



UNIVERSITY OF
LEICESTER

**Effect of Proteinuria on Cellular Expression of the Cubilin-
Amnionless CUBAM Endocytic Complex**

**Thesis submitted for the degree of Doctor of Philosophy
at the University of Leicester**

By

Nura Faraj Benfaed

MBChB (Libya), MMedsci (UK)

**Department of Infection, Immunity and Inflammation
(Nephrology)**

University of Leicester

June 2019

Statement of originality

This accompanying thesis submitted of the degree of Doctor of Philosophy entitled “Effect of Proteinuria on Cellular Expression of the Cubilin Amnionless CUBAM Endocytic Complex” is based on work conducted by the author at University of Leicester mainly during the period between August 2014 and July 2018.

All work recorded in this thesis is original unless otherwise acknowledged in the text or by references.

None of the work has been submitted for another degree in this or any other University,

Signed: Dr Nura Faraj Benfaed

Date: 14 June 2019

Effect of Proteinuria on Cellular Expression of the Cubilin-Amnionless CUBAM Endocytic Complex

Nura Faraj Benfaed

Abstract

Albumin is protein filtered by the glomerulus and subsequently reabsorbed in the proximal tubule. Reabsorption is mediated at least in part by cubilin-amnionless (cubam) endocytic receptor complex. Proteinuria is an important renal biomarker correlated with the poor prognosis of the kidney disease. However, expression of the cubam complex is not well studied in disease. These studies aimed to investigate the expression and turnover of the cubam complex in proteinuria and the effect of matrix metalloproteinase inhibition on the expression of the cubam complex.

In a mouse model of protein overload proteinuria, cubam complex was significantly reduced in the proximal tubule associated with a rise of urinary shedding of both cubilin and amnionless. An increase in renal matrix metalloprotease activity in proteinuria accompanies the urinary loss of these receptors. Furthermore, matrix metalloprotease inhibition (MMPI) treatment has an antiproteinuric effect by reducing urinary proteins excretion in proteinuric animals. Similarly, MMPI ameliorated cubam endocytic complex shedding in the urine. In addition, the studies investigated the degree of tubulointerstitial injury in experimental animals finding an increase in renal proinflammatory cytokines, inflammatory cell infiltration, collagen and apoptosis in proteinuria reversed by MMPI. Moreover, cubam complex expression was significantly downregulated in the proximal tubules of the patients with minimal change disease (MCD), membranous nephropathy (MN) and focal segmental glomerulosclerosis (FSGS), consistent with the findings in the mouse models.

In conclusion, this indicates a renoprotective action of MMPI in proteinuric nephropathies. This may have important clinical implications in the therapeutic approach to proteinuria.

Acknowledgements

I would like to thank the following people for their appreciated assistance in the production of this thesis. Firstly, my supervisor Professor Nigel Brunskill for this continuous support, patience and giving me the opportunity to have this experience. His guidance helped me in all the time of the research and writing of this thesis, and for allowing me to grow my confidence as an independent researcher. I would also like to thank my second supervisor Professor Jonathan Barratt for this insightful feedback and constructive criticism.

Besides my supervisor, I would like to thank my PRP members, Dr James Burton and Dr Peter Topham for their insightful comments and encouragement. I would also like to thank Dr Rachid Tazi-Ahnini at the University of Sheffield, who provided me with an opportunity to learn the qPCR technique.

I would like also to thank Dr Ravinder Chana, who helped me to learn various techniques during my laboratory work. I would like to thank my colleague's Dr Samy Alghadban and Dr Hiwa Falah, who have helped me in conducting the present animal's models. Many thanks to Dr Kees Straatman, whose help and advice during using advanced imaging facility.

I would like to give my special thanks to the University of Leicester for giving me an opportunity to complete my PhD study and all the people of infection, inflammation and immunity department for their continuous support.

I would like to thank the Ministry of Higher Education in Libya for sponsoring and financially support me throughout my PhD study.

Finally, I would like also to thank my parents, without them I would never have been able to complete this project. I would like to acknowledge the important contribution that my family has made toward the completion of this research, my husband Dr Sirag Bannaser has been supportive throughout my PhD study, I greatly appreciate how much he has helped me and made completing this project possible. Also, my lovely children Mohammed, Malak and Nuri for all their moral support and patience.

Dedication,

This thesis is heartily dedicated to the spirit of my father who taught me the essence of life.

Publication, Poster and Oral Presentation

Reduced proximal tubular expression of protein endocytic receptors in proteinuria is associated with urinary receptor shedding

Hiwa Fatah, **Nura Benfaed**, Ravinder S Chana, Mohamed H Chunara, Jonathan Barratt, Richard J Baines, Nigel J Brunskill. 2017, Nephrology Dialysis Transplantation

Does the Expression of Protein Endocytic Receptors Change in Human Nephrotic Syndrome?

Nura Benfaed, Nigel Brunskill, Jonathan Barratt. International RENALTRACT Conference 12-13 April 2018, University of Manchester, UK

Urinary Shedding of Protein Endocytic Receptors in Proteinuria is Associated with an Increase of Matrix Metalloproteinase Activity

Nura Benfaed, Nigel Brunskill, Jonathan Barratt. Midlands Academy of Medical Sciences Festival, 23 March 2018, Loughborough University, UK

Reduced Cubilin Expression in Proteinuric Rodents and Human Proteinuric Renal Disease

Nura Benfaed, Nigel Brunskill, Jonathan Barratt. Postgraduate conference, 11 October 2016, Department of Infection, Immunity and Inflammation, University of Leicester, UK

Cubilin Expression in Protein Overload Proteinuria model

Nura Benfaed, Nigel Brunskill, Jonathan Barratt. Renal seminar presentation, 13 April 2016, Department of Infection, Immunity and Inflammation, University of Leicester, UK

Table of Contents

Abstract	I
Acknowledgements	II
Publication, Poster and Oral Presentation	IV
Table of contents	V
List of figures	XII
List of tables	XVIII
List of abbreviation	XIX
Chapter 1. Introduction	1
1.1. Gross anatomy of Kidney	1
1.2. Nephron structure and functions	2
1.2.1. Renal Corpuscle	3
1.2.1.1. Glomerular filtration barriers	5
1.2.1.1.1. Endothelium	6
1.2.1.1.2. Glomerular basement membrane	8
1.2.1.1.3. Podocytes	8
1.2.1.2. Mesangium	10
1.2.2. Proximal tubule	11
1.3. Mechanisms of proteinuria	12
1.3.1. Glomerular proteinuria	12
1.3.2. Tubular proteinuria	13
1.4. Renal handling of protein	15
1.4.1. Glomerular filtration of albumin	15
1.4.2. Tubular reabsorption of proteins	16
1.4.2.1. Endocytosis process in proximal tubule	17
1.4.2.1.1. Fluid-phase endocytosis	18
1.4.2.1.2. Receptor-mediated endocytosis	18

1.5. Cubilin-amnionless complex endocytic receptors -----	21
1.5.1. Cubilin -----	21
1.5.1.1 Structure of cubilin-----	21
1.5.1.2. Expression and synthesis of cubilin-----	24
1.5.1.3. Regulation of expression of cubilin-----	24
1.5.1.4. Cubilin ligands-----	25
1.5.1.5. Cubilin interaction with other endocytic receptors-----	26
1.5.2. Amnionless -----	29
1.5.2.1. Structure of amnionless-----	29
1.5.2.2. Expression and distribution of amnionless-----	31
1.5.2.3. Function and regulation of amnionless-----	31
1.5.3. Cubam complex dysfunction in renal disorders -----	33
1.5.3.1. Imerslund-Gräsbeck syndrome in human-----	33
1.5.3.2. Imerslund-Gräsbeck syndrome in an animal model-----	35
1.5.3.3. Albuminuria and chronic kidney disease (CKD)-----	35
1.6. Tubular toxicity of proteinuria -----	36
1.6.1. In vitro studies-----	37
1.6.2. In vivo studies-----	40
1.7. Importance of proteinuria in CKD -----	44
1.7.1. The prevalence and progression of CKD-----	44
1.7.2. Correlation between proteinuria and renal failure-----	45
1.7.2.1. Correlation in animal studies-----	45
1.7.2.1. Remnant kidney-----	45
1.7.2.2. Puromycin Aminonucleoside nephrosis model-----	46
1.7.2.3. Protein overload model-----	48
1.7.2.2. Correlation in human studies -----	49

1.8. Matrix metalloproteinases	50
1.8.1. Structure of MMPs	51
1.8.2. MMP activation and expression	52
1.8.3. Mechanisms of MMP action in kidney disease	54
1.8.4. The beneficial effect of MMP inhibition in animals models	55
1.8.5. Synthetic Inhibitor batimastat	56
1.9. Aim and objectives	58
1.10. Hypothesis	58
Chapter 2. Materials and Methods	60
2.1. Materials	60
2.1.1. Chemicals reagents	60
2.1.2. Immunoblotting	60
2.1.3. Immunostaining	61
2.1.4. Materials used in the gene study	61
2.1.5. Commercial kits	62
2.1.6. Polyacrylamide Gels	62
2.1.7. Antibodies	62
2.1.7.1. Antibodies used in Immunoblot	62
2.1.7.2. Antibodies used in Immunohistochemistry	63
2.1.7.3. Antibodies used in Immunofluorescences	64
2.1.8. TaqMan Gene Expression Assays	64
2.2. Experimental studies	64
2.2.1. in-vivo studies in mice	64
2.2.1.1. Characterization of protein receptors expression in normal wild-type mice	65
2.2.1.2. Protein overload nephropathy	65
2.2.1.2.1. Unilateral nephrectomy surgery	65
2.2.2.1.2. Bovine serum albumin (BSA) to induce protein overload proteinuria	66
2.2.2.1.3. BSA to induce protein overload proteinuria plus MMPI	66

2.2.2.1.4. Collection of samples-----	67
2.2.1.3. Adriamycin-induced nephropathy-----	70
2.2.2. Human renal biopsy samples-----	70
2.2.3. Determination of biochemical markers-----	71
2.2.3.1. Determination of the total protein concentrations in serum and urine-----	71
2.2.3.2. Measurement of creatinine in urine and serum-----	71
2.2.3.3. Measurement of albumin in urine and serum-----	72
2.2.3.4. Measurement of serum vitamin B ₁₂ levels-----	72
2.2.4. Preparation of protein in samples-----	73
2.2.4.1. Preparation of lysate from tissues-----	73
2.2.4.2. Determination of the protein concentration in tissue homogenates-----	74
2.2.4.3. Preparation of urine samples-----	74
2.2.5. Methods-----	76
2.2.5.1. Immunoblotting-----	76
2.2.5.1.1. SDS-polyacrylamide gel electrophoresis of proteins-----	76
2.2.5.1.2. Coomassie staining for SDS-PAGE gels-----	76
2.2.5.1.3. Transfer of proteins separated by SDS-PAGE to PVDF-----	77
2.2.5.1.4. Membrane blocking and immunoblotting-----	77
2.2.5.1.5. Analysis of immunoblot images-----	78
2.2.5.2. Histological examination of tissues-----	78
2.2.5.2.1. Haematoxylin and Eosin staining-----	78
2.2.5.2.2. Immunohistochemistry staining-----	79
2.2.5.2.2.1. Analysis of immunohistochemistry images -----	81
2.2.5.2.3. Immunofluorescences-----	82
2.2.5.2.3.1. Analysis of immunofluorescence images -----	83
2.2.5.2.4. Detection of apoptosis cells-----	84
2.2.5.2.4. Sirius Red staining-----	85
2.2.5.3. Determination of the cubilin and amnionless in urine and tissue by ELISA----	86

2.2.5.4. Quantitative polymerase chain reaction-----	88
2.2.5.4.1. Extraction of Ribonucleic acid (RNA) from tissue experiments-----	88
2.2.5.4.2. Generation of complementary DNA (cDNA) -----	89
2.2.5.4.3. Quantitative real-time PCR-----	89
2.2.5.5. Measurement of matrix metalloproteinase (MMP) activity-----	90
2.2.5.5.1. General MMP activity assay-----	90
2.2.5.5.2. Zymography-----	91
2.2.5.6. Statistical analysis-----	92
Chapter 3. Characterization of the expression of endocytic receptors in wild-type mice-----	93
3.1. Introduction-----	93
3.2. Results-----	94
3.2.1. Cubilin expression in the mouse kidney-----	94
3.2.2. Cubilin expression in the mouse small intestine-----	98
3.2.3. Amnionless expression in the mouse kidney-----	102
3.3. Discussion-----	106
Chapter 4. Expression of Cubilin and Amnionless in Mouse Protein Overload Nephropathy -----	107
4.1. Introduction-----	107
4.2. Results-----	108
4.2.1. Effect of protein overload on blood and urine biochemistry-----	108
4.2.2. Renal histopathology in protein overload proteinuria-----	110
4.2.3. Effect of protein overload proteinuria on cubam complex-----	113
4.2.3.1. Cubilin expression in the kidney of proteinuric and control mice-----	113
4.2.3.2. Cubilin expression in the small intestine of proteinuric and control mice-----	120
4.2.3.3. Kidney cubilin expression in adriamycin nephropathy-----	125
4.2.3.4. Amnionless expression in the kidney of proteinuric and control mice-----	132
4.2.4. Effect of protein overload proteinuria on proximal tubular DPP-IV-----	138

4.2.5. Effect of protein overload on the Aquaporin-1-----	141
4.2.6. Effect of protein overload proteinuria on MMPs-----	144
4.3. Discussion-----	150
Chapter 5. Effect of Matrix Metalloproteinase Inhibition on the Kidney Expression of Cubam in Protein Overload Proteinuria in Mice-----	158
5.1. Introduction -----	158
5.2. Results-----	159
5.2.1. Effect of MMPI treatment on urine biochemistry in proteinuria -----	159
5.2.2. Effect of MMPI treatment on blood biochemistry in proteinuria-----	161
5.2.3. Effect of MMPI treatment on enzymatic activity of MMPs-----	163
5.2.4. Effect of MMPI treatment on MMPs expression in proteinuria-----	166
5.2.5 Effect of MMPI treatment on the expression of MMPs gene in proteinuria-----	178
5.2.6. Effect of MMPI treatment on cubam complex-----	180
5.2.6.1. MMPI ameliorates cubilin expression in proteinuria-----	180
5.2.6.2. MMPI ameliorates amnionless expression in proteinuria-----	187
5.2.6.3. Colocalization of the cubam complex in proteinuria-----	194
5.2.4.4. Effect of MMPI on DPP-IV marker in proteinuria-----	198
5.3. Discussion-----	203
Chapter 6. Matrix Metalloproteinase Inhibitor Ameliorates Renal Tubulointerstitial Fibrosis and Apoptosis in Proteinuric Mice-----	209
6.1. Introduction-----	209
6.2. Results -----	210
6.2.1. Renal histopathological in protein overload proteinuria and MMPI-----	210
6.2.2. Effect of MMPI treatment on collagen deposition in proteinuria-----	213
6.2.3. Effect of MMPI treatment on renal macrophages in proteinuria-----	216
6.2.4. Effect of MMPI treatment on renal interleukin-6 expression in proteinuria-----	221
6.2.5. Effect of MMPI treatment on renal tumour necrosis factor-alpha expression in proteinuria-----	226

6.2.6. Effect of MMPI treatment on renal transforming growth factor-beta expression in proteinuria-----	231
6.2.7. Effect of MMPI treatment on apoptosis in proteinuria-----	236
6.2.8. Effect of MMPI treatment on caspase-3 expression in proteinuria-----	239
6.3. Discussion-----	245
Chapter 7. Expression of Cubam complex in Human Nephrotic Syndrome-----	251
7.1. Introduction-----	251
7.2. Results-----	252
7.2.1. Cubilin expression in human nephrotic syndrome-----	254
7.2.2. Amnionless expression in human nephrotic syndrome-----	257
7.2.3. DPP- IV expression in human nephrotic syndrome-----	260
7.3. Discussion-----	263
Chapter 8. General Discussion-----	264
8.1. Summary thesis-----	264
8.2. Conclusion-----	271
8.3. Future work-----	272
Appendices-----	273
Appendix 1. Buffers, solutions and Materials used in this study-----	273
Appendix 2. Standard curve -----	281
Appendix .3. Automated image analysis macro code-----	287
Reference-----	289

List of Figures

Figure.1.1. Coronal section of the kidney structure-----	1
Figure.1.2. Schematic diagram of the nephron-----	2
Figure.1.3. Schematic diagram of the renal corpuscle and juxtaglomerular apparatus structures-----	4
Figure.1.4. Schematic diagram of the glomerular filtration barrier-----	9
Figure.1.5. Schematic diagram of endocytosis -----	20
Figure.1.6. Schematic diagram of the cubilin structure-----	23
Figure.1.7. Schematic diagram illustrates the interaction of cubam complex and megalin-----	28
Figure.1.8. Schematic diagram illustrates amnionless structure-----	30
Figure.1.9. Schematic diagram illustrates protein overload induce renal impairment----	43
Figure.2.1. Schematic diagram illustrated the protein overload proteinuria experiment-	68
Figure.2.2. Schematic diagram illustrated the protein overload proteinuria plus MMPI treatment experiment-----	69
Figure.3.1. Immunoblotting analysis of mouse renal cortex for cubilin-----	95
Figure.3.2. IHC analysis of mouse kidney tissue for cubilin-----	96
Figure.3.3. IF staining for cubilin in WT mouse kidney-----	97
Figure.3.4. Immunoblotting analysis of mouse small intestine for cubilin-----	99
Figure.3.5. IHC analysis of WT small intestine tissue for cubilin-----	100
Figure.3.6. IF analysis of mouse kidney tissue for cubilin-----	101
Figure.3.7. Immunoblotting analysis of mouse renal cortex for cubilin-----	103
Figure.3.8. IHC analysis of mouse kidney tissue for amnionless-----	104
Figure.3.9. IF analysis of mouse kidney tissue for amnionless-----	105
Figure.4.1. Urine biochemistry and protein excretions in mice-----	109
Figure.4.2 Serum biochemistry and proteins levels in mice-----	110
Figure.4.3. Kidney histology in proteinuric and control mice-----	112

Figure.4.4. Analysis of cubilin protein expression in mouse kidneys by immunoblotting-- -----	115
Figure.4.5. IHC analysis of mouse kidney tissue for cubilin in control and proteinuric mice with protein overload proteinuria-----	116
Figure.4.6. ELISA determination of the concentration of cubilin in mouse kidney-----	117
Figure.4.7. Fold change in cubilin mRNA expression in mouse kidneys of proteinuric vs. normal mice-----	118
Figure.4.8. Urinary excretion of cubilin in mouse urine-----	119
Figure.4.9. Analysis of cubilin protein expression in mouse small intestine by immunoblotting-----	121
Figure.4.10. Determination of mouse small intestine cubilin by ELISA-----	122
Figure.4.11. IHC analysis of mouse small intestine tissue for cubilin-----	123
Figure.4.12. Fold change of cubilin mRNA in the small intestine of protein overload proteinuria vs control mice-----	124
Figure.4.13. Analysis of cubilin protein expression in mouse kidney by immunoblotting-- -----	127
Figure.4.14. IHC analysis of mouse kidney tissue for cubilin in Adriamycin-induced proteinuria-----	128
Figure.4.15. Urinary excretion of cubilin in mouse urine by ELISA-----	129
Figure.4.16. Cubilin mRNA in the kidney of adriamycin-induced proteinuric and control mice-----	130
Figure.4.17. Renal histology and parameters of protein excretions in urine and serum of adriamycin mice -----	131
Figure.4.18. Analysis of amnionless expression in mouse kidneys by immunoblotting---- -----	134
Figure.4.19. IHC analysis of mouse kidney tissue for amnionless in control and proteinuric mice with protein overload proteinuria-----	135
Figure.4.20. Fold change in amnionless mRNA expression in kidneys of proteinuric and controls mice-----	136

Figure.4.21. Urinary excretion of amnionless in mouse urine-----	137
Figure.4.22. Analysis of DPP-IV expression in mouse kidney by immunoblotting-----	139
Figure.4.23. IHC analysis of mouse kidney tissue for DPP-IV in control and proteinuric mice with protein overload proteinuria-----	140
Figure.4.24. Analysis of AQP-1 in mouse kidneys by immunoblotting-----	142
Figure.4.25. IHC analysis of mouse kidney tissue for AQP-1 in control and proteinuric mice with protein overload proteinuria-----	143
Figure.4.26. Analysis of MMPs expression in mouse kidneys by immunoblotting-----	145
Figure.4.27. IHC analysis of mouse kidney sections for MMP-2 in control and proteinuric mice with protein overload proteinuria-----	146
Figure.4.28. IHC analysis of mouse kidney sections for MMP-3 in control and proteinuric mice with protein overload proteinuria-----	147
Figure.4.29. IHC analysis of mouse kidney sections for MMP-7 in control and proteinuric mice with protein overload proteinuria-----	148
Figure.4.30. IHC analysis of mouse kidney tissue for MMP-9 in control and proteinuric mice with protein overload proteinuria-----	149
Figure.5.1. Urine biochemistry and protein levels-----	160
Figure.5.2. Serum biochemistry and proteins levels in mice-----	162
Figure.5.3. Effect of the MMPI on kidney cortex MMPs activity-----	164
Figure.5.4. Gelatinase activity of MMP-2 and MMP-9 in control, proteinuric mice and protein injected mice treated with the MMPI-----	165
Figure.5.5. Analysis of MMPs expression in mouse kidney by immunoblotting-----	167
Figure.5.6. Densitometric analysis of MMPs expression-----	168
Figure.5.7. IHC analysis of mouse kidney tissue for MMP-2 in control, proteinuric mice and protein injected mice treated with the MMPI-----	170
Figure.5.8. Semi-quantitative analysis of renal MMP-2 staining in control, proteinuric mice and protein injected mice treated with the MMPI-----	171
Figure.5.9. IHC analysis of mouse kidney tissue for MMP-3 in control, proteinuric mice and protein injected mice treated with the MMPI-----	172

Figure.5.10. Semi-quantitative analysis of renal MMP-3 staining in control, proteinuric mice and protein injected mice treated with the MMPI-----	173
Figure.5.11. IHC analysis of mouse kidney tissue for MMP-7 in control, proteinuric mice and protein injected mice treated with the MMPI-----	174
Figure.5.12. Semi-quantitative analysis of renal MMP-7 staining in control, proteinuric mice and protein injected mice treated with the MMPI-----	175
Figure.5.13. IHC analysis of mouse kidney tissue for MMP-9 in control, proteinuric mice and protein injected mice treated with the MMPI-----	176
Figure.5.14. Semi-quantitative analysis of renal MMP-9 staining proteinuria in control, proteinuric mice and protein injected mice treated with the MMPI-----	177
Figure.5.15. Fold change of MMPs mRNA expression in mice kidneys control, proteinuric mice, and protein injected mice treated with the MMPI-----	179
Figure.5.16. Analysis of cubilin expression in mouse kidneys by immunoblotting-----	182
Figure.5.17. IHC analysis of mouse kidney tissue for cubilin in control, proteinuric mice and protein injected mice treated with the MMPI-----	183
Figure.5.18. Semi-quantitative analysis of renal cubilin staining in control, proteinuric mice, and protein injected mice treated with the MMPI-----	184
Figure.5.19. Fold change of cubilin mRNA expression in mouse kidneys of control, proteinuric mice and protein injected mice treated with the MMPI-----	185
Figure.5.20. Urinary excretion of cubilin in mouse urine-----	186
Figure.5.21. Analysis of amnionless expression in mouse kidneys by immunoblotting-----	189
Figure.5.22. IHC analysis of mouse kidney tissue for amnionless in control, proteinuric mice and protein injected mice treated with the MMPI-----	190
Figure.5.23. Semi-quantitative analysis of renal amnionless staining in control, proteinuric mice and protein injected mice treated with the MMPI-----	191
Figure.5.24. Fold change in amnionless mRNA expression in mouse kidneys of control, proteinuric mice and protein injected mice treated with the MMPI-----	192
Figure.5.25. Urinary excretion of the amnionless in mouse urine-----	193

Figure.5.26. IF analysis for colocalization of cubilin and amnionless staining in mouse kidney tissue-----	195
Figure.5.27. Semi-quantitative analysis of renal cubilin and amnionless staining in control, proteinuric mice and protein injected mice treated with the MMPI-----	196
Figure.5.28. IF analysis for colocalization of cubilin and amnionless staining in mouse small intestine tissue-----	197
Figure.5.29. Analysis of DPP-IV expression in mouse kidney by immunoblotting-----	199
Figure.5.30. IHC analysis of mouse kidney tissue for DPP-IV in control, proteinuric mice and protein injected mice treated with the MMPI-----	200
Figure.5.31. IF analysis of mouse kidney tissue for DPP-IV-----	201
Figure.5.32. Semi-quantitative analysis of renal DPP-IV staining in control, proteinuric mice and protein injected mice treated with the MMPI-----	202
Figure.6.1. Kidney histology in control, proteinuric mice and protein injected mice treated with the MMPI-----	211
Figure.6.2. Renal tubular injury scoring in mouse kidney from control, proteinuric mice, and protein injected mice treated with the MMPI-----	212
Figure.6.3. Sirius red staining of mouse kidney section for collagen deposition-----	214
Figure.6.4. Semi-quantitative analysis of collagen deposition mouse kidney from control, proteinuric mice and protein injected mice treated with the MMPI-----	215
Figure.6.5. Analysis of macrophage F4/80 expression in mouse kidneys by immunoblotting-----	217
Figure.6.6. IHC analysis of mouse kidney tissue for macrophage F4/80 in control, proteinuric mice and protein injected mice treated with the MMPI-----	218
Figure.6.7. Semi-quantitative analysis of renal macrophage F4/80 staining in mouse kidney from control, proteinuric mice and protein injected mice treated with the MMPI-----	219
Figure.6.8. Fold change in macrophage F4/80 mRNA expression in mouse kidneys from control, proteinuric mice and protein injected mice treated with the MMPI-----	220
Figure.6.9. Analysis of IL-6 expression in mouse kidneys by immunoblotting-----	222

Figure.6.10. IHC analysis of mouse kidney tissue for IL-6 in control, proteinuric mice and protein injected mice treated with the MMPI-----	223
Figure.6.11. Semi-quantitative analysis of renal IL-6 staining in mouse kidney from control, proteinuric mice and protein injected mice treated with the MMPI-----	224
Figure.6.12. Fold change in IL-6 mRNA expression in mice kidneys from control, proteinuric mice and protein injected mice treated with the MMPI-----	225
Figure.6.13. Analysis of TNF- α expression in mouse kidneys by immunoblotting-----	227
Figure.6.14. IHC analysis of mouse kidney tissue for TNF-alpha in control, proteinuric and protein injected mice treated with the MMPI-----	228
Figure.6.15. Semi-quantitative analysis of renal TNF-alpha staining in mouse kidney from control, proteinuric mice and protein injected mice treated with the MMPI-----	229
Figure.6.16. Fold change in TNF- α mRNA expression in mice kidneys from control, proteinuric mice and protein injected mice treated with the MMPI-----	230
Figure.6.17. Analysis of TGF- β expression in mouse kidneys by immunoblotting-----	232
Figure.6.18. IHC analysis of mouse kidney tissue for TGF- β in control, proteinuric and protein injected mice treated with the MMPI-----	233
Figure.6.19. Semi-quantitative analysis of renal TGF- β staining in control, proteinuric mice and protein injected mice treated with the MMPI-----	234
Figure.6.20. Fold change in TGF- β mRNA expression in mice kidneys from control, proteinuric mice and proteinuric mice treated with the MMPI-----	235
Figure.6.21. TUNEL stained mouse kidney sections for detection apoptosis-----	237
Figure.6.22. Numbers of apoptotic cells counted by Image J in control, proteinuric mice and protein injected mice treated with the MMPI-----	238
Figure.6.23. Analysis of caspase-3 expression in mouse kidneys by immunoblotting--	240
Figure.6.24. IHC analysis of mouse kidney tissue for caspase-3 in control, proteinuric mice and protein injected mice treated with the MMPI-----	241
Figure.6.25. Semi-quantitative IHC analysis of renal caspase-3 staining in control, proteinuric mice and protein injected mice treated with the MMPI-----	242
Figure.6.26. IF analysis of mouse kidney tissue for caspase-3. -----	243

Figure.6.27. Semi-quantitative IF analysis of renal caspase-3 staining in control, proteinuric mice and protein injected mice treated with the MMPI-----	244
Figure.7.1. IHC analysis of human kidney biopsies for cubilin in patients with nephrotic syndrome-----	255
Figure.7.2. Semi-quantitative analysis of renal cubilin expression in human nephrotic syndrome-----	256
Figure.7.3. IHC analysis of human kidney biopsies for amnionless in patients with nephrotic syndrome-----	258
Figure.7.4. Semi-quantitative analysis of renal amnionless expression in human nephrotic syndrome. -----	259
Figure.7.5. IHC analysis of human kidney biopsies for DPP-IV in patients with nephrotic syndrome-----	261
Figure.7.6. Semi-quantitative analysis of renal DPP-IV expression in human nephrotic syndrome-----	262
Figure. 8.1. Schematic diagram illustrates the normal physiology endocytic process of proteins in the proximal tubules-----	268
Figure.8.2. Schematic diagram illustrates the pathophysiological effect of protein overload proteinuria on the proximal tubules-----	269
Figure.8.3. Schematic diagram illustrates the effect of MMP inhibition treatment on the proximal tubules in protein overload proteinuria-----	270

List of tables

Table.7.1. Clinical parameters of nephrotic syndrome patients were provided that kidney biopsy samples-----	253
---	-----

List of abbreviations

ACEI	Angiotensin-converting enzyme inhibitor
AKI	Acute kidney injury
ARB	Angiotensin II receptor blocker
AQP-1	Aquaporin -1
BSA	Bovine serum albumin
CKD	Chronic kidney disease
CHO	Chinese hamster ovary
CL	Capillary lumen
Cubam	Cubilin-amnionless complex
DAB	Diaminobenzidine
DCCT	Diabetic control and complication trial
DPP-IV	Dipeptidyl peptidase-IV
ECM	Extracellular matrix
EC	Endothelial cells
EDIC	Epidemiology diabetes intervention and complication
EF	Endothelial fenestrate
EGF	Epidermal growth factor
ELISA	Enzyme-linked immunosorbent assay
ESRD	End-Stage Renal Diseases
ERK	Extracellular signal-regulated- kinase
ESL	Endothelial cell surface layer
FFPE	Formalin-fixed, Paraffin-embedded
FSGS	Focal segmental glomerulosclerosis
FP	Foot processes
GBM	Glomerular basement membrane
GFR	Glomerular filtration rate
H&E	Haematoxylin and eosin
HDL	High-density lipoprotein
HRP	Horseradish peroxidase
IF-B12	Intrinsic factor-cobalamin complex
IF	Immunofluorescence
IGS	Imerslund-Gräsbeck syndrome
IHC	Immunohistochemistry

IL-6	Interleukin-6
IP	Intraperitoneal
HKC-8	Human kidney cell clone-8 cells
K/DOQI	Kidney Disease Outcomes Quality Initiative
LDLR	Low-density lipoprotein receptor
MAPK	Mitogen-activated protein kinase
MCD	Minimal change disease
MCP-1	Monocyte chemotactic protein-1
MDRD	Modification of Diet in Renal Disease Study
MDCK	Madin Darby canine kidney cell line
MMP	Matrix metalloproteinase
MMPI	Matrix metalloproteinase inhibitor
MN	Membranous nephropathy
NF- κ B:	Nuclear factor-KB
NKF	National Kidney Foundation
OK	Opossum kidney cells
PAN	Puromycin Aminonucleoside
PBS	Phosphate buffered saline
PKB	Protein kinase B
PC	Podocytes
PKC	Protein kinase C
PTC	Proximal tubular cells
PTs	Proximal tubules
PVDF	Polyvinylidene Difluoride
PPARs	Peroxisome proliferator-activated receptors
PKC	Protein kinase C
PAN	Puromycin Aminonucleoside
PTECs	Proximal tubular epithelium cells
PT	Proximal tubule
qPCR	Quantitative real-time polymerase chain reaction
RAP	Receptor-associated protein
RANTES	Regulated on activation normal T-cell expressed and secreted
REIN	Ramipril Efficacy In Nephropathy
RFU	Relative fluorescence unit
RIPA	Radio-immunoprecipitation assay

ROS	Reactive oxygen species
SD	Slit diaphragm
SDS	Sodium dodecyl sulphate
SDS-PAGE	SDS-Polyacrylamide Gel Electrophoresis of Protein
STAT	Signal transducer activator of transcription
TBS	Tris-buffered saline
TBS	Tris-buffered saline with tween 20
TGF- β	Tumour growth factor- β
TNF- α	Tumour necrotic factor- α
UUO	Unilateral tract obstruction
VDBP	Vitamin-D binding protein
WT mice	Wild-type Mice

Chapter One. Introduction

1.1. Gross anatomy of Kidney

The kidneys are reddish-brown organs, situated in the retroperitoneal space of the posterior abdominal wall on either side of the vertebral column mainly under cover of the costal border (Wallace, 1998). On the superior part of each kidney is the adrenal gland (Richard S. Snell, 2000). Each adult kidney is about 12 cm long, weigh around 150 g and represents about 0.4 % of total body weight (Cohen, 2006). Also, the kidneys are receiving around 25 % of the cardiac output (Wallace, 1998). The cut surface of the kidney displays into two different regions, the pale outer region is the cortex, and a darker inner region is the medulla divided into a series of wedges, called the renal pyramids, which in turn open into the renal calyces. The renal pelvis is formed by linking the major and minor calyces and extends to the upper end of the ureter. The renal columns are connective tissue extensions that radiate down from the cortex through the medulla to separate into renal pyramids and renal papillae (Richard S. Snell, 2000, Lote, 2012). The renal hilum is a slit on the medial surface of each kidney where the renal artery, vein, lymphatic vessels, renal nerve and renal pelvis enter and exit the kidney (Richard S. Snell, 2000, Lote, 2012).

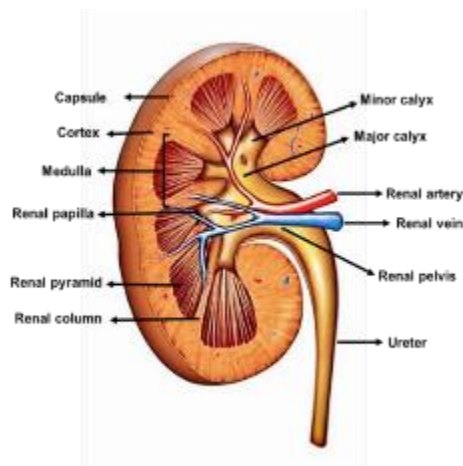


Figure.1.1. Coronal section of the kidney structure, adapted from (Lote, 2012)

1.2. Nephron structure and functions

The key roles of kidneys are to regulate water and electrolyte balance of the body, maintain the acid-base balance of the blood and excrete waste products into the urine (Wallace, 1998, Asanuma et al., 2007). The basic functional unit of kidneys is known as the nephron. Each human kidney has about 1.3 million nephrons (Kriz and Elger, 2010). Each of which consists of a renal corpuscle including glomerular tuft capillaries attached to the mesangium and Bowman's capsule. The glomerulus connects to the proximal convoluted tubule that empties into the collecting duct, which is located in the cortex and separated into superficial, mid-cortical, and juxtamedullary nephrons (Kriz and Elger, 2010). The tubular part of the nephron comprises a proximal tubule and a distal tubule connected by Henle's loop and collecting duct (Kriz and Elger, 2010).

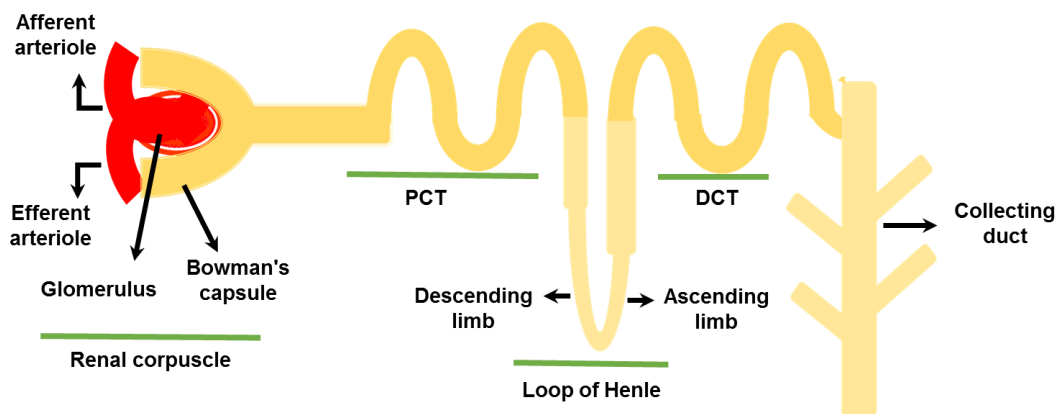


Figure.1.2. Schematic diagram of the nephron.

Proximal convoluted tubule (PCT), distal convoluted tubule (DCT), adapted from (Kriz and Bankir, 1988).

1.2.1. Renal Corpuscle

1.2.1. Renal Corpuscle

The renal corpuscle has a central role in the filtration of blood plasma. It comprises the glomerular tuft capillaries attached to the mesangium and Bowman's capsule and has a vascular pole and a urinary pole (Figure 1.3). The vascular pole is the site where the arterioles from the renal circulation enter and leave the glomerulus. The urinary pole is where glomerular filtrate leaves the Bowman's capsule and enters the renal tubule (Kriz and Elger, 2010). The glomerular capillaries, together with the mesangium, are covered by epithelial cells forming the visceral epithelium layer of Bowman's capsule known as podocytes. At the vascular pole, this is reflected to become the parietal epithelium of Bowman's capsule. The glomerular basement membrane (GBM) is developed at the border between the glomerular capillaries and the mesangium on one side and the podocyte layer on the other side. While at the urinary pole, the space between both layers of Bowman's capsule represents the urinary space which continues as the tubule lumen (Kriz and Elger, 2010).

In the glomerular tuft, the afferent arteriole directly divides into numerous primary capillary branches. These capillaries give rise to an anastomosing capillary network, the glomerular lobule. The efferent arteriole is already created inside the tuft by the union of capillaries from each lobule (Elger et al., 1998). The glomerular capillary wall is a living ultrafiltration membrane, comprised of a fenestrated endothelium, GBM and podocytes with the interdigitated foot processes of epithelial cells (Deen, 2004). Most glomerular capillaries form bulges towards the urinary space and are enclosed by the GBM and podocyte layer. The mesangium

is directly bound to the outer aspect of this capillaries tube. This peripheral portion of the capillary wall represents the filtration area (Kriz and Elger, 2010).

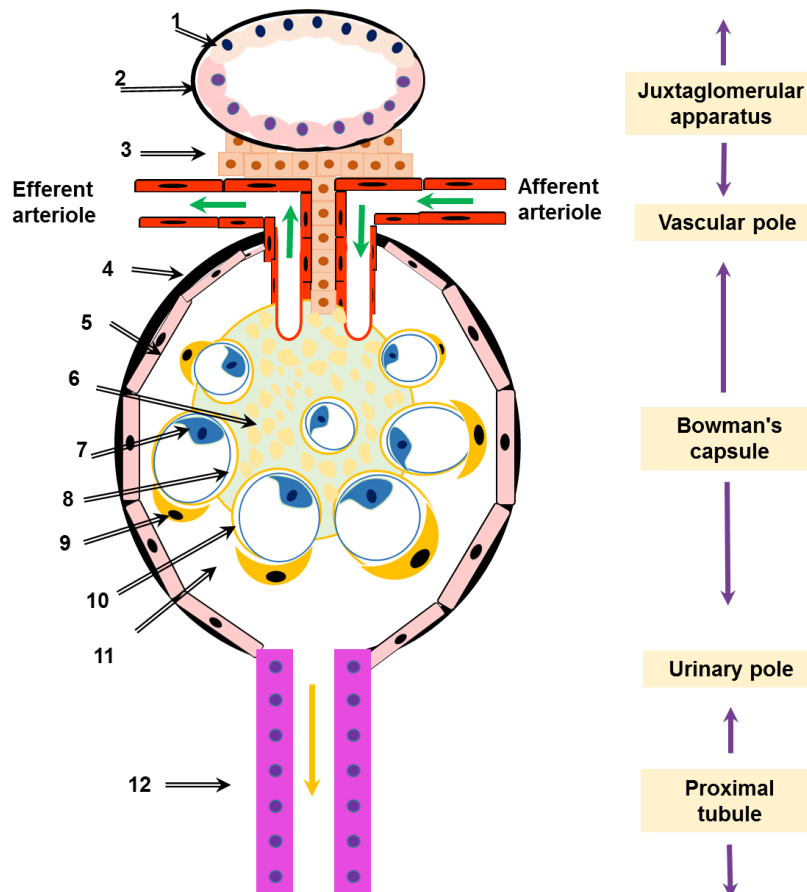


Figure.1.3. Schematic diagram of the renal corpuscle and juxtaglomerular apparatus structures.

(1) Distal convoluted tubule. (2) Macula dense. (3) Extraglomerular mesangium. (4) Bowman's capsule. (5) Parietal epithelium. (6) Matrix and mesangium cell. (7) Endothelial cell. (8) Glomerular basement membrane. (9) Podocyte. (10) Foot process, (11) Urinary space. (12) Proximal convoluted tubule, adapted from (Kriz and Elger, 2010).

1.2.1.1. Glomerular filtration barriers

The glomerular filter consists of three major cell layers which perform a mutual function of selective ultrafiltration of blood plasma, a fenestrated endothelium, the glomerular basement membrane (GBM) and the podocytes (Brenner et al., 1978) (Figure.1.4). This three-layer structure facilitates the passage of plasma, water and small solutes, whilst preventing the passage of macromolecules such as large plasma proteins (albumin) (Arif and Nihalani, 2013). Therefore, an increase of urinary protein excretion might indicate a defect in either one or all of these layers of the glomerular filtration barrier (Arif and Nihalani, 2013). The glomerular filtration barrier selects molecules according to their size, shape, and charge. This allows the free movement of water and small molecules whilst preventing large macromolecules from reaching Bowman's space (Deen et al., 2001). The fenestrated endothelium with its glycocalyx, the GBM, and the epithelial filtration slits are organised in series to form the highly selective sieving filter (Deen et al., 2001).

Evidence from human and experimental studies using variously sized dextrans, Ficolls and proteins found that solutes are restricted in their passage across the glomerular barrier depending on their molecular size (Chang et al., 1975, Ohlson et al., 2000, Lund et al., 2003). Theoretical models on glomerular permeability recognise that a group of small restrictive pores allow for movement of molecules with a radius close to 45–50 Å, but then large pores enable movement of molecules with a radius around 80–100 Å (Haraldsson et al., 2008). Blouch et al (1997) stated that the sieving coefficient of dextran and Ficoll is about 42 to 44 Å compared with albumin in terms of molecular size (Blouch et al., 1997), where elongated dextran molecules permeate the membrane more freely than spherical

macromolecules (Blouch et al., 1997, Ruggenenti et al., 1999). Other evidence also suggests that the shape of molecules may have an essential role in the filtration of protein cross the glomerular capillary wall (Sumpio and Hayslett, 1985). Horseradish peroxidase has a significantly lower sieving coefficient compared to dextrans of similar size and charges possible due to their molecular structure and rigidity (Rennke et al., 1978). Ultimately the glomerulus differentiates molecules on the combined basis of their molecular size, charge, and shape (Sumpio and Hayslett, 1985).

Loss of GFB integrity often leads to increased filtration of macromolecules such as albumin and the appearance of glomerular proteinuria (Menon et al., 2012). The herein described model of protein overload proteinuria is associated with the increased glomerular permeability to proteins such as albumin. Once filtered however the presence of receptors for ultrafiltered macromolecules on the proximal tubular epithelial cells may further modify the composition of the glomerular filtrate and determine the quality and quantity of the final proteinuria.

1.2.1.1.1. Endothelium

Glomerular endothelial cells have transcytoplasmic holes or fenestrations and are specialized for their distinctive role as essential contributors to filtration across the glomerular capillary wall (Satchell and Braet, 2009). Fenestrations present a pore size of 60-80 nm diameter. These cells also possess a gelatinous surface coat known as the glycocalyx, which consists of proteoglycans and sialoproteins (Weinbaum et al., 2007). The composition of the glycocalyx in the fenestration is noteworthy for its permeability properties (Singh et al., 2007). Glomerular filtration rate depends in part on the fractional area of the fenestrations and its glycocalyx content (Satchell and Braet, 2009). The size of glomerular EC fenestrations alone

is much too large to exclude albumin and other large proteins from the glomerular filtrate. Therefore, the glomerular capillary wall is not a perfect barrier to macromolecules and would potentially permit proteins to pass freely into the glomerular filtrate (Russo et al., 2007, Obeidat et al., 2012). An ultimate size-selective portion of the glomerular barrier is represented by the podocyte slit membrane, mainly by a zipper-like arrangement of structures in this membrane (Rodewald and Karnovsky, 1974). Previous studies found the most charge-selective barrier may be situated close to the plasma compartment in the endothelial glycocalyx (Rostgaard and Qvortrup, 2002). Whereas the furthestmost size-selective barrier may be more distally situated (Ohlson et al., 2001). Measurements of the charge-barrier properties of isolated GBMs revealed a similar to neutral and negatively charged Ficoll molecules or for native (anionic) and cationized albumin, which indicates the charge selectivity may be found in the endothelial glycocalyx (Bolton et al., 1998, Bertolatus and Klinzman, 1991).

Human and animal studies revealed that the glomerular endothelial surface layer (ESL) prevents macromolecules passage especially albumin which is mainly excluded from the glomerular filtration barrier (Satchell, 2013). Recent studies show that microalbuminuria in patients with type 1 diabetes may be associated with glycocalyx damage (Nieuwdorp et al., 2006). Furthermore, adriamycin administration causes disruption of ESL in mouse glomerular capillaries, in association with albuminuria and increased glomerular albumin clearance (Jeansson et al., 2009). Therefore, glomerular endothelial cell fenestrations and their glycocalyx play an important role in regulating the glomerular filtration barrier.

1.2.1.1.2. Glomerular basement membrane (GBM)

The GBM is originally formed by the glomerular endothelial cells that line the glomerular capillaries and the podocytes that sit on the opposite side of the GBM within the urinary space (Miner, 2012). The GBM is a thick network of extracellular matrix proteins that is an essential part of the glomerular filtration barrier (Suh and Miner, 2013, Miner, 2012). It is composed mainly of type IV collagen, laminins and heparan sulfate proteoglycans, which are produced and secreted by both endothelial cells and podocytes (Suh and Miner, 2013). The GBM restricts the passage of plasma proteins across the glomerular filtration barrier (Suh and Miner, 2013). Previous studies have found that mutations in key proteins of the GBM lead to proteinuria in Alport syndrome and Pierson syndrome (Kruegel et al., 2013, Matejas et al., 2010).

1.2.1.1.3. Podocytes

Podocytes are cells in the Bowman's capsule that cover the external surface of the glomerulus capillaries. Podocytes are comprised of cell bodies, major processes and foot processes which interdigitate with those of neighbouring cells (Asanuma et al., 2007). The foot processes wrap around the capillaries and leave slits between them to form a slit diaphragm, and cover the glomerular capillaries (Reiser and Altintas, 2016). The role of podocytes is dependent on their specific cell architecture and functions to stabilise the glomerular capillaries and to support in the barrier function of the glomerular filter through the slit diaphragms (Kriz et al., 1994, Drumond et al., 1994). Consequently, podocytes form the last barrier to protein loss, restricting the passage of large macromolecules such as serum albumin (Asanuma et al., 2007). Podocyte injury may result in effacement of foot

processes and the substantial leak of plasma proteins into the urine (Mundel and Reiser, 2010)

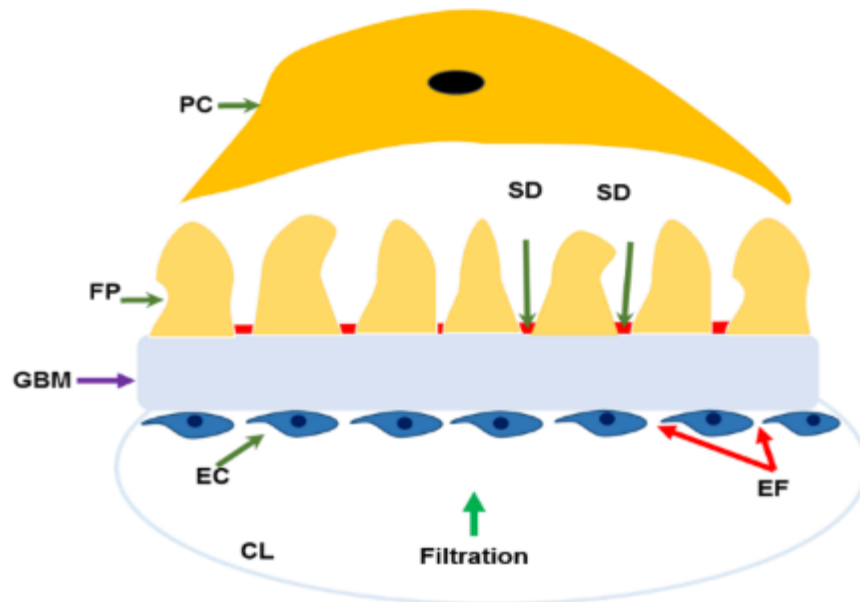


Figure.1.4. Schematic diagram of the glomerular filtration barrier.

Podocyte cell (PC), podocyte foot process (FP), slit diaphragm (SD), glomerular basement membrane (GBM), endothelial cell (EC), endothelial fenestrae (EF), capillary lumen (CL), adapted from (Kriz and Elger, 2010).

1.2.1.2. Mesangium

The mesangium is a structure that consists of predominantly intrinsic mesangial cells that resemble contractile endocytic capillary pericytes, embedded in an extracellular mesangial matrix (Sterzel et al., 1982). Mesangial cells also divide into extraglomerular or intraglomerular mesangial cells according to their location relative to the glomerulus. The mesangial cells are irregular in shape with numerous processes extending from the cell body into the surrounding matrix (Davies, 1994). The intraglomerular mesangial cells are found between the glomerulus capillaries and toward the GBM, whereas the extraglomerular mesangial cells are situated between the afferent and efferent arterioles towards the vascular pole of the glomerulus (Barajas, 1997, Scindia et al., 2010) (Figure.1.3). Processes of mesangial cells are dense assemblies of microfilaments, which contain actin, myosin, and α -actinin. The processes are attached to the GBM and the juxta-glomerular apparatus either directly or through the extracellular microfibrillar proteins (Scindia et al., 2010).

The mesangial cells have a contractile ability that constricts the capillary lumen causing regulation of blood flow into the glomerular tuft (Scindia et al., 2010). This contractile character enables them to alter the intraglomerular capillary flow and glomerular ultrafiltration surface area and thereby co-regulate single nephron glomerular filtration rate (GFR) (Stockand and Sansom, 1998). However, the indirect change of mesangial function might also disturb the function of GFB and leads to albuminuria (Zheng et al., 2004). Mesangial cells also have a wide range of receptors, for example, angiotensin II (Ang II), vasopressin, atrial natriuretic factor, prostaglandins, transforming growth factor β (TGF- β), and other growth factors (Kriz and Elger, 2010). The mesangial matrix fills the irregular spaces

between the mesangial cells and attaches the mesangial cells to the GBM (Kriz and Elger, 2010). Their matrix component may directly or indirectly influence mesangial cell growth and proliferation. It is evident that matrix metalloproteinase activity and releasing TGF- β from the mesangial matrix contributes to glomerular sclerosis (Ronco et al., 2007).

1.2.2. Proximal tubule

Renal tubules are an essential part of the nephron and tubular fluid filtered via the glomerulus (Zhuo and Li, 2013). The proximal tubule (PT) has a fundamental role in the reabsorption of filtered solutes and water (Zhuo and Li, 2013). It divides into proximal convoluted tubules and proximal straight tubules. It is distributed into three segments (S1, S2 and S3) in several animal species, but only the proximal convoluted and straight tubules are present in the normal human kidney (Kanwar Nasir M. Khan, 2013). The S1 segment is short, connecting with the Bowman capsules. The cells of this segment have the highest rate of oxidative metabolism in the kidney. The S2 segment comprises most of the proximal convoluted tubule and extends a short distance into the pars recta. Whereas, the vast bulk of the pars recta consists of the S3 segment (Kanwar Nasir M. Khan, 2013). The PT has a prominent brush border to support an increase of the luminal cell surface area and extensive interdigitation by basolateral cell processes to increase the basolateral cell surface area (Kriz and Elger, 2010). The apical endocytotic apparatus has a prominent lysosomal system and processes macromolecules such as albumin that have passed through the glomerular filter (Kriz and Elger, 2010).

1.3. Mechanisms of proteinuria

1.3.1. Glomerular proteinuria

Glomerular proteinuria can be associated with changes in one or all the three different levels of GFB, the endothelial cells, the GBM or the podocyte (Menon et al., 2012). There is evidence that shows the importance of the components of the GBM structure in proteinuria. For instance, a mutation in one of the genes that encode collagen IV may alter the structure of the GBM and this is clearly detected in Alport's syndrome, which displays extensive GBM fragmentations, and progressive glomerulosclerosis (Hudson et al., 2003, Sugimoto et al., 2006). Patients with this genetic disorder also have proteinuria and haematuria mainly due to these abnormalities in the GBM (Hudson et al., 2003). In mice, deficiency in the genes encoding collagen chains results in GBM thinning and proteinuria (Miner and Sanes, 1996).

Another study revealed that proteinuria is related to the glomerular podocyte damage in renal disorders. Disruption of the slit diaphragm and FP effacement are most common in podocyte injury and possibly the main causes of proteinuria especially albumin leakage in glomerular damage (Reiser and Altintas, 2016). Nephrin, among others, is considered the most important protein in the composition of the glomerular podocyte (Ruotsalainen et al., 1999). For example, in diseases associated with nephrin abnormalities in Finnish-type congenital nephrotic syndrome where the gene responsible for nephrin is mutated, the slit pores are disrupted and as a result, proteinuria is massively developed (Ruotsalainen et al., 1999, Tryggvason, 1999). In minimal change nephrotic syndrome, reduction of nephrin protein leads to enlargement of SD followed by massive non-selective proteinuria (Tojo and Kinugasa, 2012).

In addition, the podocyte actin cytoskeleton is also essential for the correct assembly of the slit diaphragm (Ding and Saleem, 2012). Different models of podocyte injury with proteinuria have revealed the abnormality of actin and reduction of slit diaphragm molecules (Lee et al., 2004, Otaki et al., 2008, Greka and Mundel, 2012). For instance, mice with Cdc42 deficiency in their podocyte, one of the GTPases in Rho family that regulate the actin cytoskeleton, develop heavy proteinuria associated with slit diaphragm abnormality (Scott et al., 2012). All these studies indicate that abnormalities in the components of the GFB result in abnormal passage of plasma proteins and in the absence of tubular function significant amount of these proteins may leave and are found in the urine. In a later section, the significance of tubular dysfunction in defining final proteinuria will be described.

1.3.2. Tubular proteinuria

Tubular proteinuria is described by the urinary excretion of a substantial amount of low molecular weight (LMW) proteins due to impaired tubular reabsorption of these proteins in the PT. LMW proteins, for example, α 1- and β 2-microglobulin, retinol-binding protein, urine protein 1 and β 2-glycoprotein I are normally filtered by the glomeruli because of their smaller size, charge and glomerular permeability to LMW proteins (Norden et al., 2000). Conversely, intermediate and high molecular weight (HMW) proteins are largely retained by the glomeruli and only small amounts are found in the glomerular filtrate (D'Amico and Bazzi, 2003). It has been shown that using metabolic inhibitors to inhibit proximal reabsorption of filtered proteins (Maack et al., 1979, Sumpio and Maack, 1982), the glomerular sieving coefficient for lysozyme, a 14 000 molecular weight endogenous protein found in circulating plasma, is about 0.75 in rat (Maack, 1975) in comparison with

the 0.01 for albumin estimated in the early portion of the PTs by direct puncture method (Oken and Flamenbaum, 1971). These data show that proteins of low molecular size can easily pass through GFB compared to the intermediate protein size such as albumin.

It is supposed in nephrotic condition that albumin filtered across the glomerular capillary wall and this amount of proteins is reabsorbed by the PTs, but if there is inhibition of the retrieval process in the PTs which may result of albuminuria (Russo et al., 2007, Comper et al., 2008a, Marshansky et al., 1997, Tojo and Kinugasa, 2012). Several studies have revealed that tubular dysfunction may cause urinary excretion of a substantial amount of albumin. For instance, Russo et al. (2007) demonstrated that impairment of tubular function leads to albuminuria in nephrotic rats (Russo et al., 2007). Likewise, in patients with acute tubular necrosis albuminuria is resulted from defective reabsorption of this protein by the endocytic receptors (West et al., 2006).

Even though increasing glomerular permeability of circulating protein occurs in proteinuric animals, it appears that the damage to tubulointerstitium defines the final proteinuria (Eddy, 1989, Eddy et al., 2000, Landgraf et al., 2014). Also, rats with (cy/+), a model for autosomal-dominant polycystic kidney disease develop proteinuria, which is due to the loss of endocytic machinery and tubular dysfunction (Obermuller et al., 2001a). In accordance with the diabetic patient, urinary excretion of albumin, retinol-binding protein, and N-acetyl-beta-D-glucosaminidase are all increased considerably in patients with early diabetic nephropathy, which arises from tubular abnormalities indicating the loss of endocytic reabsorption of these proteins (Gibb et al., 1989).

Additionally, the essential role of tubular dysfunction in developing proteinuria can also be exposed to genetic disorders. For example, the reduced tubular function in Fanconi syndrome is clearly revealed by numerous studies, and the most important is that this genetic disorder is always accompanied by proteinuria indicating the positive link between proteinuria and tubular dysfunction (Leheste et al., 1999, Norden et al., 2001). Reduced resorption of proteins from glomerular filtrate can also be acquired and caused by tubulointerstitial damage. In this case, tubular or interstitial injury prevents the PTs from reabsorbing LMW proteins leading to tubular proteinuria (Gorriz and Martinez-Castelao, 2012, Viswanathan and Rani, 2016).

1.4. Renal handling of protein

Numerous procedures and studies have revealed that, in normal humans, urine contains only a small amount of proteins. This is most probably because filtered proteins are reabsorbed efficiently by PT cells. Impairment in glomerulotubular balance may result in the loss of a large volume of necessary proteins and excretion into the urine. For instance, proteinuria results from glomerular injury and severe tubulointerstitial injury which may lead to adverse clinical outcomes.

1.4.1. Glomerular filtration of albumin

In normal conditions, in addition to small molecular weight proteins, macromolecules such as albumin (66kDa) and transferrin (81kDa) are filtered but in small amounts by glomeruli (Christensen et al., 2012a). The excretion of plasma albumin in the urine depends on a composite of glomerular filtration and tubular reabsorption (Castrop and Schiessl, 2017). Various techniques have been identified to measure the amount of albumin which is normally found in the glomerular filtrate. According to these techniques, including micropuncture of rats

and dogs, the concentration of albumin in the ultrafiltrate is between 1 and 50 µg/ml which equals 170 mg and 9 g/24hr in the healthy humans (Birn and Christensen, 2006). The fractional filtration of albumin estimated by micropuncture in rats is the concentration ratio between proximal tubular filtrate and blood and ranges between 0.0005 and 0.0007 (Lund et al., 2003, Tojo and Endou, 1992). The fractional filtration of albumin in human is about 0.0001 (Norden et al., 2001). Moreover, the minimum amount of albumin concentration in the glomerular filtrate is calculated to be 281 µg/min corresponding to about 400mg/24 hr whilst blocking tubular albumin uptake with lysine in humans (Mogensen and Solling, 1977). Likewise, inhibition of tubular albumin reabsorption by lysine in rats led to the excretion of approximately 2.5-25 mg/24hr which equates to 0.7-7 g/24hr in humans (Tencer et al., 1998, Thelle et al., 2006).

Micropuncture and inhibition of tubular albumin uptake are considered to be conventional techniques and largely depend on immunoassay for detecting albumin in the urine. A significant amount of albumin fragments is detected in the urine of rats and humans using radiolabelled albumin and high-performance liquid chromatography. These fragments are thought to result from degradation of filtered albumin by proximal tubular cells. Standard urinalysis by radioimmunoassay does not detect these fragments in the urine (Osicka et al., 1997, Russo et al., 2002, Comper et al., 2004, Gudehithlu et al., 2004). Thus, according to the findings of these studies; a significant amount of albumin is filtered and subsequently reabsorbed by PT cells.

1.4.2. Tubular reabsorption of proteins

Although the GFB is highly permselective, some proteins do enter the glomerular filtrate. However, the urine is almost free from protein, as a consequence of these

proteins being effectively reabsorbed by PT cells (Christensen et al., 2012a). Under physiological conditions, only a small amount of albumin, the most abundant protein in the circulation, can pass through GFB due to size and charge selectivity of the barrier towards proteins of intermediate and HMW; while the passage of LMW proteins (40,000 D and radius lower than 30 Å) is not restricted by the glomerular barrier and freely reaches proximal lumen (D'Amico and Bazzi, 2003). The majority of these proteins that enter the proximal lumen are reabsorbed by receptor-mediated endocytosis in the PT and absorbed proteins are completely hydrolyzed within lysosomes and the resulting amino acids cross the contraluminal membrane to return back to circulation and only traces are found in the urine (D'Amico and Bazzi, 2003).

11.4.2.1. Endocytosis process in proximal tubule

Endocytosis plays a fundamental role in the reabsorption of proteins in the PTs (Jefferson et al., 2008). Endocytic uptake of proteins consists of nonspecific fluid-phase endocytosis and receptor-mediated endocytosis (Jefferson et al., 2008). The apical endocytic apparatus is more complex in the S1 and S2 segments of the PT (Christensen et al., 2012b), and contains coated pits, coated vesicles, endosomes, lysosomes and dense apical tubules which facilitate membrane and receptor recycling from endosomes back to the apical plasma membrane (Christensen, 1982). Small plasma membrane invaginations are formed at the microvillar base, termed clathrin-coated pits, and contain some tubular fluid and its solute load of dissolved molecules (Gekle, 2005, Gekle, 1998). The endocytic invaginations separate from the plasma membrane to create endocytic vesicles that then deliver their contents to the sorting endosomal (SE) compartment from where it is transported to the early endosomal compartment and eventually the

lysosomal (LY) compartment via late endosomes (LE). Some endosomal material is transported back to the plasma membrane through recycling endosomes (RE) (Gekle, 2005).

1.4.2.1.1. Fluid-phase endocytosis

Fluid phase endocytosis is non-specific and plays an insignificant role in PT macromolecules retrieval (Park and Maack, 1984). Contents of this process are endocytosed at the same concentration as in the extracellular space, indicating that these contents are not enhanced at the plasma membrane and uptake increases consistently in relation to the extracellular concentration of the content (Gekle, 2005, Gekle, 1998).

1.4.2.1.2. Receptor-mediated endocytosis

Receptor-mediated endocytosis requires the specific binding of a ligand to a receptor in the apical plasma membrane of PT cells (Birn and Christensen, 2006). The receptor-ligand complex is internalized by invagination of the plasma membrane-initiated by adaptor molecule-mediated formation of a clathrin cytoplasmic coat (Goldstein et al., 1979, Robinson, 1994). In clathrin-coated mediated endocytosis, the adaptor molecules interact with the NPXY motif 17 regions in a number of endocytic receptors (Robinson, 1994) (Figure.1.5). Internalisation is followed by a detachment of the invaginations from the plasma membrane to form intracellular vesicles. Then, the cytoplasmic coat detaches, and vesicles may fuse to form new vesicles. Subsequently, acidification of the intravesicular lumen leads to detachment of the ligand from the receptor.

Furthermore, the ligand may be transported into lysosomes for storage or degradation, or otherwise into the cytosol for further processing/transport (Birn

and Christensen, 2006). Receptors may be either recycled back to the luminal membranes via a recycling dense apical tubules compartment or transported to lysosomes for degradation (Christensen, 1982) Tenten et al (2013) postulated that the presence of a transcytosis mechanism for filtered albumin and IgG across tubular cells in a neonatal Fc receptor-dependent manner (Tenten et al., 2013). For instance, genetic deletion of the neonatal Fc receptor, which rescues albumin and IgG from lysosomal degradation, abolished transcytosis of transgenic albumin and IgG in proximal tubular cells. This is evidence of a transcytosis process within the kidney tubular system that protects albumin and IgG from lysosomal degradation, permitting these proteins to be recycled intact (Tenten et al., 2013).

Albumin reabsorption in PTs occurs by the receptor-mediated endocytosis (Figure.1.5). The concentration of albumin at the plasma membrane might follow interactions with the negative surface charges of adjacent microvilli or from binding to specific sites (Gekle, 2005). Numerous studies on isolated PT segments and cells in vitro have identified albumin binding sites on PTs (Park and Maack, 1984, Gekle et al., 1996, Schwegler et al., 1991, Brunskill et al., 1997). Recognition of binding sites for albumin in opossum kidney (OK) cells provides important evidence that this protein is mostly reabsorbed by receptor-mediated endocytosis (Brunskill et al., 1997). The endocytic process of albumin is visible by electron microscopy where gold-labelled albumin is seen bound to the plasma membrane and in intracellular vesicles (Brunskill et al., 1996). Several essential receptors seem to be involved in receptor-mediated endocytosis and responsible for uptake of a range of filtered plasma proteins and variety of vitamins in complex with their binding proteins (Zhai et al., 2000, Christensen et al., 1998b). Most recent research has established that megalin, cubilin and amnionless are possibly the

most important receptors in the PT mediating endocytosis (Negri, 2006) (Figure.1.5).

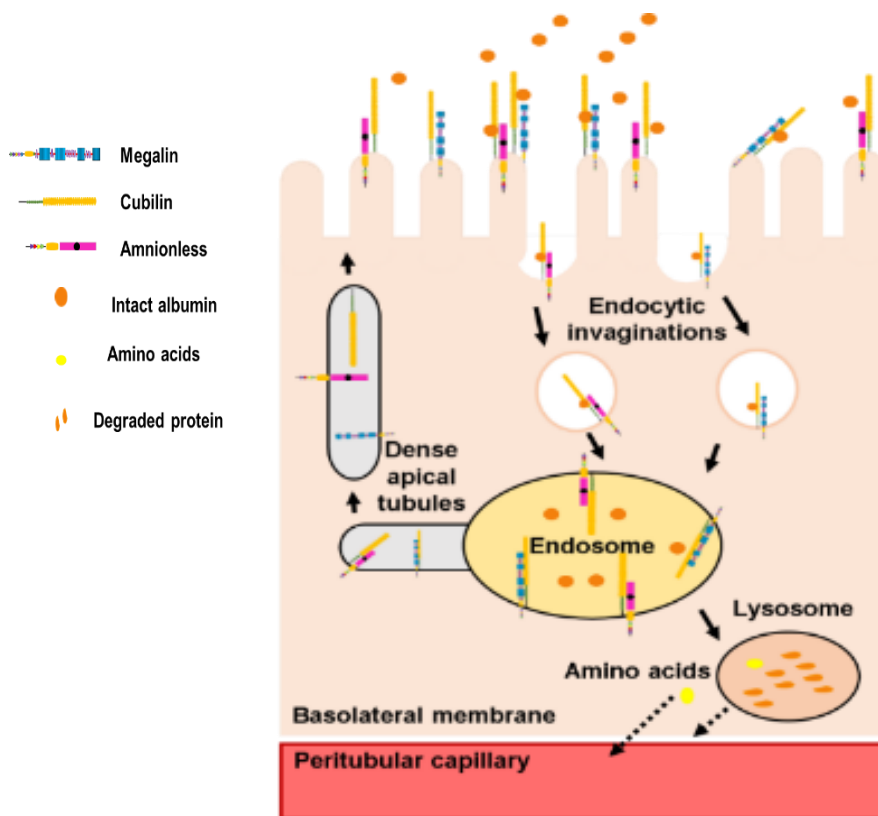


Figure.1.5. Schematic diagram showing the endocytosis processes.

Cubam complex and megalin mediated proximal tubular uptake of filtered protein, adapted from (Birn and Christensen, 2006, Christensen and Birn, 2013).

1.5. Cubilin-amnionless complex endocytic receptors

1.5.1. Cubilin

Cubilin was initially discovered as the target of teratogenic anti-gp280 antibodies and consequently revealed to be localised in clathrin-coated pits in renal PTs and yolk sac epithelial (Nielsen et al., 1998, Seetharam et al., 1997). It was also identified as the receptor for the intrinsic factor-vitamin B₁₂ (IF-B₁₂) complex in the intestine (Seetharam et al., 1981). Seetharam et al. 1988 revealed that an IF-B₁₂ binding protein isolated from renal brush borders was identical to the small intestinal IF-B₁₂ receptor (Seetharam et al., 1988) and later demonstrated IF-B₁₂ receptor and gp280 were similar to 460-kDa protein, RAP-binding protein facilitating endocytosis (Seetharam et al., 1997, Birn et al., 1997). The receptor was cloned from humans and rats and found to be a 460-kDa glycoprotein (Kozyraki et al., 1998, Moestrup et al., 1998). The cubilin gene is situated on chromosome 10p12,33-p13 in humans (Christensen and Birn, 2001).

1.5.1.1 Structure of cubilin

Cubilin is divided into three major regions, an amino-terminal region composed of 110 amino acids, a cluster of eight epidermal growth factor (EGF)-like domains and a cluster of 27 CUB [Complement c1r/C1s, Uegf (epidermal growth factor-related sea urchin protein) and Bone morphogenetic protein 1 (BMP)] domains found in the C-terminal part of the protein in that order (Moestrup et al., 1998, Kozyraki et al., 1998) (Figure.1.6). Cubilin lacks a transmembrane segment and has no cytoplasmic tail, thus represents a peripheral membrane receptor rather than an integral component of the plasma membrane. Therefore, for endocytosis, it interacts with other membrane proteins (Christensen et al., 2012a, Birn et al., 1997, Moestrup et al., 1998).

The 27 CUB domains most probably constitute numbers of the ligand-binding domains (Kristiansen et al., 1999). For instance, the binding site for intrinsic factor-cobalamin has been placed within CUB domains (5–8), whereas the binding site for RAP is placed within CUB domains (13–14), and CUB domain (12–17), (22–27) for megalin (Kristiansen et al., 1999, Moestrup et al., 1998, Amsellem et al., 2010).

The cluster of EGF repeat-like domains consists of 53 amino acids which are involved in interactions with many extracellular proteins such as, blood coagulation factors, complement activation components, development determination of cell fate, cell adhesion molecules, and connective tissue structural proteins (Appella et al., 1988). EGF repeats are widely expressed and contribute to a number of receptor-ligand interactions (Davis, 1990), which might also be the explanation for some of the binding properties of cubilin. Two of the EGF repeats in cubilin have a consensus sequence for calcium-binding (Rao et al., 1995, Selander-Sunnerhagen et al., 1992) and might be involved in the calcium-dependent binding of RAP or IF-B₁₂ (Birn et al., 1997). In addition, Ca²⁺ bound to EGF-like domains can stabilise protein structure (Rao et al., 1995).

The amino-terminal region of cubilin is about 110 amino acids regions in length. It has three remarkable features: a consensus sequence for cleavage by furin, a putative amphipathic α -helix motif, and a candidate site for palmitoylation (Verroust and Christensen, 2002). A stretch of amino acids of cubilin situated at 8 - 12 in rat and 8-11 in humans matches the consensus sequence Arg-X-Arg/Lys-Arg for cleavage by the trans-Golgi proteinase furin (Hosaka et al., 1991), which is involved in activation cleavage of other receptors and enzymes (Willnow et al., 1996, Bravo et al., 1994). Therefore, the post-translational processing of cubilin

might include furin-mediated cleavage in the trans-Golgi network (Christensen and Birn, 2001). Many studies indicated that furin-mediated cleavage is essential for the transformation of inactive precursor proteins into a bioactive form (Kozyraki et al., 1998). Cubilin has palmitoylation features that play an important role in the attachment of membrane proteins to the membrane and in the processing of certain proteins (Wedegaertner et al., 1993, Evanko et al., 2000). Cubilin may be functionally a monomer, but once shed from the membrane, the short hydrophobic region causes self-assembly into homodimer/ homotrimers (Kristiansen et al., 1999). Alternatively, the amphipathic α -helix motif might be involved in interactions with phospholipid of the plasma membrane contributing to the attachment of cubilin at the cell surface with other proteins (Bernstein et al., 2000, Mishra and Palgunachari, 1996).

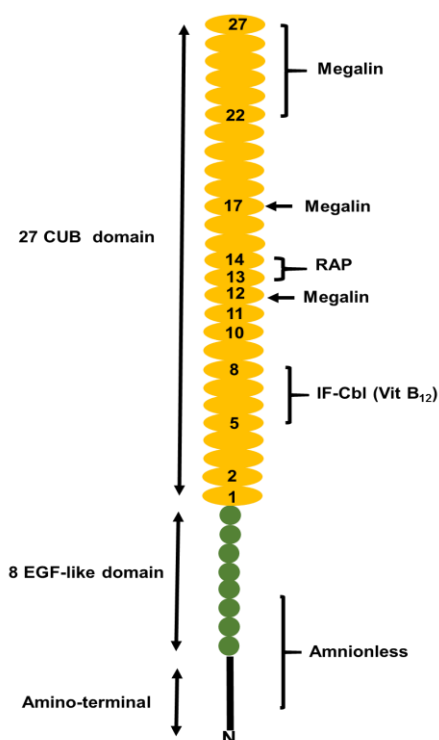


Figure.1.6. Schematic diagram of the cubilin structure.

Special binding sites for amnionless, megalin, vitamin B₁₂, receptor-associated proteins (RAP), adapted from (Moestrup et al., 1998, Kozyraki et al., 1998).

1.5.1.2. Expression and synthesis of cubilin

Cubilin is highly expressed in the proximal tubular cells of the kidney (Christensen et al., 1998a), small intestine epithelial cells (Xu and Fyfe, 2000) and visceral yolk sac (Drake et al., 2004). In the PT cells, the cubilin expression locates on the apical membrane, alongside other constituents of the coated pit endocytic and the membrane recycling pathway (Seetharam et al., 1997, Sahali et al., 1988, Christensen et al., 1998a, Christensen et al., 1998b). A small amount of cubilin is also recognised in the lysosomes (Christensen et al., 1998b). Cubilin is also expressed in the S-shaped body through renal development but later expression is restricted to the PT (Sahali et al., 1993). The post-translational processing of cubilin is involved through furin-mediated cleavage in the trans-Golgi network. For example, affinity-purified human cubilin is truncated at a recognition cleavage site for furin in the amino-terminal region of cubilin (Kozyraki et al., 1998). After synthesis, cubilin travels to the plasma membrane via the Golgi apparatus where it undergoes final processing (Kozyraki et al., 1998). Cubilin is also highly glycosylated with N-linked carbohydrates, which may guide apical sorting in polarised cells (Scheiffele et al., 1995, Gut et al., 1998). The lack of glycosylation and a basolateral sorting signalled to the cubilin proteins accumulating in the Golgi complex of MDCK and CHO cells (Gut et al., 1998).

1.5.1.3. Regulation of expression of cubilin

A little is known about the regulation of cubilin expression. In vitro studies show that cubilin expression is stimulated by retinoic acid treatment (Hammad et al., 2000). Although retinoic acid signalling is mediated by retinoic acid receptor (RARs) and retinoid X receptors (RXRs) (Hurst and Else, 2012), it is still unidentified whether the cubilin promotor region has RAREs or RXREs, or whether

the influence of retinoic acid on cubilin expression is utilised through these receptors (Hurst and Else, 2012).

Transcriptional regulation of cubilin is associated with transcription and activation by peroxisome proliferator-activated receptors (PPARs). Both PPAR and cubilin are regulated by DNA methylation or histone deacetylation and inhibition of these mechanisms increases cubilin mRNA and protein levels in renal and intestinal cell lines (Aseem et al., 2013). Cubilin and megalin expression are decreased in mouse models of acute kidney injury (AKI) and streptozotocin-induced diabetes (Schreiber et al., 2012, Zhou et al., 2011). Interestingly, in albumin overload model, it was observed a reduction of megalin expression in the kidney improves with treatment by either PPAR α or PPAR γ agonists (Cabezas et al., 2011). This suggests that cubilin is co-expressed with megalin regulated by PPAR dependent mechanisms (Aseem et al., 2013).

1.5.1.4. Cubilin ligands

Cubilin is mediated through the uptake of proteins and protein-bound materials both in the intestine and in the kidneys (Christensen et al., 2013). In the intestine, intrinsic factor is synthesized by the gastric parietal cells and complexed to B₁₂ in the duodenum which is a functional ligand for cubilin (Christensen et al., 2013). Strong evidence shows that cubilin is the physiological receptor for intrinsic factor-vitamin B₁₂ complexes (Fyfe et al., 2004). Cubilin is crucial for normal reabsorption of albumin in the renal PT and mediates the uptake of numerous filtered proteins, lipids, vitamins and hormones resulting in an almost protein-free final urine (Amsellem et al., 2010, Birn et al., 2000, Zhai et al., 2000, Christensen et al., 2009, Christensen et al., 2012a).

Cubilin has other ligands such as vitamin carrier proteins, lipoproteins, immune- and stress-related proteins and drugs (Christensen et al., 2009). Most of the ligands have been identified through studies in patients with Imlerslund-Gräsbeck syndrome (Storm et al., 2011), urinary excretion studies in mouse (Amsellem et al., 2010, Weyer et al., 2011) and dog models (Birn et al., 2000, Nykjaer et al., 2001, Kozyraki et al., 2001). It has been shown that megalin/cubilin-mediated reabsorption of vitamin D binding protein is responsible for the renal conversion of 25(OH) D₃ to 1, 25(OH)₂ D₃ in the PT (Nykjaer et al., 2001). Similarly, iron is taken up by the cubilin-amnionless-megalyn-mediated reabsorption of transferrin and haemoglobin (Kozyraki et al., 2001, Gburek et al., 2002) and cubilin binds to apolipoproteins A-I, and High-density lipoprotein (Kozyraki et al., 1999).

1.5.1.5. Cubilin interaction with other endocytic receptors

Being entirely extracellular cubilin has no apparent sites for interaction with any adaptor proteins or other mediators of clathrin-coated endocytosis (Verroust et al., 2002) (Figure.1.7). Cubilin is binding to other endocytic receptors, which colocalise at the subcellular compartments of the kidney, the intestine and yolk sac (Birn et al., 1997). It seems that intracellular internalization and recycling of cubilin relies on interaction with its partners, megalin and amnionless (Moestrup et al., 1998, Christensen et al., 2012a). Megalin, a 600 kDa transmembrane protein, is a member of the low-density lipoprotein (LDL) receptor family and present in many epithelial cells, but it is most abundantly expressed in the renal PT (Negri, 2006). The cytoplasmic tail of megalin contains three NPXY motifs that mediate clustering in coated pits and also probably have intracellular signalling functions (Christensen and Birn, 2001). In vitro uptake of the cubilin ligands transferrin, Clara cell secretory protein, apolipoprotein A-I and high-density

lipoprotein are inhibited by anti-megalin antibodies and by megalin antisense oligonucleotides (Kozyraki et al., 2001, Burmeister et al., 2001, Kozyraki et al., 1999, Hammad et al., 2000). In addition, following cubilin mediated endocytosis transferrin is not completely processed in megalin knockout mice, which accumulate large amounts of transferrin in the PT cells (Kozyraki et al., 2001). Thus, megalin appears closely involved in the normal endocytic function of cubilin (Birn et al., 2000). Cubilin is co-localised with amnionless in the renal PT to form the cubam complex. Amnionless interacts with cubilin at the EGF-type repeats and this is essential for the translocation of the cubam complex from the endoplasmic reticulum (ER) to the plasma membrane and then for endocytosis (Fyfe et al., 2004). Mutation of the amnionless gene in animal models revealed a defect in the apical expression of cubilin (He et al., 2005, Strope et al., 2004). Essentially, cubilin is reliant on amnionless and megalin, which bind to cubilin and are involved in the endocytosis of this receptor (De et al., 2014).

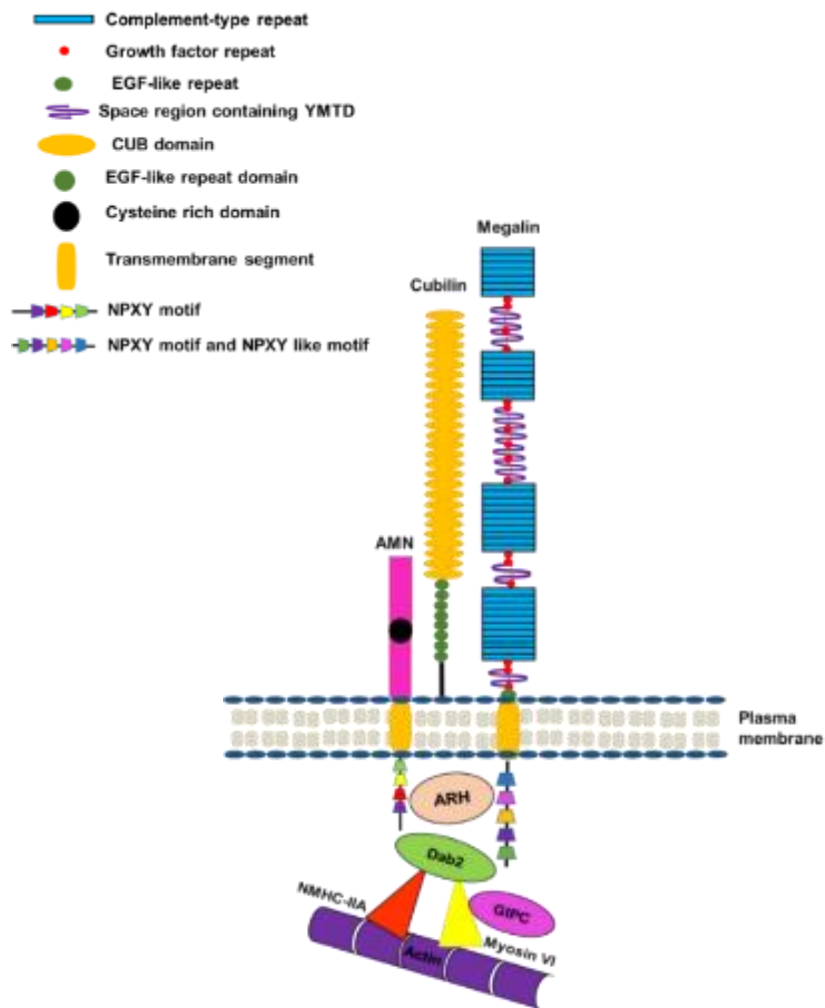


Figure.1.7. Schematic diagram illustrates cubam complex and megalin.

ARH and Dab2 are involved in the vesicle trafficking binding, to the NPXY motif present in both megalin and amnionless, but interacting with diverse adaptor proteins as ARH and Dab2 GIPC bind to actin filaments *via* Myosin VI (Birn and Christensen, 2006, De et al., 2014).

1.5.2. Amnionless

1.5.2.1. Structure of amnionless

Amnionless, a 38–50-kDa protein is important for amnion and primitive streak development in mice (Tanner et al., 2003, Tomihara-Newberger et al., 1998, Kalantry et al., 2001). It is a type I transmembrane protein with a cytoplasmic tail containing two NPXY motifs and a cysteine-rich stretch as the only identified specific feature of the extracellular domain (Fyfe et al., 2004, Tanner et al., 2003) (Figure.1.8). The amnionless protein has one transmembrane domain separating it into two parts: a large part, which is represented by the N-terminal extracellular region and the small part which is represented by the C-terminal cytoplasmic region (Tanner et al., 2003).

The extracellular region harbours a cysteine-rich domain and shares similarities with the cysteine-rich domains found in bone BMP-binding proteins and may play a role in the modulation of BMP signalling (Tanner et al., 2003). The 453 amino acid (aa) human amnionless precursor comprises a 19 aa signal sequence cleavage site, a 338 aa extracellular domain, a 21 aa transmembrane domain, and a 75 aa cytoplasmic domain. The extracellular domain also contains two potential N-glycosylation sites and a cysteine-rich vWFC domain (He et al., 2005). The alignment of amnionless amino acid sequences of human, dog, rat and mouse has been discovered to show two highly conserved copies of the sequence Phe-X-Asn-Pro-X-Phe in the cytoplasmic domain (Fyfe et al., 2004).

Amnionless has two putative internalisation signals of the FXNPXF sequence type within its cytoplasmic domain, which are a signal for internalisation of the receptor through clathrin-coated pits, and therefore, it might mediate endocytosis of compounds bound by cubilin (He et al., 2005, Boll et al., 2002). This kind of signal

closely resembles the FXNPXY signal found in receptors of the low-density lipoprotein (LDL) receptor superfamily (Chen et al., 1990). This sequence also founds in AP-2 adaptor protein-binding signal (Phe-X-Asn-Pro-X-Phe) for ligand-independent internalization via clathrin-coated pits (Tanner et al., 2003, Stolt and Bock, 2006).

FXNPXY signals mediate endocytosis through interaction with clathrin-associated sorting proteins (CLASPs) harbouring phosphotyrosine-binding (PTB) domains (Stolt and Bock, 2006). Also, the CLASPs, Disabled-2 (Dab2) and autosomal recessive hypercholesterolemia (ARH), have both been found to interact with FXNPXY signals that directly contact to AP-2, which was initially identified to mediate internalisation of the LDL receptor, megalin and low-density lipoprotein receptor-related protein (LRP) (Morris and Cooper, 2001, He et al., 2002). The novel mechanism of amnionless, via two seemingly functionally redundant FXNPXF signals, stimulates clathrin-dependent internalisation using the CLASPs pathway (ARH or Dab2) that leads amnionless to mediate uptake of cubam ligands (Pedersen et al., 2010).

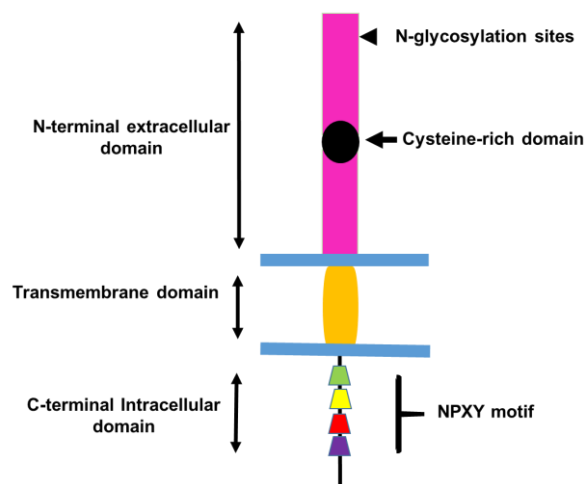


Figure.1.8. The schematic diagram shows the amnionless protein structure, adapted from (He et al., 2005, Fyfe et al., 2004).

1.5.2.2. Expression and distribution of amnionless

Amnionless is expressed exclusively in the extra-embryonic tissue, visceral endoderm (VE), during the early post-implantation stages, as well as, in kidney proximal tubules and small intestinal epithelium (Strope et al., 2004). During fetal development in the mouse, amnionless is expressed in mesonephric tubules at E11.5-12.5 and in the metanephric kidney beginning at E14.5. In addition, is expressed in the fetal intestine is detected at E16.5 (Strope et al., 2004). In the adult kidney, it is also identified in the outer cortex and the outer stripe of the outer medulla as well as the apical surface of proximal tubules and small intestine (Strope et al., 2004).

1.5.2.3. Function and regulation of amnionless

Amnionless localises in epithelial cells of the kidneys (Christensen et al., 1998a), small intestine (Xu and Fyfe, 2000) and visceral yolk sac (Drake et al., 2004). The amnionless with cubilin is a partner in a functional complex for endocytosis of IF-cobalamin and other ligands. In the ileum, the single function of the cubam complex is to facilitate uptake of dietary vitamin B₁₂ in complex with its transport protein, IF, while cubam complex in the PTs of the kidney is involved in reabsorption of numerous proteins from the glomerular ultrafiltrate such as albumin, transferrin, apolipoprotein A-I and vitamin D-binding protein (Birn et al., 2000, Pedersen et al., 2010). The cubam complex has a significant role during fetal development in rodents (Sahali et al., 1988, Strope et al., 2004), however, currently, its role in the human yolk sac is uncertain.

In polarized epithelial cells, amnionless has structures that facilitate membrane anchorage, biosynthetic processing, trafficking of cubilin to the plasma membrane, and then supports endocytosis of cubilin ligands and subsequent receptor

recycling (Fyfe et al., 2004). Cubam complex interactions take place early in the biosynthetic pathway of the rough endoplasmic reticulum (Fyfe et al., 2004). Therefore, amnionless interacts with cubilin at EGF-type repeats which is essential for the translocation of the cubam complex from the endoplasmic reticulum (ER) to the plasma membrane and then for progress in endocytosis (Fyfe et al., 2004).

Recent evidence demonstrates that amnionless is essential during biosynthesis and trafficking of cubilin. An in vitro study found cubam complex to be endocytically active consequent upon the intracellular endocytic FXNPXF motifs in the tail of amnionless (Fyfe et al., 2004, Pedersen et al., 2010). Other investigators have introduced a hypothesis that cubilin and amnionless to allow transfer out of the ER and subsequent expression as the cubam complex at the apical membrane (Coudroy et al., 2005). Another study in CHO cells shows co-expression of cubilin and amnionless is fundamental for the cubam complex to internalize IF-B₁₂ (Fyfe et al., 2004).

Accumulation of cubilin in the early biosynthetic compartment and loss of expression on the apical membrane has previously been detected in dogs with IF-cobalamin absorption deficiency (Fyfe et al., 1991b). In this dog, there is no defect in a cubilin gene, but cubilin cannot localise to the apical plasma membrane (Xu et al., 1999, Ramanujam et al., 1994). Amnionless mutations most likely affect cell surface expression of cubilin as posttranslational modifications and apical membrane expression of cubilin is extremely reliant on proper amnionless function and localization (Fyfe et al., 1991b, Strobe et al., 2004, He et al., 2005, Amsellem et al., 2010).

1.5.3. Cubam complex dysfunction in renal disorders

1.5.3.1. Imlerslund-Gräsbeck syndrome (IGS) in human

Familial selective vitamin B₁₂ (cobalamin, Cbl) malabsorption known as IGS (IGS, OMIM 261100) is a rare autosomal recessive syndrome, which is usually presented with failure to thrive, recurrent infections and fatigue along with megaloblastic anaemia in the early juvenile period (Christensen et al., 2013). IGS is categorised by selective malabsorption of Cbl from the distal small intestine and proteinuria, which results from deficient reabsorption of low molecular weight proteins in proximal tubules of the kidney (Namour et al., 2011). It can be effectively treated by supplementation with regular doses of cobalamin (Grasbeck, 2006).

IGS has also been described with mutations in either the cubilin or amnionless gene which are located on chromosomes 10 and 14, respectively (Tanner et al., 2004). These mutations have been recorded in patients from Finland and Norway, while an increasing number of mutations in both genes are being identified in eastern Mediterranean countries (Tanner et al., 2004).

It has been found that these different mutants lack the capability to mediate intestinal absorption of IF- B₁₂. For instance, a single amino acid substitution in CUB domain 8 leads to impairment in IF-B₁₂ binding. Another mutation is represented by gene deletion that leads to a truncation of the receptor in CUB domain 6, which is characterised by the absence of expression of functional cubilin (Aminoff et al., 1999, Hauck et al., 2008) as well as mutations in amnionless gene (He et al., 2005, Fyfe et al., 2004). The cubilin gene was found to be mutated in Finnish patients with the selective malabsorption of cobalamin and proteinuria (Aminoff et al., 1999), whereas the amnionless gene in Norwegian and Middle

Eastern patients also have selective B₁₂ malabsorption with proteinuria (Broch et al., 1984).

In patients with cubilin deficiency, proteinuria is as a result of defective tubular reabsorption of filtered proteins such as albumin (Storm et al., 2011). Truncation of the cubilin receptor might lead to an increase in urinary excretion of the cubilin ligand vitamin-D binding protein (VDBP) in the Finnish group of patients with IGS. However, no proteinuria was detected in patients with a single amino acid substitution within the IF-B₁₂ binding site (Nykjaer et al., 2001). Therefore, the varying proteinuria in these patients supports the hypothesis that different degrees of albuminuria depend on the type of mutation (Birn and Christensen, 2006).

Interestingly, a mutation in Finnish IGS patients with an amino acid substitution results in a diverse degree of proteinuria whereas, in gene deletion, proteinuria was always obvious (Wahlstedt-Froberg et al., 2003). Also, the urinary excretion of proteins of those patients was increased concomitant with excretion of cubilin ligands such as albumin, immunoglobulin light chains, and transferrin and α_1 - and β_2 -microglobulins (Wahlstedt-Froberg et al., 2003). As a consequence, proteinuria in Finnish IGS patients is due to a defect in tubular reabsorption of proteins due to a lack of cubilin function (Wahlstedt-Froberg et al., 2003).

In Norwegian patients with homozygous amnionless mutations affecting exons 1-4 of the amnionless gene-selective malabsorption of vitamin B₁₂ and proteinuria results, suggesting that the 5' end of amnionless is unnecessary for embryonic development but essential for the absorption of vitamin B₁₂ (Densupsoontorn et al., 2012). Interestingly, no consistent abnormalities in the kidney structure have been observed in biopsies from patients with IGS; although one patient presenting

with haematuria had focal mesangial expansion and IgA deposits, similar to IgA nephropathy (Storm et al., 2011). The tubular proteinuria in IGS does not accompany the progressive loss of kidney function (Grasbeck, 2006). Proteinuria identified in IGS patients is related to a defect in protein the endocytic pathway, normally mediated by the cubam complex in the PT (Nielsen and Christensen, 2010).

1.5.3.2. IGS in an animal model

IGS has been observed firstly in the giant Schnauzers family of dogs (Fyfe et al., 1991a). Locus heterogeneity in IGS was observed early through findings in a homologous animal model of IGS. Similar to the human disorder, canine IGS is a disorder categorised by failure to thrive, and selective intestinal vitamin B₁₂ malabsorption with proteinuria (Fyfe et al., 1991a). In amnionless, mutations show that cubilin is expressed in the tissues of IGS affected dogs, but the cubilin does not fold correctly and is not trafficked to the apical membrane (He et al., 2005). This suggested that the lack of amnionless expression leads to a defect in a cubam complex expression. Cubam complex endocytic receptors depend on each other for trafficking and membrane expression (Fyfe et al., 1991b, Fyfe et al., 1991a, Xu and Fyfe, 2000).

1.5.3.3. Albuminuria and chronic kidney disease (CKD)

Albuminuria is a biomarker of poor prognosis in patients with renal diseases (Levey et al., 2011). A defect cubam complex results in a reduction in protein reabsorption and subsequent proteinuria (Amsellem et al., 2010). Some studies have highlighted a relationship between cubilin dysfunction and the progression of kidney disease. In genome-wide association studies, missense single nucleotide polymorphism (SNP) in the cubilin gene is related to the degree of

albuminuria among normal European and African populations (Boger et al., 2011). In addition, cubilin SNPs are associated with microalbuminuria in patients with type 1 diabetes in the DCCT/EDIC study (Boger et al., 2011). This supports a role for cubilin in regulating urinary albumin excretion (Christensen et al., 2013).

Alteration in cubilin function has been described in animal models of CKD. In the remnant rat kidney study established that proteinuria and heavy lipid accumulation in the PT cells in ESRD animal are associated with strong staining for cubilin (Kim et al., 2009). As a sequence, it seems that tubular reabsorption of filtered protein-bound lipid occurs through the cubam complex and megalin by activation of several signal transduction pathways. These pathways stimulate apoptosis of tubular epithelial cells and the production of inflammatory and profibrotic mediators. Ultimately, the lipid accumulation in reduced renal mass might lead to proteinuria, glomerulosclerosis and tubulointerstitial injury (Kim et al., 2009). An increased loss of cubilin in type 1 diabetic patients could also contribute to albuminuria and the deficiency of essential hormones and vitamins (Thraill et al., 2009b). In a mouse model of cystic fibrosis, it was found that a defect in PT endocytosis causes an increase in urinary excretion of cubilin and proteinuria. This correlation was recognised also in patients with cystic fibrosis (Jouret et al., 2007).

1.6. Tubular toxicity of proteinuria

Abnormally filtered macromolecules (protein) has direct toxicity on the proximal tubular epithelial cells (Baines and Brunskill, 2011). Overloading of albumin exposure in the proximal tubular cells led to the production of a mixture of chemoattractants, profibrotic agents, matrix protein and vasoconstrictive agents by the proximal tubular epithelial cells (Baines and Brunskill, 2011) (Figure.1.9).

In the sections below the toxic effect of albumin on the proximal tubular epithelial cells in cell cultures and animal studies are shown.

1.6.1. In vitro studies

Albumin is the predominant protein in the glomerular filtrate and exerts a toxic effect on the proximal epithelial cells through activation of signalling pathways and transcription factors. For instance, NF- κ B is a transcription factor normally found in the cytoplasm of the cell as an inactive form and bound to inhibitory proteins (I κ B) (Takaya et al., 2003). Albumin has been found to activate this nuclear factor in the proximal tubular epithelial cells. Activation of NF- κ B leads to transcription of NF κ B-dependent pro-inflammatory genes such as monocyte chemoattractant protein-1 (MCP-1) and regulated upon activation, normal T cell expressed and secreted (RANTES). These chemoattractant molecules increase the recruitment of inflammatory cells to the interstitium, resulting in the release of potentially deleterious inflammatory cytokines and ultimate tubular injury (Reich et al., 2005).

In vitro studies have demonstrated that protein overload enhances the production of RANTES in the proximal tubular epithelial cells and a suggested role of this chemotactic and activating factor in the development of interstitial inflammation and kidney diseases (Zoja et al., 1998). Moreover, activation of NF- κ B and TNF- α gene expression are both associated with albumin overload in the proximal tubular epithelial cells (Wheeler et al., 2011), and their contribution to renal inflammation and fibrosis has been very well-documented in obstructive and diabetic nephropathy (Grande et al., 2010, Navarro-Gonzalez and Mora-Fernandez, 2008).

Albumin can also stimulate signal transducer and activator of transcription (STAT). It has been revealed that albumin can activate STAT in murine proximal tubular epithelial cells (Nakajima et al., 2004). Likewise, stimulation of STAT leads to upregulation of MCP-1 and RANTES which in turn results in inflammatory cell infiltration and consequent tubular damage (Rodriguez-Iturbe and Garcia Garcia, 2010). Nakajima et al. (2004) found that STAT activation depends on the generation of reactive oxygen species (ROS) by albumin in the proximal tubular epithelial cells. ROS may itself contribute to the progression of renal disease (Nakajima et al., 2004). The evidence is available that increased albumin endocytosis by proximal tubular epithelial cells leads to the activation of Rac1. Rac1 is a Rho-family small GTPase, which is responsible for activation of NADPH oxidase and ROS generation. A recent study has revealed that albumin overload increases the formation of ROS via activation of Rac1 and NADPH oxidase (Whaley-Connell et al., 2007).

Other studies have found that albumin overload in cultured proximal tubular epithelial cells activates p38 MAPK and ERK1 and 2 signalling pathways, which in turn increases the production of pro-inflammatory markers of kidney damage including IL-6 (Pearson et al., 2008). Consistent with the previous study, regulation of IL-6 synthesis is greatly dependent on both p38 and ERK/MAPK pathways in the proximal tubular epithelial cells and glomerular mesangial cells of the kidney nephron (Leonard et al., 1999). It is believed that IL-6 may contribute to renal fibrosis via modulating TGF- β signalling (Pearson et al., 2008). Albumin is also able to stimulate growth and proliferation of proximal tubular cells that is dependent on the ERK family of mitogen-activated protein kinase (MAPK). It has

been shown to be involved in the regulation of MCP-1 and cell proliferation in the PT cells (Takaya et al., 2003, Dixon and Brunskill, 2000).

It has been demonstrated that incubation of human proximal tubular epithelial cells with human serum albumin significantly increases the expression of proinflammatory markers (IL-6, IL-8, TNF- α , CCL-2, CCL-5) as well as α -SMA, and collagen IV, indicating the toxic effect of this plasma protein which may result in inflammation and fibrosis (Wu et al., 2014). Likewise, albumin is able to induce the production of IL-8, a potent chemokine that plays a major role in attracting inflammatory cells especially neutrophils to the site of inflammation and also promotes angiogenesis in the proximal tubular epithelial cells, in human PT cell dose-dependently, which occurs via NF- κ B dependent pathways through PKC activation and ROS generation (Tang et al., 2001). These proinflammatory markers are involved in the pathophysiology of CKD (Kayama et al., 1997). TNF- α has long been recognised as a proinflammatory cytokine to play an important role in tissue damage and the progression of CKD (Vielhauer and Mayadas, 2007).

There is evidence that albumin plays a critical role in the activation and expression of transforming growth factor in the proximal tubular epithelial cells. For example, Diwakar et al. (2007) have demonstrated that incubation of proximal tubular epithelial cells (opossum kidney cells and human kidney cell clone-8 cells) with albumin results in overproduction of TGF- β 1. This study also observed the role of albumin endocytosis and its interaction with megalin in the secretion of TGF- β 1 and found that there is no correlation between megalin and the amount of TGF- β 1 produced by a proximal tubular epithelial cell (Diwakar et al., 2007). Altogether, these studies have provided strong evidence that albumin overload, the most

widely used protein in tissue culture studies and most abundant protein in the glomerular filtrate, is toxic to the proximal tubular epithelial cells and may lead to inflammation and fibrosis, the main causes of CKD.

1.6.2. In vivo studies

Animal models of protein overload proteinuria, a model of tubulointerstitial injury in experimental animals, have clearly revealed the toxic effects of glomerular ultrafiltered proteins on the proximal tubular epithelial cells which may lead to tubulointerstitial inflammation and fibrosis and eventually chronic damage (Eddy et al., 2000). In addition, there are other models of proteinuria that show the influence of filtered proteins due to glomerular permeability on the proximal tubular epithelial cells. In rats treated with increasing doses of bovine serum albumin (BSA) for two weeks, tubulointerstitial changes have been recognised (Eddy, 1989). At one week, macrophage infiltration into the interstitium was clearly detected, consequently followed by T helper and T cytotoxic cells. The PT presented increased expression of vimentin and increased deposition of complement component C3 and neoantigens. The severity of tubular damage was closely associated with proteinuria in these animals (Eddy, 1989). Likewise, Landgraf et al. (2014) have found that protein overload proteinuria produces substantial alterations in the kidney interstitium related to the increased levels of proinflammatory cytokines, TNF- α and IL-6. Tubulointerstitial fibrosis was identified as evaluated by marked collagen deposition (Landgraf et al., 2014).

Tubular injury has been reported in protein overload proteinuria rats. In these animals reduced tubulointerstitial damage induced by proteinuria was found to be associated with inactivation of NF- κ B, which in turn leads to suppression of MCP-1, TGF- β and fibronectin in tubulointerstitial injury lesions (Takase et al., 2003).

It is well-known that protein overload in mice results in proteinuria, interstitial inflammation and the development of interstitial fibrosis. Increased protein in the tubular lumen changes the mRNA levels of matrix genes procollagens $\alpha 1$ (I), $\alpha 1$ (III), and $\alpha 2$ (IV) and TGF- $\beta 1$ and Timp-1 (Eddy et al., 2000). According to protein overload proteinuria in rats leads to activation of tubular NF- κ B with interstitial inflammation and upregulation of MCP-1 and osteopontin (Eddy and Giachelli, 1995). Another study revealed that mice overloaded with protein display tubular injury and increased macrophage infiltration into the interstitium, evaluated by F4/80 immunostaining and that was associated with increased mRNA expression of MCP-1 and TNF- α (Yang et al., 2011).

In animal models of progressive proteinuric nephropathies (5/6 nephrectomy and passive Heymann nephritis), It has been shown that increased urinary excretion of protein over time is associated with a significant increase in NF- κ B activity, which is being localised to the PTs (Donadelli et al., 2000). Activation of NF- κ B was paralleled by renal up-regulation of MCP-1 gene expression and consequent accumulation of ED-1-positive monocytes/macrophages and CD8-positive T cells in the interstitium, suggesting that the initial recruitment of mononuclear cells may occur at least in part by on MCP-1 dependent mechanism in these models (Donadelli et al., 2000).

The relationship between proteinuria and tubulointerstitial nephritis has long been identified in the puromycin aminonucleoside (PAN) nephrosis model (Tang et al., 1997). In this model, administration of PAN led to a significant increase in MCP-1 and interferon-inducible protein-10 (IP-10) mRNA expression after 6-8 days and gradually declined on reaching day 21. The MCP-1 and IP-10 mRNA expression were mainly localised to the intrinsic tubulointerstitial cells and not to infiltrating

monocytes or macrophages. The most interesting fact here is that using neutralising Ab to rat MCP-1 considerably reduced interstitial accumulation of macrophages and T lymphocytes, supporting the idea that inflammatory responses in the interstitium are greatly dependent on the MCP-1 mechanism (Tang et al., 1997).

The central role of TGF- β in the development of renal fibrosis has long been recognised. TGF- β may contribute to renal scarring through activation of its downstream Smad signalling pathways (Lan, 2011). TGF- β can also lead to renal fibrosis through the induction of tubular cell epithelial-mesenchymal transition (EMT) (Zhao et al., 2013). In experimental animals, protein overload proteinuria has been shown to upregulate the cortical mRNA and protein levels of TGF- β , which in turn leads to interstitial fibrosis and progressive renal injury (Eddy and Giachelli, 1995). Eddy (2001) believed that the initial inflammatory cells recruited in response to interstitial injury produced as a result of protein overload may participate in interstitial fibrosis (Eddy, 2001). Infiltration of monocytes, the main source of TGF- β , into the interstitium in protein overload proteinuria which might be explained by the recruitment mechanism of osteopontin, ICAM-I and VCAM-I expression, indicating the role of inflammatory cell infiltrate in the tubulointerstitial fibrosis (Eddy and Giachelli, 1995).

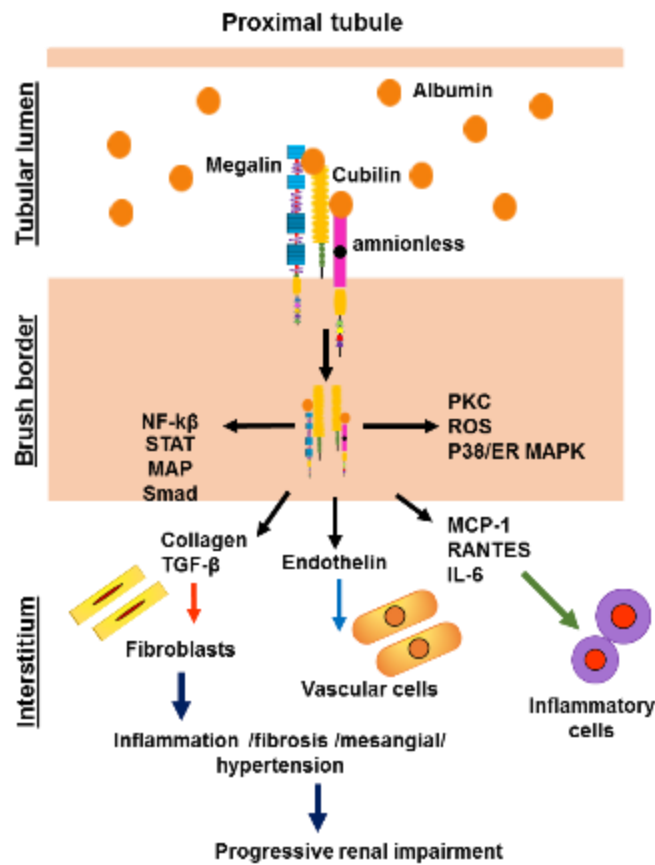


Figure.1.9. Schematic diagram illustrates protein overload-induced progressive renal impairment.

extracellular signal-regulated-kinase (ERK), nuclear factor- κ B (NF- κ B), protein kinase C (PKC), monocyte chemotactic protein-1(MCP-1), regulated on activation normal T-cell expressed and secreted (RANTES), reactive oxygen species (ROS), tumor growth factor- β (TGF- β), P38 mitogen-activated protein kinases (P38/MAPK), signal transducer and activator of transcription (STAT), adapted from (Roscioni et al., 2014).

1.7. Importance of proteinuria in CKD

1.7.1. The prevalence and progression of CKD

CKD has increased worldwide, indicating that it is a significant public health concern that affects up to 10% of the adult population (El Nahas, 2005, Levey et al., 2007). The incidence and prevalence of end-stage renal diseases (ESRD) have doubled in the last decade and are expected to continue to rise steadily in the future. In 2001, the annual average cost of therapy for ESRD was \$70 - \$75 billion internationally. This excludes kidney transplantation (Szczzech and Lazar, 2004). The number of ESRD patients is expected to reach over 2 million by 2030, which may create future budgetary problems (Szczzech and Lazar, 2004).

Early intervention of CKD would be essential to reduce the economic burden of renal replacement therapy. To achieve this, it is important to know which individuals may progress to renal disease. Identification of risk factors for CKD is essential such as black ethnicity, older age, low birth weight and a family history of kidney disease. In addition, factors such as smoking, obesity, hypertension, proteinuria, anaemia, dyslipidaemia and diabetes mellitus can lead to kidney disease (Kazancioglu, 2013). Numerous studies in general populations have observed that low eGFR and elevated albuminuria are accompanied by cardiovascular disease (Chronic Kidney Disease Prognosis et al., 2010, Gansevoort et al., 2013). Also, the cardiovascular mortality in a high-risk population is about twofold higher in patients with stage 3 CKD and three times higher at stage 4 CKD compared to individuals with normal kidney function (van der Velde et al., 2011). High albuminuria and reduced eGFR are both independent risk factors for cardiovascular and renal effects in patients with type 2 diabetes (Ninomiya et al., 2009).

1.7.2. Correlation between proteinuria and renal failure

A strong association between the degree of proteinuria and progression of renal failure has been identified (Eddy, 2004). Proteinuria can be either glomerular or tubular in origin (Gorriz and Martinez-Castelao, 2012). Bioactive macromolecules which are present in the glomerular filtrate interact with PT cells, leading to progressive of proteinuric nephropathy (Brunskill, 2004). The toxic effect of these molecules has clearly defined such as activation of tubular-dependent pathways of interstitial fibrosis and inflammation, together with alterations in PT cell growth, apoptosis and gene transcription (Baines and Brunskill, 2011, Birn and Christensen, 2006). Evidence from animals and human studies have demonstrated that proteinuria is closely associated with loss of renal function.

1.7.2.1. Correlation in animal studies

1.7.2.1.1. Remnant kidney

In experimental animals, reduction in kidney mass leads to heavy proteinuria and progressive renal impairment. For example, the remnant kidney is exposed to a high amount of filtered proteins in the residual part of the nephrons and an increase of GFR eventually led to the development of proteinuria (El Nahas, 1989a). However, reduction in proteinuria appears more beneficial in these animals. In the remnant kidney model, rats on the low-protein diet showed less proteinuria and significantly reduced the development of progressive renal impairment (El-Nahas et al., 1983). Another study revealed that rats exposed to a low dietary protein have a beneficial effect on maintaining the renal function in the remaining renal mass (Williams et al., 1987). Similarly, rats with a remaining kidney and treated with angiotensin-converting enzyme (ACE) inhibitors showed

reduced proteinuria and development of renal injury via reducing intraglomerular capillary pressure (Anderson et al., 1985).

Furthermore, in the remnant kidney model, reduction in renal mass of rats may result in glomerulosclerosis (Shimamura and Morrison, 1975). In these animals, the remaining glomeruli undergo various morphological and functional changes, which result in increases in single nephron glomerular filtration (GFR) and then an increase in the intraglomerular pressure, consequently, glomerular injury and ultimate sclerosis may develop (Hostetter et al., 1981). Therefore, a strong association between glomerulosclerosis and proteinuria has been detected in these animals (Williams and Coles, 1994). There is direct evidence from animals and human studies that tubulointerstitial injury is more probable to be triggered by poor control of systemic blood pressure which consequences from proteinuria in the remnant kidney (Novick et al., 1991, Bidani et al., 1990). In contrast, the better control of systemic blood pressure results in the lower the rate of decline of GFR in the diseased kidney (Remuzzi et al., 1990). Overall, the amount of proteinuria, the degree of structural renal damage and the severity of renal impairment all are closely associated.

1.7.2.1.2. Puromycin aminonucleoside nephrosis model

In the puromycin aminonucleoside (PAN) nephrosis model, a single dose administration of PAN (15mg/100g) to rats may produce direct toxicity to the glomerular epithelial cells and the development of nephritic range proteinuria (Eddy et al., 1991). In these animals, a significant change in the glomerular structure is observed. A detachment of podocyte FP from the GBM is the most prominent effect of PAN (Whiteside et al., 1993). According to the previous studies, there is a positive association between proteinuria and separation of

podocyte from the GBM (Whiteside et al., 1993, Messina et al., 1987). It is clear that the extent of pro-inflammatory infiltrates and tubulointerstitial injury are closely associated with the degree of proteinuria (Jones et al., 1992). Likewise, a relationship between an increased influx of pro-inflammatory cells such as macrophages and T-lymphocytes into interstitium and proteinuria has been described in PAN nephrosis (Eddy et al., 1991). Another probable mechanism of podocyte detachment contributing to renal impairment is that separation of this FP may change the permeability of the glomerular barrier; as a result, an enormous amount of circulating macromolecules accumulates in the glomerulus and glomerulosclerosis develops, this association was clearly detected in the remnant kidney model of rats (El Nahas, 1989b).

Additionally, according to PAN nephrosis model, a single intraperitoneal injection of the PAN to rats produces a cellular alteration in the interstitium. Following these alterations, massive proteinuria develops after 14 days of treatment in association with the mononuclear cells infiltrating into the tubulointerstitial area (Eddy and Michael, 1988). Thus, the number of interstitial cells is prominently correlated to the degree of proteinuria. Moreover, the same model displayed a substantial decline in GFR related to extent of interstitial damage (Eddy and Michael, 1988). Furthermore, in the PAN model, animals treated with a low-protein diet and enalapril show significantly reduced proteinuria and a reduced number of interstitial macrophages (Eddy et al., 1991). Similarly, chronic PAN-induced nephrosis, rats on dietary-protein restriction showed less proteinuria and reduced tubulointerstitial injury (Marinides et al., 1990).

1.7.2.1.3. Protein overload model

In the protein overload proteinuria model, intraperitoneal injection of bovine serum albumin (BSA) (1g / day) to rats may result in heavy proteinuria. There is no evidence that glomerular and /or interstitial damage is whether due to immune complex deposition or increased circulating anti-BSA antibodies in the glomeruli or the interstitium. As proteinuria increases, there is an influx of chronic inflammatory cells such as macrophages and T lymphocytes into the interstitium and an accumulation of the extracellular of matrix (ECM) protein (Eddy, 1989, Eddy and Giachelli, 1995). Eddy et al (1995) suggested that proteinuria is the only causative agent in this model, leading to recruitment of macrophages and T lymphocytes, with increased matrix protein synthesis and altered matrix degradation and remodelling contributing to the interstitial fibrogenic development (Eddy and Giachelli, 1995). Additionally, there is a significant increase in a renal message for chemotactic MCP-1 and osteopontin in association with the progress of interstitial inflammation (Eddy and Giachelli, 1995).

Further study of protein-overload displays that injection of BSA to uninephrectomized rats leads to proteinuria and the development of acute tubulointerstitial nephritis. There is a significant increase in the number of macrophages and T lymphocytes in the interstitium in response to tubulointerstitial inflammation (Eddy et al., 1991). Tubular cell apoptosis also increases especially in the PT cells as a result of proteinuria (Thomas et al., 1999). In another experimental study, rats injected repeatedly with protein via intravenously develop heavy proteinuria related to the increased permeability of glomerular properties. Therefore, the toxic effects of filtered proteins directly appear on the PTs by

increasing the process of reabsorption and recruitment of macrophages and T lymphocytes into the interstitium (Zoja et al., 1998).

1.7.2.2. Correlation in human studies

In patients with diabetes, the hallmark of diabetic nephropathy is proteinuria. In these patients, proteinuria develops, particularly when the GBM loss its selective-permeability, which is very common in diabetic kidney disease, for a different amount of proteins (Ruggenti et al., 1998). Previous studies displayed that in diabetic patients, inhibition of ACE using different doses of ramipril decreases proteinuria through diminishing the size of large non-selective pores in the GFB (Morelli et al., 1990, Lewis et al., 1999). Furthermore, in experimental diabetes ACE inhibitors reduced intraglomerular capillary pressure and reduced the development of renal impairment (Zatz et al., 1986).

Similarly, patients with type 2 diabetic nephropathy are at greater risk of proteinuria. Therefore, in these patients, reduction in proteinuria especially albuminuria to the lowest level is a major goal and particularly this is closely related to reducing the risk of renal failure. For instance, losartan, which is antiproteinuric therapy can effectively decrease the higher risk of renal function loss in patients with type 2 diabetic nephropathy (de Zeeuw et al., 2004). Losartan has been identified as an ACE inhibitor and/or angiotensin II receptor blocker which, in turn, can slow the progression of chronic renal failure (Hou et al., 2007).

Likewise, in type-1 diabetic patients, the degree of diabetic glomerulosclerosis is correlated with proteinuria. It is known that reducing proteinuria positively delays the progression of diabetic glomerulosclerosis. This is because lowering proteinuria might decrease the overflow of plasma lipoproteins through injured

glomeruli (Hebert et al., 1994). Therefore, captopril has a renoprotective effect by decreasing proteinuria and lowering blood pressure. Recent studies have revealed that captopril can inhibit angiotensin II formation. It is well-known that angiotensin II stimulates the formation of growth factors and TGF- β and these factors may lead to collagen formation and glomerular hypertrophy (Gibbons et al., 1992, Johnson et al., 1992). Captopril can also decrease proteinuria by its direct or indirect effects on GFB (Sorbi et al., 1993).

A study of the Modification of Diet in Renal Disease (MDRD) in 840 non-diabetic patients showed that proteinuria is the strongest predictor of the progressive renal failure among other baseline factors including serum creatinine, blood glucose, blood pressure and cholesterol levels (Peterson et al., 1995). Additionally, De Zeeuw et al. (2004) found that baseline proteinuria can increase the risk of renal disease to the endpoint by 5.2-fold, and an 8.1-fold rise risk for progressing to ESRD (de Zeeuw et al., 2004). MDRD study showed that reducing protein intake and stricter blood pressure control did not significantly alter the rate of decline in GFR in patients with moderate or severe renal failure (Klahr et al., 1994). Overall, the degree of chronic renal insufficiency is closely associated with the degree of proteinuria.

1.8. Matrix metalloproteinases

Matrix metalloproteinases (MMPs) are a large family of zinc-dependent matrix degradation enzymes (Tan and Liu, 2012). MMPs are extracellular proteins, which include collagenases (MMP-1, MMP-8, and MMP-13), stromelysins (MMP-3, MMP-10, and MMP-11), gelatinases (MMP-2, MMP-9), matrilysins (MMP-7, MMP-26) and membrane-type MMPs (MT-MMPs) (Tan and Liu, 2012). The physiological function of MMPs is the modulation and regulation of ECM turnover.

These enzymes act by a direct proteolytic degradation of the ECM proteins via destroying the collagen meshwork of the ECM and basement membrane components such as collagen IV, fibronectin, laminin and gelatin (Woessner, 1991). MMPs are essential for tissue development and homeostasis but also in controlling several cell behaviours such as cell proliferation, migration, differentiation, angiogenesis, and apoptosis (Tan and Liu, 2012).

MMPs have a role in cleavage of a wide range of substrates, which consist of cell surface receptors, adhesion molecules to growth factors and cytokines (Tan and Liu, 2012): for example, the release of biologically active proteins as cytokines, growth factors and chemokines from their membrane-anchored proforms (so-called shedding). Consequently, these protein cleavage effects are modifying the signalling environment of the cell (Butler and Overall, 2009). Several MMPs and their inhibitors have unique expression profiles along the nephron regarding physiological and pathological conditions (Tan and Liu, 2012). For examples, upregulation of MMP-2, MMP -7, MMP -9, MMP -12, MMP -14 and TIMP-1 are identified in the glomerulus in renal pathological disorders. While expression of MMP-1 is reduced in kidney disorders, MMP-2, MMP -3, MMP -7, MMP -9, - MMP 14, and MMP 24 are recognised as upregulated in PCT in kidney dysfunctions (Tan and Liu, 2012).

1.8.1 MMP structure

The fundamental structure of the MMPs is similar and comprises four distinct domains, the propeptide domain, the catalytic domain, a linker peptide domain and a hemopexin (Hpx) domain (Nagase, 1997, Visse and Nagase, 2003, Arnold et al., 2011). The propeptide domain has about 80 amino acids and the PRCXXPD sequence in this domain is highly conserved. The cysteine “cysteine switch”

residue within this motif maintains the pro-form (inactive form) or latency of these enzymes by binding to the zinc atoms in the active site which prevents from cleavage (Nagase and Woessner, 1999). The cysteine-zinc coordination can be cleaved by limited proteolysis of the pro-peptide, treatment with chaotropic agents or organomercurials which in turn activates the enzyme (Van Wart and Birkedal-Hansen, 1990). There are also numerous potential furin recognition sites (RX(R/K)R) on the carboxy terminus of pro-peptide domain in various MMPs, which allow intracellular activation by furin-like pro-hormone convertases in the Golgi apparatus (Liu et al., 1997, Molloy et al., 1992, Nagase and Woessner, 1999).

The catalytic domain consists of 170 amino acids, with highly conserved zinc-binding motif HEXXHXXGXXH (Bode et al., 1993). The catalytic zinc in this motif is supported by three histidine residues which form a “Met-turn” (Cerdeira-Costa and Gomis-Ruth, 2014). The zinc-binding motif and the conserved methionine in the catalytic domain are found in all members of the metzincin (Gomis-Ruth, 2009). Moreover, catalytic zinc MMPs have non-catalytic zinc and calcium ions to protect the tertiary structure of the enzyme, and the calcium ions play an essential role in the expression of MMPs (Zhang et al., 1997, Lovejoy et al., 1994). The catalytic domain in all MMPs except MMP-7, -23 and -26, is connected to the Hpx domain by a proline-rich linker known as the hinge region (Peng et al., 2012).

1.8.2 MMP activation and expression

MMPs initially are produced and secreted in latent proenzyme form and then depending on the extracellular events they will be activated and changed to active-form (active MMPs) (Obermuller et al., 2001b, Loffek et al., 2011). When released, MMPs can be activated either by the already activated MMPs or other proteolytic

enzymes (Murphy et al., 1999, Sternlicht and Werb, 2001). MMP-2 and MMP-9, among the other MMP classes, are responsible for the cleavage of collagen types, particularly collagen IV, and laminin, the basic components of tubular basement membrane (Catania et al., 2007). MMP-9 is released by inflammatory cells, whereas MMP-2 is mostly secreted by fibroblasts and endothelial cells (Pittayapruek et al., 2016).

MMPs are expressed at low levels and are closely regulated via interactions between their activators and inhibitors during normal conditions (Tokito and Jougasaki, 2016). The expression of these peptidases is increased in response to high albumin doses in culture supernatants of podocytes (Fang et al., 2009). Likewise, in vitro albumin overload can encourage overexpression and activation of MMP-9 in the proximal epithelial cells via the activation of P44/42 MAPK pathway (Zhang et al., 2015).

Furthermore, the expression of MMP-9, the most expressed MMP with MMP-2 in the kidney, is increased modestly but not considered in the kidney of proteinuric mice compared to controls (Eddy et al., 2000). It has also been revealed that MMP-2, MMP-8 and MMP-9 levels are increased in the urine and serum of patients with diabetic nephropathy, indicating that these endopeptidase enzymes may be involved in the progression of diabetic nephropathy (Thraillkill et al., 2007, Thraillkill et al., 2009a, Gharagozlian et al., 2009, Lauhio et al., 2008, Tashiro et al., 2004, van der Zijl et al., 2010). Additionally, upregulation of MMPs particularly MMP-2 and MMP-9 has been demonstrated in animal models of focal segmental glomerulosclerosis (FSGS), lupus nephritis and Thy-1.1 nephritis, a model for membranoproliferative glomerulonephritis (Liu et al., 2006, Tveita et al., 2008, Mitani et al., 2004, Steinmann-Niggli et al., 1998). Regardless of the great

involvement of MMPs in degrading the ECM proteins in the kidney, these studies suggest that high levels of these endopeptidases may contribute to the development of various kidney diseases.

1.8.3. Mechanisms of MMP in kidney disease

Various mechanisms may explain the contribution of MMPs to kidney diseases. The previous study has demonstrated that MMP-2 and MMP-9, the most expressed MMPs in the kidney, are involved in the progression of renal fibrosis through the induction of tubular cell epithelial-mesenchymal transition (EMT) (Tan et al., 2010, Cheng and Lovett, 2003). Therefore, MMP-2 and MMP-9 are responsible for the EMT is the collagen and laminin component of the tubular basement membrane (Lenz et al., 2000). An additional possible mechanism of MMPs leading to kidney fibrosis is that products of collagen degradation have chemotactic properties for neutrophils and are also able to encourage MMP-9 production (Xu et al., 2011). Furthermore, it has been long documented that TGF- β and fibroblast growth factor (FGF)-2-binding proteins are components of ECM proteins and are released during ECM degradation, which in turn may regulate cell migration and induce EMT (Benezra et al., 1993, Falcone et al., 1993). (Benezra et al., 1993, Falcone et al., 1993). Recent studies have also revealed that MMP-9 is able to cleave osteopontin, potent macrophage infiltration and induce tubular cell EMT; which in turn activates TGF- β , a key inducer of renal fibrosis (Zheng et al., 2009, Tan et al., 2013).

Numerous other roles have been determined for MMPs in renal fibrosis such as destruction of the basement membrane, angiogenesis, cell migration, cell-cell adhesion and cell apoptosis (Gialeli et al., 2011, Morrison et al., 2009). In accordance with microvasculature, MMPs have a significant role in regulating

endothelial cell behaviour, vascular wall stiffness/elasticity (Tan and Liu, 2012). For examples, an increase of perivascular MMP-9 in acute ischemic injury plays a role in microvascular integrity (Lee et al., 2011). Similarly, dialysed CKD patients also demonstrated higher levels of MMP-2 /MMP-9 in extrarenal arteries associated with calcification and loss of elasticity (Chung et al., 2009a). Ultimately, continuous research is required to provide a further understanding of MMPs mechanisms in the pathogenesis of kidney disorders.

1.8.4. The beneficial effect of MMP inhibition in animal models

Overexpression or activation of MMPs has been revealed to be correlated with different kidney diseases. As well as, inhibition of the MMPs activity has been widely shown in human and animal's kidney diseases. For example, in animal models of acute kidney injury (AKI), it has been shown that the expression and activity of MMP-2, MMP-7 and MMP-9 are increased in kidney tissues exposed to ischemia-reperfusion injury; while inhibition of the activity of MMPs in AKI models ameliorates the progression of acute tubular injury and improves renal dysfunction at 24hr (Kunugi et al., 2011). Furthermore, in a rat model of autosomal-dominant polycystic kidney disease (cy/+) inhibition of MMP activity significantly reduced cyst numbers and kidney weight (Obermuller et al., 2001b). Additionally, in a mouse model of ischemic acute kidney injury (AKI) inhibition of MMPs activity significantly reduced reperfusion AKI (Kunugi et al., 2011). An inhibitor of MMPs led to a reduction in vascular permeability following ischemia-reperfusion injury (Sutton et al., 2005). Similarly, MMP inhibitors ameliorate vascular relaxation in dialysed CKD patients (Chung et al., 2009b).

The inhibition of MMP-2 and MMP-9 in a murine model of bleomycin-induced pulmonary fibrosis was effective in reducing pulmonary fibrosis in mice (Corbel et

al., 2001). Other studies have revealed the importance of MMPs inhibitor in decreasing the growth of tumours (Low et al., 1996, Prontera et al., 1999, Watson et al., 1996). Together, these findings suggest that MMPs inhibition might be an important target in the treatment of different diseases.

Previous studies showed that transmembrane receptors such as megalin undergo regulated intramembrane proteolysis (RIP). By this process, megalin is subject to metalloproteinase-mediated ectodomain shedding regulated by protein kinase-C and releases the megalin ectodomain into the tubular lumen (Zou et al., 2004, Biemesderfer, 2006). The importance of MMP inhibition in RIP has been reported in in-vitro studies (Hooper et al., 1997, Werb and Yan, 1998, Zou et al., 2004). Cubam complex, on the other hand, is not to be subject to RIP but the complex is physically close to megalin. This suggests that cubam complex may be affected by this mechanism. Based on this, in order to investigate whether the inhibition of MMPs activity may effectively reduce ectodomain shedding of both cubilin and aminonless in mice, we used a synthetic MMP inhibitor batimastat.

1.8.5. Synthetic inhibitor batimastat

Batimastat, also known as BB-94, is a potent broad-spectrum matrix metalloproteinase inhibitor (Rasmussen and McCann, 1997). Its mechanism depends on the inhibition of MMPs activity by the binding of a hydroxamate to the zinc ion in the active site of MMPs (Botos et al., 1996). Batimastat was first synthetic inhibitor used in clinical trials as an anticancer, anti-invasive and anti-metastatic drug inhibiting a broad spectrum of MMPs particularly MMP-2, MMP-9 and MMP-3 (Prontera et al., 1999, Yamamoto et al., 1998, Parsons et al., 1997, Zempo et al., 1996, Fingleton, 2007, Fingleton, 2008). It is believed that batimastat regulates MMPs at the transcriptional level by interfering with the signalling

pathways of MMP production. It has been demonstrated that batimastat can reduce the activation of ERK1/2, p38 MAPK and AP-1 pathways in skeletal muscle of mdx mice, which in turn reduces the production of MMP (Kumar et al., 2010). Inhibition of MMPs activity by batimastat has been widely used in various animal models of kidney diseases and in clinical trials to treat cancer and prevent the growth of a tumour in adult populations (Obermuller et al., 2001b, Ermolli et al., 2003, Lutz et al., 2005, Kunugi et al., 2011, Novak et al., 2010, Rasmussen and McCann, 1997). Additionally, very low toxicity has been reported in animals treated with batimastat (Wojtowicz-Praga et al., 1997, Wang et al., 1994).

1.9. Aims and objectives

CKD is a global public health problem. The number of patients affected by ESRD with a decline in renal function has increased internationally and predicted to reach over 2 million by 2030 which may produce more difficulties with the future budget. Proteinuria is one of the prognostic factors of deterioration in renal function in a patient with CKD. In proteinuria, proximal tubular cells are adversely affected by abnormal filtered proteins, leading ultimately to renal inflammation and scarring. This creates a pressing need for a better understanding of the molecular mechanisms of proteinuria. To do this, a mouse model of protein overload proteinuria was established and the effect of protein overload on the cubam complex expression was studied. After this, a mouse model of protein overload proteinuria and matrix metalloproteinase inhibitor (MMPI) was established to determine whether this inhibitor can preserve the apical expression of cubam complex and prevent proteinuria in proteinuric animals.

Expression of the cubam complex is not well studied in human proteinuric diseases. Therefore, human patients' kidney biopsies from different nephrotic diseases were investigated to assess change in cubam expression.

1.10. Hypothesis

In proteinuria changes in expression of PT endocytic receptors is a key feature in the pathophysiology of the disease. Altered expression of PT endocytic receptors may represent a maladaptive response to proteinuria mirrored by changes in expression elsewhere in the body. Manipulating this process may be therapeutic in proteinuric nephropathy.

The specific objectives of this project are

1. To study the pattern of cubam complex expression in normal wild-type mice
2. To study the effect of the proteinuria on the cubam complex expression and influence of MMPs on the cubam complex in the kidneys of proteinuric mice.
3. To investigate whether MMP inhibition could prevent proteinuria and influence on cubam complex expression in proteinuric mice.
4. To study the effect of MMP inhibition in reducing tubulointerstitial inflammation and fibrosis in the kidney of proteinuric mice.
5. To study the alteration of cubam complex expression in renal biopsies from patients with nephrotic syndrome.

Chapter Two

Materials and Methods

2.1. Materials

2.1.1. Chemicals reagents used in buffer solutions

All common chemicals were purchased from Sigma-Aldrich- (Dorset, UK) and Fisher Scientific- (Loughborough, UK) unless otherwise specified. Glycerol (Sigma-Aldrich, G6279), Glycine (Sigma-Aldrich, G8898), normal goat serum (Sigma-Aldrich, G9023), normal donkey serum (Sigma-Aldrich, D9663), normal swine serum (Vector Laboratories, S4000), potassium chloride (Sigma-Aldrich, P-9333), potassium phosphate, monobasic (Fisher scientific, 205920025), skim milk powder (Sigma-Aldrich, 70166), sodium dodecyl sulphate (SDS) (Sigma-Aldrich, L4390), sodium chloride (Fisher scientific, PB358-212), sodium citrate tribasic dihydrate (Sigma-Aldrich, S4641), Tris-base (Sigma-Aldrich -T1503), and Tween® 20 (Sigma-Aldrich, P1379).

2.1.2. Immunoblotting

All the materials were purchased from Bio-Rad Laboratories (Hemel Hempstead, UK), Sigma-Aldrich or Fisher Scientific unless otherwise specified. acrylamide 30% (Proto Gel) (National Diagnostics, EC-890), ammonium persulfate (Sigma-Aldrich, A3678), Amersham ECL western blotting detection reagent (Scientific Laboratory, RPN 2106), cellophane Membrane (Bio-Rad Laboratories, 1650963), Laemmli sample buffer 4x (Bio-Rad Laboratories, 1610747), 2-mercaptoethanol (Sigma- Aldrich, M3148-100ml), Quick Start bovine serum albumin standard (Bio-Rad Laboratories, 5000207), precision plus protein standards (Bio-Rad Laboratories, 1610373), polyvinylidene difluoride membrane (PVDF) (Fisher Scientific, IPVH00010), resolving gel buffer 1L 1.5 M Tris-HCl (Fisher Scientific, 12794165), SDS solution (20%) (National Diagnostics, EC-874), Tris 1.0

M buffer solution PH 6.8 (AVOCADO Research Chemicals, J63831.K2), tetramethyl-ethylene diamine TEMED (Sigma- Aldrich,T-8133) and lastly, X-ray film RX NIF sheets 130 mm x 180 mm (Fisher Scientific, 12705325).

2.1.3. Immunostaining

Materials were bought from Vector Laboratories (Peterborough, UK) and Sigma-Aldrich (Dorset, UK) and Fisher Scientific (Loughborough, UK) unless otherwise specified. animal-free blocker (Vector Laboratories, SP-5030), antibody diluent (Dako, S0809), account differentiating solution (Sigma-Aldrich, A3179-1L), DAPI (4', 6-Diamidino-2-Phenylindole, Dihydrochloride) (Life Technologies, D1306), DPX mountant (Sigma-Aldrich, 6522-100 ml), coverslip No.1 glass 22mm x 22mm (Fisher scientific ,12705325), eosin Y solution (Sigma-Aldrich, HT110132-1L), haematoxylin solution, gill no 2 (Sigma-Aldrich,GHS232-1L), horseradish peroxidase streptavidin (Vector Laboratories, SA-5704), H₂O₂ hydrogen peroxidase 30% (Sigma-Aldrich,H1009), prolong™ gold antifade mountant (Life Technologies , P10144), Scott water (Sigma-Aldrich, S5134) and xylene (Fisher scientific, X/0200/17).

2.1.4. Materials used in the gene study

The materials of gene study were bought from Applied Biosystem and Invitrogen except unless otherwise specified. Adhesive seals absolute qPCR (X50) (Fisher Scientific, 12144741), 10-20 µl graduated tip one filter tip (sterile) (STAR LAB, S1120-3810), 200 µl graduated tip one filter tip (sterile) (STAR LAB, S1120-8810), 1000 µl graduated tip one filter tip (sterile) (STAR LAB, S1120-1830), RNase-free microfuge tube (2.0ml) (Invitrogen, AM12425), RNase-free microfuge tube (1.5ml) (Invitrogen, AM12400), TaqMan universal master Mix II, with UNG (Applied

Biosystem, 4440038), TaqMan® gene expression assays (Applied Biosystem, 4331182) and Thermo-Fast 96 PCR plate (Fisher Scientific, AB0900P).

2.1.5. Commercial kits

The ready-made kits were purchased from Vector Laboratories (Peterborough, UK), BioAssay Systems, Universal Biologicals Ltd, (Cambridge, UK) and Bio-Rad Laboratories (Hemel Hempstead, UK) (see Appendix 1.2).

2.1.6. Polyacrylamide Gels

The 6% resolving gels were prepared from 7.9 ml H₂O, 30% Acrylamide (3 ml), 1.5M Tris-base pH 8.8 (3.8 ml), 20% SDS (0.15 µl), 10 % ammonium persulfate (0.15 µl) and TEMED (0.012 µl). While 5% stacking gel made as follows in order 2.1 ml H₂O, 30% Acrylamide (0.5 ml), 0.5M Tris-base pH 6.80 (38 ml), 20% SDS (0.03 µl), 10 % ammonium persulfate (0.0.3 µl) and TEMED (0.003 µl). A variety of pre-cast gels were obtained from Bio-Rad Laboratories and ThermoFisher Scientific (UK) (see Appendix 1.3).

2.1.7. Antibodies

The antibodies that were applied in the method sections are divided into three kinds according to the procedures.

2.1.7.1. Antibodies used in Western blot

The primary antibodies were purchased from Santa Cruz Biotechnology, Inc. (Heidelberg, Germany) such as, amnionless (K-14) goat polyclonal (cat no: sc-46727), cubilin (A-20) goat polyclonal (cat no: sc-20609), cubilin (T-16) goat polyclonal (cat no: sc-23644), aquaporin-1 (B-11) mouse monoclonal (cat no: sc-25287), interleukin-6 (10E5) mouse monoclonal (cat no: sc-57315), macrophage F4/80 (C-7) mouse monoclonal (cat no: sc-377009), MMP-3 (1B4) mouse monoclonal (cat no: sc-21732), MMP-7 (A-5) mouse monoclonal (cat no: sc-

515703), transforming growth factor- β (3C11) monoclonal (cat no: sc-130348) and tumour necrosis factor- α (52B83) monoclonal (cat no: sc-52746). Except for Beta-actin monoclonal (AC-15) (cat no: ab6276) was purchased from Abcam, UK. Also, CD26/DPP IV goat polyclonal (cat no: (AF954), MMP-2 goat polyclonal (cat no: AF909-SP), MMP-9 goat polyclonal (cat no: AF902-SP) were obtained from Novus Biologicals, USA. The secondary antibodies were purchased from Dako, UK as peroxidase-conjugated rabbit anti-goat immunoglobulin (cat no: P044901-2) and peroxidase-conjugated rabbit anti-mouse immunoglobulin (cat no: P0260).

2.1.7.2. Antibodies used in Immunohistochemistry

Primary antibodies were purchased from Santa Cruz Biotechnology, Inc. (Heidelberg, Germany) such as, amnionless (K-14) goat polyclonal (cat no: sc-46727), aquaporin-1 (B-11) mouse monoclonal (cat no: sc-25287), caspase-3 (H-277) rabbit polyclonal (cat no: (sc-7148), cubilin (A-20) goat polyclonal (cat no: sc-20609). Interleukin-6 (M-19) goat polyclonal (cat no: sc-1285), macrophage F4/80 (M-300) rabbit polyclonal (cat no: sc-25830), MMP-3 (1B4) mouse monoclonal (cat no: sc-21732), MMP-7 (A-5) mouse monoclonal (cat no: sc-515703), transforming growth factor- β (H-112) rabbit polyclonal (cat no: sc-7892), and tumour necrotic factor- α (M-18) goat polyclonal (cat no: sc-1348), Human cubilin sheep polyclonal (cat no: AF3700), CD26/DPP IV goat polyclonal (cat no: AF954), MMP-2 goat polyclonal (cat no: AF902-SP) and MMP-9 goat polyclonal (cat no: AF909-SP) were brought from Novus Biologicals and R&D Systems, USA. The secondary antibodies were purchased from Vector Laboratories, Peterborough, UK such as, biotinylated rabbit anti-goat polyclonal IG (cat no: BA-5000), biotinylated goat anti-mouse polyclonal IG (cat no: BA-9200), biotinylated rabbit anti-sheep polyclonal

IG (cat no: BA-6000) but biotinylated swine anti-rabbit polyclonal IG (cat no: E0431) purchased from Dako, UK.

2.1.7.3. Antibodies used in immunofluorescences

All immunofluorescences antibodies were obtained from ThermoFisher Scientific, UK as, goat anti-rabbit IgG (H+L) cross-adsorbed secondary antibody, Alexa Fluor 488 (cat no: A-11034), donkey anti-goat IgG (H+L) cross-adsorbed secondary antibody, Alexa Fluor 568 (cat no: A-11057) and donkey anti-goat IgG (H+L) cross-adsorbed secondary antibody, Alexa Fluor 488 (cat no: A-11055).

2.1.8. TaqMan Gene Expression Assays

All TaqMan gene expression assays were used in quantitative polymerase chain reaction were obtained from ThermoFisher Scientific, UK (see Appendix.1.4).

2.2. Experimental studies

2.2.1. In vivo studies in mice

All animal procedures were subject to institutional ethical review and approved under UK Home Office Project Licence PPL (PPL60/4438). Male Balb/c mice or female C57BL/6 mice, eight weeks old, weighing 26-30 g were purchased from Charles River Laboratories (Harlow, UK) and housed 5 per cage kept in an environment controlled at 22 ± 2 °C, with relative humidity 60 % and a 12 /12-hour light/ dark cycle. Mice were fed on standard diet pellets and water ad libitum during the whole studies.

2.2.1.1. Characterization of protein receptors expression in normal wild-type mice

Wild-type mice (C57BL/6, female, age 14 months) were sacrificed by cervical dislocation. The midline longitudinal incision was made in the anterior abdominal wall in order to harvest the kidney and small intestine. The small intestine was recognised between two fixed points, the end of stomach pylorus and the beginning of the large intestine and excised. Then, the small intestine was opened longitudinally from end to end and washed 4 times for 5 min with ice-cold PBS. The small intestinal tissue was cut into small thin pieces, collected in Eppendorf tubes and stored at -80 °C for further investigations. A further segment of small intestine was rolled up longitudinally with mucosa, around an orange stick and carefully placed in 10% formalin fixative prior to paraffin-embedding. The samples were dewaxed and sections prepared on slides by the histology facility department of the core biotechnology service, University of Leicester. In terms of renal tissue, both kidneys were harvested, the renal cortex of one was cut into small pieces, collected in Eppendorf tubes and stored at -80 °C for further investigations. The other kidney was placed in formalin fixative prior to paraffin-embedding. The samples were dewaxed and sections prepared on slides by the histology facility department of the core biotechnology service, University of Leicester.

2.2.1.2. Protein overload nephropathy

2.2.1.2.1. Unilateral nephrectomy surgery

Male Balb/c mice, eight weeks of age were allowed to acclimatise for 1 week and then subject to left unilateral nephrectomy, Meloxicam (Metacam) 5mg/kg analgesia was given for four doses at 24-hour pre- and post-operatively. Mice were anaesthetised with 2.5% isoflurane in 1.5L/min oxygen and local anaesthetic

bupivacaine (Marcain) was administered once during the operation. An incision was made in the left flank in order to expose to the left kidney. The blood vessels of the left kidney and the ureter were ligated using polyglactin suture (6/0) and the kidney was excised. Then, the wound was sutured using polyglactin suture (6/0) and mice allowed to recover for seven days before beginning the protein overload protocol.

2.2.2.1.2. Bovine serum albumin (BSA) to induce protein overload proteinuria

Overload proteinuria was induced as described (Fatah et al., 2017). Nephrectomised animals were divided into two groups, 5 mice in each. One group received intraperitoneal (IP) injections of low-endotoxin bovine serum albumin (BSA) (Thermo Fisher Scientific, cat no: 12891630) treatment for 15 days. BSA was prepared as a 40% solution in saline, the final concentration was determined. BSA dissolved in 1ml of saline was administered by intraperitoneal (IP) injection in increasing doses. On Day 1, a BSA dose was administered to animals beginning at 2mg/g body weight (BW), increasing subsequently by daily increments of 2mg/g BW to a maximum dose of 15mg/g BW on Day 6, which then continued at a fixed dose (15mg/g BW) until Day15. The second group of animals received only IP injections of the same volume of saline (1ml/animal) and served as non-proteinuric controls (Figure.2.1).

2.2.2.1.3. BSA to induce protein overload proteinuria plus MMPI treatment (Batimastat, BB-94)

Proteinuria was induced in nephrectomised mice as described above. In experiments, the matrix metalloproteinase inhibitor, Batimastat (BB-94) 30 mg/g

BW, was administered IP each day at the same time as the BSA injections. Control animals received only IP injections of the equivalent volume of saline (Figure.2.2).

2.2.2.1.4. Collection of samples

At the end of the study, each group of mice were placed in individual metabolic cages to collect 24 hr urine samples. The urine samples were collected in tubes containing protease inhibitors (P8340, Sigma-Aldrich, USA) to avoid protein degradation. Next, urine samples were centrifuged at 10,000xg for 5 min at 4⁰C to remove cellular materials, the pellets were also discarded, and the supernatants were collected and stored at -80 ⁰C for further analysis.

Blood samples were collected by direct cardiac puncture of anaesthetised mice. Briefly, a hypodermic needle (0.4X12mm) was inserted via diaphragm into the heart and 0.75ml of blood was withdrawn into a 2.5 ml sterile syringe. Then, blood samples were transferred to microcentrifuge tubes. The samples incubated on ice or at room temperature for 30 - 60 min to allow clotting. Then, blood samples were centrifuged at 10,000xg for 5 min at 4⁰C. Moreover, the separated serum was collected and transferred to new microcentrifuge tubes. The samples stored at -80⁰C for further investigations. Finally, animals were sacrificed by cervical dislocation, and various tissues were collected and processed for further investigation. For future protein and gene studies, tissue samples were stored at -80⁰C, whereas, other tissue samples were placed in formalin for future histological examination.

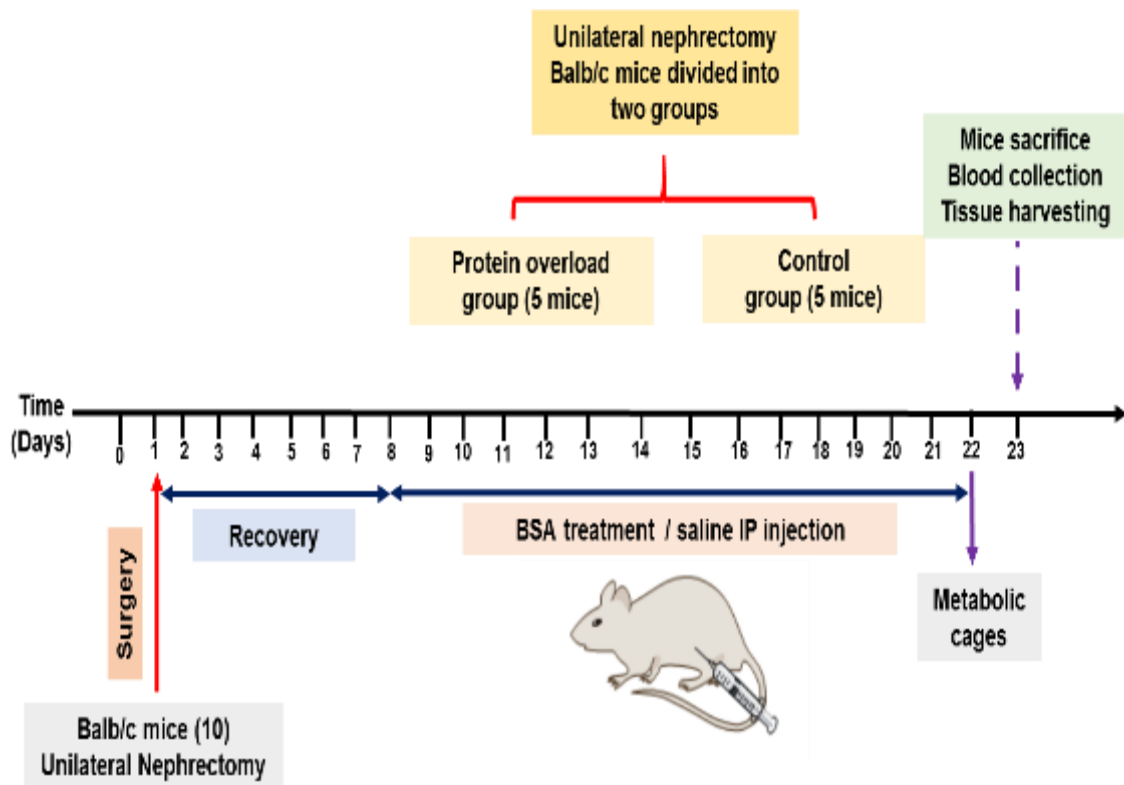


Figure.2.1. Schematic diagram illustrated the protein overload proteinuria experiment.

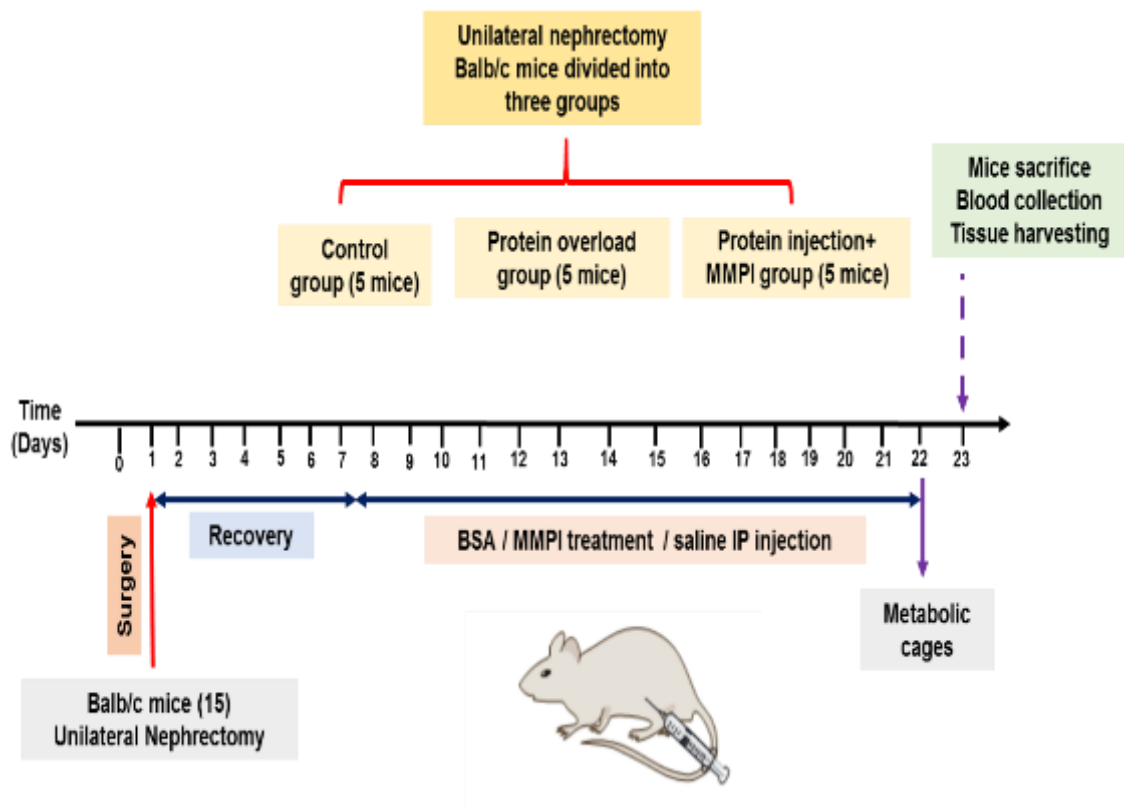


Figure.2.2. Schematic diagram illustrated the protein overload proteinuria plus MMPI treatment experiment.

2.2.1.3. Adriamycin-induced nephropathy

Male Balb/c mice were divided into groups. One group received an intravenous injection of a single dose of 10.5mg/kg adriamycin hydrochloride (Sigma, cat no: D1515), dissolved in 100 µl normal saline for 3 weeks. Control mice were injected with only normal saline. Three weeks after adriamycin and saline injection, mice were placed in individual metabolic cages to collect 24 hr urine samples. Samples of urine were then centrifuged at 10,000xg for 5 min at 4°C to remove cellular materials, the pellets were also discarded, and the supernatants were collected and stored at -80°C for further protein analysis. Thereafter, mice were sacrificed by cervical dislocation, and tissues were harvested and processed for further analysis.

2.2.2. Human renal biopsy samples

Renal biopsy samples obtained from patients presenting with nephrotic syndrome due to minimal change disease (MCD) (n=9), membranous nephropathy (MN) (n=10) and focal segmental glomerulosclerosis (FSGS) (n=9). All patients were aged 18 years or over, normotensive with a Modification of Diet in Renal Disease (MDRD) estimated glomerular filtration rate (eGFR) > 60mL/min/1.73 m² and a urine PCR 350mg/mmol creatinine. Patients were not diabetic, and none were receiving renin-angiotensin system modifying agents and had not received any immunosuppressive treatment in the 12 months prior to biopsy. The biopsy material used in this study was from their first diagnostic biopsy. All biopsies had been done in the 30 months preceding the study and had been stored for similar lengths of time under the same conditions in fully accredited NHS clinical laboratories. Normal tissue was obtained from the unaffected pole of nephrectomy specimens (n=11) well clear of the tumour margin from age-matched renal cell

carcinoma patients with normal eGFR. Use of patient biopsy material was approved by the North Leicestershire Research Ethics Committee.

2.2.3. Determination of biochemical markers

2.2.3.1. Determination of the total protein concentrations in serum and urine

Total protein concentrations in urine and serum were measured based on the Lowry method, using the Bio-Rad DC Protein Assay Kit (Bio-Rad Laboratories, UK). The samples were diluted with distilled water (1:20 for urine and 1:200 for serum). Then, 5 µl of standard (cat no: 500-0207, Bio-Rad Laboratories) and unknown samples were pipetted into a well of 96-well plate in duplicates. 25 µl of working reagents were prepared from 20 µl of Reagent S added to 1ml of Reagent A and also pipetted into 96 well plates in duplicate. Next, 200 µl of Reagent B was pipetted into wells and the plate incubated for 15 min at room temperature. Colour development was read using a plate reader at wavelength 595 nm (Infinite F50/Robotic Absorbance Microplate Readers from Tecan, Magellan™ for F50 data analysis software). The calculation was done by subtracting blank OD from all the standard OD reading and the optical density plotted against the concentration of each protein standard and a standard curve was created to determine the concentration of proteins in samples using Graph Pad Prism 7 (GraphPad Software, La Jolla, California, USA).

2.2.3.2. Measurement of creatinine in urine and serum

Creatinine concentrations in serum and urine samples of experiments were determined using the QuantiChrom™ Creatinine Assay Kit (BioAssay Systems, UK). The samples were diluted in distilled water (1:20 for urine and 1:200 for serum). For urine, 5 µl of urine samples and standards (50 mg/dl) were pipetted in duplicate into wells of 96-well plate. The working solution was prepared as 50

µl Reagent A, 50 µl Reagent B and 200 µl of water. Then, 200 µl of working solution was pipetted into each well. For serum, 30 µl of serum sample and standard (2 mg/dl) pipetted into a well of 96-well plate in duplicates. The working solution was prepared as 100 µl of Reagent A and 100 µl of Reagent B. Next, 200 µl of working solution was pipetted into each well. After that, the plate was tapped gently to mix and immediately read at 520 nm wavelength (OD₀) and after 5 min (OD₅). Protein concentrations were calculated from the following equation: sample concentration = [(OD₅ sample - OD₀ sample) / (OD₅ standard - OD₀ standard)] X standard concentration (mg/dl).

2.2.3.3. Quantification of albumin in urine and serum

Albumin concentrations in serum and urine were estimated using the QuantiChrom™ Albumin Assay Kit (BioAssay Systems, UK). The albumin standard was prepared in serial dilutions as 0, 0.5, 1.0, 1.5, 2.0, 3.0, 4.0, 5.0 g/dl. Next, 5 µl of diluted standard or urine or serum samples were pipetted into a well of 96-well plate in duplicates. After that, 200 µl of working solution was pipetted into each well with slight mixing and incubated for 5 min at room temperature. Subsequently, the optical density (OD) was read by using a plate reader at a wavelength of 570 nm. The calculation was done by subtracting blank OD (water) reading from the standard protein OD reading. The OD was plotted against standard albumin concentrations. Finally, the albumin concentrations in the sample were calculated from the standard curve via Graph Pad Prism 7 analysis software.

2.2.3.4. Measurement of serum vitamin B₁₂ levels

Vitamin B₁₂ level was measured in the serum samples from both proteinuric mice and their relevant control group by vitamin B₁₂ ELISA kit (Elabscience, UK). Serum

samples were thawed for 2 hours and centrifuged. 1ml of sample diluent was added to the 50 pg/ml stock standard protein to mix and centrifuged at 10,000xg for 1 min and allowed to stand for 10 min. The standard protein was diluted at 0.0, 0.78, 1.56, 3.125, 6.25, 12.5, 25, 50 pg/ml proteins. 50 µl of each concentration of standard was added into well of 96 wells plate in duplicate.

Serum samples from proteinuria overload proteinuria model were diluted. Duplicate 50 µl samples were then added into separate wells of 96 well plate. Then, 50 µl of a biotinylated detection antibody was immediately added to each well and incubated for 45 minutes at 37°C. The contents of the well were aspirated and washed by washing buffer 3 times. Next, 100 µL of HRP conjugate was added to each well and incubated for 30 min at 37°C. Then, HRP conjugate was aspirated and plates again washed by washing buffer 5 times. The reaction was visualized by adding 90 µl chromogenic substrate (TMB) and incubation at 37°C for 15 min in the dark. The reaction was stopped with 50 µl stop solution and immediately measured at an optical density (OD) 450 nm using an ELISA plate reader (Infinite 50 Microplate Readers, Magellan™ for F50 data analysis software). The OD reading of a water blank reading was subtracted from all OD of standards reading and from experimental samples as well. Vitamin B₁₂ concentrations were calculated by interpolating absorbance against a standard curve using Graph Pad Prism 7 analysis software.

2.2.4. Preparation of protein in samples

2.2.4.1. Preparation of lysate from tissues

Renal cortex and unfixed segments of the small intestine were homogenized in RIPA lysis buffer system (Santa Cruz Biotechnology, Germany). The 1ml of RIPA buffer was prepared by adding 10 µl of 200mM PMSF, 10 µl of 100mM sodium

orthovanadate, and 20 μ l of protease inhibitor cocktail solution. For kidney, 5 mg - 10 mg of tissue was added rapidly to Eppendorf tubes containing 600 μ l of ice-cold RIPA buffer. The samples were homogenized using an electric homogenizer (IKAT 18 digital Ultra-Turrax) for 5 min at 50Hz, whilst maintaining the temperature at 4⁰C. For small intestine, 15 mg of tissue pieces were placed into 750 μ l of ice-cold RIPA buffer and homogenized by an electric homogenizer for 15 min at 50Hz whilst maintaining the temperature at 4⁰C. Samples were then kept on a shaker with constant agitation for 2 hr at 4⁰C. Then, lysates were transferred to microcentrifuge tubes and centrifuged (Heraeus Fresco 17, Thermo Fisher Scientific) at 10,000xg for 30 min at 4⁰C. Finally, the supernatants were collected and stored at -20⁰C for further proteins analysis.

2.2.4.2. Determination of the protein concentration in tissue homogenates

The protein concentrations in tissue homogenates were determined by the Bio-Rad DC protein assay kit (Bio-Rad Laboratories, UK). 5 μ l of standards or tissue homogenates were pipetted in duplicate into wells of 96-well standard plate. 25 μ l of reagent solution was then added into the wells of 96-well plate. Then, 200 μ l of reagents B pipetted into wells. The plate was incubated for 15 min at room temperature. The OD was measured at 590 nm using a plate reader and the measurements were plotted against standard concentrations to make a standard curve. The standard curve was used to determine protein concentration in tissue homogenates.

2.2.4.3. Preparation of urine samples

The urine samples were thawed, centrifuged at 17000 g for 15 min at 4⁰C and the resulting supernatants were further centrifuged at 200,000g for 1 hour at 4⁰C to remove all particulate material. The supernatants were then stored at -20⁰C. Urine

samples were dialysed against 3 L of PBS buffer pH 7.4 at 4⁰C. Briefly. Slide-A-Lyzer™ Dialysis Cassettes (ThermoFisher, cat no: 66005) were hydrated for 30 min in PBS buffer pH 7.4. A syringe needle was inserted into the gasket via one of the corner ports and 100 µl urine samples were injected, excess air was withdrawn and then the needle was removed. The dialysis cassettes were attached to a floating buoy and placed in the PBS buffer pH 7.4. The urine samples were dialysed for 4 hr at 4⁰C, with vigorous stirring, against 3 L of PBS buffer pH 7.4 with one change after 1hr. Samples were then withdrawn from cassettes and stored at -80 °C for further analysis.

Proteins in urine samples were separated by using ProteoSpin Urine protein concentration Micro Kit (Norgen. Biotek, cat no: 17400) according to manufacturers instructions. To concentrate proteins in the samples, 40 µl of binding buffer A was added to 150 µl urine sample in column tubes and the pH adjusted to pH 3.5 – 4. The spin columns were placed on collection tubes and 500 µl of wash solution C was added to activate the spin column, followed by centrifugation for 2 min at 3,300g. Then, 150 µl of the pH-adjusted urine samples were added to the spin column tubes and centrifuged again for 5 min to bind the protein to the membrane. The flow-through was then discarded and the spin column placed on new collection tube. Subsequently, 500 µl of wash solution C was added to the spin column and centrifuged for 3 min. For protein elution and neutralization, 9.3 µl of protein neutraliser was added into a 1.7 ml elution tube and a spin column was then placed into the elution tube. Then, 100 µl of elution buffer C was added to the columns and centrifuged for 2 min to elute bound proteins. Then the urine proteins were ready for downstream applications.

2.2.5. Methods

2.2.5.1. Immunoblotting

2.2.5.1.1. SDS-polyacrylamide gel electrophoresis of proteins (SDS-PAGE)

The 60-80 µg of protein sample was diluted in 4x Laemmli sample buffer (Bio-Rad Laboratories, UK) and then denatured by heating at 95°C of kidney lysate for 5 min and small intestine lysate for 10 min. Samples containing equal amounts of protein were loaded alongside the appropriate protein standard molecular weight markers (Pre-stained Precision Plus, Bio-Rad Laboratories, UK) onto gels and run at 100-150V using a PowerPac HC power (Bio-Rad, UK) for approximately 1.5-2 hr depending on the percentage acrylamide in the gel, and until the dye front ran off the bottom of the gel. The gel was transferred onto the PVDF membrane by using the semi-dry transfer method or stained with Coomassie blue.

2.2.5.1.2. Coomassie staining for SDS-PAGE gels

Coomassie staining to visualise separated proteins in gels was performed using Coomassie Brilliant Blue R-250 staining kit (Bio-Rad Laboratories, 161-0435). Gels were stained for 2 hr then the stain was removed and replaced with a destaining solution (methanol: H₂O (1:1 v/v), glacial acetic acid). Gels were destained overnight on a rocker at room temperature. Next day, gels were immersed in a fresh destaining solution containing 3% Glycerol for 30 min and then wrapped in moistened cellophane sheets. Any bubbles between the gel and the cellophane sheets were expelled, wrinkles in the cellophane smoothed out, and the gel dried using GelAir drying system.

2.2.5.1.3. Transfer of proteins separated by SDS-PAGE to PVDF

Proteins separated by gel electrophoresis were transferred onto a PVDF membrane by using the semi-dry transfer method (Trans-Blot® SD Semi-Dry Transfer Cell, Bio-Rad). PVDF membranes were activated in 7ml of 100% methanol for 30 sec and then washed in distilled water for 2 min. Next, a sandwich was made from filter paper immersed in transfer buffer with 10% methanol/membrane /gel /filter paper moistened in the transfer buffer, but without methanol. After this, the proteins were transferred from the gel to the membrane by applying voltage for 1-2 hr depending on the percentage acrylamide in the gel. The transfer was confirmed by the transfer of pre-stained Precision Plus molecular weight markers.

2.2.5.1.4. Membrane blocking and immunoblotting

After semi-dry transfer, the membrane was blocked to prevent antibodies from binding to the membrane non-specifically and to reduce background. The PVDF membranes were blocked in 2.5% non-fat milk in Tris/Tween buffered saline (TBST) for 1 hr at room temperature. Then, membranes were probed with the primary antibodies (see appendix 1.5) diluted in 2.5% non-fat milk in TBST overnight at 4 °C. The following day, membranes were washed 3 x 5 min in 25 ml of TBST. Membranes were incubated by secondary antibodies HRP-conjugated rabbit anti-goat Immunoglobulin, or rabbit anti-mouse Immunoglobulin (Dako, UK) diluted 1:2000 in TBST for 2 - 3 hr. After this, the membranes were washed 3 x 5 min in 25 ml TBST. Detection and staining of proteins were performed using Amersham ECL Western Blotting Detection Reagent (Scientific Lab, UK). A mixture of enhanced-chemiluminescence (ECL) reagent (1ml of reagent 1 and 1ml of reagent 2) was applied to the membrane for 3 min at room temperature. Next,

the reagent was removed, and the membrane was wrapped in Saran Wrap. Images of ECL treated blots were acquiring using the ChemiDoc^{Touch} imaging system (Bio-Rad Laboratories, UK). All blots were performed in triplicate for samples derived from three or more individual animals.

2.2.5.1.5. Analysis of immunoblot images

Densitometry analysis was performed using ImageJ Software v 1.49 (National Institutes of Health, USA). The intensity of protein bands was measured in samples from different experimental conditions and the intensity of the target protein was then divided by the intensity of either the β -actin or dipeptidyl peptidase (DPP)-IV loading control for that blot. This target protein/loading control ratio was used to express relative target protein abundance in the experiments. Data are presented as the ratio of intensity for the protein of interest/loading control expressed as a percentage of the corresponding ratio under control conditions.

2.2.5.2. Histological examination of tissues

2.2.5.2.1. Haematoxylin and Eosin staining

To investigate the morphological changes in tissues from the experimental animal's sections of fixed tissue were stained with hematoxylin and eosin (H&E). The formalin-fixed paraffin-embedded (FFPE) tissue sections were dewaxed 2 x 5 min in the xylene and rehydrated in a series of graded alcohols: 100 % ethanol twice, 90% ethanol and 70% ethanol once for 5 min each. The slides were then washed with deionised water for 3x5 min each. The slides were stained with Hematoxylin Solution Gill No.2 (Sigma-Aldrich, cat no: GHS232) for 3 min, then washed in the deionised water. Slides were placed in differentiation account solution (Sigma-Aldrich, cat no: A31179) for 60 sec followed by a wash in water.

The slides were placed in Scott's Tap Water substitute (Sigma-Aldrich, cat no: S5134) for 1 min and washed again in water for 5 min. The slides were placed in 95% ethanol for 1 min for destaining and then washing twice with tap water followed by deionized water for 2 min. The slides were then immersed in Eosin Y Solution (Sigma-Aldrich, cat no: HT-1101132) from 30 – 45 sec. Slides were then dehydrated with increasing concentration of serial dilutions of ethanol (70%, 90%, and 100%) respectively for 3x5 min each and then placed in xylene 3x 5 min. The slides were mounted by a drop of DPX mounting and covered with a coverslip. The mounted slides were left to dry overnight and observed under an Olympus Cytology Microscope using Spectral imaging acquisition software 4.0.

The tubular injury was evaluated in 10 non-overlapping fields at x200 magnification from each section were captured using an Olympus Cytology Microscope with identical illumination and exposure. According to the previous studies, the tubular injury was scored as follows: 4 for severe tubular damage; 3 for moderate tubular damage; 2 for mild tubular damage; 1 for small focal areas and 0 for normal tubules (Guan et al., 2013). In addition, the tubular damage was scored independently and blind by two researchers in the infection, immunity and inflammation department. The results presented as a mean \pm SEM of triplicates

2.2.5.2.2. Immunohistochemistry staining

Four-micron sections from FFPE samples of human kidney biopsies or experimental mouse kidneys or small intestines were used in the immunohistochemistry staining. The sections were dewaxed in xylene and rehydrated in a series of graded ethanol. The sections were treated with 2.4 ml of 30% hydrogen peroxide (Sigma-Aldrich, UK) in 400 ml of PBS, which was incubated for 10 min at room temperature to block endogenous peroxidase

activity. To maximise antigen retrieval, the sections were submerged in pre-heated sodium citrate buffer pH 6 (Sigma-Aldrich, UK) in a pressure cooker for 12 min at 800W in a microwave. The sections were then left to cool at room temperature for 20 min in sodium citrate buffer. Then, the sections were placed in a glass chamber containing 400 ml of water. To enhance the binding of the antibody to the sections the slides were kept moistly and then encircled using a PAP pen (ThermoFisher Scientific, UK). To prevent non-specific antibody binding, sections were blocked with 100 µl of Animal-Free Blocker (Vector Laboratories, SP-5030) or 100 µl of Mouse on Mouse (MOM) Blocking (Vector Laboratories, BMK-2202) for 1 hr at room temperature. Next, the sections were washed with PBS for 3 x 5 min.

To block endogenous biotin and avidin binding, the sections were then treated with the Avidin/Biotin Blocking System reagent kit (Vector Laboratories, SP-2001). Three drops of avidin were added to each section and incubated for 15 min at room temperature. Next, the avidin was drained and the slides washed 3x5 min in PBS. Immediately, three drops of biotin were added to each slide and incubated for 15 min at room temperature. Biotin was then drained, and the slides washed 3x5 min in PBS. The sections were then incubated with primary antibodies diluted in antibody diluent (Dako, UK), or 10 % swine serum or 10 % goat serum in PBS overnight at 4⁰C (see appendix 1.6). Negative controls were treated with an animal-free blocker only. Slides were then washed in PBST for 5 min. The secondary antibodies were diluted 1:200 dilution in PBS and applied for 30 min (see appendix 1.6). Then, the sections were washed 3 times with PBS for 5 min. Then, Streptavidin/Horseradish Peroxidase (SA/HRP) Reagent (Vector Laboratories, SA-5704) was applied to each section for 25 min. Then, SA/HRP was drained and the slides washed 3 times 5 minutes in PBS.

Peroxidase (DAB) Substrate kit (Vector Laboratories, SK-4100,) allowing the formation of a brown-coloured precipitate at the antigen site. A solution of DAB was prepared from a one drop of buffer stock solution, two drops of DAB stock solution and one drop of the hydrogen peroxide solution. These were added to 2.5 ml of distilled water and mixed well. The staining was completed by 3 -10 min incubation. Then, the DAB solution was drained, and the slides washed 3 x 5 min in water. Then, sections were quickly counterstained with hematoxylin and for 1 min, before being washed in running water for 5-10 min. The slides were again submerged in Differentiating Account Solution for 10 sec and washed with tap water then immersed in the Scott Tap Water for 5 sec before being washed again in running water for 5-10 min. The slides were dehydrated using 70%, 90%, and 100% ethanol, 3 min for each and then twice in 100% xylene for 5 min. One drop of DPX (Sigma-Aldrich, UK) was placed in each section and covered with a coverslip. The mounted slides were left to dry for 3 hr and viewed subsequently under an Olympus monochrome CCD camera and Olympus Cytology Microscope using Spectral imaging acquisition software 4.0.

2.2.5.2.2.1. Analysis of immunohistochemistry images

The computerised analysis of the images was performed using macros in ImageJ analysis software 1.51h (Schneider et al., 2012). The percentage of antibody staining areas in renal cortex of each section was quantified by colour deconvolution method using ImageJ, which separates the image colours reliant on the section staining and a threshold feature demonstrated the selected area depending on the intensity of staining (Ruifrok and Johnston, 2001, Wang et al., 2011, Ross, 2014, Varghese et al., 2014, Haub and Meckel, 2015). Photographs were captured from 20 nonoverlapping fields of renal cortex just under the renal

capsule around the whole kidney section. Photographs were imported into the ImageJ. Then, the colour deconvolution plugin was selected from the colour tool. The image was separated into 3 images colour (Haematoxylin, DAB, and complimentary) and then background subtracted from the DAB image. The threshold of images was set to a similar pixel using threshold settings. After threshold was adjusted and then the intensity of interesting staining (brown staining area only) was determined by selection analysis plugin of ImageJ. The threshold of the total area of no staining (adjacent to an interesting area of DAB) was also determined with the analysis plugin of ImageJ.

The data were calculated using Microsoft Office Excel software (2010) and according to this equation (IHC stained area = (IHC of the interesting stained area)/ (total area) multiply by 100%). The average percentages were calculated that represents the percentage of antibody binding area in the kidney section and expressed as a (%) per field of view and presented as a Mean \pm SEM of triplicates.

2.2.5.2.3. Immunofluorescences

FFPE samples were dewaxed in xylene and rehydrated in 100%, 90%, and 70% ethanol for 5 min. The sections were immersed in 400 ml of distilled water for 10 min. the sections were submerged in pre-heated sodium citrate buffer pH 6 (Sigma-Aldrich, UK) in a pressure cooker for 12 min at 800W in a microwave. The sections were then left to cool at room temperature for 20 min in sodium citrate buffer. The sections were placed in a glass chamber containing 400 ml of water. Slides were kept moist and then encircled using a PAP pen (ThermoFisher Scientific, UK). Next, sections were blocked with 100 μ l of Animal-Free Blocker (Vector Laboratories, UK) for 60 min at room temperature.

The sections were then incubated with primary antibodies diluted in antibody diluent (Dako, UK) and incubated overnight at 4°C (see appendix 1.7). Negative controls were treated with an animal-free blocker only. The sections were washed in PBST for 5 min. followed by incubating the sections with Alexa Fluor secondary antibody diluted 1:100 dilution in PBS with 10% of donkey serum or 10 % goat serum for 1 hr in the dark at room temperature and then washed 3 x 10 min by PBST (see appendix 1.7). Next, 100 µl of DAPI 1:1000 dilution (Life Technologies, UK) was applied to each section for 10 min in the dark and followed by washed in PBST for 8 min twice. One drop of Prolong Gold Reagent (Life Technologies, UK) was then added to each section and covered with a coverslip. Mounted slides then left to dry and stored at 4°C in darkness. Immunofluorescence staining was viewed under Olympus monochrome CCD camera and Fluorescence Olympus Cytology Microscope using Applied Spectral Imaging's version 6.

2.2.5.2.3.1. Analysis of immunofluorescence images

The analysis of immunofluorescence (IF) staining was performed by threshold analysis using ImageJ. The images were captured using a fluorescence Olympus Cytology Microscope (Applied Spectral Imaging's version 6). Images were captured from 15 non-overlapping fields of the section of a kidney and then imported to the ImageJ. The image was split into three channels using a split channel tool. The images were stored on the 8-bit greyscale. The threshold of images was set to a similar pixel using threshold settings. After threshold was adjusted and then the intensity of fluorescence staining was determined by selection analysis plugin of ImageJ. The threshold of the total area of no fluorescence (adjacent to an interesting area of fluorescence) was also determined with the analysis plugin of ImageJ.

The data were calculated using Microsoft Office Excel software (2010) and calculated as fluorescence area = (the interesting fluorescence area) / (Total area of no fluorescence) multiply by 100%. The average percentages were calculated as the percentage of antibody binding area in the section and expressed as a (%) per field of view and presented as a mean \pm SEM of triplicates.

The caspase-3 positive cells were examined under Fluorescence Olympus Cytology Microscope using Applied Spectral Imaging's version 6 and counted in 15 fields of adjacent non-overlapping random field using automatically ImageJ analysis software 1.51h. The caspase-3 positive cell numbers were expressed as a (%) of staining per field of view, and the results presented as a mean \pm SEM of triplicates.

2.2.5.2.4. Detection of apoptotic cells

Apoptotic cells in the kidney sections were stained using ApopTag Peroxidase In Situ Apoptosis Detection Kit (Millipore, S7100), according to the manufacturer's protocol (Newbold et al., 2014). The paraffin-embedded kidney sections were dewaxed by washing with xylene for three changes for 5 min each, then another two washes with 100% ethanol for 3 min each, followed by further washes in 95 % ethanol and in 70% ethanol for 3 min each. Lastly, the sections were washed twice for 2 min in water and one change of PBS for 5 min. To expose DNA, the tissue sections were pre-treated by applying a freshly diluted solution of Proteinase K (20 μ g/ml) for 15 min at room temperature and the sections were washed with distilled water twice for 2 min each. Endogenous peroxidase activity was inactivated by incubating the slides with 3% H₂O₂ in PBS for 5 min and washing twice for 5 min in PBS. Excess liquid was removed by gentle tapping.

To detect fragmented DNA, 60 µl of equilibrium buffer was applied to each section and incubated at room temperature for at least 30 sec. Excess of liquid was removed. Each section was tapped and 50 µl of a working solution of TdT enzyme was applied to each section for 1 hr in a humidity chamber. Sections were washed in stop/wash buffer under agitation for 15 sec and then incubated for another 10 min at room temperature. Next, the sections were washed 2 min 3 times in PBS. 50 µL of HRP-conjugated anti-digoxigenin antibody was applied to each section and incubated for 30 min at room temperature. The sections were then washed 2 min for 4 times in PBS and then 60 µL of peroxidase substrate (DAB) was added to each of the sections for 1-5 min at room temperature followed by washing in distilled water. Subsequently, the sections were counterstained with hematoxylin solution for 2-4 min and washed in water. Sections were then dehydrated through graded ethanol solutions and then placed twice in xylene for 5 min and then mounted with DPX.

Brown coloured apoptotic cells were examined under x400 magnification using an Olympus light microscope and counted using automatically ImageJ in 20 fields adjacent non-overlapping random fields. Apoptotic cells were counted, and the cell numbers were expressed as a number of per field of view, and the results presented as a Mean \pm SEM of triplicates.

2.2.5.2.4. Sirius Red staining

In order to determine renal fibrosis, 4 µm paraffin-embedded kidney sections were stained with picosirius red staining specific for collagen (Junqueira et al., 1979, Whittaker et al., 1994), according to picosirius red stain kit (Abcam, ab150681) protocol. The sections were de-waxed in xylene, rehydrated in a series of graded ethanol for 5 min and washed 2 min in water. Nuclei were stained by hematoxylin

solution as described above. Slides were then washed in running tap water for 10 min and then stained with Picro Sirius Red Solution (Abcam, ab150681) for 1 hr. The acidified water was prepared by adding 5 ml Acetic Acid Solution (0.5 %) (Abcam, ab150681) to 1 L of distilled water. Slides were washed in two changes of acidified water for 5 min. Sections were dehydrated in three changes of 100 % ethanol, followed by two changes of xylene for 5 min. The sections were mounted in one drop of DPX (Sigma-Aldrich, UK) and left to dry overnight. Finally, the staining was visualized by Nikon microscope using NIS Elements Advanced Research, Microscopy Imaging Software.

Sirius Red staining images were examined under x200 magnification using Nikon microscope and analysis using ImageJ in 10 adjacent non-overlapping random fields. The images were stored on 8-bit greyscale and the threshold was set using the colour adjustment tool. After the threshold was adjusted and then the intensity of the stained was calculated. The results were expressed as % percentage of the stained area and presented as a mean \pm SEM of triplicates.

2.2.5.3. Determination of the cubilin and amnionless in urine and tissue by ELISA

The content of cubilin and amnionless in urine and tissue was determined using the Mouse Cubilin ELISA Kit (CSB-EL006213MO, General Ltd, UK) or the Amnionless Mouse ELISA kit (CSB-EL001675MO, Generon Ltd, UK), according to the manufacturer's instruction. 1ml of Sample Diluent Buffer was added to 500 pg/ml of stock standard protein and mixed by agitation for 15 min. Then, protein standards were diluted to 0.0, 7.8, 15.6, 31.25, 62.5, 125, 250 and 500 pg/ml concentrations. 100 μ l of diluted protein standards were added into wells of 96 well plate in duplicate. In some experiments, albumin 0.003 gram was added to

the protein standards and a standard curve was produced under these conditions to determine whether albumin in the urine may interfere with the ELISA assay measurements.

Kidney homogenates were diluted 1:10, small intestine homogenates were diluted 1:20 and urine samples were diluted 1:20. Protein receptor excretion was determined in urine samples, normalized to creatinine concentration from each group. 100 µl from each sample was pipetted into wells of 96 wells plate in duplicate. The plate was covered with an adhesive strip and incubated at 37°C for 2 hr. Then, the samples were removed without washing. 100 µl Biotin-antibody was added to each well and incubated for 1 hr at 37°C. The biotin antibody was aspirated from the wells and washed with 200 µl of wash buffer for 2 min three times and plates inverted against clean paper towels.

100 µl HRP-avidin antibody was added to each well and the plate covered with a new adhesive strip and incubated at 37°C for 1 hr. The HRP-Avidin antibody was aspirated and wells washed 5x 2 min in wash buffer. The reaction visualised by adding 90 µl chromogenic substrate (TMB) incubated at 37°C for 30 min in the dark. The reaction was stopped with 50 µl stop solution and absorbance at 450 nm determined within 5 min using an ELISA plate reader (LT-4500 Microplate Absorbance Reader, Labtech). The absorbance (OD) of the standard was subtracted from the OD blank reading and concentrations were calculated via interpolating absorbance against the standard curve using Graph Pad Prism 7 analysis software.

2.2.5.4. Quantitative polymerase chain reaction

2.2.5.4.1. Extraction of Ribonucleic acid (RNA) from tissue experiments

RNA was isolated from experimental tissues using RNeasy Mini Plus Kit (Qiagen Ltd, UK) according to the manufacturer's instructions (Morse et al., 2006). For each group, 10 mg kidney or small intestine tissues were homogenized in 600 μ l buffer RTL plus containing beta-mercaptoethanol (10 μ l/ml) and reagent DX for 3 min at 50 Hz using an electric homogeniser. The supernatant was transferred to gDNA eliminator spin columns and inserted into a new 2 ml collection tube. The tubes were centrifuged at $>8000xg$ for 30 sec before removing the column. A 350 μ l aliquot of 70 % ethanol was added to the tubes and mixed by frequent gentle pipetting. 700 μ l of the samples were transferred into RNeasy spin columns and placed into 2 ml collection tubes. The tubes were centrifuged at $>8000xg$ for 30 sec and the flow-through was discarded. Then, 700 μ l of buffer RW1 was added to the RNeasy spin columns in new 2 ml collection tubes and centrifuged for 15 sec at $>8000xg$ and the flow-through again discarded. 500 μ l of buffer RPE was added to the RNeasy spin columns placed in new 2 ml collection tubes and centrifuged again at $>8000xg$ for 15 sec, and the flow-through was discarded again. Finally, 500 μ l of buffer RPE was added to spin column again, centrifuged again at $> 8000xg$ for 2 min.

To dry the membrane, RNeasy spin columns were centrifuged twice at $> 8000xg$ for 3 min. To elute the RNA, the RNeasy spin columns were transferred to new 1.5 ml collection tubes and 30 μ l of RNase-free water was added before centrifuging the tubes at $> 8000xg$ for 4 min. The spin columns were removed and the extract RNA in the 1.5 ml collection tubes was stored $-80^{\circ}C$ for further step.

Finally, RNA concentration was measured (ng/ μ l) using a Thermo Scientific NanoDrop spectrophotometer 1000TM and software, 1000.Version 3.7.1.

2.2.5.4.2. Generation of complementary DNA (cDNA)

Complementary DNA was prepared from the extracted RNA using the Reverse Transcription System (First-Strand cDNA Synthesis) Kit (Promega Ltd, UK) according to the manufacturer's protocol. For each sample, 1 μ g of RNA (appropriately adjusted for each sample) was transferred to a 0.5 ml RNase free tube (on ice) and incubated at 70^oC for 10 min. The RNase free tubes were then centrifuged and incubated on ice. Each reaction mixture comprised 4 μ l of 25mM MgCl₂, 2 μ l of Reverse transcription 10x buffer, 2 μ l of dNTP mixture 10mM, 0.5 μ l of Recombinant RNasin Ribonuclease Inhibitor, 0.6 μ l of AMV reverse transcriptase, 1 μ l of oligo (dT) 15 primer, 1 μ g of RNA template (reliant on the amount and concentration of RNA in the samples of each group) and RNase-free water to a total reaction volume 20 μ l. The reaction mixtures were incubated for 15 min at 42^oC at first before the temperature was raised to 95^oC for 5 min. The procedure was completed by incubating at 0-5^oC for 5 min.

2.2.5.4.3. Quantitative real-time PCR

Quantitative real-time PCR (qPCR) was performed using TaqMan Gene Expression Assays (Applied Biosystems) (see appendix 1.3). The cDNA was diluted 1:4 with nuclease-free water. The master mix reactions were prepared from 10 μ l of TaqMan Universal PCR master mix Amplification UNE, 1 μ l of TaqMan gene expression assay and 4 μ l of cDNA. Then, 16 μ l of master mix was added to 4 μ l of diluted cDNA (from experiment and control) in each well of the 96 PCR well plate in triplicates. The same amount of master mix was added to 4 μ l of RNase-free water instead of cDNA (negative control) in each well of the 96 PCR

well plate in triplicates. After initial hold at 50°C for 5 min and initial denaturation at 95°C for 10 min, qPCR reactions were run for 40-55 cycles consisting of denaturation at 95°C for 15 sec and annealing/extension at 60°C for 60 sec.

Each sample was conducted in triplicate for each TaqMan® assay using an Applied Biosystems 7500 fast qPCR machine and software version 2.0.6. The results were analyzed according to the method of Livak ($2^{-\Delta\Delta CT}$) (Adamski et al., 2014) and using Microsoft Office Excel software (2010). The Ct value of the target gene was normalised to the Ct value of a GAPDH reference gene for both the experimental sample and control sample. For example, ΔCT (experiment) was calculated as Ct (experiment) – Ct (reference, experiment), and ΔCT (control) was calculated as Ct (control) – Ct (reference, control). Then, $\Delta\Delta CT$ was calculated as ΔCT (experiment) - ΔCT (control) and the relative expression ratio calculated as $2^{-\Delta\Delta CT}$.

2.2.5.5. Measurement of matrix metalloproteinase (MMP) activity

2.2.5.5.1. General MMP activity assay

To evaluate the activity of MMPs in protein overload and control kidneys, the MMP Activity Assay Kit (Abcam, UK) was used according to the manufacturer's protocol. First, the 25 µl of kidney lysates and 25 µl of 2 mM 4-aminophenylmercuric acetate (APMA) solution (1:500) was added to each well of a 96 well plate (ThermoFisher scientific, M33089) in duplicate and incubated for 10-15 min at 37 °C. 50 µl of assay buffer alone was added to each well in duplicate for the negative control. Then, 50 µl of the green substrate solution (1:100) (a broad-spectrum MMP fluorogenic peptide substrate) was added to each well and the fluorescence signal was monitored 1 hr after initiating the reaction using a microplate reader with a filter set for excitation/emission of 490/525 nm (Thermos Scientific Varioskan®)

flash and SkanIt[®] software version 2.4.1). The fluorogenic activity was calculated by subtracting the increase in emission of the negative control samples containing assay buffer only from the samples having kidney samples.

2.2.5.5.2. Zymography

Zymography for the analysis of MMP-2 and MMP-9 activities were performed using kidney homogenates and urine samples. Briefly, the samples were adjusted to a uniform protein content of 15 µg in a volume of 10 µl diluted in non-reducing of 4x Laemmli sample buffer (Bio-Rad Laboratories, UK). Subsequently, 15 µl of this mixture was loaded into each well of 10% polyacrylamide minigels of 0.75mm thickness containing 0.1% gelatin (Novex™10% Zymogram Plus and electrophoresis at constant 150V/cm for 2 hr. After that, the gels were incubated in Zymogram Renaturing Buffer (ThermoFisher Scientific, cat no: LC2670) for 30 min at room temperature with gentle agitation. This buffer was removed and Zymogram Developing Buffer (ThermoFisher Scientific, cat no: LC2671) was added to equilibrate the gel for 30 min at room temperature with gentle agitation and the buffer was decanted. Then, fresh Zymogram Developing Buffer was added, and the gels incubated overnight with gentle agitation at 37°C. Subsequently, zymograms were fixed and zones of lysis were visualized by staining with Coomassie Blue R250. Molecular weight standards were used for the assignment of molecular weight.

2.2.5.6. Statistical analysis

All experiments were conducted in triplicates and the average of data was calculated from three repeat experiments. All data are expressed as mean \pm SEM. The data were analysed for multiple groups by one-way ANOVA and Tukey's test for multiple comparisons. Comparisons for two groups were performed by unpaired student t-test using GraphPad Prism 7 software. The level of statistically significant difference was considered $P < 0.05$.

Chapter three

Characterization of the expression of the endocytic receptors in wild-type mice

3.1. Introduction

The reabsorption of filtered proteins in the kidney tubule and the intestinal absorption of the intrinsic factor-B₁₂ complex both require the multiligand receptor complex formed by cubilin and amnionless (Christensen et al., 2009, Fyfe et al., 2004, Nielsen et al., 2016). Cubilin is a 460-kDa multiligand receptor that mediates endocytosis of the intrinsic factor-B₁₂ complex from small intestinal chyme and is important for renal tubular reabsorption of various proteins present in the glomerular ultrafiltration (Moestrup et al., 1998, Wahlstedt-Froberg et al., 2003). Amnionless is 48-kDa apical membrane protein also expressed in intestinal and proximal tubule epithelial (Kalantry et al., 2001, Tanner et al., 2003). Cubilin does not have a transmembrane region, and the binding of its EGF-like repeats with amnionless a transmembrane protein enables its expression at the plasma membrane (Coudroy et al., 2005). Recent studies proposed that cubilin and amnionless function as subunits of a receptor complex called cubam (Fyfe et al., 2004). The main objective of this chapter is to define the normal pattern of expression of cubilin in the kidney and small intestine tissues of wild-type mice as well as the expression of amnionless within the kidney tissue of normal wild-type mice.

3.2. Results

3.2.1. Study the cubilin expression in the mouse kidney

The kidney tissue of WT mice was analysed for cubilin expression by immunoblotting, immunohistochemistry, and immunofluorescence. Cubilin bands were clearly detected at 460 kDa (Figure 3.1). To complement the immunoblotting, cubilin expression in FFPE sections of WT mouse kidney was studied. Figure 3.2 demonstrates the optimisation steps performed to identify the optimum antibody concentrations and optimum blocking procedures. Ultimately the optimum detection of cubilin was obtained by blocking for 1 hr with animal-free blocker, using a 1:800 dilution of A-20 anti-cubilin antibody and a 1:200 dilution of biotinylated rabbit anti-goat antibody. Therefore, these conditions were used for all subsequent cubilin blots unless otherwise indicated. As revealed in Figure-3.2B found that brown staining representing the cubilin expression was localized to the apical membranes of proximal tubular epithelial cells. Cubilin is mostly located on the apical membrane of proximal tubules with some staining of the parietal epithelium in glomeruli, close to the tubular pole. Cubilin expression was also studied by immunofluorescence (IF) in FFPE sections of mouse kidney (Figure.3.3.). The IF confirms cubilin expression in PT and glomeruli as seen in the IHC. Overall the IHC and IF results confirm, cubilin expression in PT apical membrane and parietal epithelium of glomeruli close to the tubular pole.

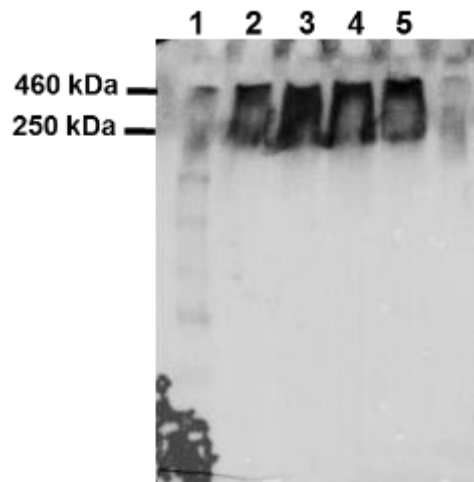


Figure.3.1. Immunoblotting analysis of mouse renal cortex for cubilin.

Renal cortex proteins were loaded onto 7.5 % SDS-PAGE gels and blots were probed with primary antibody cubilin A-20 (1:1000) (Santa Cruz Biotech, Germany). Lane 1: molecular weight standard, Lanes 2, 3, 4 and 5 loaded protein concentrations 100 $\mu\text{g}/\mu\text{l}$ and 80 $\mu\text{g}/\mu\text{l}$. A cubilin band is indicated at 460 kDa

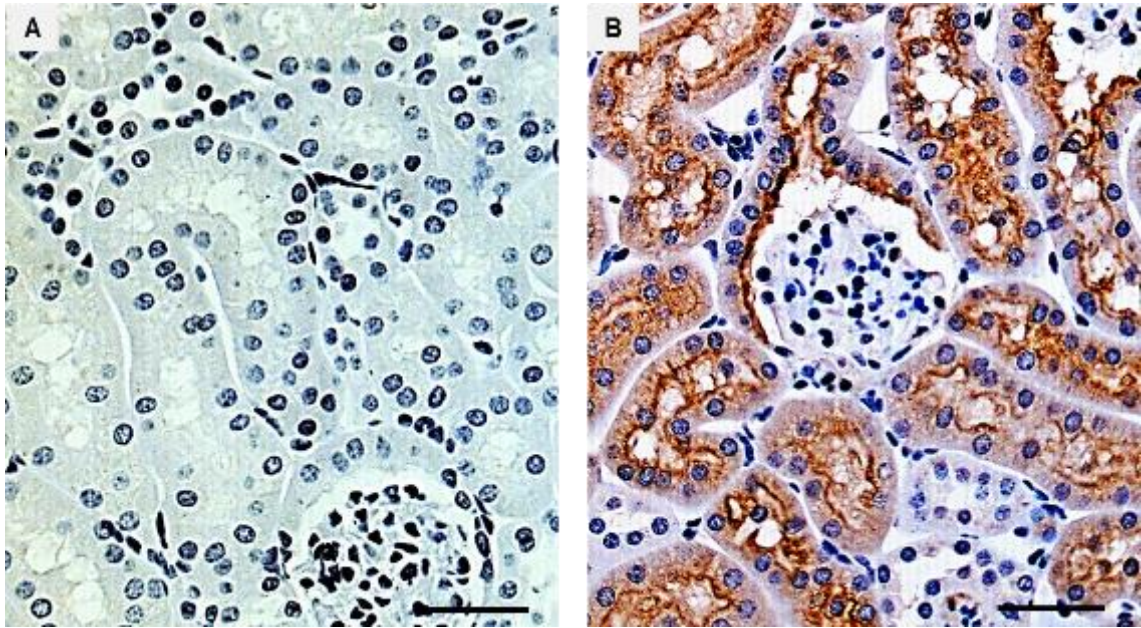


Figure.3.2. IHC analysis of mouse kidney tissue for cubilin.

Representative photomicrographs showing (A) negative control represents the normal WT mice treated without the inclusion of primary cubilin A-20 antibody. (B) Cubilin staining represents the normal WT mice staining by primary antibody cubilin A20. All photomicrographs, scale bars 100 μm .

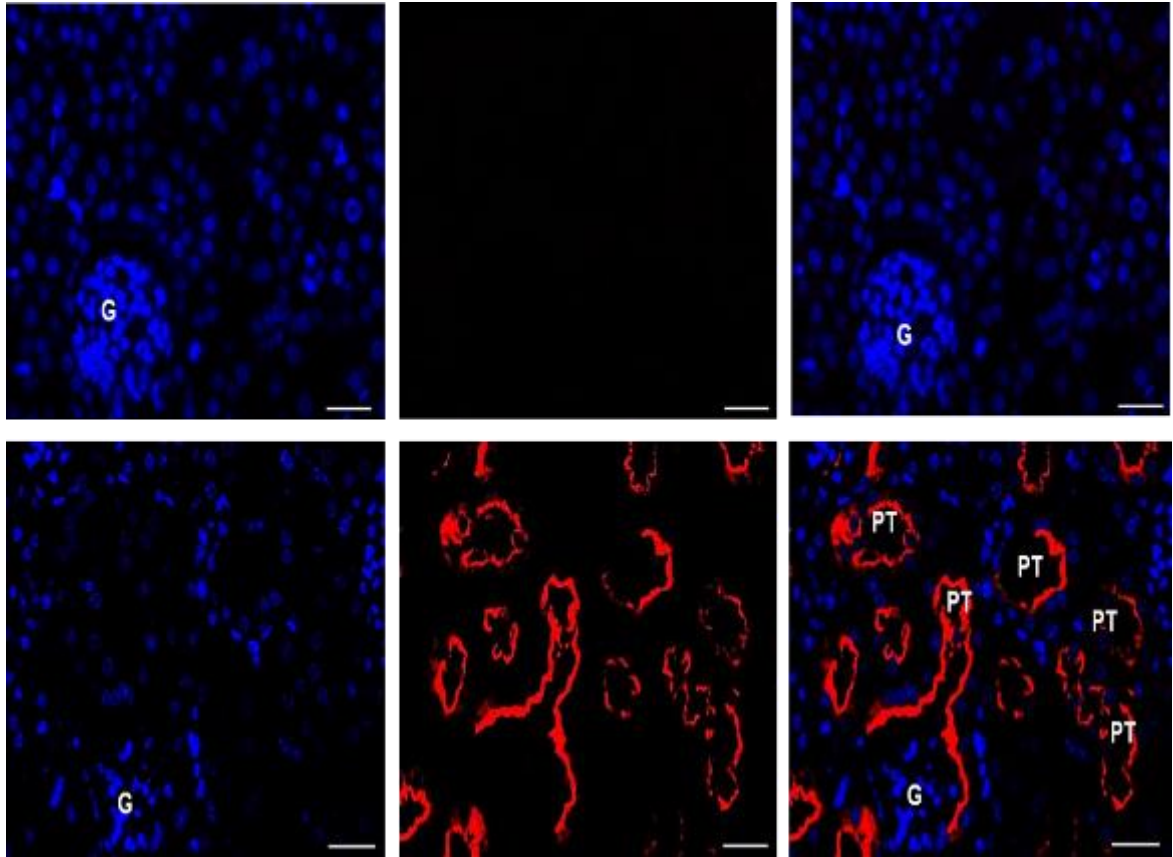


Figure.3.3. IF analysis of mouse kidney tissue for cubilin.

Representative photomicrographs showing Nuclei were stained blue with DAPI (left panels). Middle panels represent negative control (middle-upper) or anti-cubilin (cubilin A-20 antibody) red-stained (middle lower). Right-hand panels represent merged left and middle panels. All photomicrographs scale bar 100 μ m.

3.2.2. Cubilin expression in the mouse small intestine

Expression of cubilin in the small intestine of WT mice was identified the immunoblotting, IHC and IF. The immunoblotting reveals a cubilin band in the small intestine at 460 kDa, identical to the expression in kidney tissue (Figure.3.4).

Cubilin expression in the small intestine tissues of FFPE sections from WT mice was examined by IHC. Figure.3.5 shows that expression of cubilin was localised to the absorptive epithelial cells of the small intestine in WT mice. To confirm the previous results, the cubilin expression in the small intestine was also studied by IF which demonstrated a cubilin expression pattern identical to that observed with IHC (Figure.3.6).

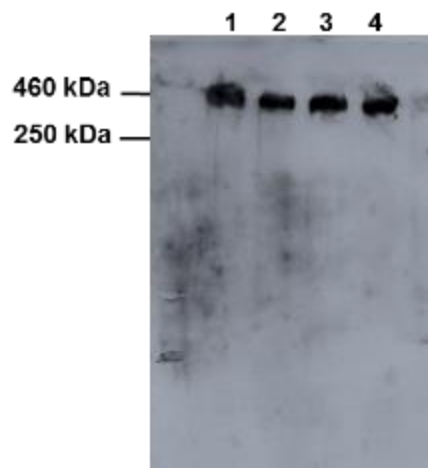


Figure.3.4. immunoblotting analysis of mouse small intestine for cubilin.

Samples were loaded onto 6% SDS-PAGE gels and probed with primary antibody cubilin A-20 (1:1000) (Santa Cruz Biotech, Germany). Cubilin is detected at 460 kDa. Lane 1 represents a mouse kidney as a positive control for cubilin expression whereas, lanes 2, 3 and 4 represent small intestine lysate protein.

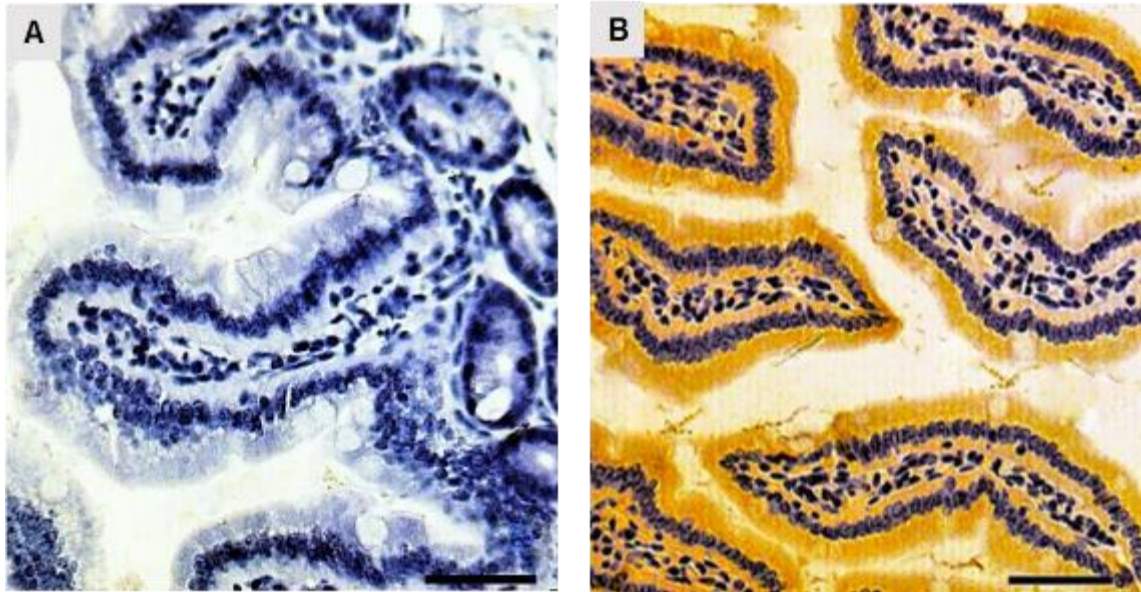


Figure.3.5. IHC analysis of WT small intestine tissue for cubilin.

Representative photomicrographs showing (A) Negative control prepared without the primary antibody. (B) Cubilin staining represents the normal WT mice staining by the primary antibody. All photomicrographs, scale bars 100 μ m.

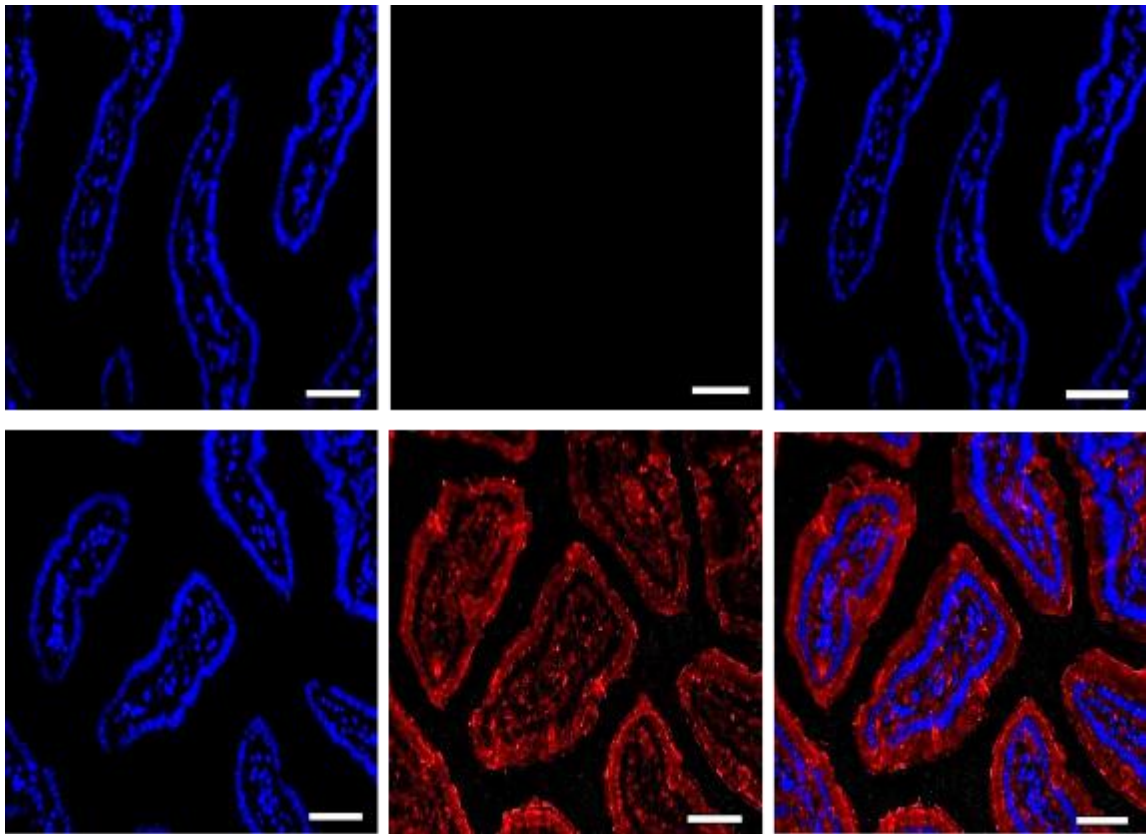


Figure.3.6. IF analysis of mouse small intestine tissue for cubilin.

Representative photomicrographs showing nuclei were stained blue with DAPI (left panels). Middle panels represent negative control (middle-upper) or anti-cubilin (cubilin A-20 antibody) red-stained (middle lower). Right-hand panels represent merged left and middle panels. All photomicrographs scale bar 100 μm .

3.2.3. Study the amnionless expression in the mouse kidney

The kidney tissue of WT mice was analysed for amnionless expression by immunoblotting, IHC, and IF. The immunoblotting reveals the amnionless band in the kidney at 48 kDa (Figure 3.7). The amnionless expression in the kidney tissues of FFPE sections from WT mice was studied by IHC. Figure 3.8 showed that brown staining representing amnionless expression is mostly situated on the apical membrane of proximal tubules with some staining of the parietal epithelium in glomeruli, close to the tubular pole. The IF confirms amnionless expression in PT and glomeruli as seen in the IHC (Figure.3.9). Overall the IHC and IF results confirm, amnionless expression in the apical membrane of PT and parietal epithelium of glomeruli, close to the tubular pole.

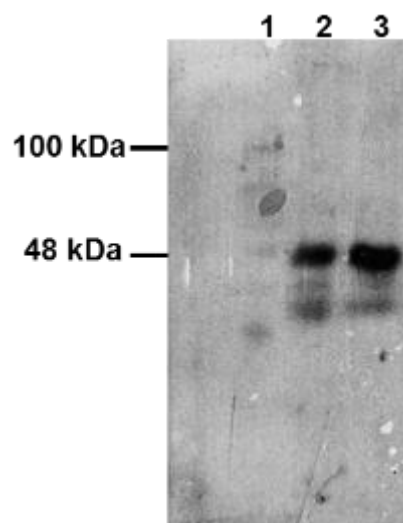


Figure.3.7. Immunoblotting analysis of mouse renal cortex for cubilin.

Renal cortex proteins were loaded onto 10 % SDS-PAGE gel and blots were probed with primary antibody amnionless (1:1000) (Santa Cruz Biotech, Germany). Lane 1 molecular weight standard, Lanes 2 and 3 loaded protein concentrations of 80 micrograms. An amnionless band is indicated at 48 kDa.

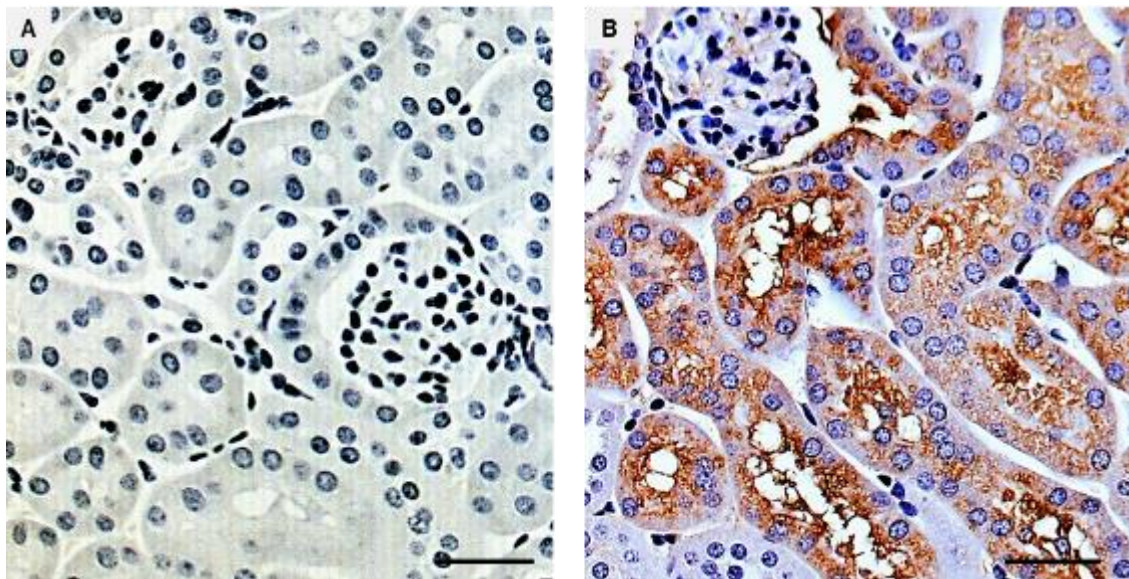


Figure.3.8. IHC analysis of mouse kidney tissue for amnionless.

Representative photomicrographs showing (A) negative control represents the normal WT mice treated without the inclusion of a primary antibody. (B) amnionless staining represents the normal WT mice staining by the primary antibody. All photomicrographs, scale bars 100 μm .

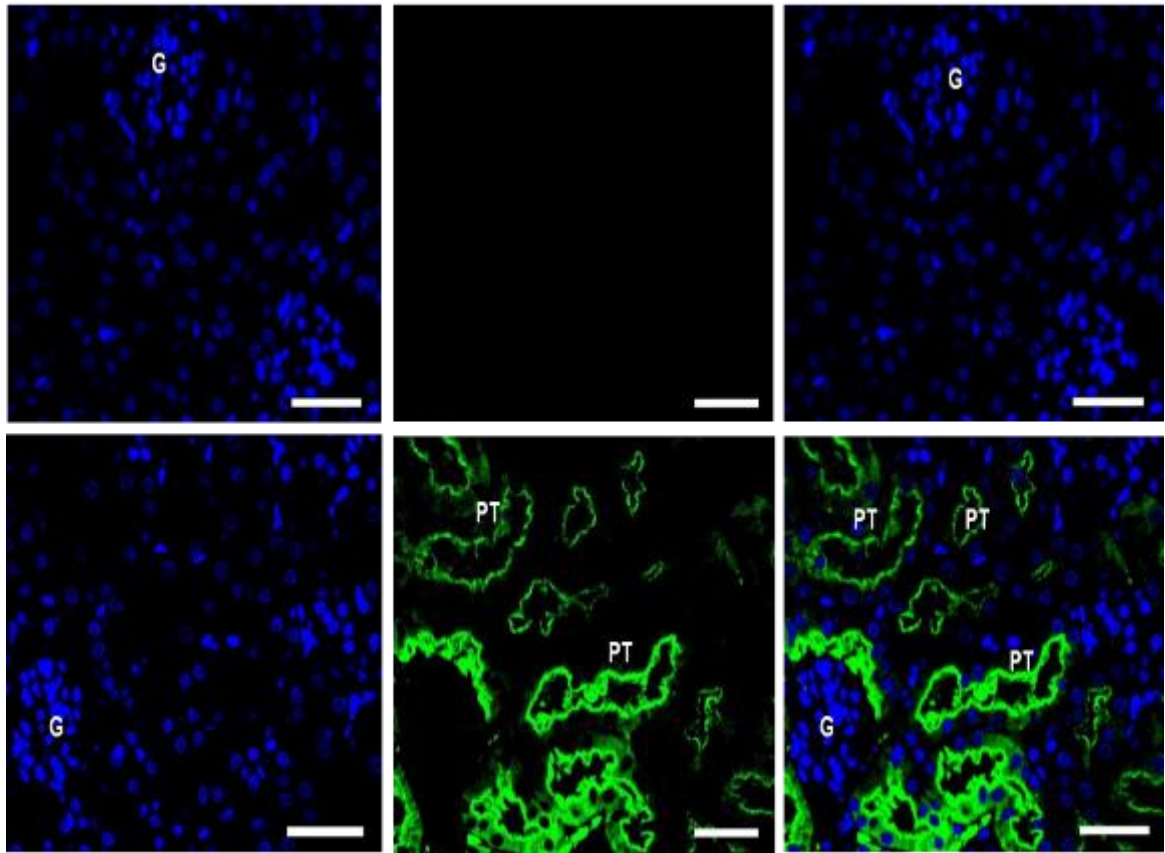


Figure.3.9. IF analysis of mouse kidney tissue for amnionless.

Representative photomicrographs showing Nuclei were stained blue with DAPI (left panels). Middle panels represent negative control (middle-upper) or anti-amnionless (amnionless antibody) stained (middle-lower). Right-hand panels represent merged left and middle panels. All photomicrographs scale bar 100 μ m.

3.3. Discussion

These present studies were performed to identify the normal pattern of cubilin and amnionless expression in mouse tissues and to set a benchmark against which potential changes in expression in disease could be measured. Our studies achieved well-optimised immunoblotting, IHC and IF for both cubilin and amnionless expression. However, our present studies exposed that the expression of both cubilin and amnionless in mouse, localised on the kidney epithelial cells. In addition, cubilin is expressed on the apical membrane of the intestine absorptive cells of WT mice. Interestingly, these results are consistent with previous literature suggesting that both these protein receptors are expressed in different absorptive epithelial cells such as the kidneys, small intestine and yolk sac (Wahlstedt-Froberg et al., 2003, Seetharam et al., 1997, Tanner et al., 2004).

Earlier research revealed that cubilin is co-localised with amnionless in the renal proximal tubule, and interacts with cubilin at EGF-type repeats which is essential for the translocation of the cubam complex from the ER to the plasma membrane and then for endocytosis (Fyfe et al., 2004). Coudroy et al (2005) showed evidence supporting the hypothesis that cubilin and amnionless work mutually in membrane anchoring and trafficking of the complex to the apical cell surface (Coudroy et al., 2005). Therefore, the results of this chapter showed that both cubilin and amnionless are expressed in mouse kidney in the apical membrane of PT and parietal epithelium of glomeruli, close to the tubular pole. This provides a baseline to the identification of the pattern of cubilin and amnionless expressions in future research on the protein endocytic reabsorptive receptors.

Chapter Four

Expression of Cubilin and Amnionless in Mouse Protein Overload Nephropathy

4.1. Introduction

Proteinuria is a strong marker for progression of CKD and cardiovascular morbidity (Gorriz and Martinez-Castelao, 2012). Excess of filtered proteins interact with PTs and induce interstitial inflammation and fibrosis, leading ultimately to progressive renal failure (Gorriz and Martinez-Castelao, 2012, Baines and Brunskill, 2011). Cubilin is an endocytic receptor on the apical cell membrane of PTs and forms a complex with amnionless. This cubilin-amnionless (cubam) complex is crucial to the handling of proteins in PTs and intrinsic factor-vitamin B₁₂ complex in the intestine (Amsellem et al., 2010, Fyfe et al., 2004). However, the expression of this complex has not been studied in proteinuria.

The main objective of this chapter is to investigate the effect of proteinuria on cubam complex expression and MMPs expressions in mice with protein overload proteinuria.

4.2. Results

4.2.1. Effect of protein overload proteinuria on blood and urine biochemistry

The effect of proteinuria on urine biochemistry and protein was determined. The total urinary protein concentration exhibited a substantial increase in proteinuric mice to 51.59 ± 3.25 mg/ml compared to 18.3 ± 1.8 mg/ml in controls (Figure 4.1A). Mice with proteinuria also demonstrated a reduction in urinary creatinine to 1.13 ± 0.1 mg/dl compared to 2.37 ± 0.14 mg/dl of controls (Figure 4.1B). Moreover, urinary albumin concentration was increased in proteinuric mice to 16.2 ± 1.1 mg/dl in comparison with 2.7 ± 0.5 mg/dl in controls (Figure.4.1D). In order to correct for urinary concentration, the urine protein /creatinine (PCR) ratio was calculated and found to be 46.71 ± 5.3 mg/mg in proteinuric mice, whereas in control mice urine PCR was 16.05 ± 2.01 mg/mg (Figure.4.1C).

Serum biochemistry was also studied in control and proteinuric mice. Protein injected demonstrated a significant increase in total serum protein concentration at 24.17 ± 1.3 mg/ml compared to 11.04 ± 0.49 mg/ml of controls (Figure. 4.2A). Serum creatinine levels increased in proteinuric mice to 2.913 ± 0.3 mg/dl compared to 0.83 ± 0.08 mg/dl in controls (Figure.4.2B). Moreover, serum albumin concentration levels showed a substantial increase in proteinuric mice to 11.1 ± 0.5 mg/dl in comparison with 3.2 ± 0.29 mg/dl in controls (Figure.4.2C). Serum Vitamin B₁₂ levels were insignificantly increased in proteinuric mice at 135 ± 11.8 ng/ml in contrast to 85 ± 11.7 ng/ml in controls (Figure. 4.2D).

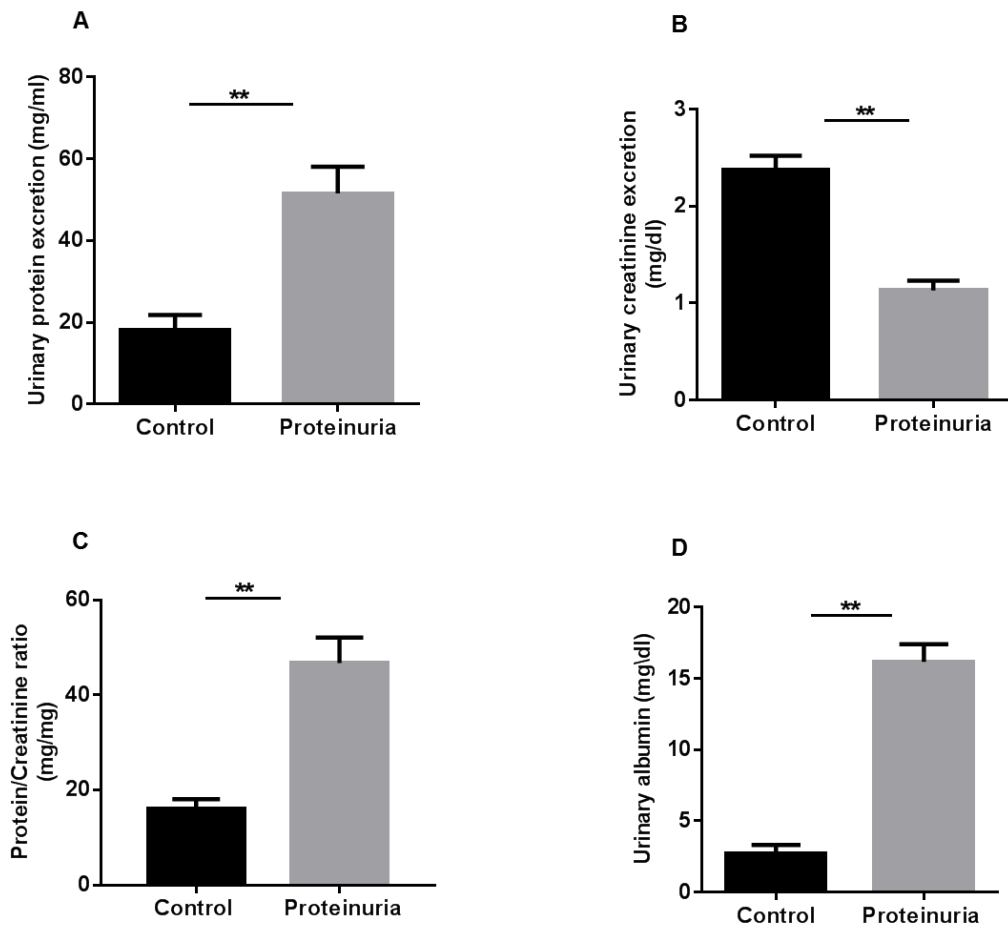


Figure.4.1. Urine biochemistry and protein excretions in mice.

(A) Total urinary protein excretion levels in proteinuric and control mice $**p < 0.01$.

(B) Mouse urinary creatinine concentration $**p < 0.01$.

(C) Mouse urine protein /creatinine ratio $**p < 0.01$.

(D) Mouse urinary albumin concentration $**p < 0.01$.

Data are expressed as mean \pm SEM of 4 mice in each group.

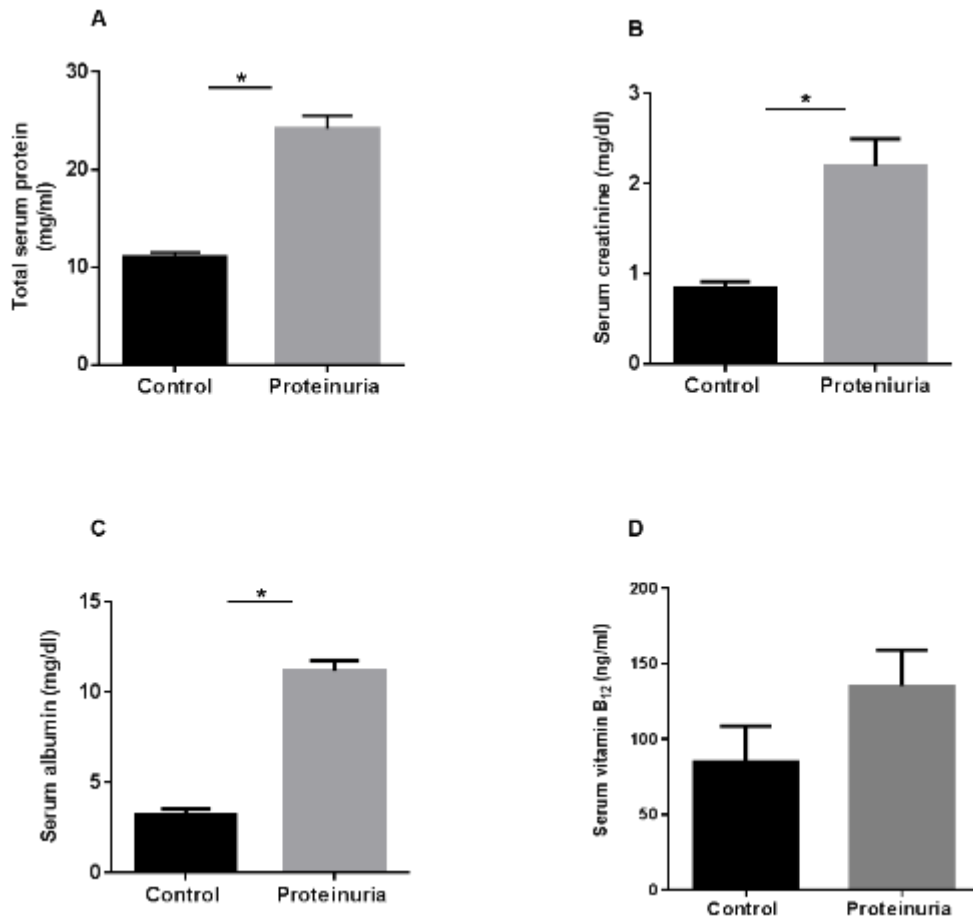


Figure.4.2 Serum biochemistry and proteins levels in mice.

(A) Mouse total serum protein concentrations in control and proteinuria mice. *p < 0.05. (B) Mouse serum creatinine levels *p < 0.05. (C) Mouse serum albumin levels *p < 0.05. (D) Mouse serum vitamin B12 concentrations not significant. Data are expressed as mean \pm SEM of 4 mice in each group.

4.2.2. Renal histopathology in protein overload proteinuria

Kidney sections from each group were stained with H&E to assess the effect of protein overload on the renal histology. Proteinuric mice displayed clear kidney histological abnormalities (Figure 4.3). The sections of a kidney from proteinuric mice showed tubular injury with brush border loss, cellular swelling, and patchy tubular dilation, accumulation of tubular lumen casts and acute tubular necrosis. By contrast, mice control showed no obvious histological changes in the kidney structure (Figure 4.3).

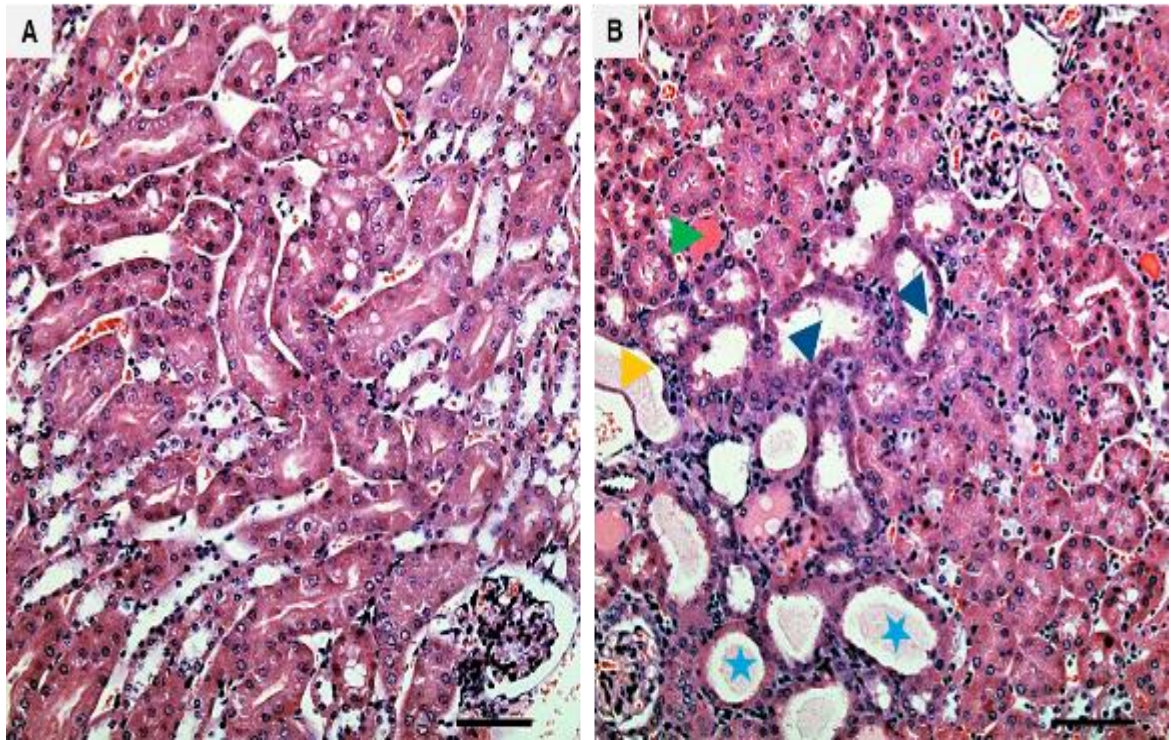


Figure.4.3. Kidney histology in proteinuric and control mice.

Kidney injury was assessed in H&E stained kidney sections. (A) Control mice, and (B) proteinuric mice, displaying loss of brush border in renal tubules (yellow arrowheads), cast formation (blue asterisk), tubular dilatation (blue arrows), and blood (green arrowheads). Scale bar 100 μm .

4.2.3. Effect of protein overload proteinuria on the cubilin complex

4.2.3.1. Cubilin expression in the kidney of proteinuric and control mice

To determine whether cubilin protein expression is affected by proteinuria, kidney tissues from control and proteinuric mice were investigated using immunoblotting. Figure.4.4A depicts cubilin expression in kidney tissue from control and proteinuria groups. Cubilin bands at 460 kDa were very faint in the proteinuric mice in comparison with controls. When quantified, the cubilin expression level was significantly decreased in proteinuric mice (0.63 ± 0.09 relative intensity) compared to controls (1.44 ± 0.1 relative intensity) when normalized to β -actin (Figure. 4.4B).

To accompany the immunoblotting, FFPE sections of a kidney from control and proteinuric mice were analysed by IHC. As described earlier (chapter 3. section 3.3.1), cubilin is mostly expressed at the apical membrane of the PTs in normal mice (Figure 4.5B). In proteinuric mice, expression of cubilin appears considerably reduced in the apical membrane of the proximal tubules (Figure.4.2.5C) compared to in control group (Figure 4.5B). Semiquantitative analysis of the sections revealed a significant decrease in cubilin staining in proteinuric mice ($15.7 \pm 0.7\%$ stained area) compared to control mice ($32.14 \pm 0.9\%$ stained area) (Figure.4.5D). Cubilin expression in kidney cortex from control and proteinuric mice was also determined by ELISA. This confirmed a significant reduction in cubilin protein in proteinuric mice (5.7 ± 0.94 ng/ml) compared to controls (13.9 ± 0.99 ng/ml) (Figure.4.6A). Expression of cubilin mRNA in mouse kidney was substantially decreased in kidney cortex of mice with proteinuria (0.26 ± 0.12 -fold) in comparison with control (1.0 ± 0.08 -fold) (Figure 4.7). These results confirmed that

the down-regulation of cubilin protein is associated with a reduction of cubilin mRNA levels in the kidney.

ELISA was also used to investigate cubilin in the urine of control and proteinuric mice. The concentrations were interpolated from the standard curve and expressed in ng/ml. The concentration of cubilin in urine samples was normalised to urinary creatinine (uCr mg/ml). The urine of proteinuric mice contained a significantly increased cubilin excretion at 2.00 ± 0.30 ng/mg creatinine compared to 0.35 ± 0.08 ng/mg creatinine for the urine of controls (Figure.4.8A). Urine was also analysed for cubilin by immunoblotting and this confirmed an excess of cubilin in the urine of proteinuric mice. No cubilin was identified in the urine of control mice in comparison with the control of mouse kidney lysate (KL) (Figure.4.8B). Overall, these data reveal that urinary excretion of cubilin in animals with proteinuria increased in association with a reduction of cubilin protein expression in the kidney of proteinuric animals.

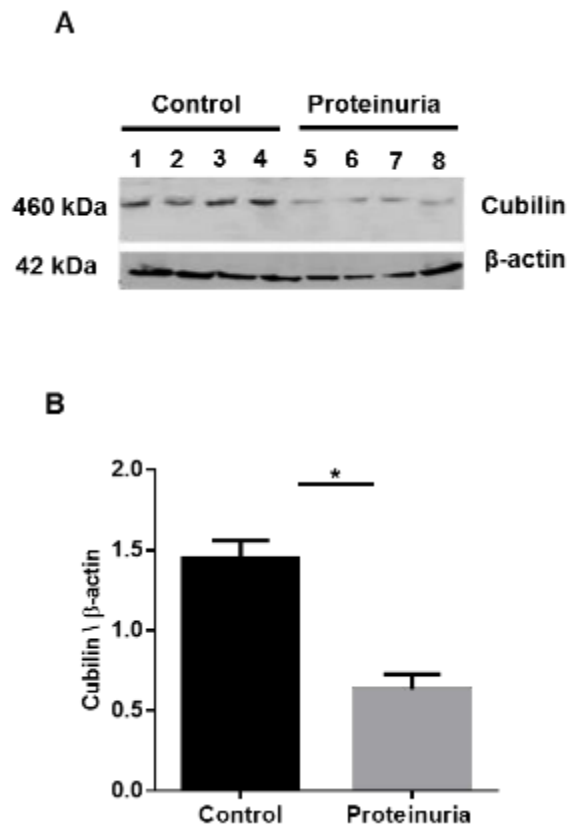


Figure.4.4. Analysis of cubilin protein expression in mouse kidneys by immunoblotting.

(A) Kidney cortex from control and proteinuria mice was assessed by immunoblotting for cubilin, each lane represents a kidney sample from a different animal. Blots stripped and reprobed for β -actin loading control. (B) Densitometric analysis of cubilin expression for control and proteinuric animals expressed as a ratio to β -actin, * $p < 0.05$, unpaired t-test, all experiments were done in triplicate.

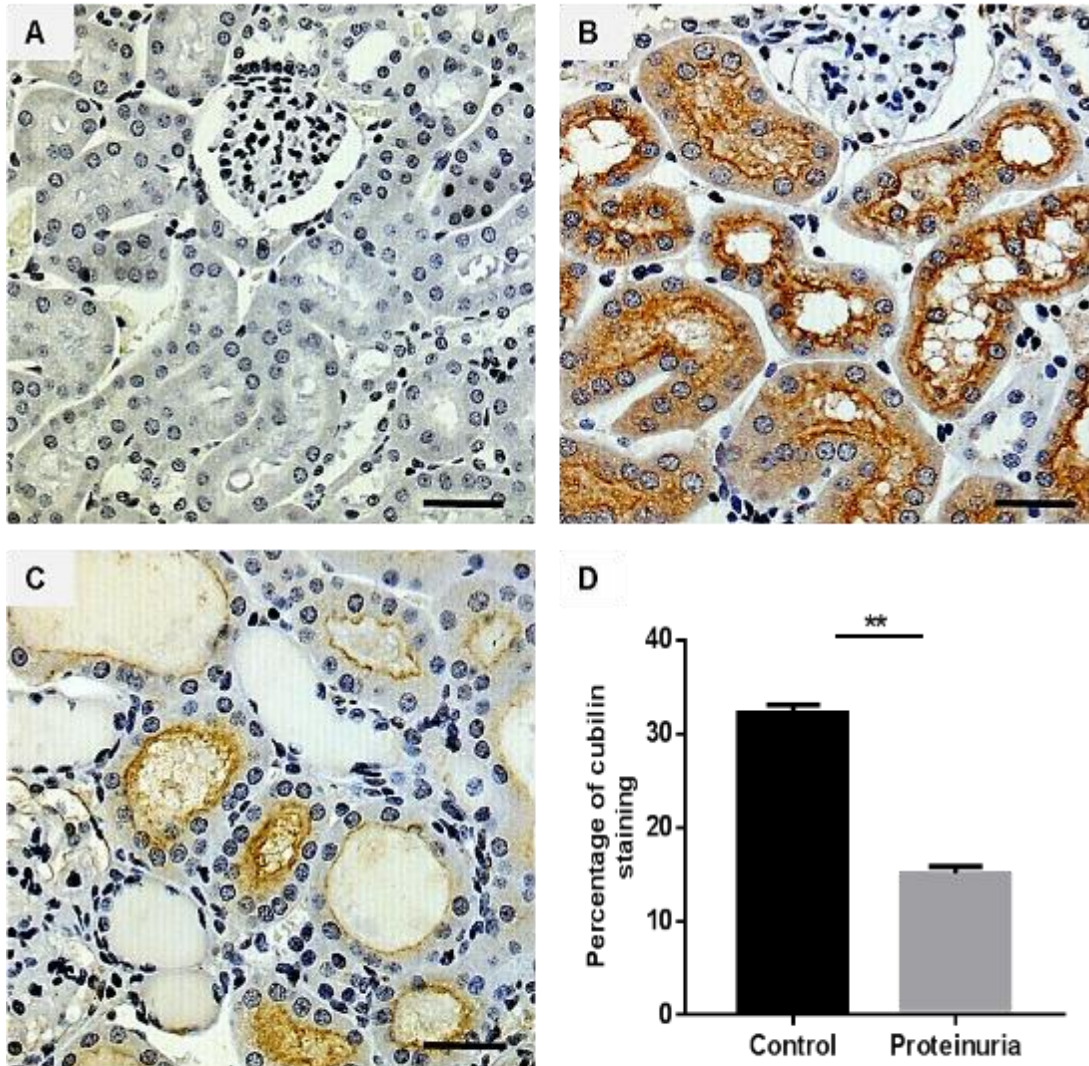


Figure.4.5. IHC analysis of mouse kidney tissue for cubilin in control and proteinuric mice with protein overload proteinuria.

Representative photomicrographs showing (A) Negative control sections from control animals prepared without primary antibody. (B) Control mice. (C) Proteinuric mice. (D) Semi-quantitative analysis of cubilin staining. Data are expressed as mean \pm SEM, ** $p < 0.01$, unpaired t-test test. Scale bars 100 μ M.

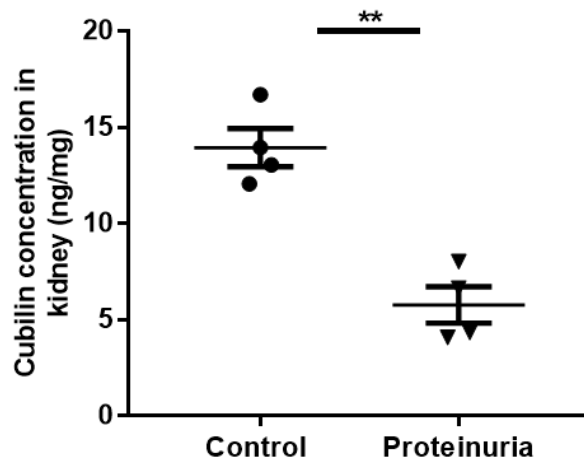


Figure.4.6. ELISA determination of the concentration of cubilin in mouse kidney. Protein samples from kidneys of control and proteinuria mice were examined by ELISA. The graph represents the cubilin concentration in both groups expressed as ng/mg kidney cortical protein. Data are expressed as mean \pm SEM of 4 mice per group. ** $p < 0.01$, unpaired t-test, ELISA was performed in triplicate for each sample.

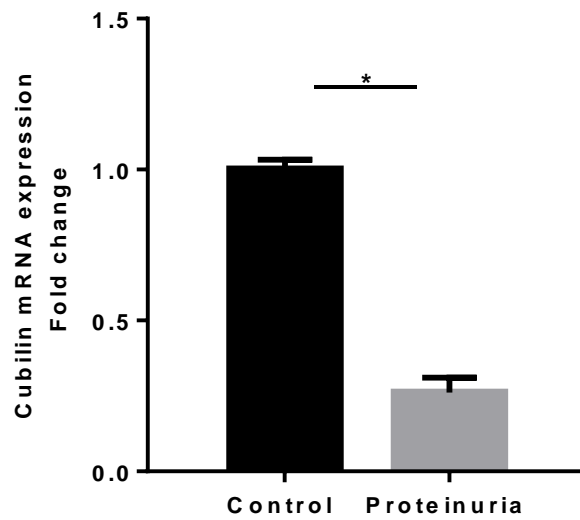


Figure.4.7. Fold change in cubilin mRNA expression in mouse kidneys of proteinuric vs. normal mice.

mRNA was extracted from the kidney cortex and subjected to qPCR. Data are mean \pm SEM of 5 mice in each group. * $p < 0.05$. qPCR was performed in triplicate for each group.

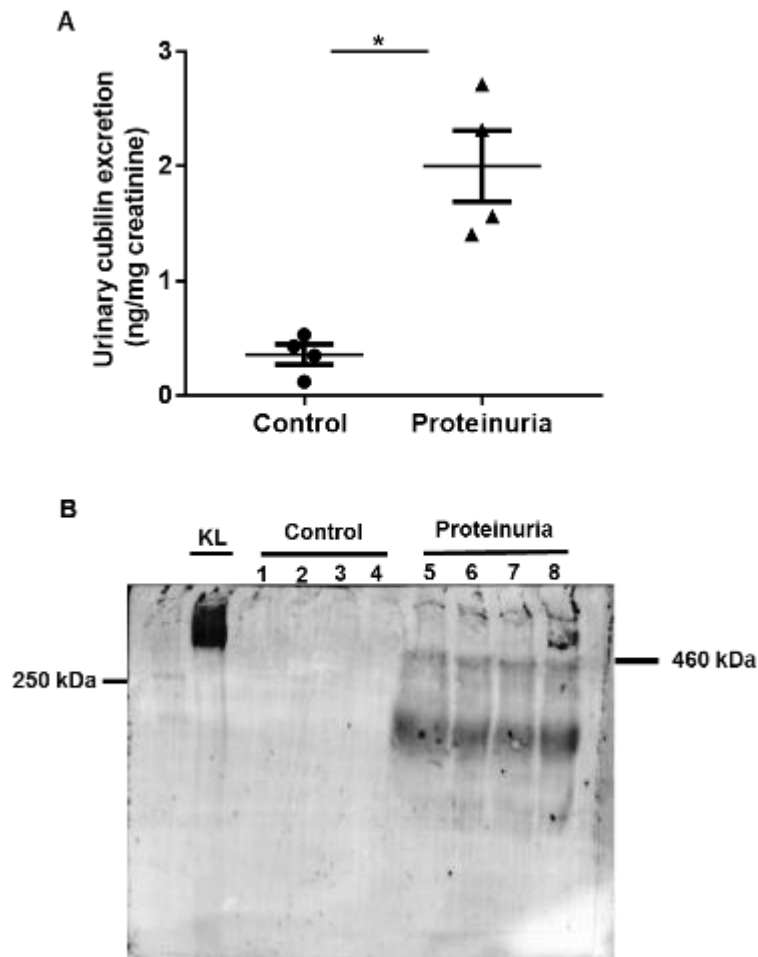


Figure.4.8. Urinary excretion of cubilin in mouse urine.

(A) Urine samples from control and proteinuric mice normalised to creatinine and analysed for cubilin by ELISA. Data are mean \pm SEM of 4 mice in each group. * $p < 0.05$, unpaired t-test, each symbol represents the mean of 3 replicates. (B) Representative immunoblot showing urinary cubilin excretion by proteinuric and control mice in comparison to the control and mouse kidney cortex lysate (KL). The cubilin band was prominently fragmented in the urine of proteinuric mice. All experiments were conducted in triplicate.

4.2.3.2. Cubilin expression in the small intestine of proteinuric and control mice

Small intestine from control and proteinuric mice was studied for cubilin expression by western blotting. A cubilin band in small intestine tissue from proteinuric and control mice was detected at 460 kDa. Cubilin expression was similar in both proteinuric animals and controls (Figure.4.9A). When quantified, cubilin protein expression was not changed in the proteinuric mice (1.158 ± 0.041 relative intensity) compared to controls (1.153 ± 0.025 relative intensity) when normalized to β -actin (Figure. 4.9B). Cubilin concentration in the small intestine of mice was also determined by ELISA. These data confirmed that the amount of cubilin in the small intestine of proteinuric mice (3.41 ± 0.66 ng/mg) was similar to the control mice (3.4 ± 0.56 ng/mg) (Figure.4.10).

IHC was also used to investigate cubilin expression in the small intestine of proteinuric mice. Cubilin expression was typically observed in the apical membrane of absorptive epithelial cells of the small intestine in control and proteinuric animals (Figure.4.11). Semiquantitative analysis of the sections confirmed no significant difference in cubilin expression between control (15.7 ± 0.68 % stained area) and proteinuric animals (15.7 ± 0.75 % stained area) (Figure.4.11D). Cubilin mRNA levels were also assessed in the small intestine of control and protein overloaded animals. Cubilin mRNA expression of cubilin was insignificantly reduced in mice proteinuria to (0.82 ± 0.12 -fold) in contrast with (1 ± 0.04) of control (Figure 4.12). Therefore, the results demonstrate that proteinuric nephropathy has no adverse impact on the protein expression of cubilin in the absorptive epithelial cells of the small intestine.

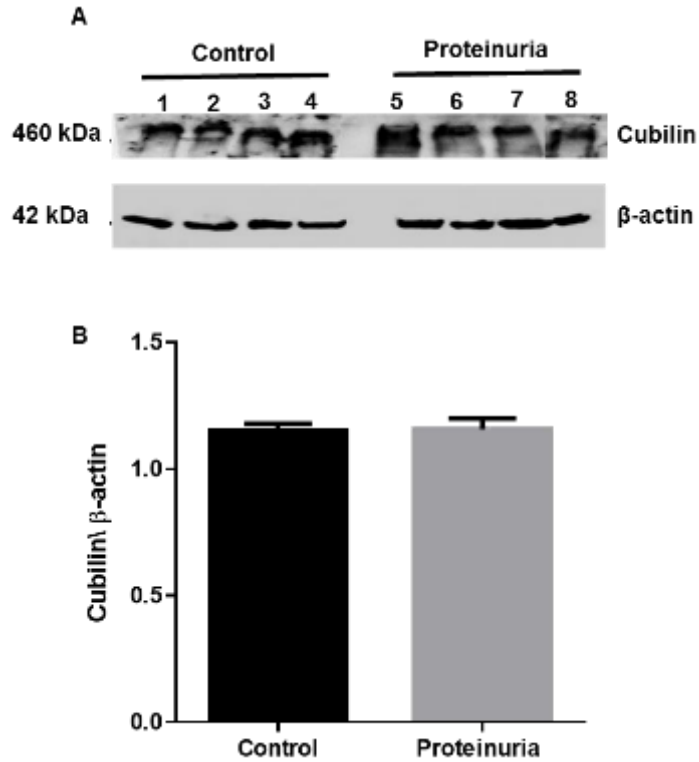


Figure.4.9. Analysis of cubilin protein expression in mouse small intestine by immunoblotting.

(A) Small intestine lysates from control and proteinuric mice were studied by immunoblotting for cubilin. Representative blots are shown in each group. The lower blots stripped and reprobed for β -actin loading control. (B) Densitometric analysis of the cubilin expression as a ratio to β -actin. Data are expressed as mean \pm SEM of 5 mice in each group. $p = ns$, unpaired t-test. All experiments were performed in triplicate.

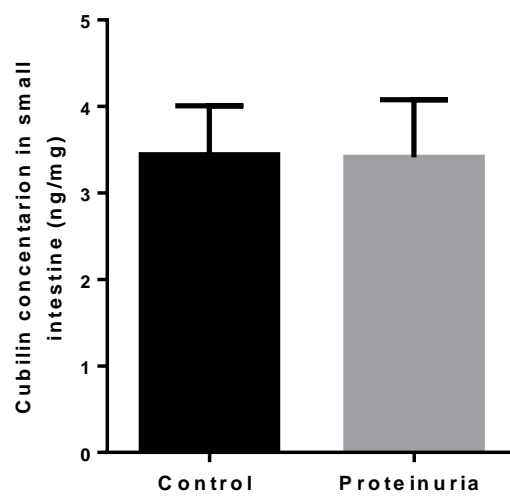


Figure.4.10. Determination of mouse small intestine cubilin by ELISA.

Small intestine protein samples from control and proteinuric mice were examined by ELISA. Cubilin content is expressed as ng/mg of total small intestine lysates. Data are mean \pm SEM of 5 mice per group, $p=ns$, ELISA was performed in triplicate for each animal samples.

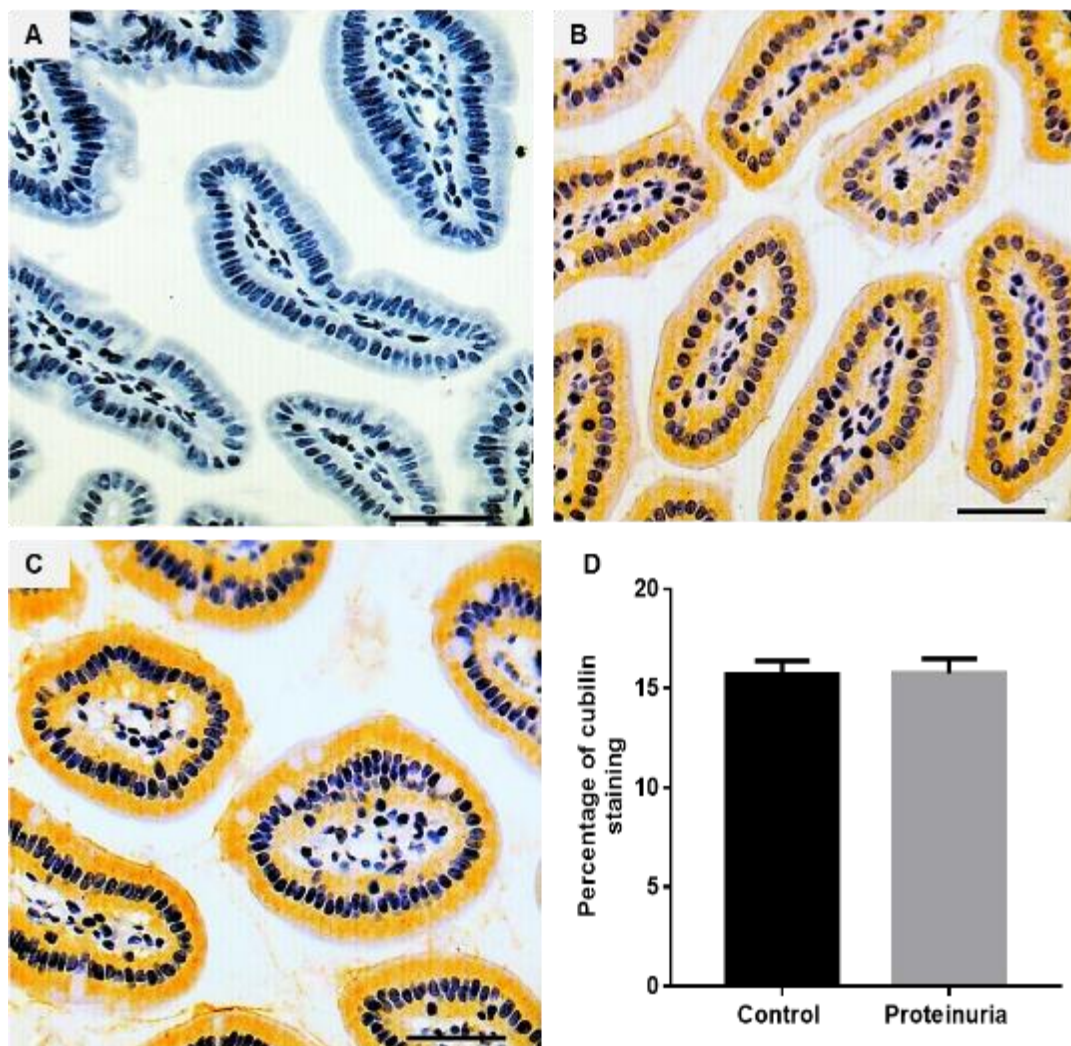


Figure.4.11. IHC analysis of mouse small intestine tissue for cubilin.

Representative photomicrographs showing (A) Negative control sections from control animals treated without primary antibody. (B) Control mice. (C) Proteinuric mice. (D) Semi-quantitative analysis of cubilin staining. $p=ns$. All IHC was performed in triplicate, Scale bars 100 μ M.

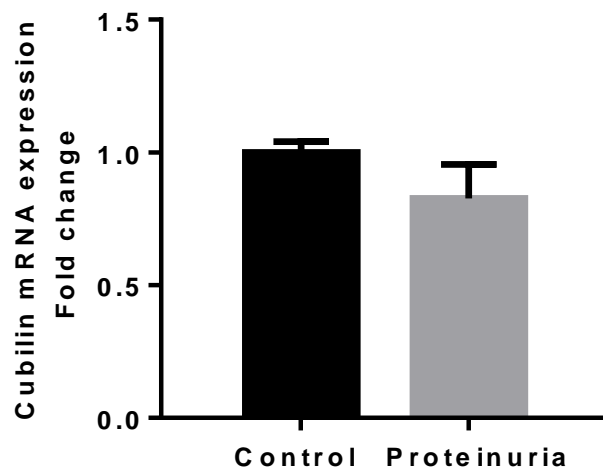


Figure.4.12. Fold change of cubilin mRNA in the small intestine of protein overload proteinuria vs control mice.

Data are expressed as mean \pm SEM of 5 animals in each group, $p = ns$. All qPCR was performed in triplicate in each group.

4.2.3.3. Kidney cubilin expression in adriamycin nephropathy

To define whether cubilin protein expression was altered in another model of proteinuria, expression in adriamycin nephropathy was studied. By immunoblotting, cubilin was clearly reduced in proteinuric animals compared to controls (Figure.4.13 A). When quantified, cubilin protein expression was significantly decreased in the proteinuric adriamycin treated mice (1.04 ± 0.05 relative intensity) compared to controls (1.3 ± 0.034 relative intensity) when normalized to β -actin (Figure. 4.13B). A similar difference was seen in IHC of mouse kidney tissues from control and proteinuric animals (Fig 4.14). The semiquantitative analysis of the sections displayed a significant decrease of cubilin expression in adriamycin mice (12.75 ± 0.45 % stained area) compared to control (19.4 ± 0.8 % stained area) (Figure.4.14 D).

Urinary excretion of cubilin was also examined in adriamycin nephropathy by ELISA. As in protein overload proteinuria, mice with adriamycin nephropathy also demonstrated an increase in urinary cubilin to 1.133 ± 0.046 ng/mg creatinine compared to control 0.146 ± 0.08 ng/mg creatinine (Figure.4.15). Cubilin mRNA expression was markedly decreased in proteinuric mice with adriamycin nephropathy to (0.85 ± 0.104 -fold) compared to control (1.0 ± 0.051 -fold) (Figure 4.16). These results reveal a reduction of kidney cubilin expression in proteinuric adriamycin treated mice, whereas in these animals urinary cubilin excretion was increased.

Effect of adriamycin-induced proteinuria on the blood and urine biochemistry was also studied. The urinary protein /creatinine (PCR) ratio showed a substantial increase in adriamycin mice to 26.2 ± 2.2 mg/mg compared to 9.7 ± 1.4 mg/mg in controls (Figure 4.17A). In adriamycin injected demonstrated a significant decline

in total serum protein concentration at 17.2 ± 1.1 mg/ml compared to 22.15 ± 1.2 mg/ml of controls (Figure. 4.17B). Serum creatinine levels also increased in adriamycin mice to 3.66 ± 0.3 mg/dl compared to 0.83 ± 0.16 mg/dl in controls (Figure.4.17C). These findings confirm that adriamycin treatment effected on the kidney parameters and induced proteinuria.

As well, the effect of adriamycin treatment on the renal histology was studied. The sections of a kidney from adriamycin mice showed tubular injury with brush border loss, cellular swelling, and patchy tubular dilation, an increase in intratubular cast formations and reduction in the glomeruli. By contrast, mice control showed no obvious histological changes in the kidney structure (Figure 4.17C and D).

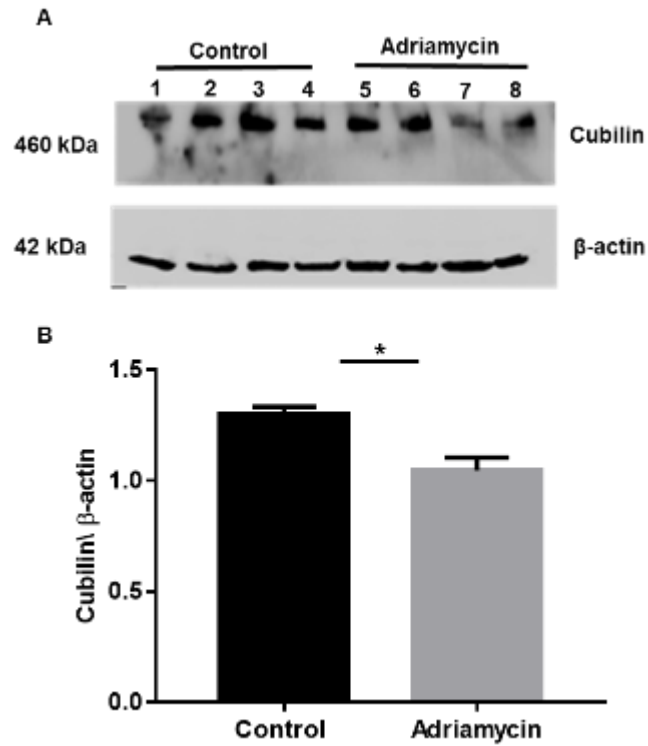


Figure.4.13. Analysis of cubilin protein expression in mouse kidney by immunoblotting.

(A) Kidney lysates from control and adriamycin mice were studied by immunoblotting for cubilin. Representative blots are shown in each group in comparison with a β -actin loading control. (B) Densitometric analysis of the cubilin expression as a ratio to β -actin. Data are expressed as mean \pm SEM of 4 mice in each group. * $p < 0.05$, unpaired t-test and all experiments were performed in triplicate.

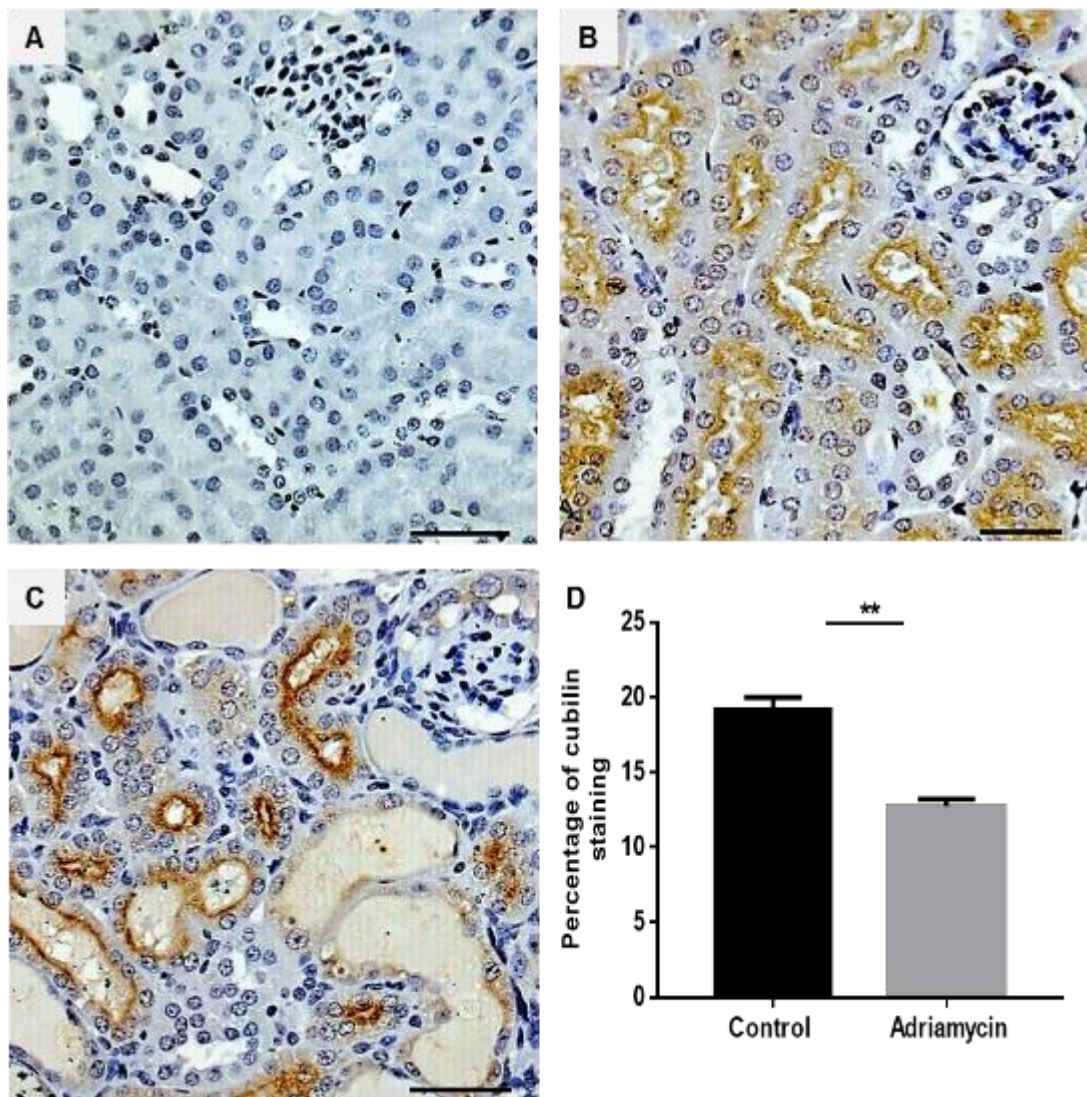


Figure.4.14. IHC analysis of mouse kidney tissue for cubilin in Adriamycin-induced proteinuria.

Representative photomicrographs displaying (A) Negative control sections from control animals treated without primary antibody. (B) Control mice. (C) Proteinuric mice treated with adriamycin. (D) Semiquantitative analysis of cubilin, Data are expressed as mean \pm SEM, **p < 0.01, unpaired t-test test. All IHC was performed in triplicate, Scale bars 100 μ M

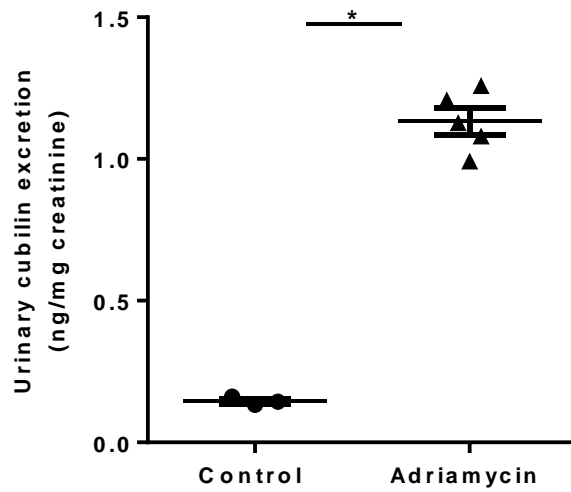


Figure.4.15. Urinary excretion of cubilin in mouse urine by ELISA.

The urine samples from control and adriamycin mice were normalized to creatinine and quantified by ELISA for cubilin. Data are expressed as mean \pm SEM of 3 control and 4 adriamycin mice. * $p < 0.05$, unpaired t-test. Cubilin level was measured in triplicate in each group of mice.

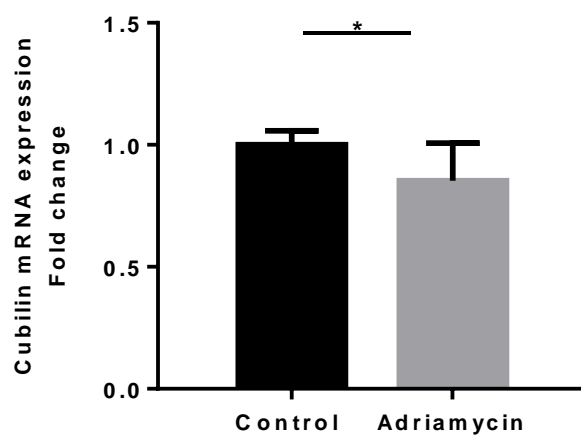


Figure.4.16. Cubilin mRNA in the kidney of adriamycin-induced proteinuric and control mice.

mRNA was extracted from kidney cortex and cubilin quantified by qPCR. Data are expressed as mean \pm SEM of 4 mice of each group, *p < 0.05, unpaired t-test. All qPCR reactions were performed in triplicate.

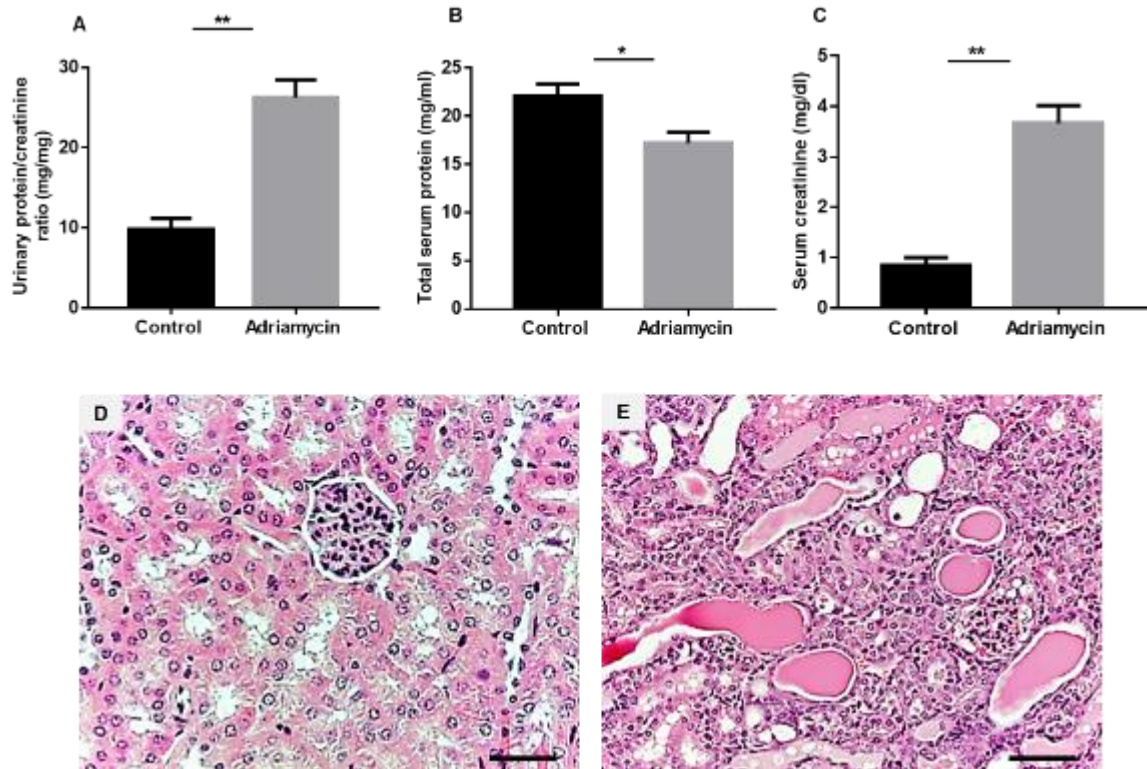


Figure.4.17. Renal histology and parameters of protein excretions in urine and serum of adriamycin mice.

(A) Mouse urine protein /creatinine ratio in adriamycin and control mice **p < 0.01. (B) Mouse total serum protein concentration *p < 0.05. (C) Mouse serum creatinine concentration **p < 0.01. Kidney injury was assessed in H&E stained kidney sections. (D) control mice, and (E) adriamycin mice. Data are expressed as mean \pm SEM of 4 mice in each group.

4.2.3.4. Amnionless expression in the kidney of proteinuric and control mice

To determine whether amnionless protein expression is affected by proteinuria, kidney tissues from each group were investigated by immunoblotting. Amnionless bands at 48 kDa were faint in samples from proteinuric mice in comparison with controls (Figure.4.18A). When quantified, amnionless expression at the protein level was significantly reduced in proteinuric mice (0.37 ± 0.04 relative intensity) compared to controls (1.23 ± 0.03 relative intensity) when normalized to β -actin (Figure.4.18 B).

By IHC, amnionless is typically expressed at the apical membrane of the PTs in normal mice (Figure.4.19 B). In proteinuric mice, amnionless immunostaining reduced in the apical membrane of the PTs (Figure.4.19 C) compared to control mice (Figure 4.19 B). Semiquantitative analysis of the sections demonstrated a significant decrease in the amnionless expression in proteinuric mice ($13.1 \pm 0.9\%$ stained area) compared to control mice ($26.85 \pm 0.8 \%$ stained area) (Figure.4.19 D).

Moreover, the expression of amnionless mRNA was substantially reduced to (0.44 ± 0.059 -fold) in kidney cortex of mice with proteinuria compared to controls (1 ± 0.079 -fold) (Figure 4.20). Amnionless excretion in the urine of proteinuric and control mice was also investigated by ELISA. It was significantly increased in the urine of proteinuric mice (1.404 ± 0.064 ng/mg creatinine) compared to controls (0.28 ± 0.02 ng/mg creatinine) (Figure.4.21 A). Urine was also examined by immunoblotting and this revealed an excess of amnionless in the urine of proteinuric mice. While the urine of control mice did not show amnionless bands (Figure.4.21 B). Mouse kidney lysate was used as a positive control. These data

demonstrated a decrease of amnionless expression associated with urinary shedding of amnionless in proteinuric animals.

.

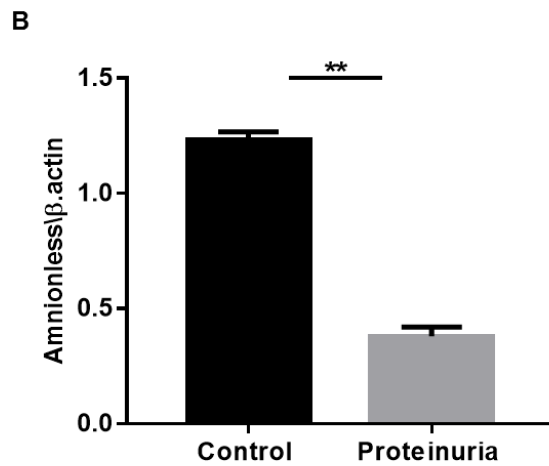
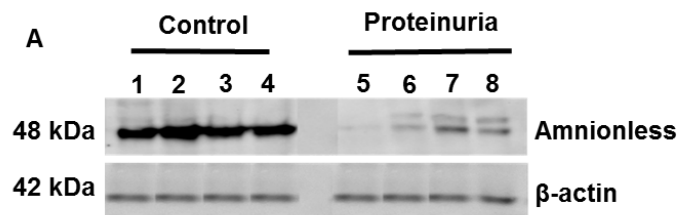


Figure.4.18. Analysis of amnionless expression in mouse kidneys by immunoblotting.

(A) Kidney cortex from control and proteinuric mice was evaluated by immunoblotting for amnionless. Each lane represents a kidney sample from different animal control and proteinuria in comparison with a β -actin loading control. (B) Densitometric analysis of amnionless expression for control and proteinuric animals expressed as a ratio to β -actin. ** $p < 0.01$, unpaired t-test. All experiments were conducted in triplicate.

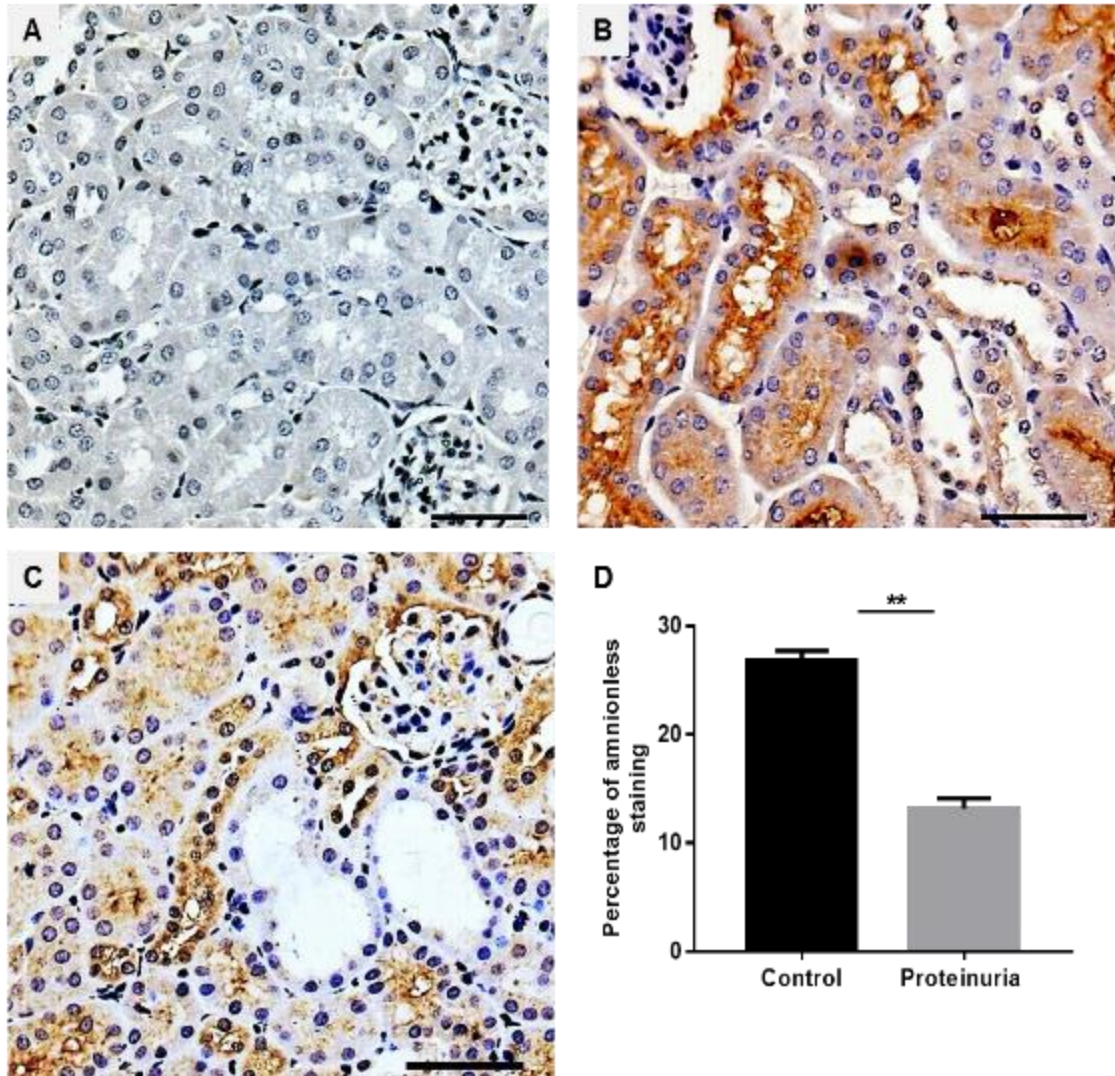


Figure.4.19. IHC analysis of mouse kidney tissue for amnionless in control and proteinuric mice with protein overload proteinuria.

Representative photomicrographs showing (A) Negative control sections prepared without primary antibody. (B) Control mice. (C) Proteinuric mice. (D) Semiquantitative analysis of amnionless staining. Data are expressed as mean \pm SEM, **p < 0.01, unpaired t-test. Scale bars 100 μ m.

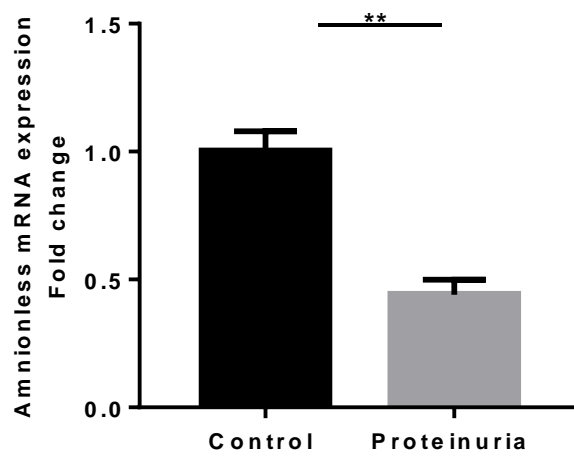


Figure.4.20. Fold change in amnionless mRNA expression in kidneys of proteinuric and control mice.

mRNA was extracted from kidney cortex and subjected to qPCR. Data are mean \pm SEM of 4 mice in each group. The ** $p < 0.01$, unpaired t-test. qPCR was performed in triplicate for each group.

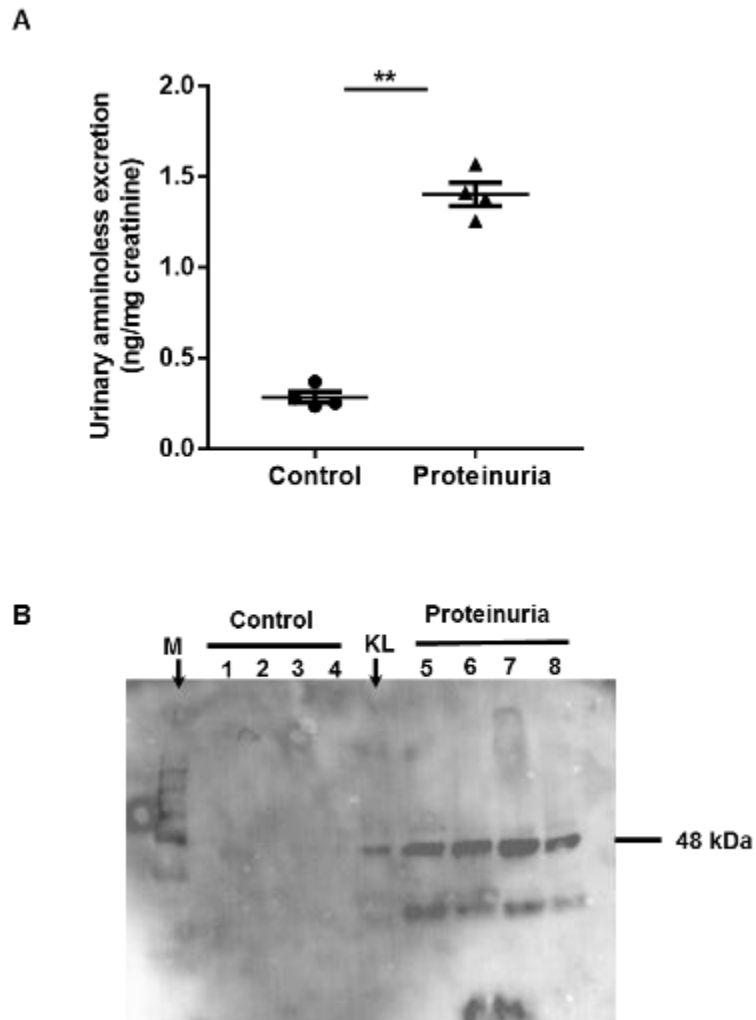


Figure.4.21. Urinary Excretion of amniocless in mouse urine.

(A) Urine samples from control and proteinuric mice normalized to creatinine were quantifying by ELISA for amniocless. Results are expressed as mean \pm SEM of 4 mice in each group. $**p < 0.01$, unpaired t-test. (B) Representative immunoblot showing the urinary amniocless excretion by proteinuric and control mice, compared to the positive control, mouse kidney lysate (KL).

4.2.4. Effect of protein overload proteinuria on proximal tubular DPP-IV

DPP-IV is commonly expressed on the brush border membranes of the absorptive epithelial such as PTs, small intestine and in the glomerular capillary walls (Hopsu-Havu and Ekfors, 1969, Chatelet et al., 1986). Previous investigators have used the proximal tubular expression of DPP-IV as a control protein (Santoyo-Sanchez et al., 2013). To investigate whether DPP-IV is affected by proteinuria, kidney tissues from control and proteinuric mice were studied using immunoblotting and IHC. By immunoblotting, DPP-IV bands at 110 kDa were similarly expressed in control and proteinuric mice (Figure.4.22 A). When quantified, both endocytic protein receptors were significantly reduced in proteinuric mice, for example, cubilin (0.29 ± 0.03 relative intensity) and amnionless (0.39 ± 0.017 relative intensity), while in controls, cubilin was at (1.05 ± 0.02 relative intensity) and amnionless was (1.1 ± 0.02 relative intensity) when normalized to DPP-IV (Figure.4.22 B).

In IHC, DPP-IV expressed at the apical membrane of the PTs and glomeruli in normal mice. In proteinuric mice, there was no alteration of DPP-IV expression (Figure.4.23). This confirms no significant difference in DPP-IV expression either in control ($20.2 \pm 0.19\%$ stained area) or proteinuric animals ($20.2 \pm 0.74\%$ stained area) (Figure.4.23 D).

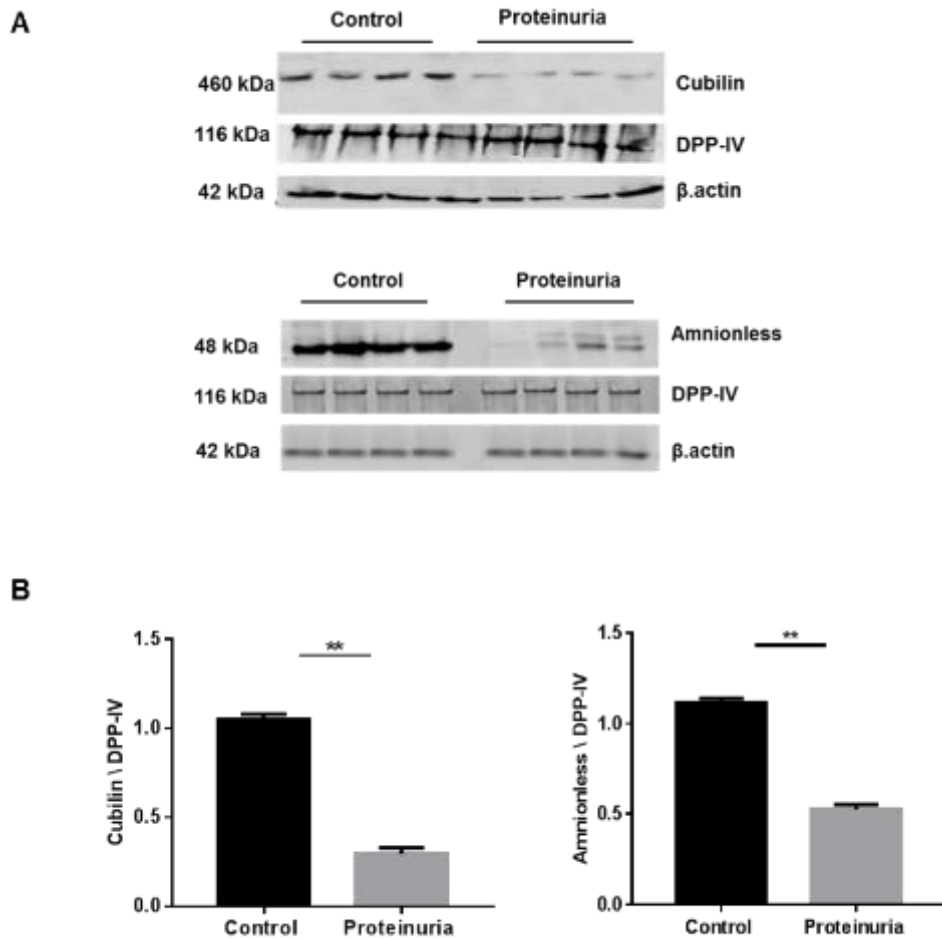


Figure.4.22. Analysis of DPP-IV expression in mouse kidney by immunoblotting. (A) Kidney cortex from control and proteinuric mice was evaluated by immunoblotting for previous amnionless and cubilin blots in comparison with DPP-IV proximal tubular marker and β -actin loading control. (B) Densitometric analysis of cubilin and amnionless expression for control and proteinuria expressed as a ratio to DPP-IV, 4 mice in each group, $**p < 0.01$, unpaired t-test.

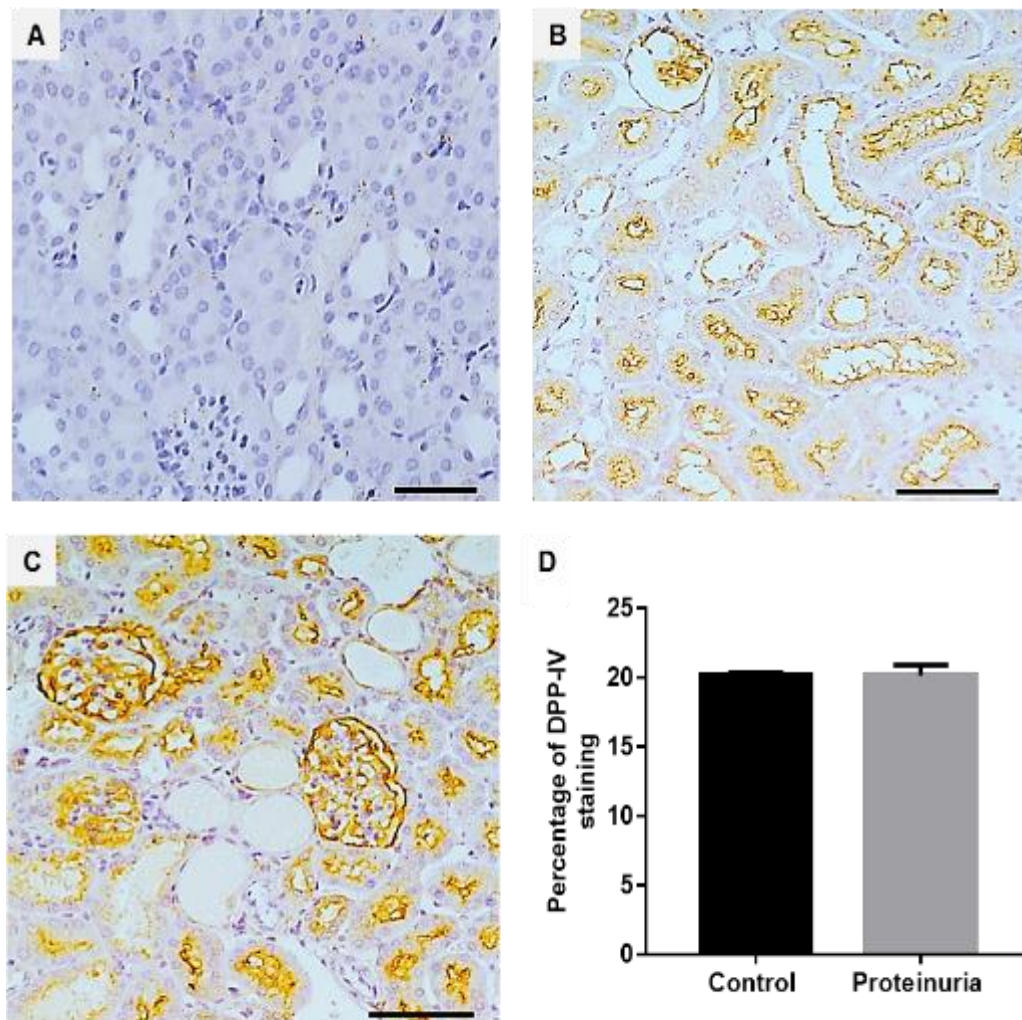


Figure.4.23. IHC analysis of mouse kidney tissue for DPP-IV in control and proteinuric mice with protein overload proteinuria.

Representative photomicrographs showing (A) Negative control sections from control animals prepared without primary antibody. (B) Control mice. (C) Proteinuric mice. (D) Semiquantitative analysis of DPP-IV staining. $p=ns$, unpaired t-test. Scale bars 100 μ M.

4.2.5. Effect of protein overload proteinuria on aquaporin-1

AQP-1 water channel protein is normally expressed in the PTs of the kidney (Maunsbach et al., 1997). To define AQP-1 protein expression in proteinuria, kidney tissues from each group of mice were studied by immunoblotting and IHC. AQP-1 bands at 32 kDa were clearly reduced in proteinuric mice in comparison with controls (Figure.4.24A). When quantified, the AQP-1 protein was significantly decreased in proteinuric mice (0.203 ± 0.03 relative intensity) compared to controls (1.024 ± 0.04 relative intensity) when normalised to β -actin (Figure.4.24B).

In comparison with the controls (Figure 4.25B), AQP-1 immunostaining was reduced at the apical membrane of PTs in mice with proteinuria (Figure 4.24C). The semiquantitative analysis confirmed a significant decline in AQP-1 expression in proteinuric mice (9.49 ± 0.147 %stained area) compared to control mice (19.64 ± 0.83 %stained area) (Figure.4.25D). For urinary AQP-1 excretion do not examine in proteinuric mice. Taken together, these results indicate that proteinuria has an adverse influence on the AQP-1 expression in the kidneys of mice.

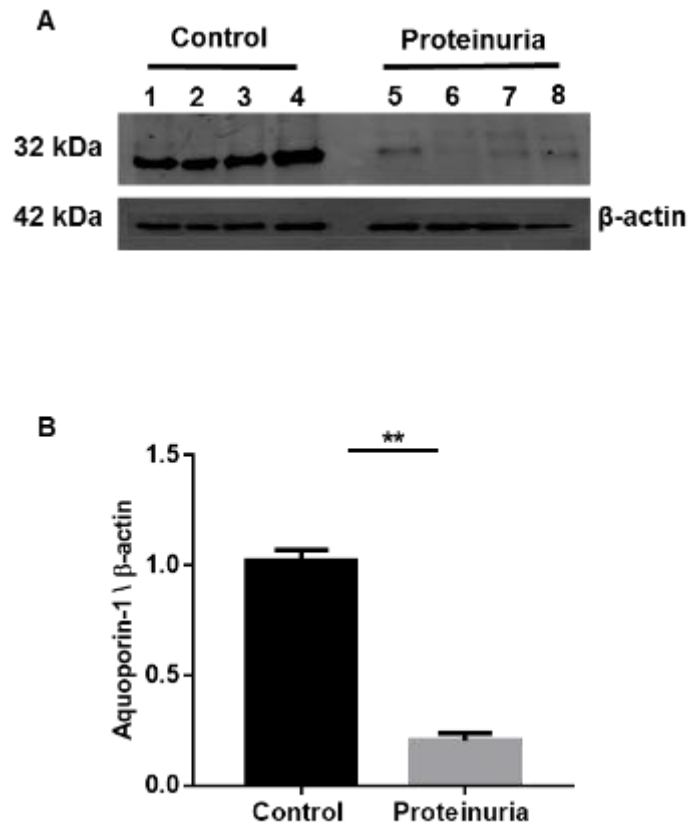


Figure.4.24. Analysis of AQP-1 in mouse kidneys by immunoblotting.

(A) Kidney cortex of control and proteinuric mice was evaluated by immunoblotting for AQP-1 alongside β -actin as a loading control. Each lane represents an individual animal. (B) Densitometric analysis of AQP-1 expression for control and proteinuric animals expressed as a ratio to β -actin. **p < 0.01, unpaired t-test and 4 mice for each group.

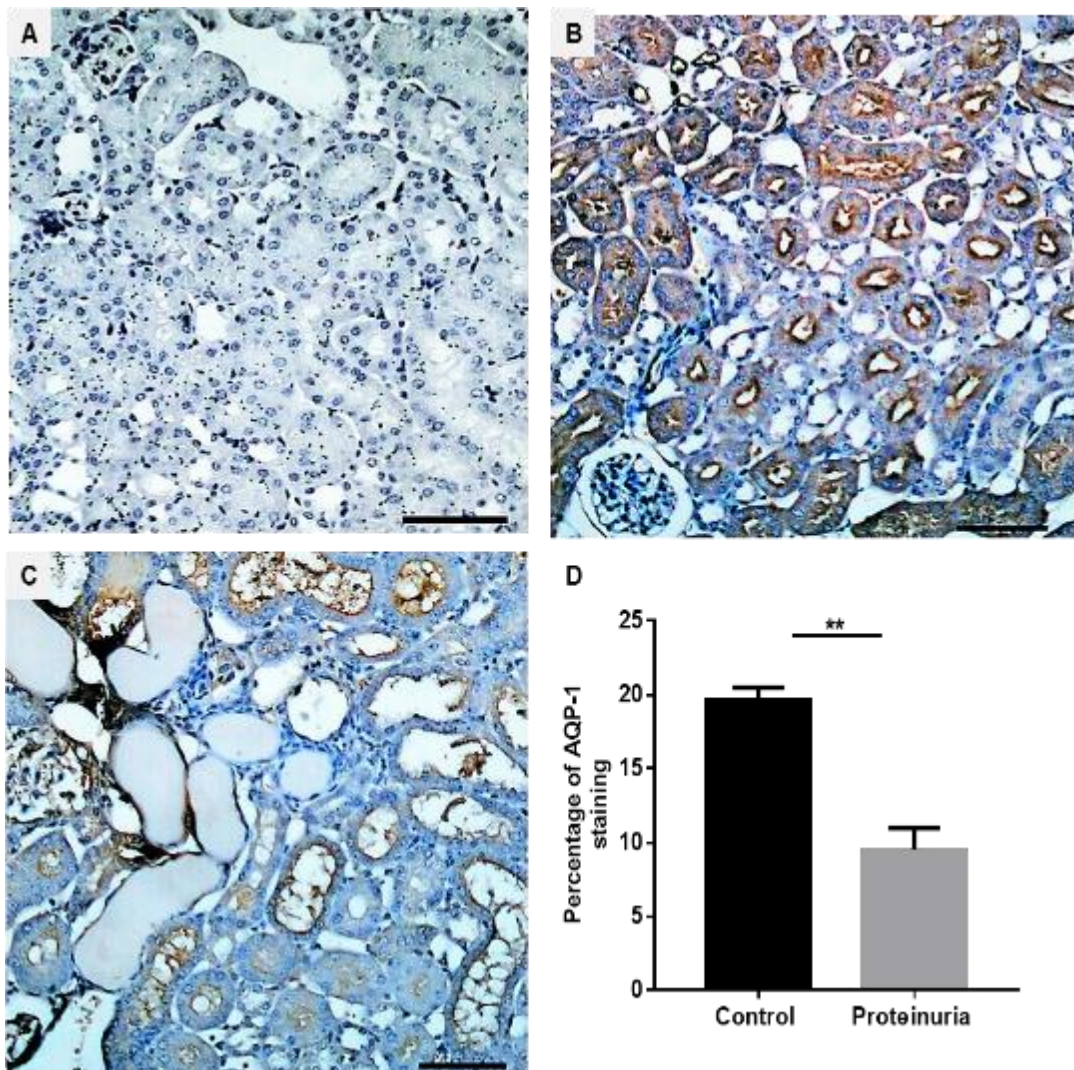


Figure.4.25. IHC analysis of mouse kidney tissue for AQP-1 in control and proteinuric mice with protein overload proteinuria.

Representative photomicrographs showing (A) Negative control sections from control animals prepared without primary antibody, (B) Control mice. (C) Proteinuric mice. (D). Semiquantitative analysis of AQP-1 staining. Data are expressed as mean \pm SEM of 4 mice in each group, ** $p < 0.01$ unpaired t-test. Scale bars 100 μ M.

.2.6. Effect of protein overload proteinuria on MMPs

MMPs are a large family of zinc-dependent matrix degradation enzymes (Tan and Liu, 2012). MMPs have an important role in proteinuria and progression of renal impairment have been identified (Zeisberg et al., 2006). To explore whether MMPs expression is affected by protein overload proteinuria, kidney tissue from each group was examined by immunoblotting and IHC. MMP2 bands at 72 kDa were observed in samples from proteinuric mice compared to controls (Figure.4.26 A). When quantified, MMP-2 expression was significantly higher in proteinuric mice (2.5 ± 0.17 relative intensity) than (0.19 ± 0.04 relative intensity) in controls (Figure.4.26 B). In addition, IHC revealed a significant rise in MMP2 expression in the PTs of proteinuric mice (26.1 ± 0.97 % stained area) compared to control mice (2.4 ± 0.11 % stained area) (Figure 4.27D).

Similarly, blotting for MMP-3 revealed bands at 53 kDa, considerably increase in mice with proteinuria (2.28 ± 0.35 relative intensity) compared to controls (0.29 ± 0.1 relative intensity) when normalized to β -actin (Figure.4.26). This finding was confirmed by IHC result which showed a noticeable increase in MMP-3 expression in glomeruli of proteinuric mice and some in tubules (16.94 ± 1.0 % stained area) in comparison with controls (1.6 ± 0.20 % stained area) (Figure 4.28).

Moreover, MMP-7 bands detected at 22 kDa, a significant rise in proteinuric mice (2.3 ± 0.26 relative intensity) compared to controls (0.76 ± 0.05 relative intensity) (Figure.4.26). This was also confirmed by IHC which revealed a significant increase in MMP-7 expression in PT of proteinuric animals (21.49 ± 0.71 % stained area) in comparison with controls (3.01 ± 0.1 % stained area) (Figure.4.29).

In addition, MMP-9 bands observed at 92 kDa, when quantified, were significantly greater in proteinuric mice (2.47 ± 0.11 relative intensity) compared to controls (0.38 ± 0.07 relative intensity) (Figure.4.26). IHC results also confirmed these findings, a significant increase of MMP-9 in PT of proteinuric animals ($22.0 \pm 0.7\%$ stained area) compared to controls ($2.1 \pm 0.3\%$ stained area) (Figure.4.30). These results, therefore, demonstrate that protein overload proteinuria results in a general increase in MMP expression in the kidneys of proteinuric animals.

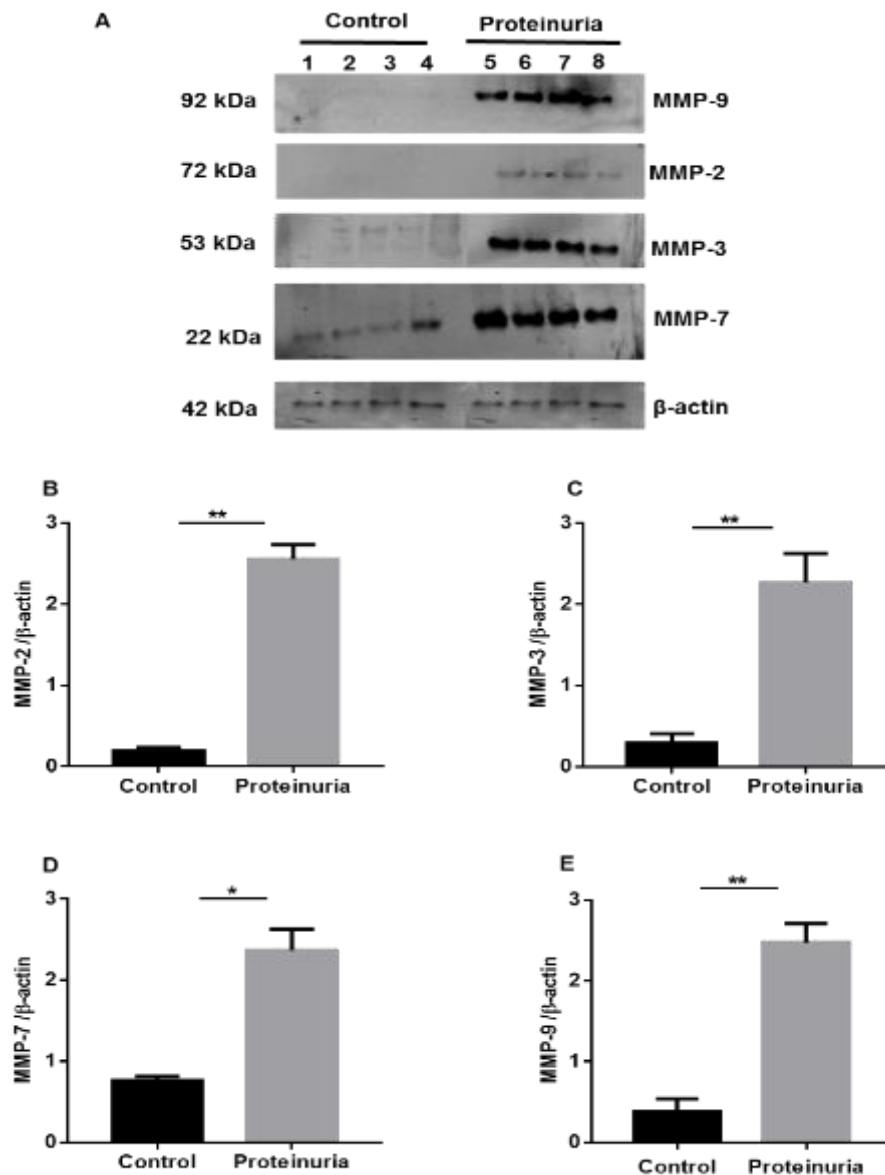


Figure.4.26. Analysis of MMPs expression in mouse kidneys by immunoblotting.

(A). Kidney cortex from control and proteinuric mice was examined by immunoblotting for MMPs. Blots stripped and reprobbed for multiple MMPs and β -actin loading control. (B, C, D, E). Densitometric analysis of MMPs expression for control and proteinuric mice expressed as a ratio to β -actin. * $p < 0.05$, ** $p < 0.01$ unpaired t-test. All experiments were done in triplicate.

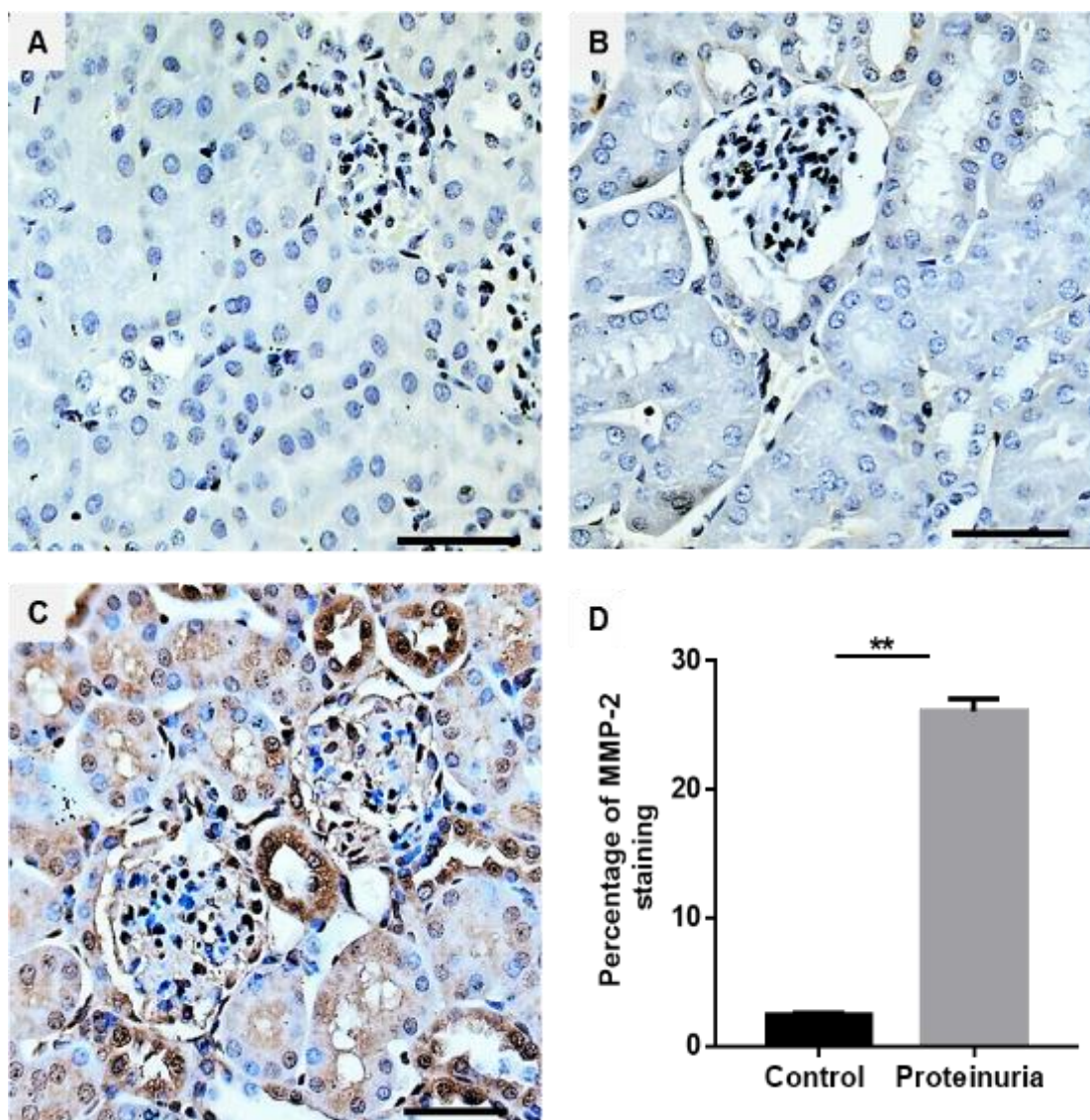


Figure.4.27. IHC analysis of mouse kidney sections for MMP-2 in control and proteinuric mice with protein overload proteinuria.

Representative photomicrographs showing (A) Negative control sections from control animals prepared without primary antibody. (B) Control mice. (C) Proteinuria mice. (D) Semiquantitative analysis of MMP-2 staining. Data are expressed as mean \pm SEM, ** $p < 0.01$, unpaired t-test. Scale bars 100 μ M.

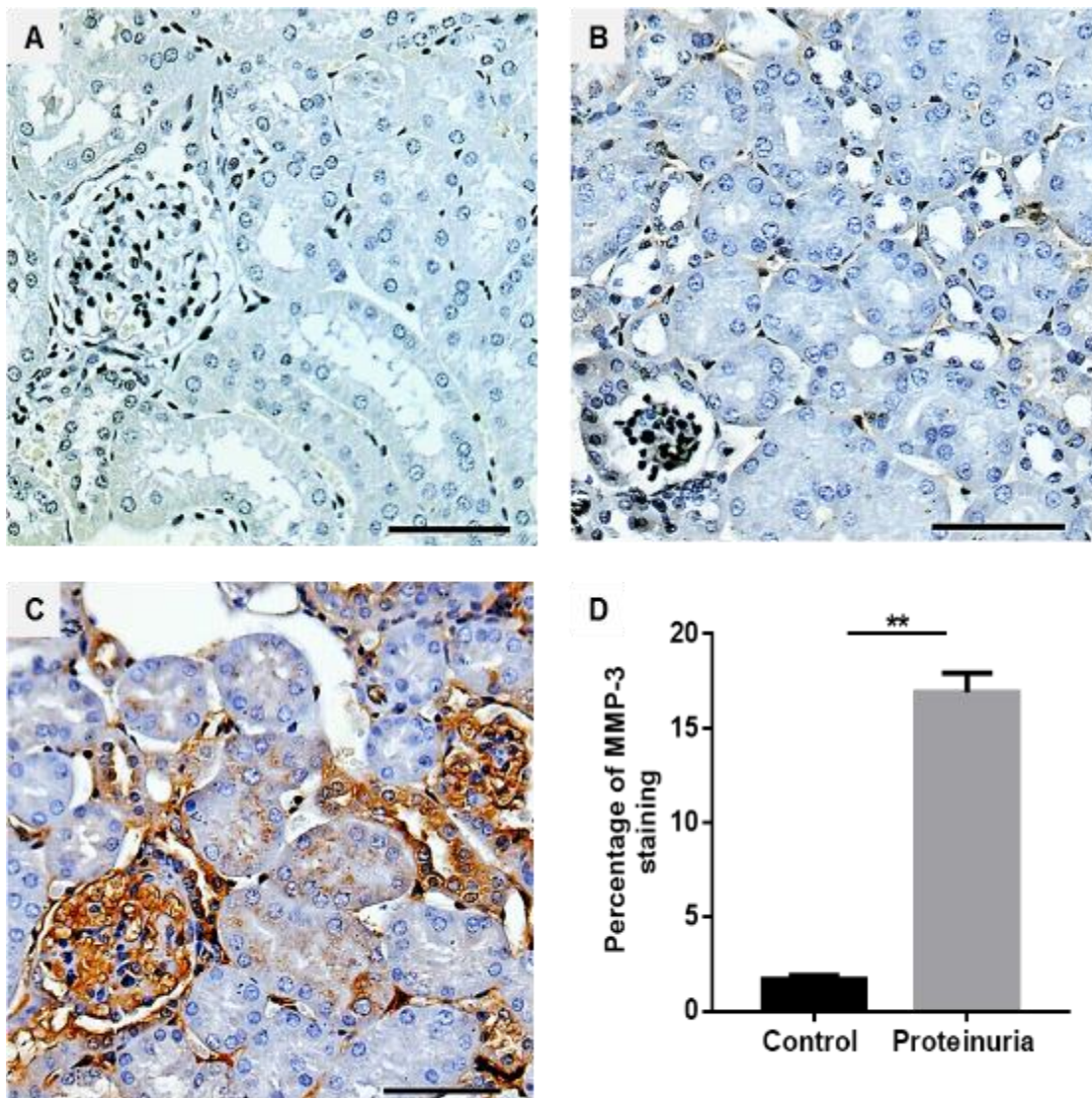


Figure.4.28. IHC analysis of mouse kidney sections for MMP-3 in control and proteinuric mice with protein overload proteinuria.

Representative photomicrographs showing (A) Negative control sections from control animals prepared without primary antibody. (B) Control mice. (C) Proteinuric mice. (D) Semiquantitative analysis of MMP-3 staining. Data are expressed as mean \pm SEM, ** $p < 0.01$, unpaired t-test. Scale bars 100 μ M.

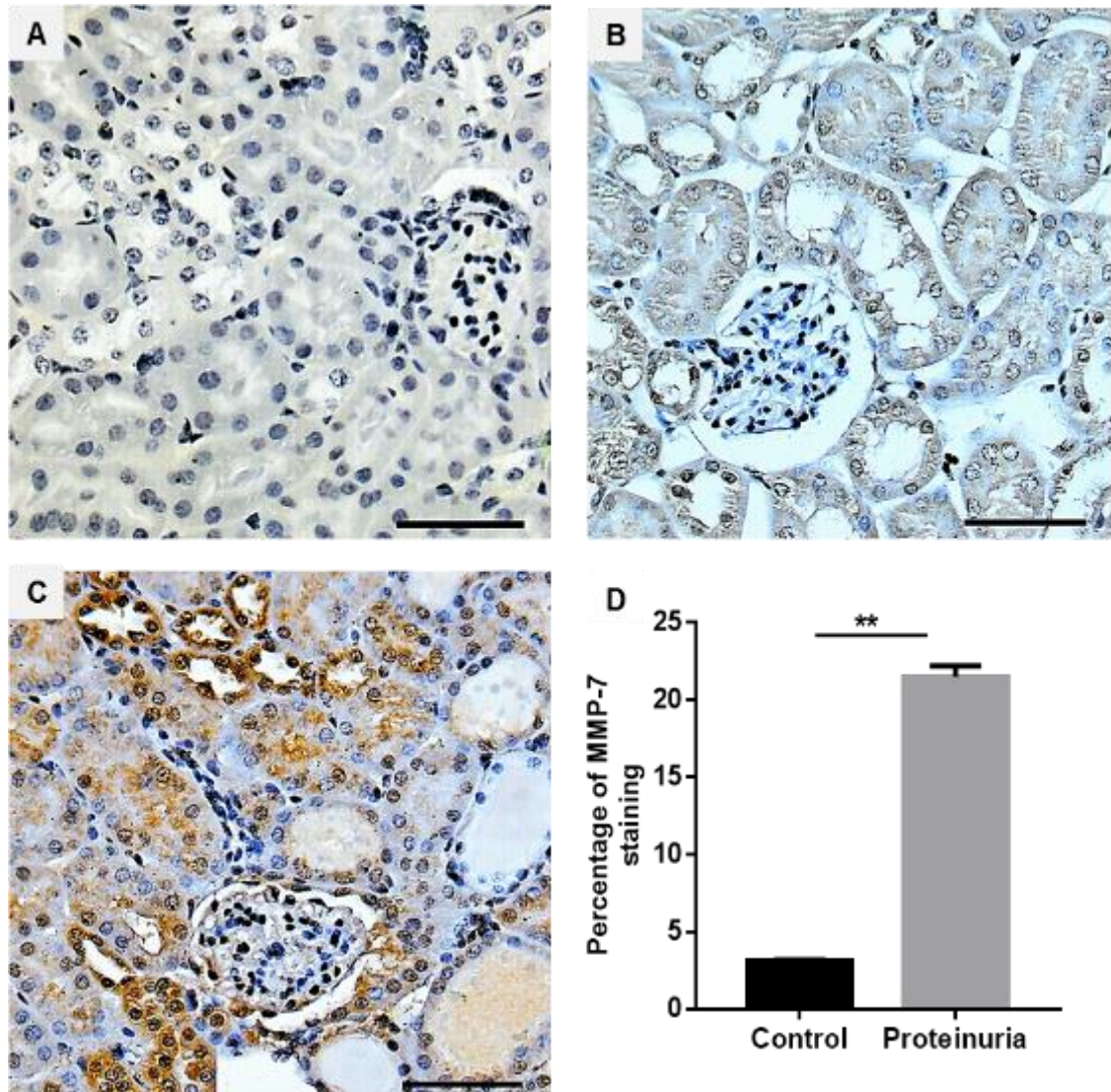


Figure.4.29. IHC analysis of mouse kidney sections for MMP-7 in control and proteinuric mice with protein overload proteinuria.

Representative photomicrographs viewing (A) Negative control sections from control animals prepared without primary antibody. (B) Control mice (C) Proteinuric mice. (D) Semiquantitative analysis of MMP-7 staining. Data are expressed as mean \pm SEM, ** $p < 0.01$, unpaired t-test. Scale bars 100 μ M.

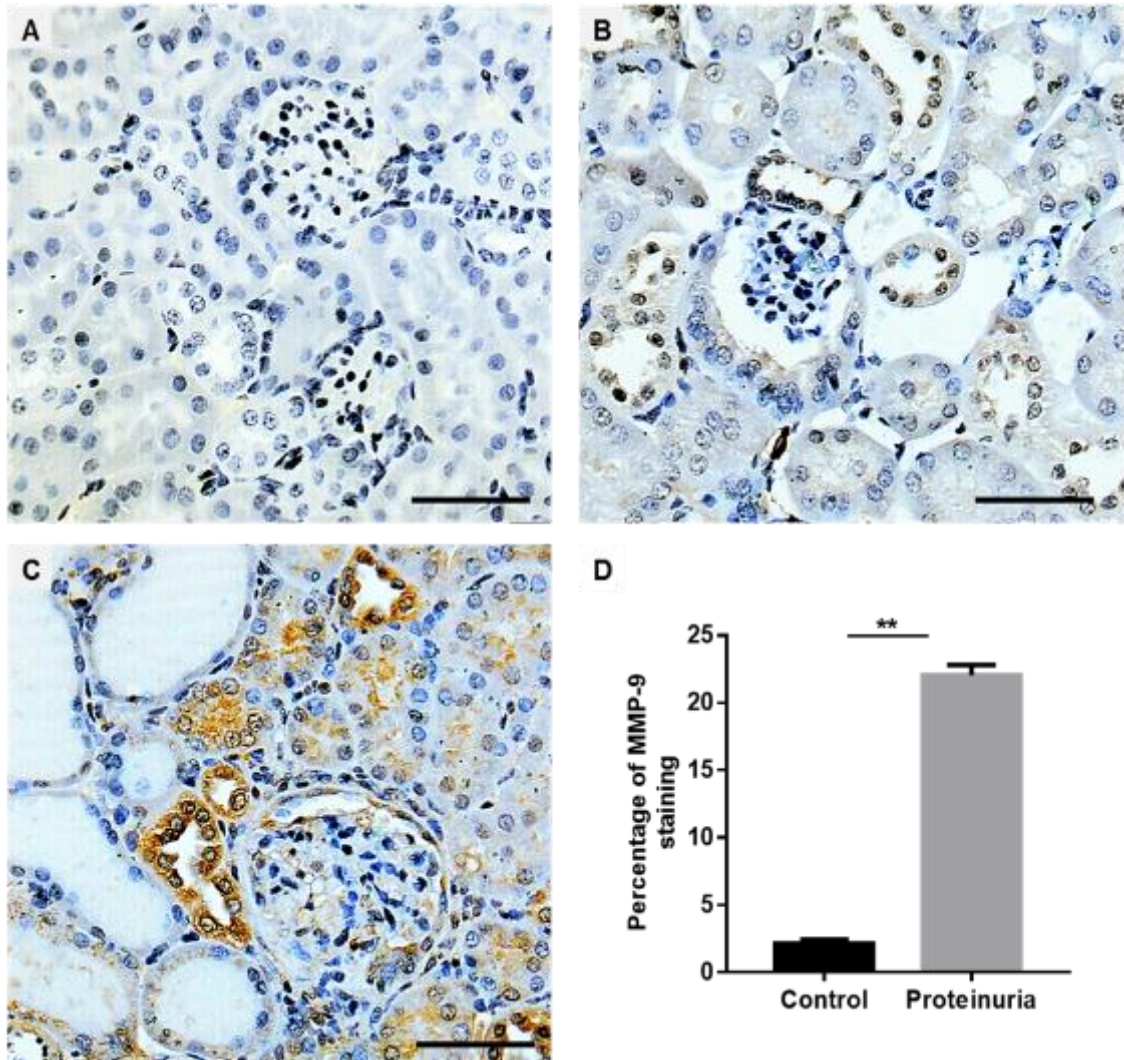


Figure.4.30. IHC analysis of mouse kidney tissue for MMP-9 in control and proteinuric mice with protein overload proteinuria.

Representative photomicrographs viewing (A) Negative control sections from control animals prepared without primary antibody. (B) Control mice. (C) Proteinuric mice. (D) Semiquantitative analysis of MMP-9 staining. Data are expressed as mean \pm SEM, ** $p < 0.01$, unpaired t-test. Scale bars 100 μ M.

4.3. Discussion

These results present a comprehensive study of the cubam protein endocytic complex expression in proteinuria. The results reveal a general reduction in protein expression of both the cubilin and amnionless components of cubam in the PTCs of proteinuric animals accompanied by a similar reduction in mRNA expression for both cubam components. At the same time, there is an increase in urinary cubam excretion. Therefore, the decrease in renal cubam expression in proteinuria is explained by a reduction in gene transcription combined with urinary receptor shedding.

Phenotypically the protein overload model in this study is similar to previously described mouse models associated with a rise in serum creatinine and a significant increase in urinary protein excretion (Ishola et al., 2006, Eddy et al., 2000, Donadelli et al., 2000, Donadelli et al., 2003). Despite different mouse models of proteinuria, the current model is identical to tubulointerstitial damage and is a non-glomerular or immune injury model (Eddy and Giachelli, 1995). Eddy et al (1995) showed that induced proteinuria increased matrix protein synthesis and changed matrix remodelling/degradation that leading to tubulointerstitial inflammation (Eddy and Giachelli, 1995). In addition, Donadelli et al (2003) revealed that an increase in serum creatinine indicates mild impairment of renal function and develops proteinuria attributed to fractalkine gene stimulation through NF-kB and p38 activation in proximal tubular cells (Donadelli et al., 2003). Therefore, the present protein overload proteinuria model allows focussing on the effect of ultrafiltered proteins such as albumin on protein expression of endocytic receptors more precisely due to an increase in transcapillary movement of albumin into the urinary space. Furthermore, in the current study mice were injected with

low endotoxin BSA fatty acid-free for two weeks to minimise tubular injury; however, albumin-bound to fatty acids has more effect on tubular damage (Kamijo et al., 2002).

In comparison with the current model, the adriamycin model develops proteinuria by damaging the glycocalyx layer of glomerular endothelial cells (Jeansson et al., 2009), with changes in renal functions and structures that resemble focal segmental glomerular sclerosis which develops over a long time (Wang et al., 2000). In the present study, creatinine increased in the serum of proteinuric mice. In the previous study experimental models showed that decreased interstitial mononuclear cell infiltration associated with improved creatinine clearance and decreased serum creatinine (Lan et al., 1993). This could explain that tubulointerstitial damage associated with an increase in serum creatinine.

The previous literature described the urinary loss of tubular protein endocytotic receptors in proteinuric patients and in animal models of renal disease. For instance, an increase of cubilin in the urine is associated with microalbuminuria in patients with Type 1 diabetes (Thraillkill et al., 2009b). Coffey et al 2015, suggested that urinary cubilin may be used as a biomarker in patients with Type 1 diabetes where urinary shedding of cubilin arises prior to the development of microalbuminuria (Coffey et al., 2015). A mouse model of type 1 diabetes showed a decline of cubilin expression in the PTs: this correlated with an increase in urinary cubilin excretion in diabetic animals (Coffey et al., 2015). Nevertheless, another study revealed that cubilin expression was increased in patients with nephrotic syndrome (YANG Jurong, 2008).

A further study describes significantly down-regulated cubilin expression in Goto-Kakizaki (GK) rats with diabetic nephropathy. This study found that advanced

glycation end products (AGEs) reduce albumin uptake by suppressing cubilin (Ke et al., 2014). In addition, a proteinuric dog model of Alport disease found cubilin in the urine of animals along with other proteins. This study suggests that an increase in glomerular permeability and change in cubilin-mediated endocytosis ultimately led to proteinuria (Vinge et al., 2010).

Previous investigators have described the joint function of cubilin and amnionless as a cubam complex (Fyfe et al., 2004). For example, Imlerslund-Grasbeck syndrome (IGS) patients with amnionless mutations also lack cubilin expression, and this leads to the excretion of protein in the urine (Amsellem et al., 2010). Similarly, IGS studies in dogs revealed that effective cubam expression does not occur in the absence of amnionless, which leads to a failure of apical cubilin expression and proteinuria (He et al., 2005). A study on chimeras with amnionless deficient cells has a proximal tubule dysfunction that showed an elevation of albumin level (Strope et al., 2004). Therefore, these studies reveal a connection between amnionless as a necessary component of the cubilin receptor. This has also been supported by the present study in which amnionless expression demonstrated a significant decrease in proteinuric animals' kidney associated with urinary shedding of amnionless. Likewise, is the similar effect of proteinuria on the cubilin receptor.

The current study shows a decrease of cubilin and amnionless mRNA levels in proteinuric mice, although the mechanism of endocytic receptor gene regulation in the proteinuric kidney is uncertain. However, expression of cubilin is regulated at both gene and protein levels in the PTs by transcriptional regulation of peroxisome proliferator-activated receptor (PPAR) (Aseem et al., 2013). Moreover, an amelioration of protein overload proteinuria by PPAR agonists was

observed in other studies, that associated with an increase of cubilin level (Aseem et al., 2013). In vivo study of acute kidney injury (AKI) revealed down-regulated expression of cubilin mRNA, which was parallel with an increase of albumin concentration and albumin/creatinine ratio in the urine of experimental endotoxemia (Schreiber et al., 2012). Cubilin may be more quickly degraded in cells that have amnionless gene silenced, this might explain an important mutual interaction between amnionless and cubilin in the intracellular stability of the cubam complex (Ahuja et al., 2008).

The present study showed a reduction of cubilin protein and mRNA level in the kidney of adriamycin-induced proteinuria associated with an increase in urinary cubilin excretion. However, anti-cubilin antisense RNA delivered by an adenoviral vector improved the albuminuria-induced glomerulosclerosis and tubulointerstitial damage in adriamycin nephrotic rats. This could be targeted by cubilin as a therapeutic agent in this model of proteinuric nephropathy (Liu et al., 2011).

Cubilin mediated endocytosis is responsible also for the absorption of proteins and nutrients in the intestine (Kozyraki et al., 2001, Barth and Argraves, 2001). Cubilin dysfunction either by deletions or mutations in the cubilin gene or its partner leads to vitamin B₁₂ deficiency because of malabsorption in the small intestine. This associated with proteinuria that developed due to PT's failure to absorb filtered proteins (Storm et al., 2011, Storm et al., 2013, Wahlstedt-Froberg et al., 2003). However, in the current study of protein overload proteinuria revealed that cubilin expression at both protein and mRNA level was not changed in the small intestine. Ultimately, according to our data, there is no systemic effect on cubilin beyond the kidney.

The current study also exhibited a substantial reduction of AQP-1 expression level in PTs of proteinuric animals. In an autosomal dominant form of diabetes patients experienced a significant decrease in cubilin expression accompanying proteinuria, whereas AQP-1 expression was significantly increased (Terry et al., 2016). Moreover, in mouse kidneys with defective endocytosis due to a defect in chloride channel CIC-5 constitutively enhanced expression of AQP-1 in the PTs was seen (Pohl et al., 2015).

Interestingly, the expression of MMP-2, MMP-3, MMP-7, and MMP-9 all significantly increased in the current study of protein overload proteinuria. Albumin at diverse doses enhances the expression and activity of MMP-2 and MMP-9 in mouse podocytes (Zheng et al., 2009). Similarly, primarily cultured rat tubule epithelial cells incubated with albumin increased the expression and secretion of MMP-9. Therefore, MMP-9 secretion may be driven by albumin endocytosis in these cells via the ERK signalling pathway (Chen et al., 2017). Eddy et al (2000) revealed that the activity of MMP-9 increased in a mouse model of protein overload (Eddy et al., 2000). These observations are consistent with the present work that showed a significant increase in the MMPs activities in proteinuric animals. MMPs activity and expression was also detected in the urine of patients with diabetic nephropathy (Thraill et al., 2007, Thraill et al., 2009a). These enzymes activity may be enhanced in the parenchyma and tubular lumen of the diabetic kidney where the cubam complex is shed from PT surfaces (Thraill et al., 2009b).

An increase in MMP activity induced by proteinuria may contribute to shedding by driving regulated intramembrane proteolysis (RIP). RIP plays an important role in the regulation of a large number of transmembrane proteins (Lichtenthaler et al.,

2011, Lal and Caplan, 2011). There are many functional sheddases including proteases of the disintegrin and metalloprotease (ADAM) family, MMPs and, gamma-secretase. These substrates of RIP are sequentially cleaved to release an extracellular domain and a small intracellular fragment called intracellular domain (Lichtenthaler et al., 2011). Shedding is generally increased by activation of protein kinase-C, occurs close to the cell membrane and blocked by metalloproteinase inhibitors (Hooper et al., 1997, Werb and Yan, 1998).

Previous studies revealed that megalin a transmembrane protein is targeted by metalloproteinase-mediated shedding regulated by protein kinase-C. The RIP process released megalin ectodomain into the tubular lumen; however, it leaves an intracellular domain of the receptor. This part works as a substrate for gamma-secretase to release intracellular megalin domain that is potentially phosphorylated and has intrinsic signalling capacity (Zou et al., 2004, Biemesderfer, 2006). There is evidence that RIP of megalin may also occur in proteinuric patients. An individual with diabetic nephropathy and albuminuria substantially increased urinary shedding of the extracellular domain of megalin compared with non-albuminuric diabetic patients. Therefore, it could be supposed that this is mediated by an increase in MMP activity in the diabetic kidney (Thraill et al., 2009a). Though the mechanism of cubam complex excretion in the urine is unresolved, as a consequence of their close association with megalin, this may potentially be pulled free from the apical membranes of PTs as a consequence of megalin ectodomain shedding (Fatah et al., 2017). This might clarify why the cubam complex was excreted in the urine and reduced in the PTs in the present studies.

Overall protein excretion in the urine, especially albumin is the result of both glomerular permselectivity and tubular reabsorption and this issue is still a debated subject (Dickson et al., 2014, Peti-Peterdi, 2009, Comper et al., 2008b). Previous studies revealed that tubular reabsorption of glomerular filtered proteins is contributing to proteinuria (Dickson et al., 2014, Comper et al., 2008b). This might show a relation between urinary protein excretion and impaired glomerular permselectivity (Peti-Peterdi, 2009). The current study could not determine between the increased glomerular leakage and /or decreased proximal tubular reabsorption of filtered protein via cubam complex endocytic receptors in proteinuria. These observations suggest that reducing tubular reabsorption of filtered proteins because of reduced expression of these endocytic receptors could likely contribute to a part of the increased urinary protein excretion.

Eventually, in proteinuria, expression of both essential protein re-absorptive receptors is considerably reduced in the proximal tubular cells connected with a rise of urinary shedding of cubilin and amnionless. Moreover, an increase of matrix metalloprotease activity in proteinuria is associated with the urinary loss of these receptors. Cubilin and amnionless may be used as potential markers in the proteinuric nephropathy.

Chapter Five

Effect of Matrix Metalloproteinase Inhibition on the Kidney Expression of Cubam in Protein Overload Proteinuria in Mice

5.1. Introduction

PTs are adversely affected by abnormal filtered proteins that contribute to renal inflammation and fibrosis. Renal fibrosis is a common process promoted by epithelial remodelling, inflammation, fibroblast activation, and reorganization of cellular interactions including extracellular matrix (Ronco and Chatziantoniou, 2008). Extracellular matrix proteins are regulated by extra-cellular MMPs zinc-dependent matrix-degrading proteases (Turck et al., 1996, Woessner, 1999). MMP activity is elevated in the urine of diabetic patients with diabetic nephropathy (Thraikill et al., 2007, Thraikill et al., 2009a) which may indicate a role for MMPs in the shedding of endocytic receptors from the proximal tubule surfaces (Thraikill et al., 2009b).

The previous chapter described reduced cubam complex in the kidneys of proteinuric animals in association with significantly increased MMP activity. The effect of inhibition of MMP activity in proteinuric kidney disease has not been studied. The main objective of the following experiments was to investigate the effect of MMP inhibition on cubam expression in protein overload nephropathy.

5.2. Results

5.2.1. Effect of MMPI treatment on urine biochemistry in proteinuria

The effect of MMPI treatment on urine biochemistry and protein excretion in the proteinuria was investigated. The total urinary protein concentration showed a significant increase in proteinuric mice to 61.2 ± 0.75 mg/ml compared with 17.6 ± 2.05 mg/ml in controls, while MMPI treated mice showed a significant reduction to 22.1 ± 2.5 mg/ml (Figure.5.1A).

Urinary albumin concentration was also increased in proteinuric mice to 6.1 ± 0.4 mg/dl in comparison with controls to 0.8 ± 0.2 mg/dl. However, the MMPI treatment showed a substantial decrease to 1.5 ± 0.21 mg/dl in protein injected mice (Figure.5.1B). Moreover, urinary creatinine was significantly raised to 2.0 ± 0.9 mg/dl in MMPI treated mice compared to proteinuric mice 1.5 ± 0.25 mg/dl, while controls mice were 2.2 ± 0.6 mg/dl (Figure.5.1C).

To correct urinary concentration, the urine PCR ratio was calculated and found to be 44.21 ± 4.1 mg/mg in proteinuric animals. While urine PCR of MMPI treatment groups reduced to 14.2 ± 2.15 mg/mg compared with controls (11.02 ± 1.67 mg/mg) (Figure.5.1D). These findings confirm that MMPI treatment preserved urine biochemistry and protein within the normal limit range by inhibition of MMP activity.

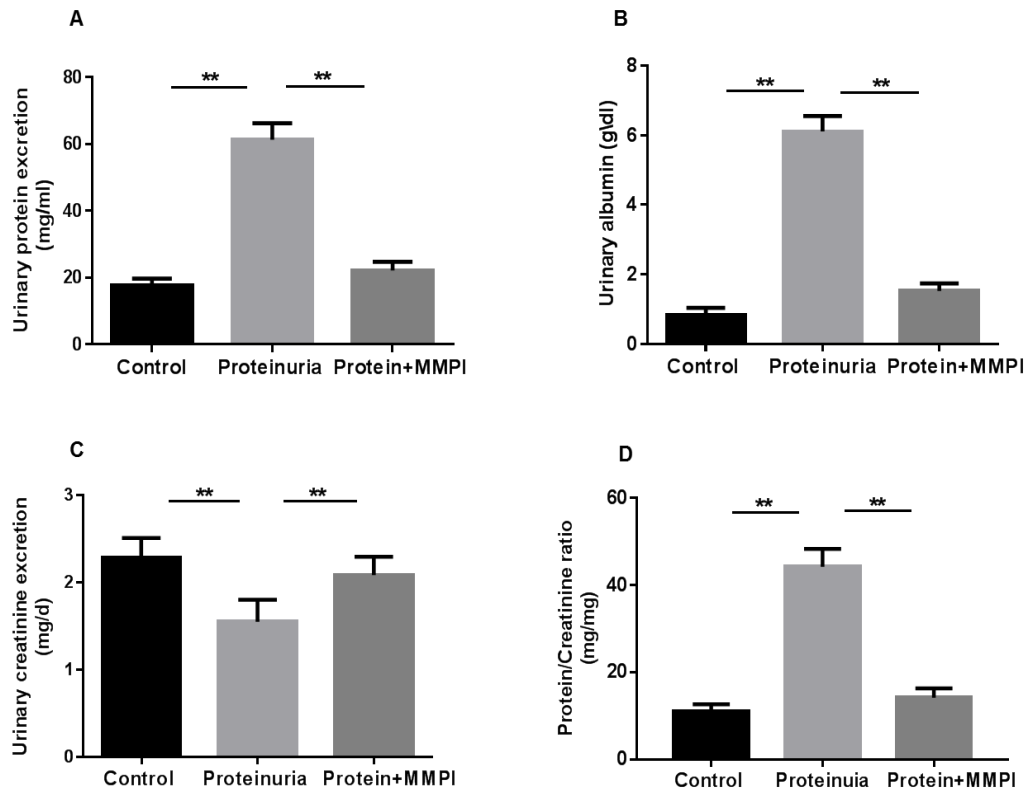


Figure.5.1. Urine biochemistry and protein levels.

(A) Total urinary protein excretion. (B) Mouse urinary albumin concentration. (C) Mouse urinary creatinine concentration. (D) Mouse urine protein /creatinine ratios. Data are expressed as mean \pm SEM of 4 mice in each group, **p < 0.01, one-way ANOVA.

5.2.2. Effect of MMPI treatment on blood biochemistry in proteinuria

Influence of MMPI on serum biochemistry and protein excretion in proteinuria was studied. Total serum protein concentration revealed a significant increase in proteinuric mice compared to controls, but serum protein in MMPI treated mice was still elevated in protein injected mice (Figure.5.2A). In addition, serum creatinine levels exhibited a significant rise in proteinuric mice (2.49 ± 0.13 mg/dl) compared to control, whereas MMPI treatment results in a decrease to (1.17 ± 0.017 mg/dl) in protein injected mice (Figure.5.2B). These results indicate that serum creatinine in proteinuric mice reverted to the normal limit range when treated with the MMPI.

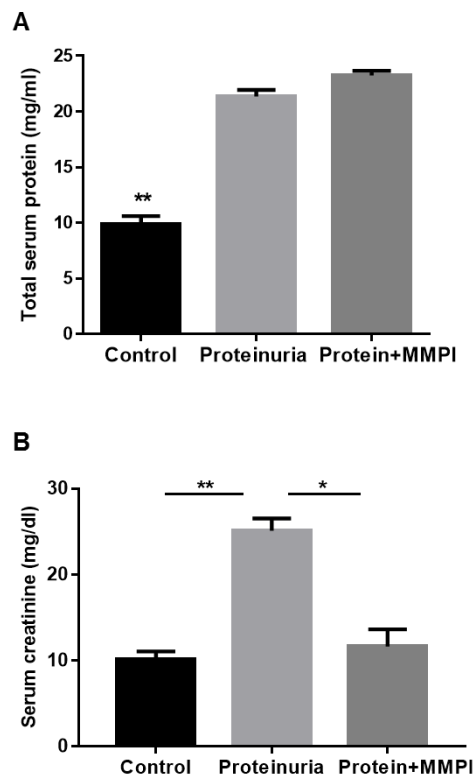


Figure.5.2. Serum biochemistry and proteins levels in mice.

(A) Mouse total serum protein concentration. (B) Mouse serum creatinine levels. Data are expressed as mean \pm SEM of 4 mice in each group, **p < 0.01, *p < 0.05, one-way ANOVA.

5.2.3. Effect of MMPI treatment on enzymatic activity of MMPs

To investigate the effect of MMPI treatment on the enzymatic activity of MMPs in proteinuria, kidney cortex homogenates from each group were evaluated for total MMP activity by a fluorometric assay. MMPs enzymatic activity was significantly augmented in proteinuric mice (808.4 ± 89.1 RFUs) in comparison with control mice (164.0 ± 27.1 RFUs) (Figure.5.3). Treatment of mice with MMPI showed a substantially reduced renal MMP activity (210.0 ± 40.2 RFUs) (Figure.5.3).

Both urine and kidney homogenates from each group were examined specifically for MMP-2 and MMP-9 activity by gelatin zymography. In proteinuric mice, these enzymes showed increased activity in both kidney and urine compared to non-proteinuric controls. In comparison, MMPI treatment substantially reduced MMP-2 and MMP-9 activity in both kidney and urine (Figure.5.4). These findings confirm that MMPI has an inhibitory effect on renal MMP-2 and MMP-9 activities in proteinuric mice.

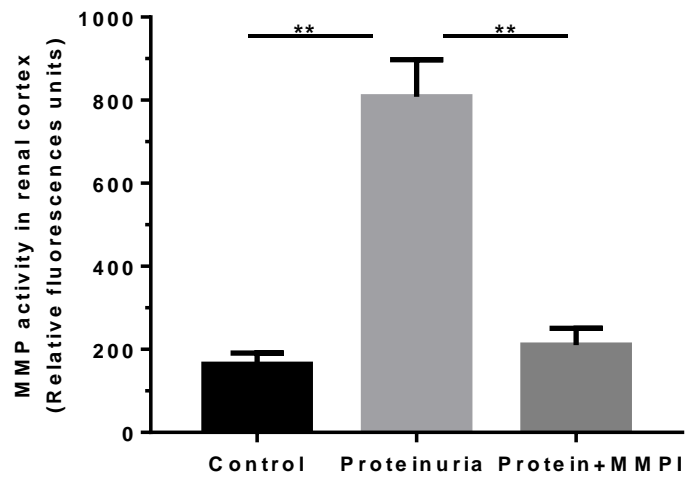


Figure.5.3. Effect of the MMPI on kidney cortex MMPs activity.

MMP activity was determined in control, proteinuric mice and protein injected mice treated with the MMPI. Data expressed as mean \pm SEM of 4 mice in each group.

** $p < 0.01$, one-way ANOVA.

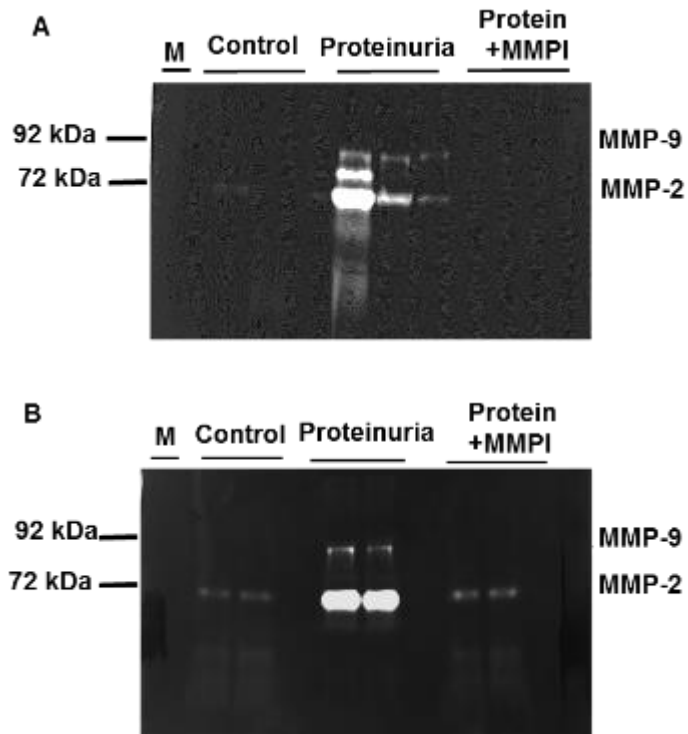


Figure.5.4. Gelatinase activity of MMP-2 and MMP-9 in control, proteinuric mice and protein injected mice treated with the MMPI.

(A) Kidney cortex homogenate and (B) urine samples were subjected to gelatin zymography. MMP-2 bands at 72-kDa gelatinase and MMP-9 bands at 94-kDa gelatinase in comparison with (M) standard ladder protein.

5.2.4. Effect of MMPI treatment on MMP protein expression in proteinuria

To investigate the effect of MMPI treatment on MMP expression in proteinuria, kidney tissues from each group were studied for MMP-2, MMP-3, MMP-7 and MMP-9 expression by immunoblotting. MMP bands were increased in proteinuric animals compared with controls. However, MMP bands in MMPI treated mice were reduced towards control levels (Figure.5.5).

These data were confirmed by densitometric analysis (Figure.5.6). For example, MMP-2 expression increased significantly in proteinuric mice to (1.35 ± 0.04 relative intensity) compared with control (0.19 ± 0.03 relative intensity), while in the MMPI treated mice decreased to (0.31 ± 0.06 relative intensity). In MMP-3 the other matrix enzyme was substantially increased in proteinuric animals to (1.7 ± 0.09 relative intensity) compared with control (0.17 ± 0.04 relative intensity), but MMPI treatment reduced this considerably to (0.36 ± 0.03 relative intensity).

Moreover, proteinuric mice showed a significant increase in expression for MMP-7 (1.6 ± 0.10 relative intensity) and MMP-9 (1.6 ± 0.1 relative intensity) when compared with control mice (0.12 ± 0.06 relative intensity), (0.1 ± 0.05 relative intensity), respectively. On the other hand, MMPI treatment gave a significant reduction in the expression of MMP-7 (0.29 ± 0.2 relative intensity) and MMP-9 (0.31 ± 0.06 relative intensity) in protein injected mice.

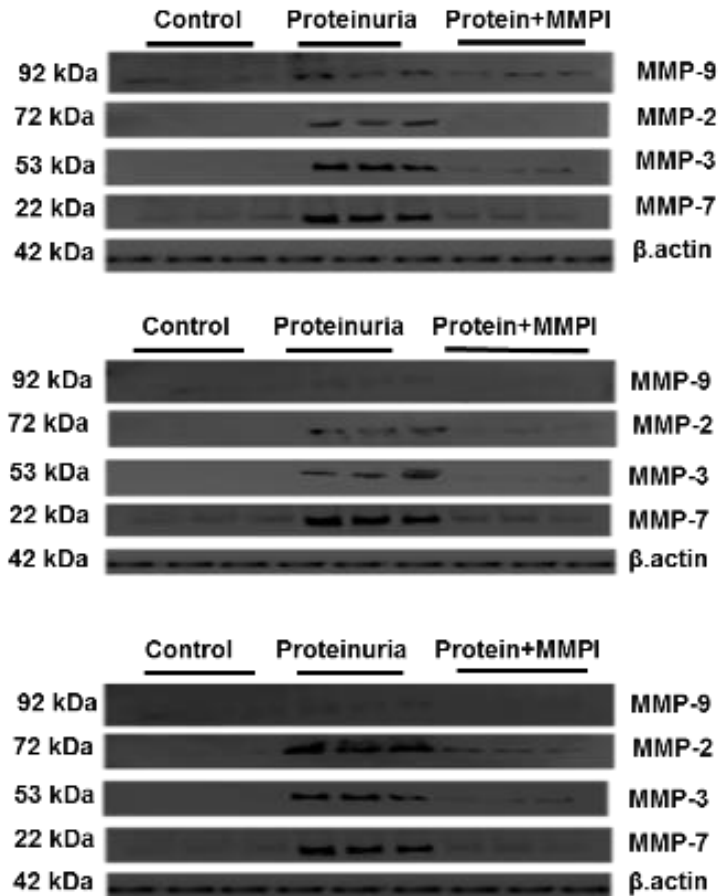


Figure.5.5. Analysis of MMPs expression in mouse kidney by immunoblotting.

Kidney cortex from control, proteinuric mice and protein injected mice treated with the MMPI were evaluated by immunoblotting for MMPs. Each lane represents a kidney sample from an individual animal from each group. Blots stripped and reprobbed for multiple MMP and β -actin loading control shown for comparison.

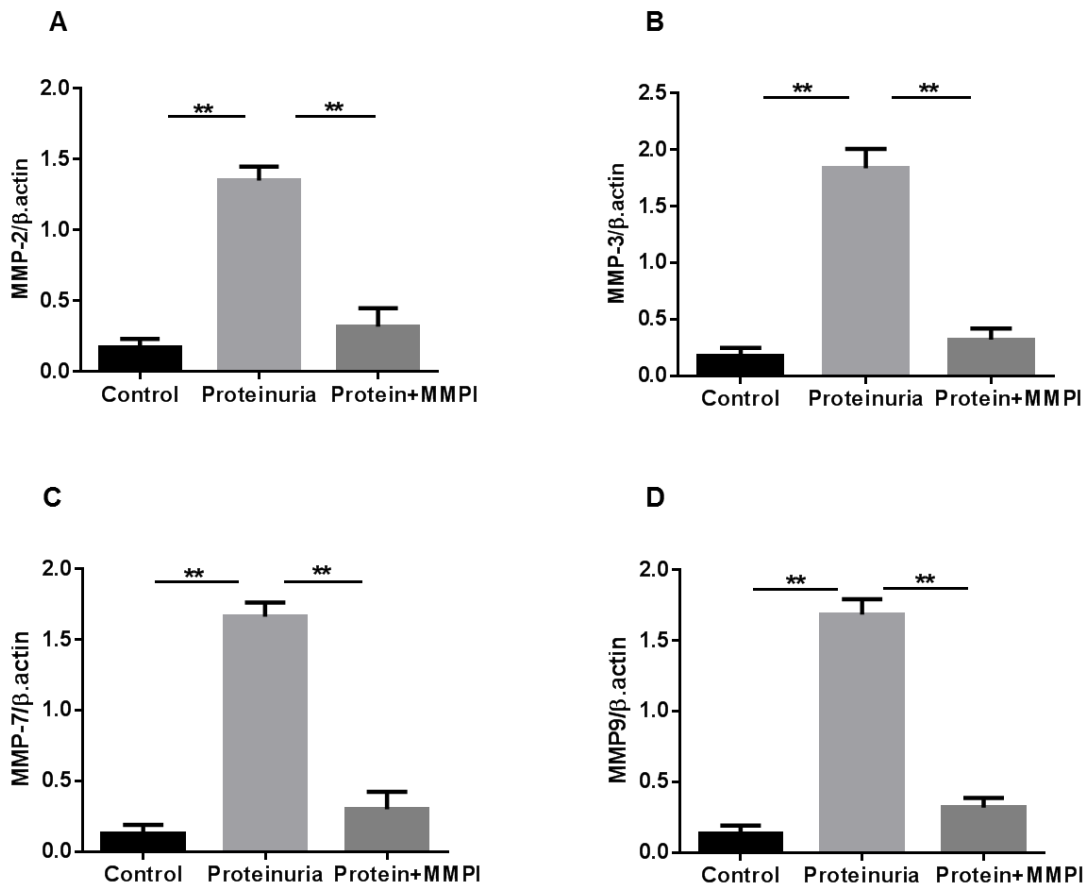


Figure.5.6. Densitometric analysis of MMPs expression.

MMPs expressed as a ratio to β -actin in control, proteinuric mice and protein injected mice treated with the MMPI mice for (A) MMP-2 (B) MMP-3 (C) MMP-7 and (D) MMP-9. Data are expressed as mean \pm SEM of 3 mice per group. ** $p < 0.01$, one-way ANOVA.

MMPs expression was also investigated by IHC in kidney sections from each group of mice. Expression levels of all MMPs studied (MMP-2, -3, -7, and -9) were increased in the kidney of proteinuric animals compared to controls. In contrast, MMPI treatment of mice reduced MMP expression towards normal.

These data were confirmed by semi-quantitative analysis for sections. For instance, MMP-2 expression was significantly increased in the PTs of proteinuric mice (29.09 ± 0.94 % stained area) compared with controls (2.4 ± 0.14 % stained area), whereas mice treated with the MMPI declined to (4.6 ± 0.49 % stained area) (Figure 5.7 and 5.8). Interestingly, MMP-3 expression was increased in the glomeruli of proteinuric mice (17.1 ± 1.6 % stained area) compared with controls (1.6 ± 0.2 % stained area). But, MMPI treatment of protein injected mice dropped to (3.2 ± 0.68 % stained area) (Figure 5.9 and 5.10).

Moreover, MMP-7 expression elevated in the PTs of mice with proteinuria (21.4 ± 0.7 % of stained area) compared to non-proteinuric mice control (2.07 ± 0.5 % stained area), whereas the MMPI treated mice was decreased to (4.2 ± 0.74 % stained area) (Figure 5.11 and 5.12). In addition, MMP-9 expression elevated in the PTs of proteinuric animals to (23.0 ± 1.66 % stained area), while MMPI treatment of protein injected animals has a reduction in MMP-9 expression to (4.2 ± 0.7 % stained area) compared with controls ($2.07 \pm 0.5\%$ stained area) (Figure.5.13 and 5.14). These finding revealed that MMPI treatment down-regulated MMPs expression in proteinuria.

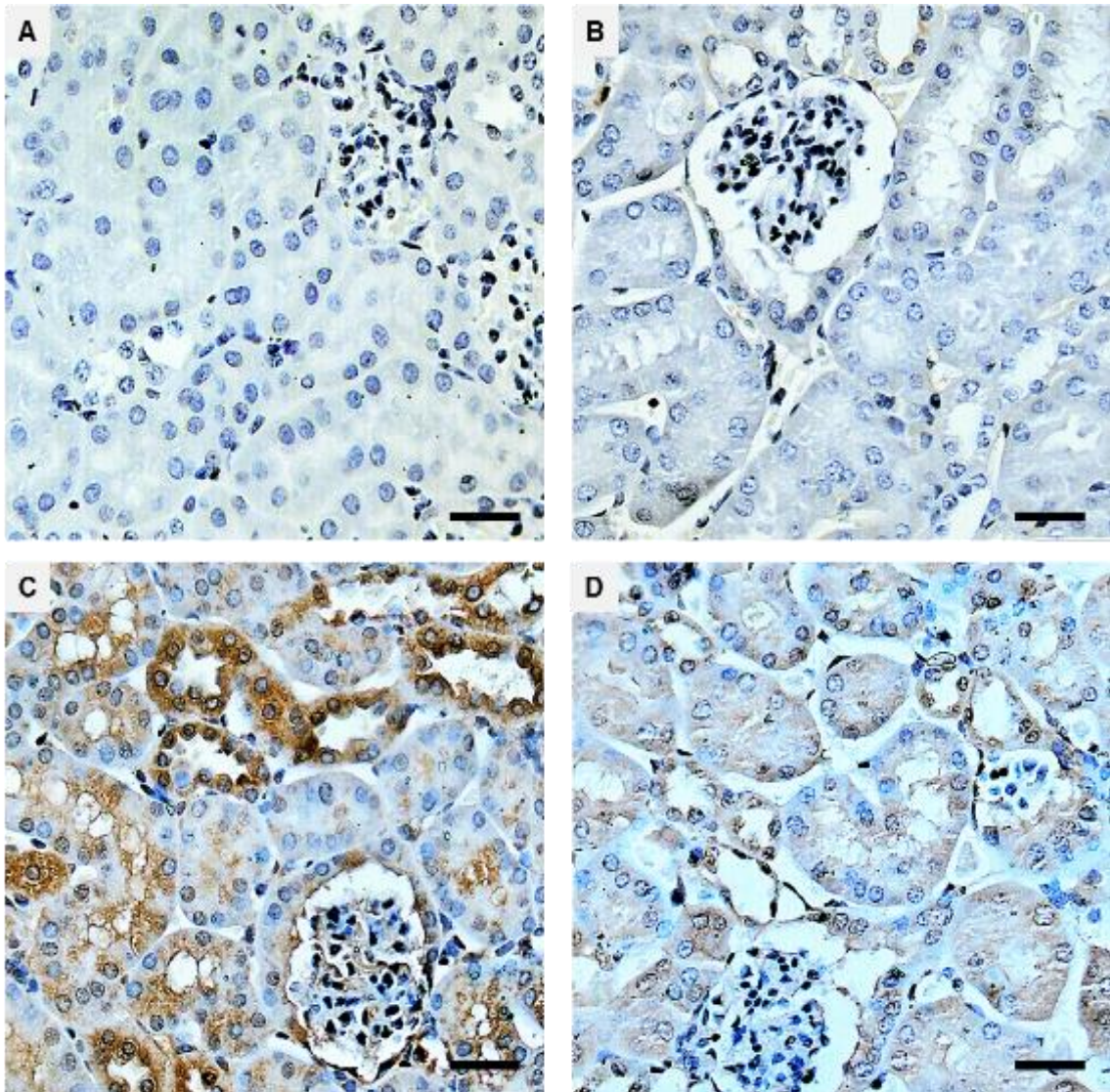


Figure.5.7. IHC analysis of mouse kidney tissue for MMP-2 in control, proteinuric mice and protein injected mice treated with MMPI.

Representative photomicrographs showing (A) Negative control sections from control animals prepared without primary antibody. (B) Control mice. (C) Proteinuric mice. (D) Protein injected mice treated with the MMPI. Scale bars 100 μ M.

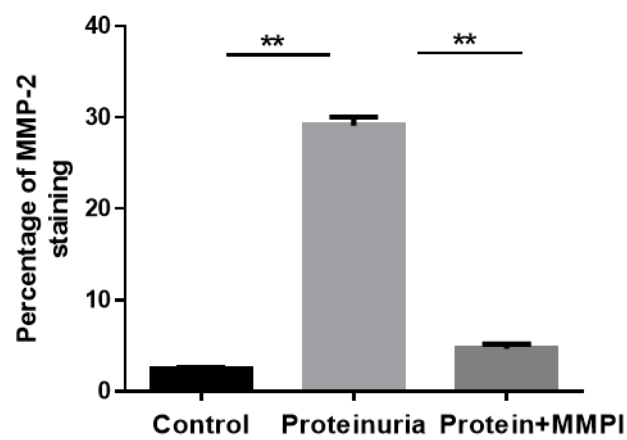


Figure.5.8. Semi-quantitative analysis of renal MMP-2 staining in control, proteinuric mice and protein injected mice treated with the MMPI.

Data are expressed as mean \pm SEM of 4 mice per group. ** $p < 0.01$, one-way ANOVA.

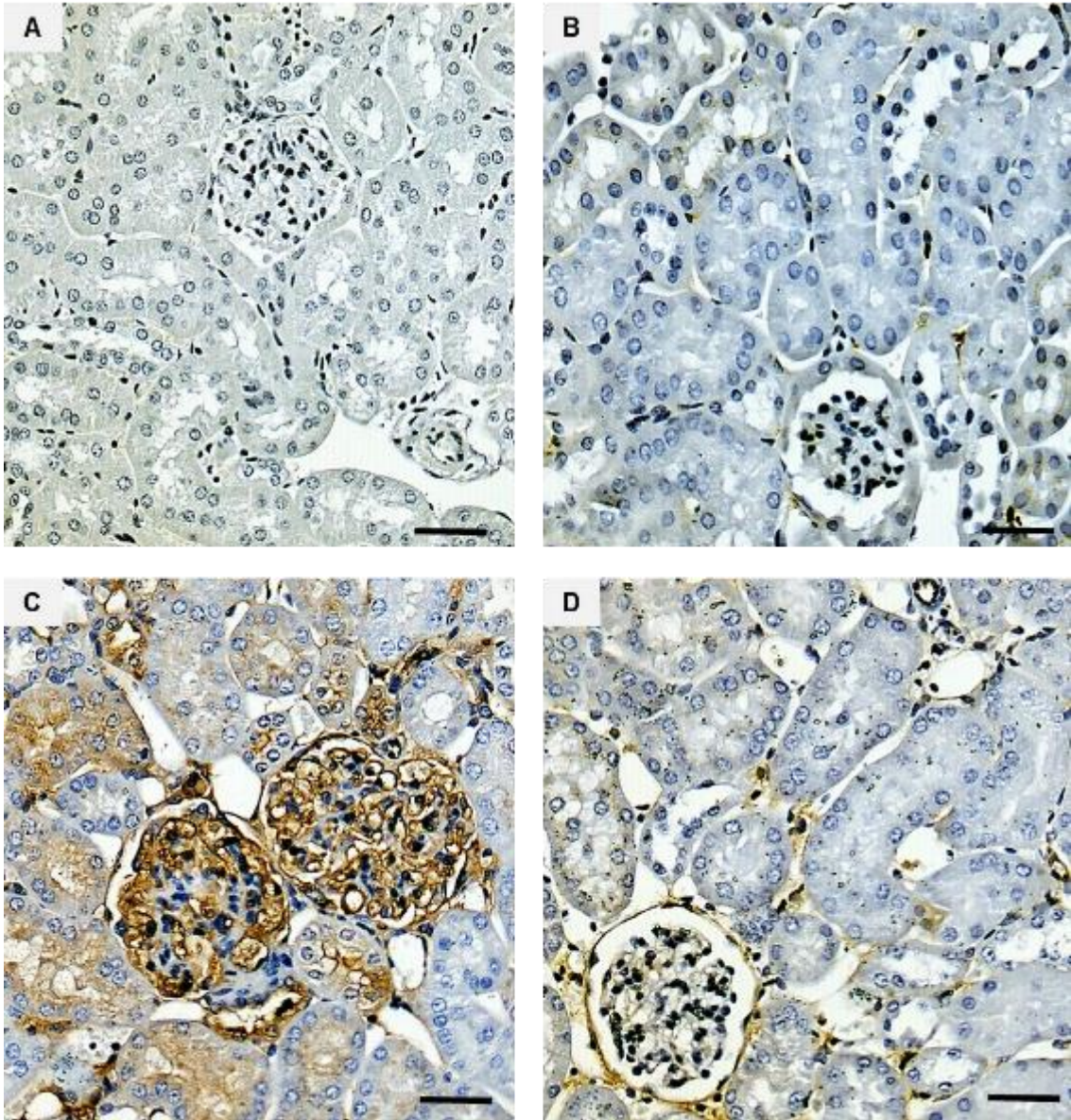


Figure.5.9. IHC analysis of mouse kidney tissue for MMP-3 in control, proteinuric mice and protein injected mice treated with MMPI.

Representative photomicrographs showing (A) Negative control sections from control animals prepared without primary antibody. (B) Control mice. (C) Proteinuric mice. (D) Protein injected mice treated with the MMPI. Scale bars 100 μ M.

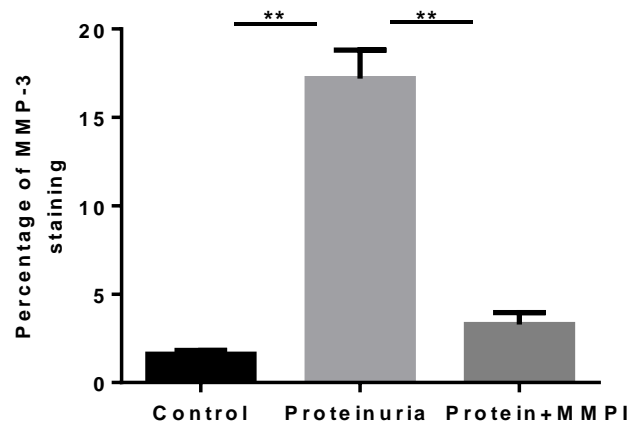


Figure.5.10. Semi-quantitative analysis of renal MMP-3 staining in control, proteinuric mice and protein injected mice treated with the MMPI.

Data are expressed as mean \pm SEM of 4 mice per group, ** $p < 0.01$, one-way ANOVA.

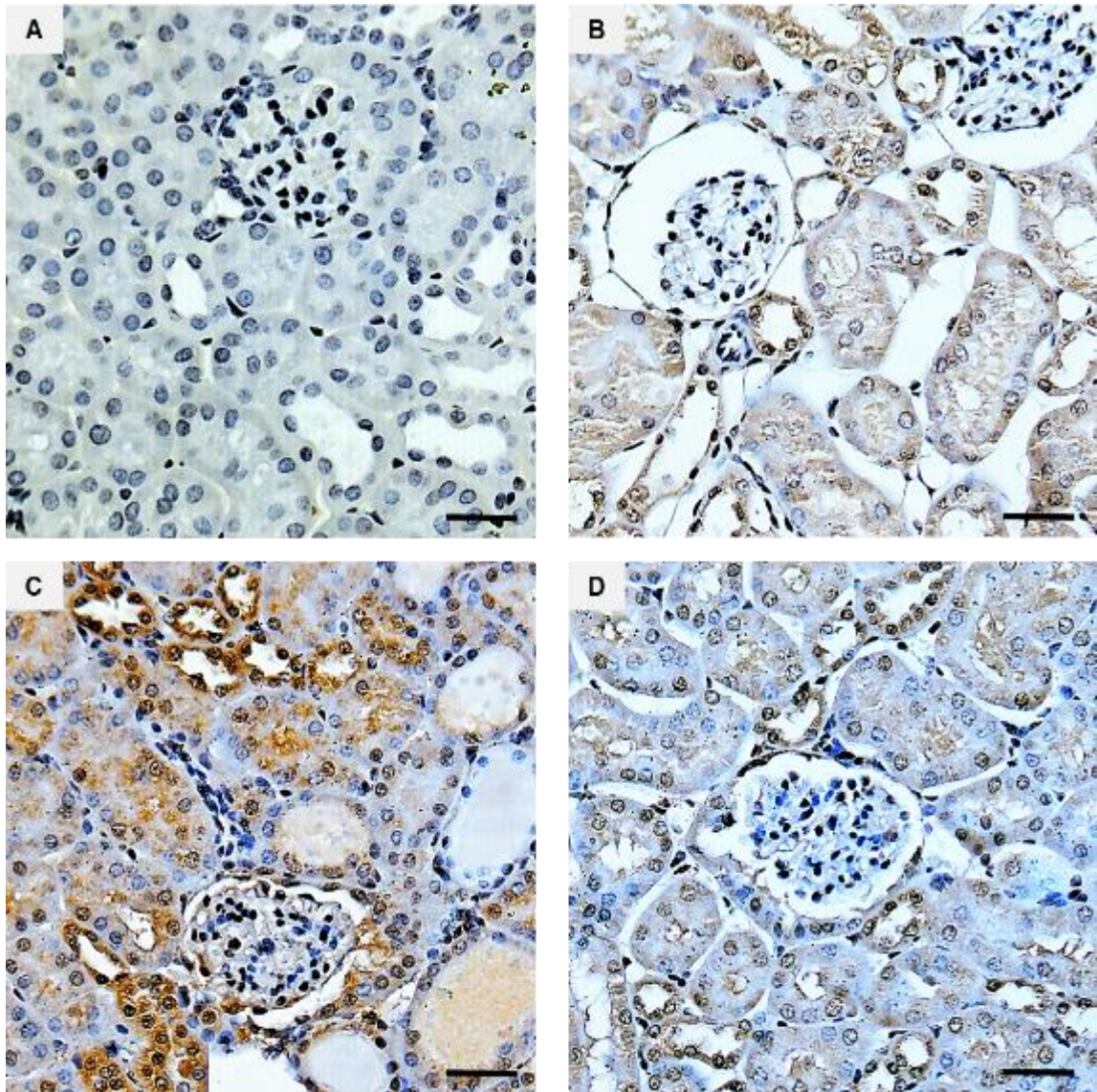


Figure.5.11. IHC analysis of mouse kidney tissue for MMP-7 in control, proteinuric mice and protein injected mice treated with MMPI.

Representative photomicrographs showing (A) Negative control sections from control animals treated without primary antibody. (B) Control mice. (C) Proteinuric mice. (D) Protein injected mice treated with the MMPI. Scale bars 100 μ M.

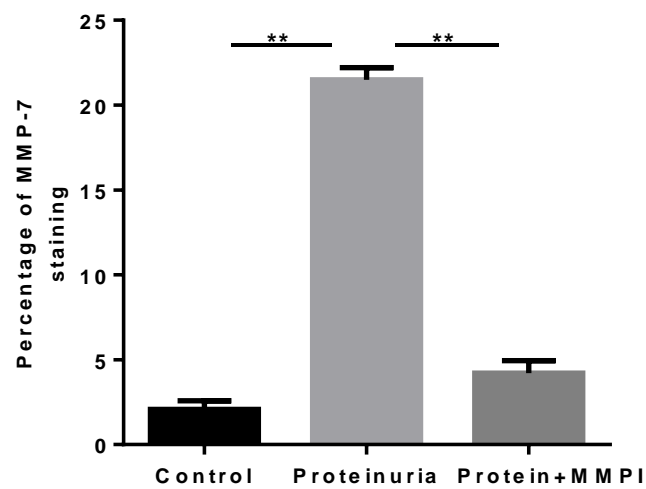


Figure.5.12. Semi-quantitative analysis of renal MMP-7 staining in control, proteinuric mice and protein injected mice treated with the MMPI.

Data are expressed as mean \pm SEM of 4 mice per group. **p < 0.01, one-way ANOVA.

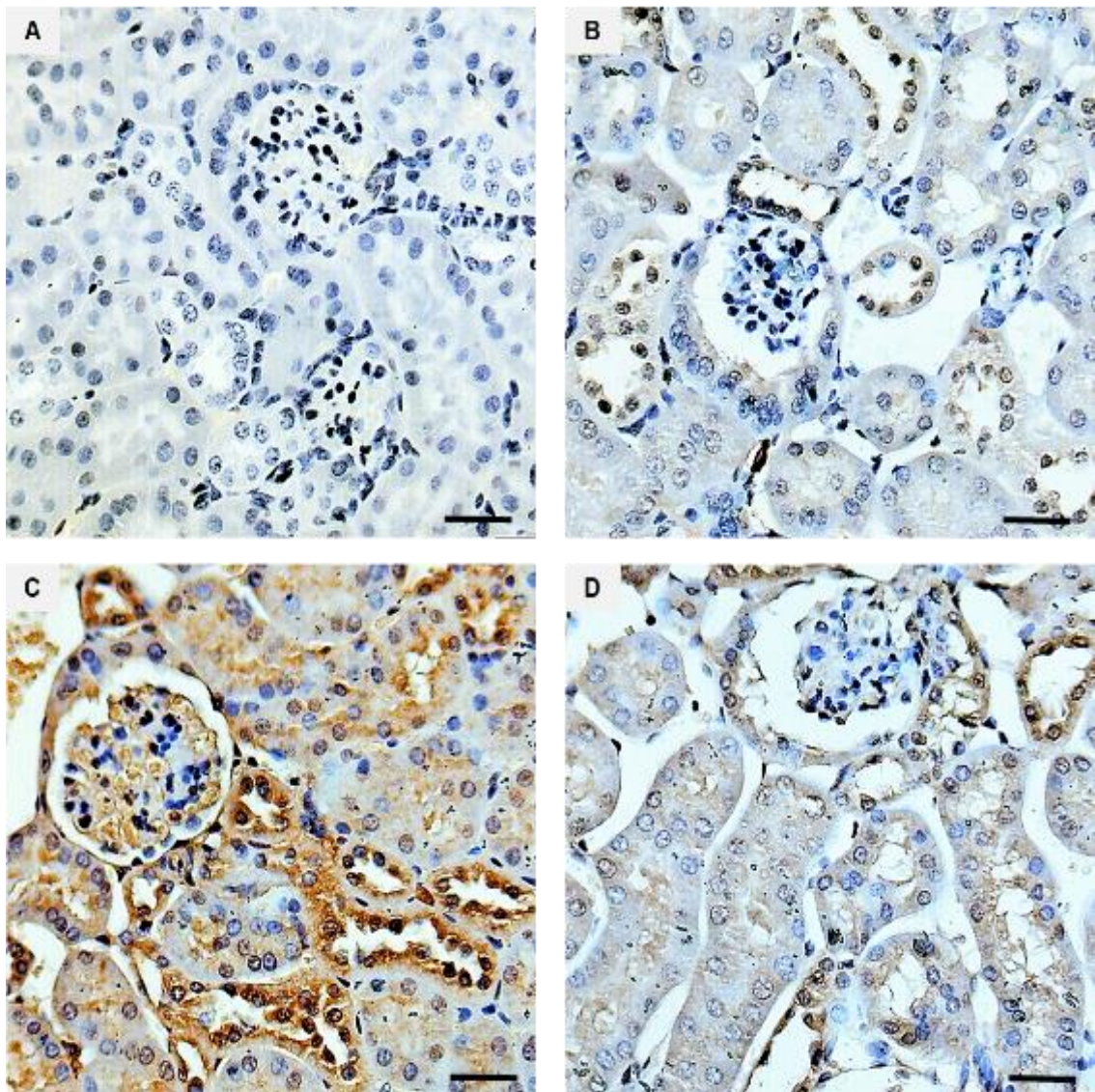


Figure.5.13. IHC analysis of mouse kidney tissue for MMP-9 in control, proteinuric mice and protein injected mice treated with MMPI.

Representative photomicrographs showing (A) Negative control sections from control animals prepared without primary antibody. (B) Control mice. (C) Proteinuric mice. (D) Protein injected mice treated with the MMPI. Scale bars 100 μ M.

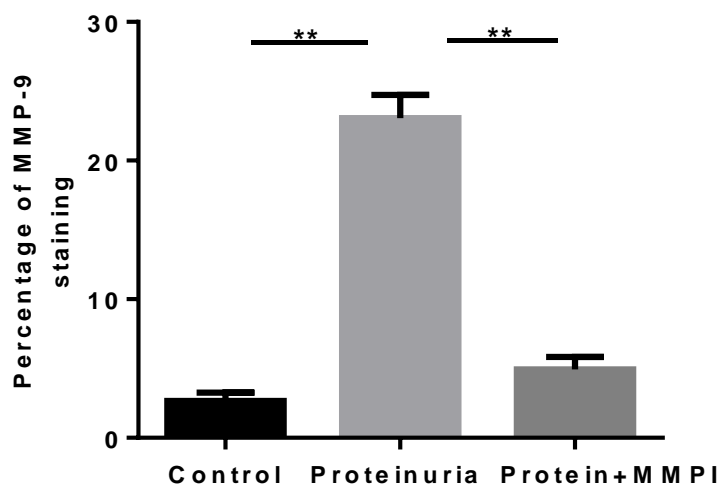


Figure.5.14. Semi-quantitative analysis of renal MMP-9 staining proteinuria in control, proteinuric mice and protein injected mice treated with the MMPI.

Data are expressed as mean \pm SEM of 4 mice per group. ** $p < 0.01$, one-way ANOVA.

5.2.5. Effect of MMPI treatment on MMPs gene expression in proteinuria

The gene expression of MMP-2, -3, -7 and -9 were assessed in kidney tissues for each group by qPCR. The expression of each MMP gene was increased in the kidney of proteinuric animals compared to non-proteinuric controls. Treatment with the MMPI normalised the expression of each gene towards control levels (Figure.5.15). For instance, the mRNA expression of MMP-2 increased significantly in mice proteinuria to (1.95 ± 0.07 -fold) compared with control animals (1 ± 0.05 -fold), while in protein injected mice treated with MMPI decreased to (0.94 ± 0.05 -fold). In mRNA expression of MMP-3 was significantly increased in mice proteinuria to (1.93 ± 0.23 -fold) compared with (1 ± 0.02 -fold) of controls, but in MMPI treatment reduced this considerably to (0.97 ± 0.06 -fold). Moreover, proteinuric mice showed a significant increase in mRNA expression for MMP-7 (1.4 ± 0.08 -fold) and MMP-9 (1.34 ± 0.10 -fold) compared with control mice (1 ± 0.02 -fold) (1 ± 0.06 -fold), respectively. On the other hand, MMPI treatment gave a significant reduction in mRNA expression of MMP-7 (0.98 ± 0.01 -fold) and MMP-9 (0.96 ± 0.05 -fold) in protein injected mice. Regarding these results, MMPI treatment diminishes the MMPs gene expression of MMP-2, MMP-3, MMP-7 and MMP-9 in proteinuria.

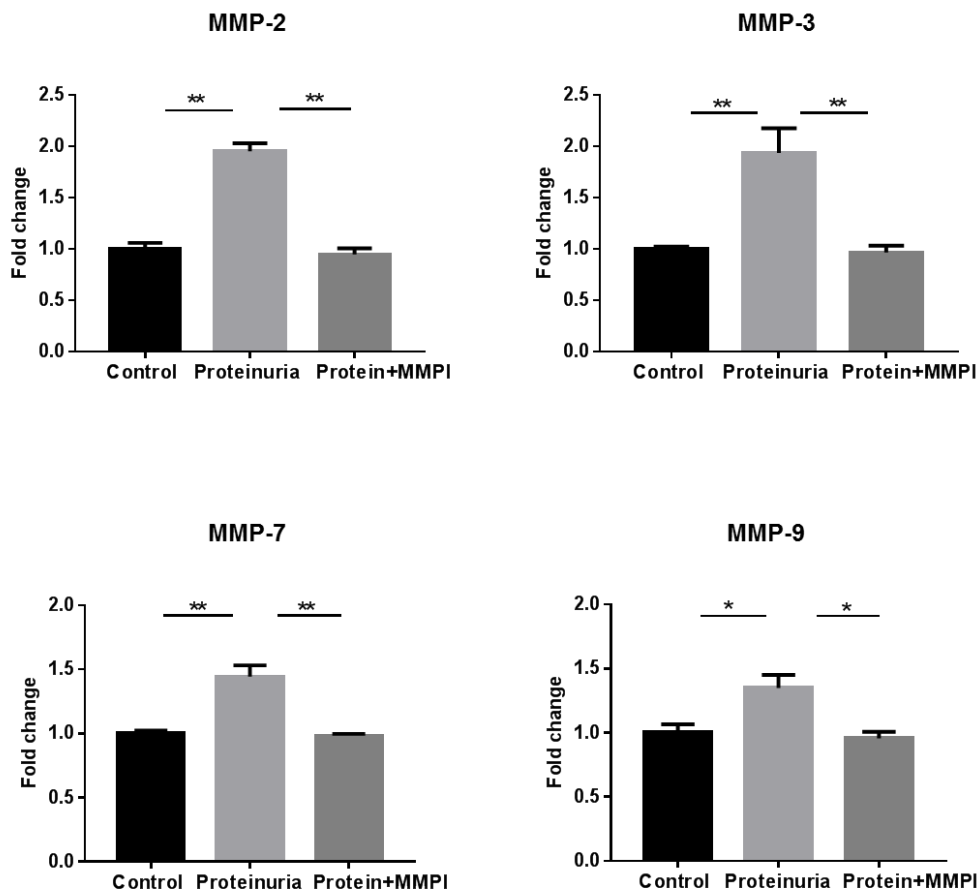


Figure.5.15. Fold change of MMPs mRNA expression in mice kidneys control, proteinuric mice, and protein injected mice treated with MMPI.

mRNA was extracted from the kidney cortex and subjected to qPCR. Data are expressed as mean \pm SEM of 4 mice per group. ** p < 0.01, one-way ANOVA

5.2.6. Effect of MMPI treatment on cubilin complex

5.2.6.1. MMPI ameliorate cubilin expression in proteinuria

To determine whether the cubilin expression is affected by MMPI in proteinuria, kidney tissues from control, proteinuric mice and protein injected mice treated with MMPI were investigated using immunoblotting. Cubilin expression was reduced in proteinuric mice to (0.56 ± 0.07 relative intensity) compared with controls (1.7 ± 0.3 relative intensity) when normalized to β -actin. While protein injected mice which treated with the MMPI showed a significantly preserved cubilin expression to (1.69 ± 0.01 relative intensity) (Figure.5.16).

IHC was also used to investigate kidney sections from each group. Cubilin immunostaining was decreased in the PTs of proteinuric animals compared with controls. However, in protein injected mice treated with the MMPI, cubilin staining was preserved in the apical membranes of PTs (Figure 5.17). By semiquantitative analysis, cubilin staining significantly fell in proteinuric animals (13.8 ± 0.43 % stained area) compared with controls (36.6 ± 0.9 % stained area). However, MMPI treatment restored cubilin expression to (33.6 ± 0.46 % stained area) (Figure.5.18).

Effect of MMPI on cubilin gene expression was also studied by qPCR. Cubilin mRNA expression was noticeably reduced to (0.51 ± 0.02 -fold) in the kidney cortex of proteinuric mice compared with controls (1 ± 0.07 -fold). Though, protein injected mice treated with the MMPI had increased expression of cubilin mRNA to (0.94 ± 0.05 -fold) (Figure.5.19). These data indicate that MMPI treatment can efficiently normalise cubilin gene expression.

In addition, the effect of MMPI treatment on the urinary cubilin excretion of proteinuric mice was determined by ELISA. The urine of proteinuric mice has substantially increased cubilin excretion to (2.58 ± 0.13 ng/mg creatinine) compared with urine controls (0.523 ± 0.02 ng/mg creatinine), but, urinary cubilin excretion declined on MMPI treatment to (0.526 ± 0.023 ng/mg creatinine) in protein injected mice (Figure.5.20). These findings suggest that MMPI treatment can protect cubilin from being shed into the urine of proteinuric mice. This associated with improvement of cubilin expression in the kidney of proteinuric animals.

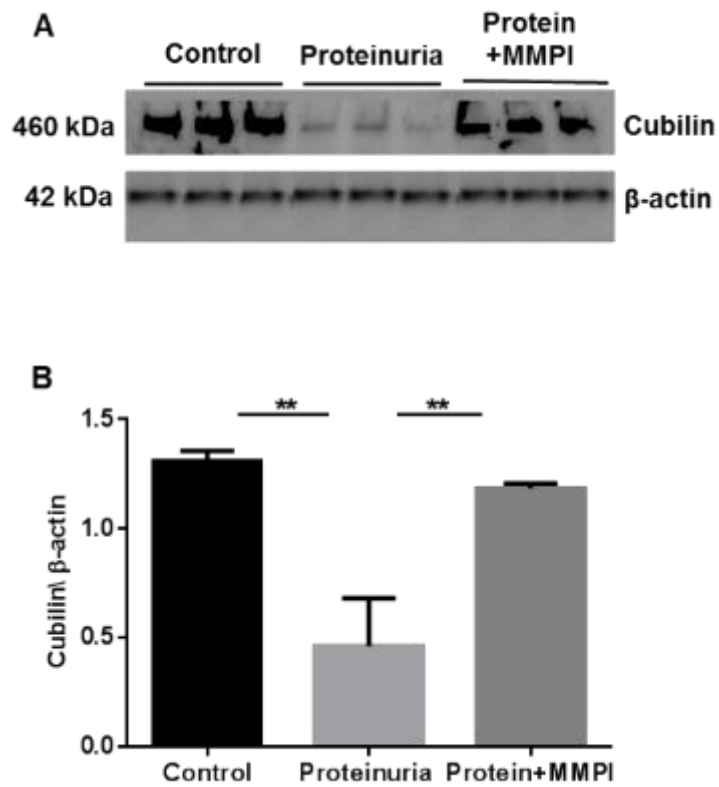


Figure.5.16. Analysis of cubilin expression in mouse kidneys by immunoblotting.

(A) Kidney cortex from control, proteinuric mice and protein injected mice treated with the MMPI were evaluated by immunoblotting for cubilin in comparison with a β -actin loading control. (B) Densitometric analysis of cubilin expression as a ratio to β -actin, Data are expressed as mean \pm SEM of 3 mice per group. ** $p < 0.01$, one-way ANOVA.

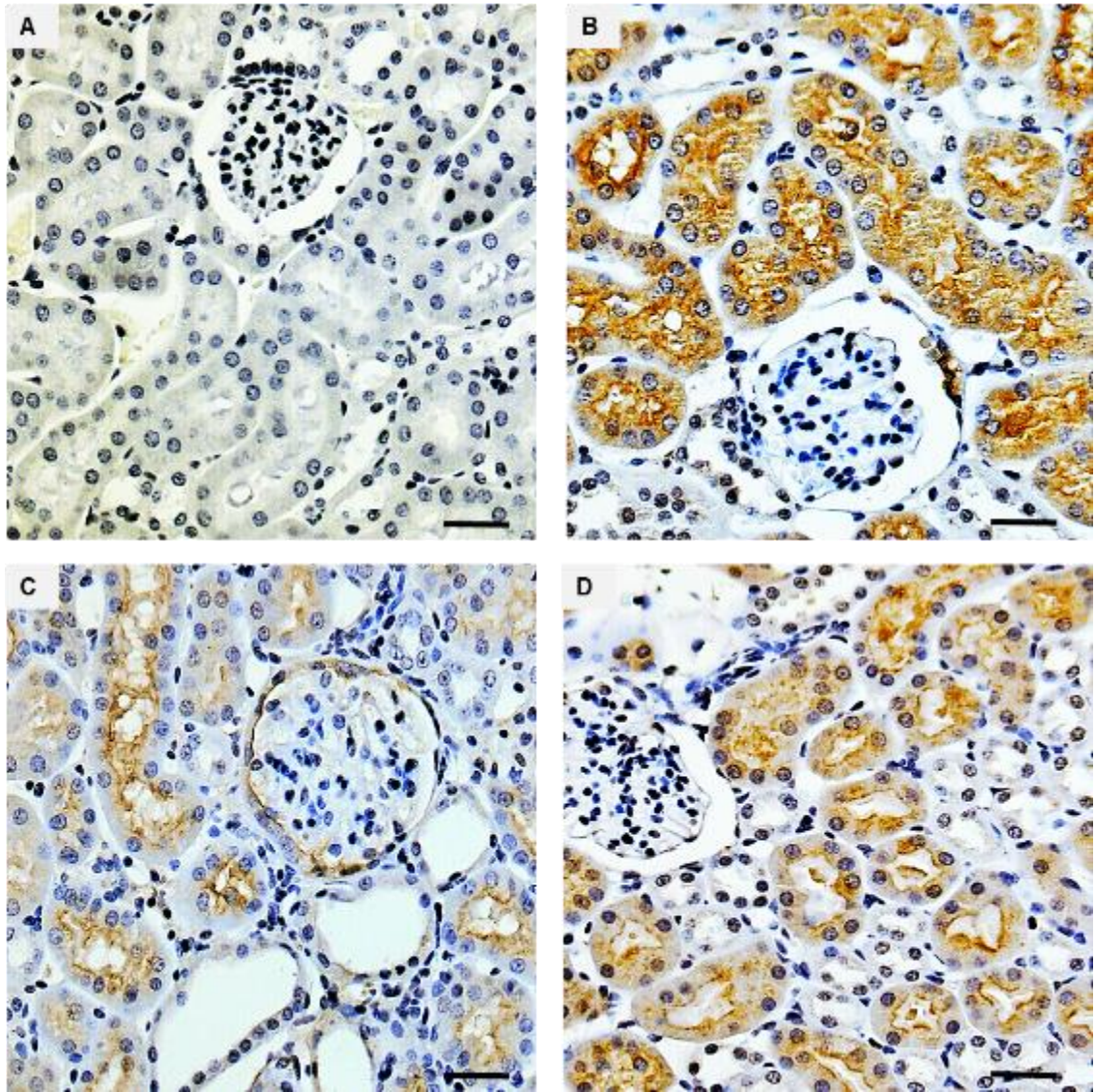


Figure.5.17. IHC analysis of mouse kidney tissue for cubilin in control, proteinuric mice and protein injected mice treated with the MMPI.

Representative photomicrographs showing (A) Negative control sections from control animals prepared without primary antibody. (B) Control mice. (C) Proteinuric mice. (D) Protein injected mice treated with the MMPI. Scale bars 100 μ M.

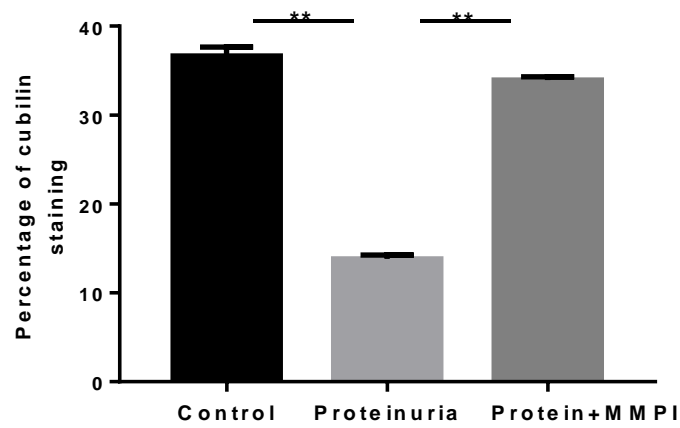


Figure.5.18. Semi-quantitative analysis of renal cubilin staining in control, proteinuric mice, and protein injected mice treated with the MMPI.

Data are expressed as mean \pm SEM of 4 mice per group. **p < 0.01, one-way ANOVA.

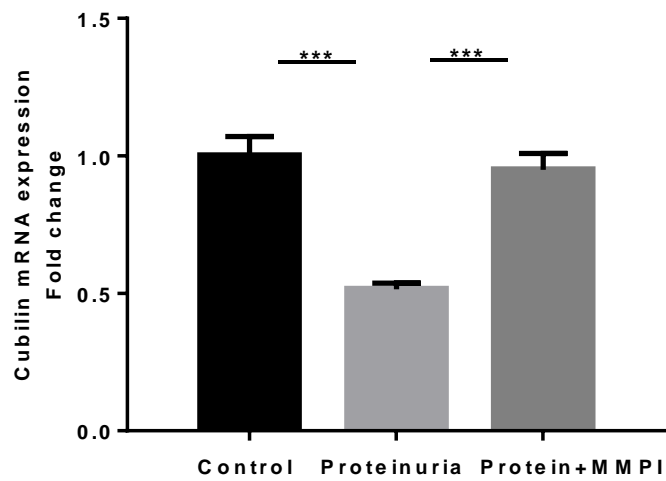


Figure.5.19. Fold change of cubilin mRNA expression in mouse kidneys of control, proteinuric mice and protein injected mice treated with the MMPI.

mRNA was extracted from the kidney cortex and subjected to qPCR. Data are expressed as mean \pm SEM, 4 mice per group, *** $p < 0.001$, one-way ANOVA.

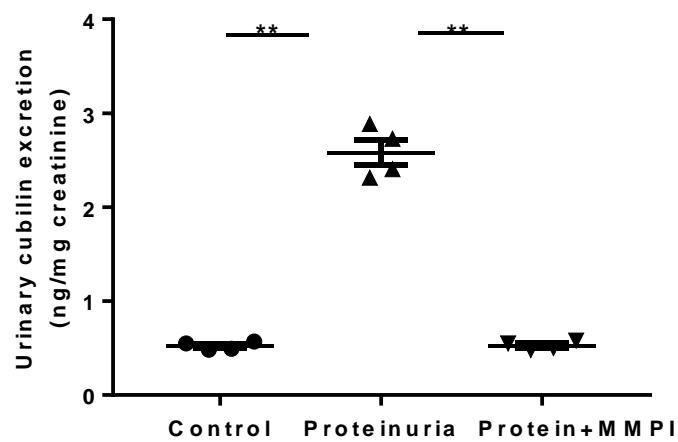


Figure.5.20. Urinary excretion of cubilin in mouse urine.

Urine samples from control, proteinuric mice and protein injected mice treated with the MMPI normalised to creatinine and analysed for cubilin by ELISA. Data are mean \pm SEM of 4 mice per group. ** $p < 0.01$, one-way ANOVA.

5.2.6.2. MMPI ameliorate amnionless expression in proteinuria

To investigate whether the amnionless expression is affected by MMPI in proteinuria, kidney tissues from each group were examined using immunoblotting. Amnionless expression at protein level substantially declined in proteinuric animals to (0.7 ± 0.07 relative intensity) compared with controls (1.6 ± 0.13 relative intensity) when normalized to β -actin. However, in protein injected animals treated with the MMPI, expression was substantially maintained to (1.57 ± 0.10 relative intensity) (Figure.5.21).

To confirm the immunoblotting results, Kidney sections from each group were analysed by IHC. Amnionless expression was reduced at the apical membrane of the PTs in proteinuric mice compared with control mice. While the MMPI treated mice showed preservation of amnionless expression (Figure 5.22). The quantification of amnionless staining revealed a significant decline in proteinuric animals (14.4 ± 0.98 % stained area) compared to controls (27.8 ± 0.39 %). However, amnionless staining was significantly improved in protein injected animals treated with the MMPI to (24.7 ± 0.70 %) (Figure.5.23).

By qPCR, the expression of amnionless mRNA was significantly decreased to (0.49 ± 0.04 -fold) in proteinuric mice compared with controls (1 ± 0.07 -fold). Interestingly, the amnionless mRNA was increased to normal in the MMPI treatment of protein injected animals to (1.0 ± 0.10 -fold) (Figure.5.24).

By ELISA, it was found that urine of proteinuric mice contains a significant excretion of amnionless (2.72 ± 0.10 ng/mg creatinine) compared with control (0.55 ± 0.016 ng/mg creatinine). However, the amnionless excretion was reduced

in the urine of protein injected mice treated with MMPI to (0.55 ± 0.04 ng/mg creatinine) (Figure.5.25).

Overall these results suggest that MMPI treatment protect amnionless from being lost in the urine of proteinuric animals. Likewise, the treatment preserves its expression in proteinuric kidney and regulates the gene expression.

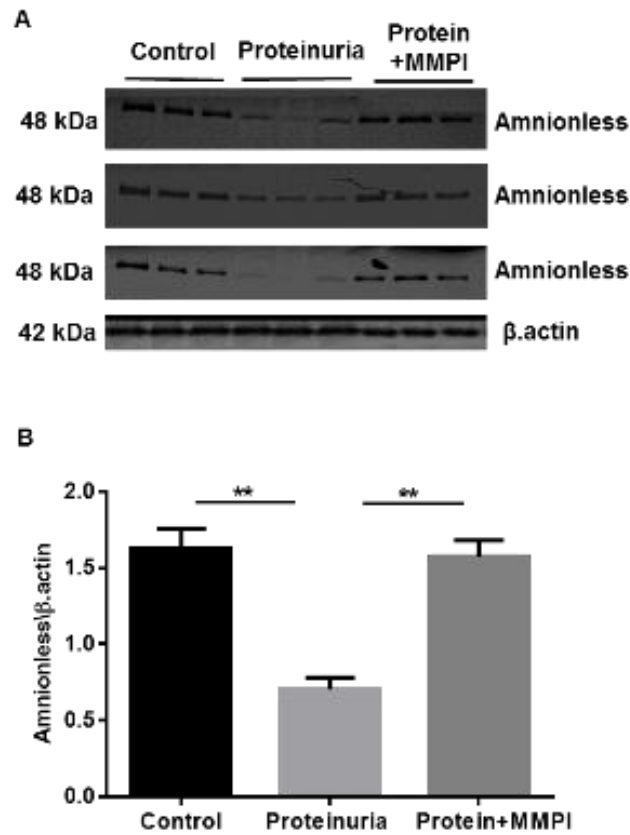


Figure.5.21. Analysis of amnionless expression in mouse kidneys by immunoblotting.

(A) Kidney cortex from control, proteinuric mice and protein injected mice treated with the MMPI were assessed for amnionless, each lane represents a kidney from each group in comparison with β -actin loading control. (B) Densitometric analysis of amnionless expression as a ratio to β -actin. Results are expressed as mean \pm SEM of 3 mice per group. ** $p < 0.01$, one-way ANOVA.

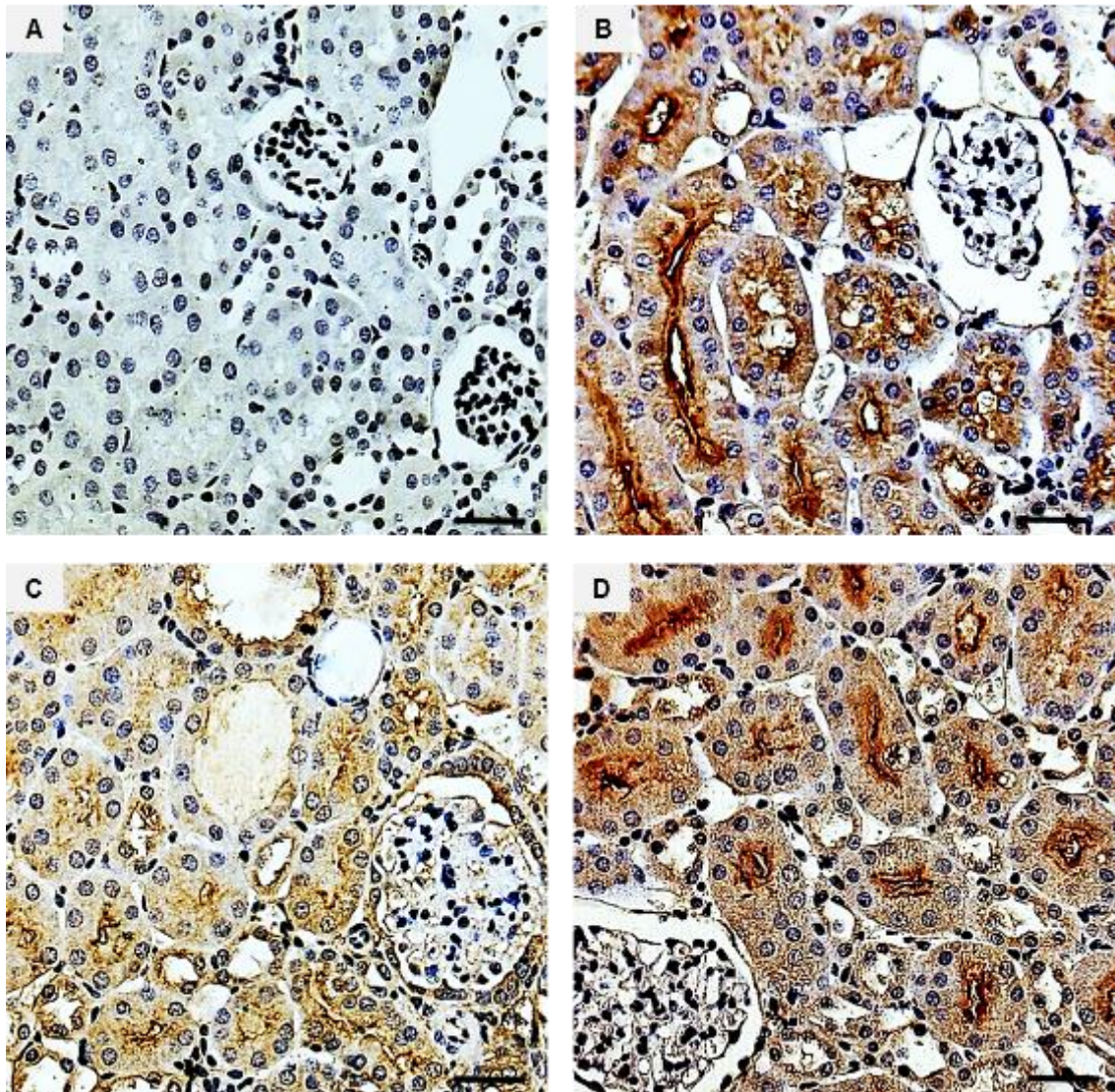


Figure.5.22. IHC analysis of mouse kidney tissue for amnionless in control, proteinuric mice and protein injected mice treated with the MMPI.

Representative photomicrographs showing (A) Negative control sections from control animals prepared without primary antibody. (B) Control mice. (C) Proteinuric mice. (D) Protein injected mice treated with the MMPI. Scale bars 100 μ M.

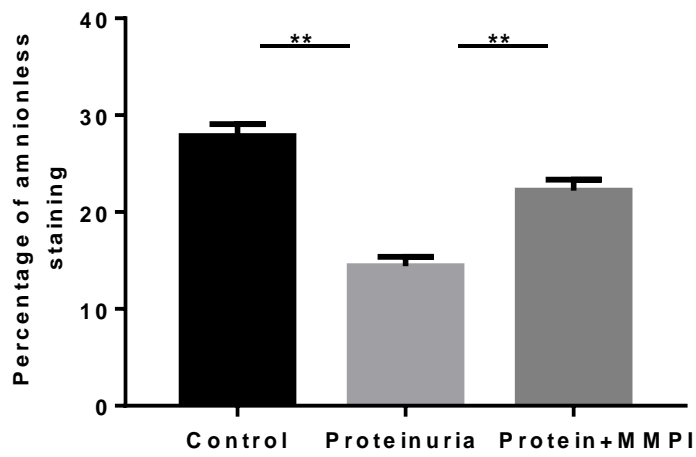


Figure.5.23. Semi-quantitative analysis of renal amnionless staining in control, proteinuric mice and protein injected mice treated with the MMPI.

Results are expressed as mean \pm SEM of 4 mice per group. ** $p < 0.01$, one-way ANOVA

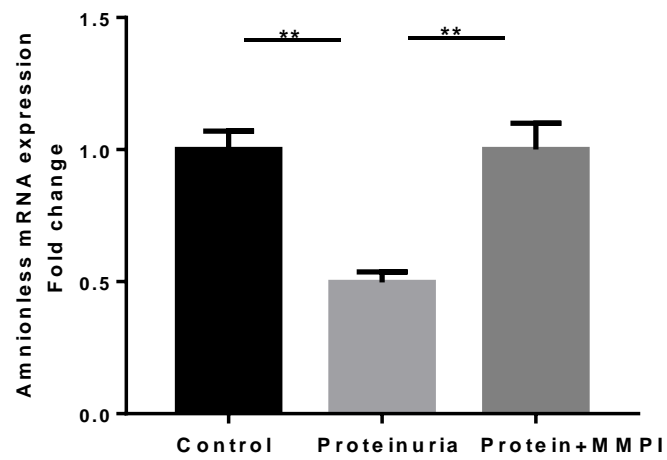


Figure.5.24. Fold change in amnionless mRNA expression in mouse kidneys of control, proteinuric mice and protein injected mice treated with the MMPI.

mRNA was extracted from the kidney cortex and subject to qPCR. Data are mean \pm SEM of 4 mice per group, **p < 0.01, one-way ANOVA.

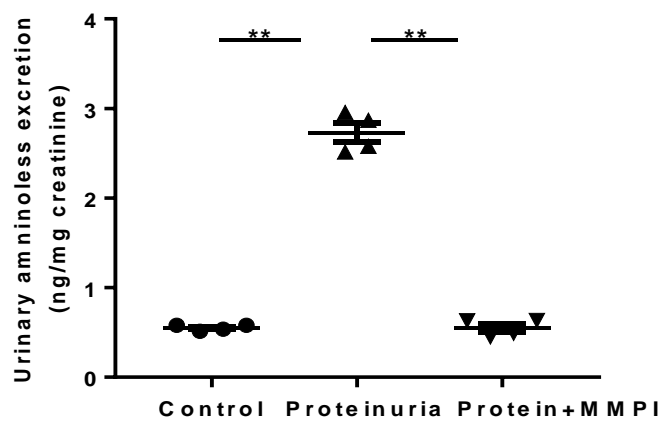


Figure.5.25. Urinary excretion of the amnioless in mouse urine.

Urine samples from control, proteinuric mice and protein injected mice treated with the MMPI normalised creatinine and analysed for amnioless by ELISA. Data are expressed as mean \pm SEM of 4 mice per group. ** $p < 0.01$, one-way ANOVA.

5.2.6.3. Colocalization of the cubam complex in protein overload proteinuria

Kidney tissues from each group were studied for cubilin and amnionless colocalization by IF. Cubilin and amnionless expression were similar in the kidney of protein injected mice treated with the MMPI and controls. In proteinuric mice, cubilin and amnionless receptors were significantly reduced (Figure.5.26). According to quantification analysis, the percentage of staining significantly declined in proteinuric mice for cubilin (12.8 ± 0.43 % stained area) and amnionless (13.4 ± 0.98 % stained area) compared with the control of cubilin (26.6 ± 0.4 % stained area) and amnionless (26.8 ± 0.39 % stained area). MMPI treatment showed substantial preservation of cubilin to (25.9 ± 0.46 % stained area) and amnionless to (25.7 ± 0.7 % stained area) in protein injected mice (Figure.5.27).

Colocalisation of cubilin and amnionless in the small intestine of mice were also investigated by IF. Interestingly, these data showed that colocalization of cubilin and amnionless expression in proteinuric mice were similar to control mice (Figure.5.28). Therefore, although the expression of receptors was down-regulated in the diseased kidney and improved by MMPI, in the intestinal tissue, this cubam complex compared with control had not expressed any change.

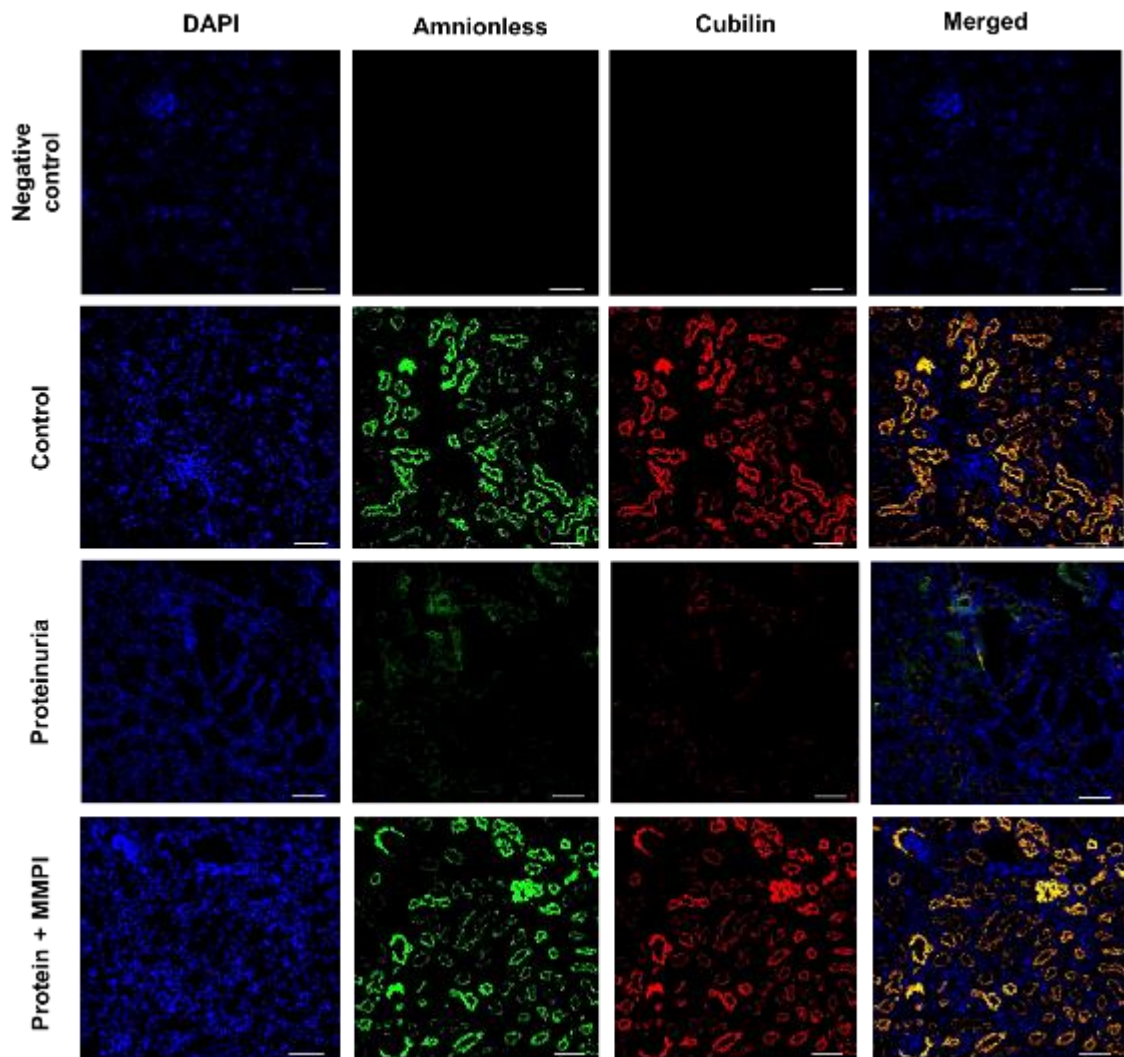


Figure.5.26. IF analysis for colocalization of cubilin (red) and amnionless (green) staining in mouse kidney tissue.

Representative photomicrographs showing negative control, control mice, proteinuric mice and protein injected mice treated with the MMPI. Nuclei were stained blue with DAPI (left panels). Middle panels represent cubilin (cubilin A-20 antibody) stained and amnionless (amnionless antibody) stained. Right-hand panels represent merged (DAPI, cubilin and amnionless). All photomicrographs scale bars 100 μ m.

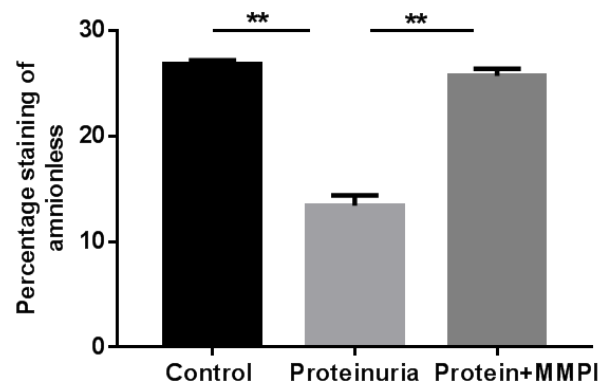
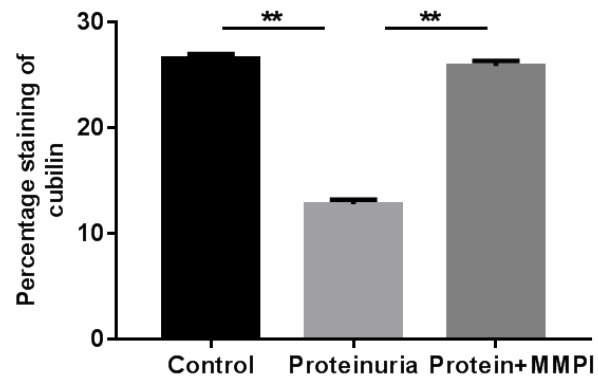


Figure.5.27. Semi-quantitative analysis of renal cubilin and amnionless staining in control, proteinuric mice and protein injected mice treated with the MMPI.

Data are expressed as mean \pm SEM of 4 mice per group. ** $p < 0.01$. one-way ANOVA.

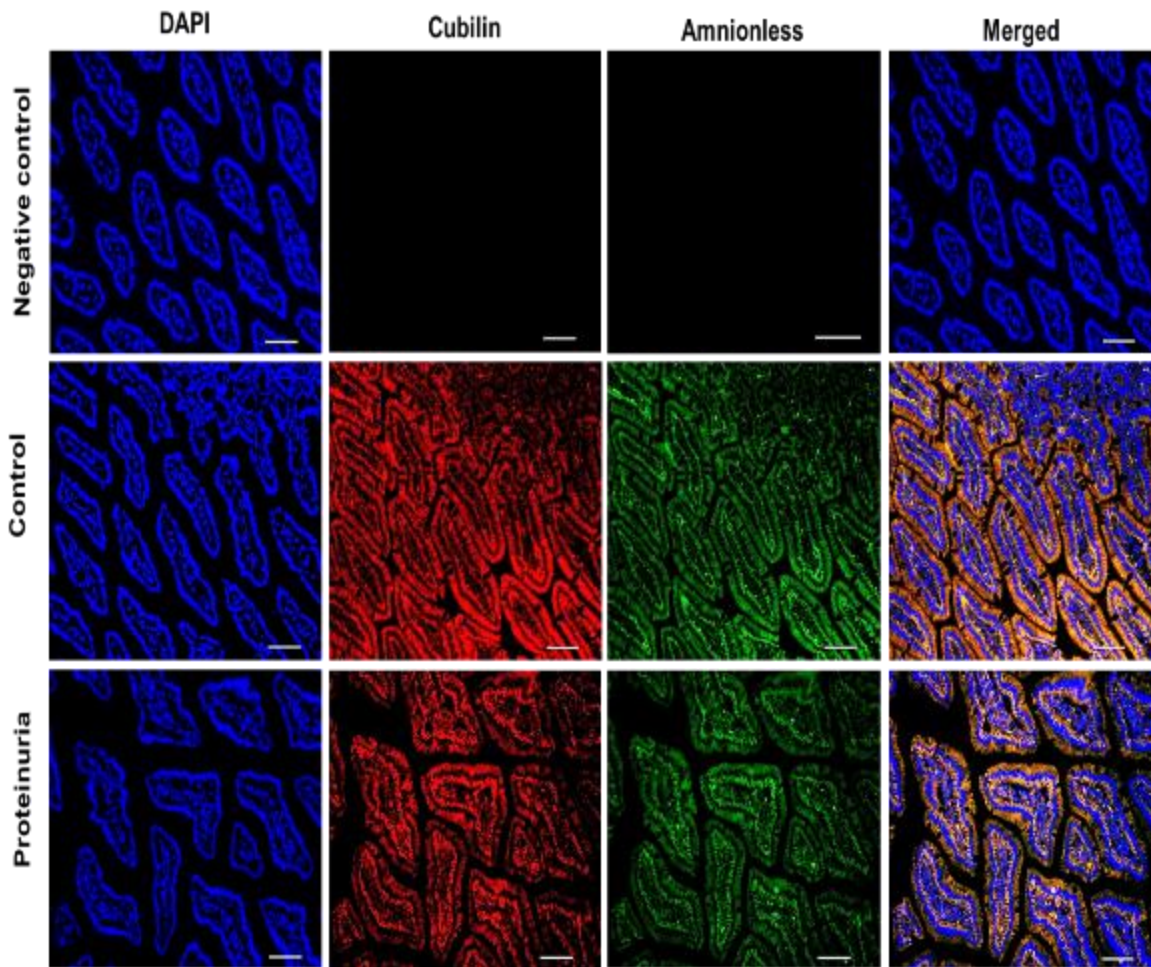


Figure.5.28. IF analysis for colocalization of cubilin and amnionless staining in mouse small intestine tissue.

Representative photomicrographs showing nuclei were stained blue with DAPI (left panels). Middle panels represent cubilin (cubilin A-20 antibody) red-stained and amnionless (amnionless antibody) green-stained. Right-hand panels represent merged (DAPI, cubilin and amnionless). All photomicrographs scale bars 100 μ m.

5.2.6.4. Effect of MMPI treatment on DPP-IV marker in proteinuria

Kidney tissue from each mice group was investigated for DPP-IV expression using immunoblotting, IHC and IF. DPP-IV expression at 116 kDa in proteinuric mice was similar to protein injected mice treated with the MMPI and controls (Figure.5.29A). Quantification of both endocytic protein receptors and normalised to DPP-IV found a significant decrease in proteinuric animals. For example, cubilin was (0.43 ± 0.05 relative intensity) and amnionless (0.38 ± 0.03 relative intensity). However, control mice, the cubilin was (1.4 ± 0.07) and amnionless was (1.3 ± 0.09 relative intensity). While MMPI treated animals, cubilin was obviously increased to (1.4 ± 0.05 relative intensity) as well as amnionless to (1.3 ± 0.07 relative intensity) (Figure.5.29B).

Additionally, IHC and IF results showed that DPP-IV expression was identical in each group (Figure.5.30 and 5.31). Quantification analysis depicted no significant difference in proteinuric mice, protein injected mice treated with the MMPI and controls (Figure.5.32).

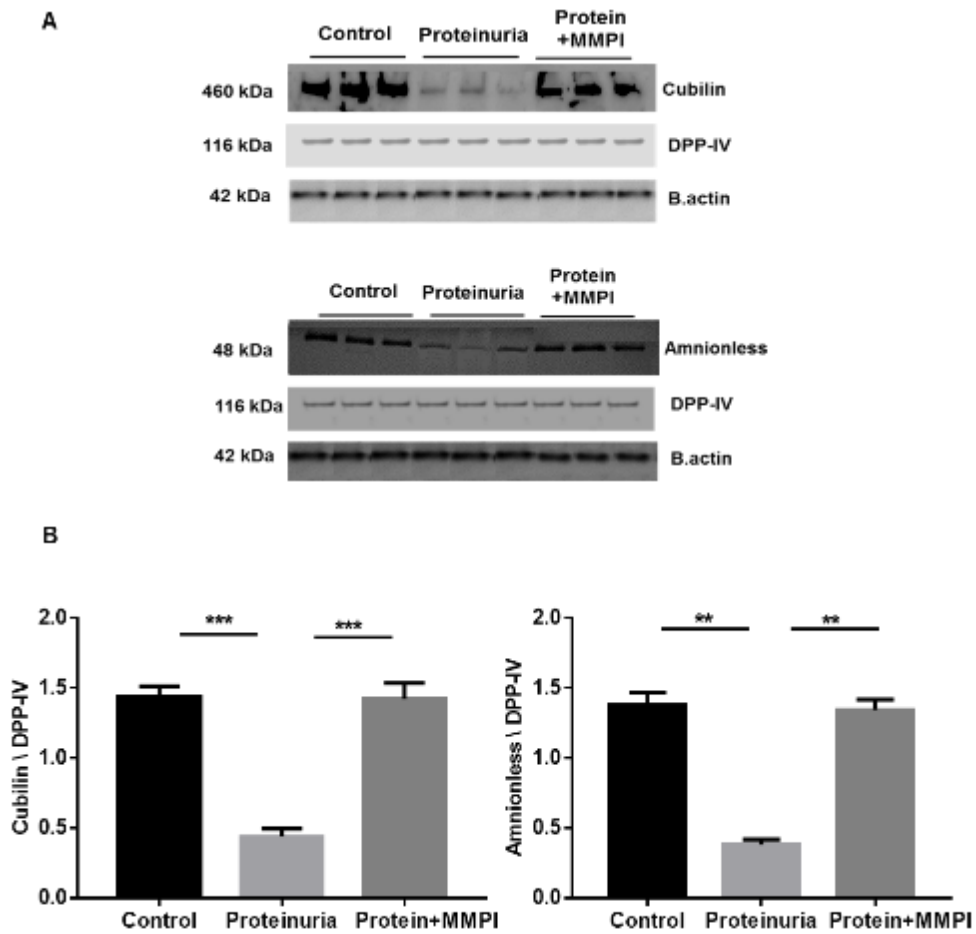


Figure.5.29. Analysis of DPP-IV expression in mouse kidney by immunoblotting.

(A) kidney cortex from control, proteinuric and protein injected mice treated with the MMPI was assessed by immunoblotting for previous cubilin and amnionless blots in comparison with DPP-IV proximal tubular marker and β -actin loading control. Blots stripped and reprobred for DPP-IV and β -actin loading control. (B) Densitometric analysis of cubilin and amnionless expression as a ratio to DPP-IV. **p<0.01 and ***p<0.001, one-way ANOVA.

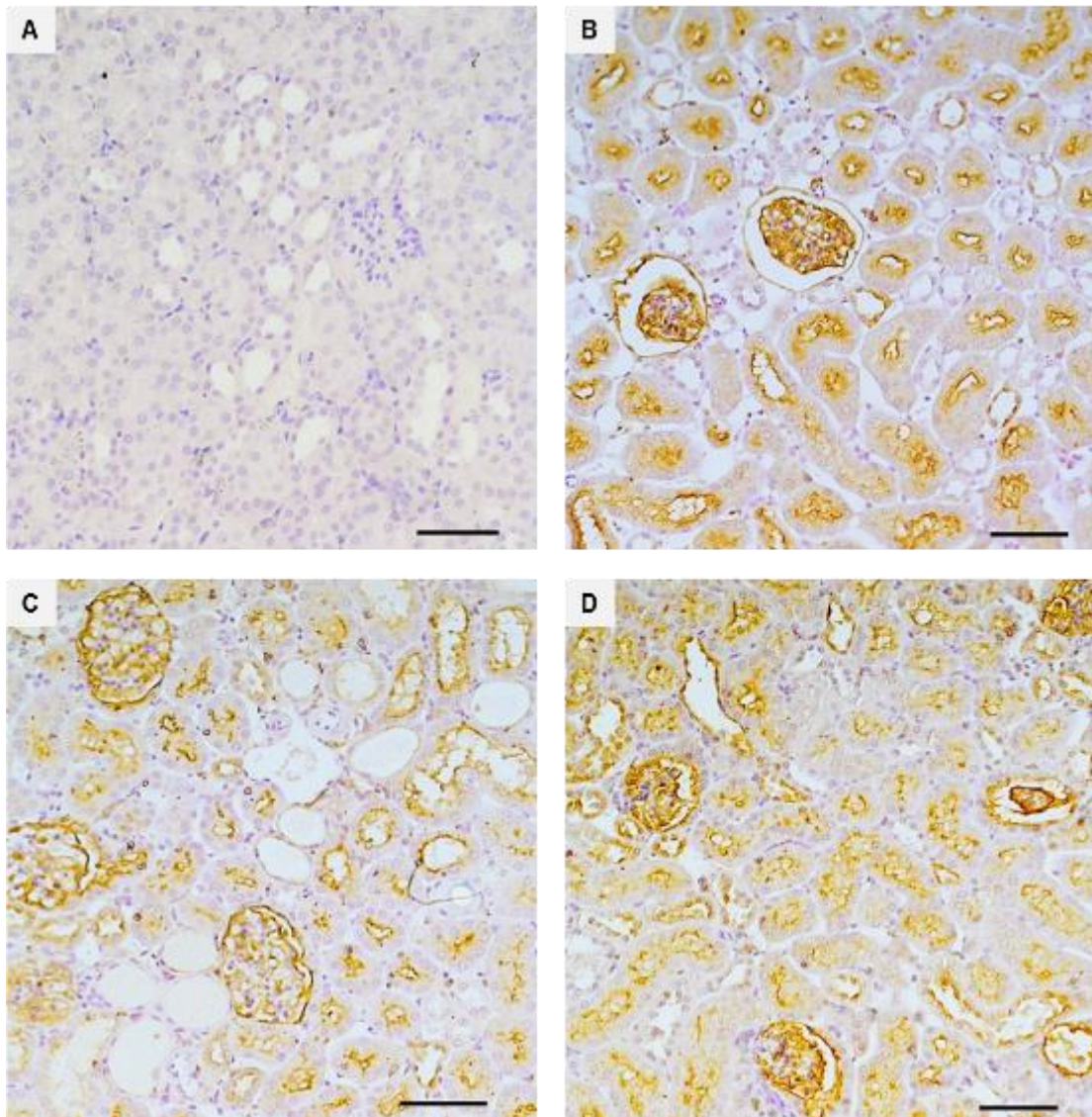


Figure.5.30. IHC analysis of mouse kidney tissue for DPP-IV in control, proteinuric mice and protein injected mice treated with the MMPI.

Representative photomicrographs showing (A) Negative control sections from control animals prepared without primary antibody. (B) Control mice. (C) Proteinuric mice. (D) Protein injected mice treated with the MMPI. Scale bars 100 μ M.

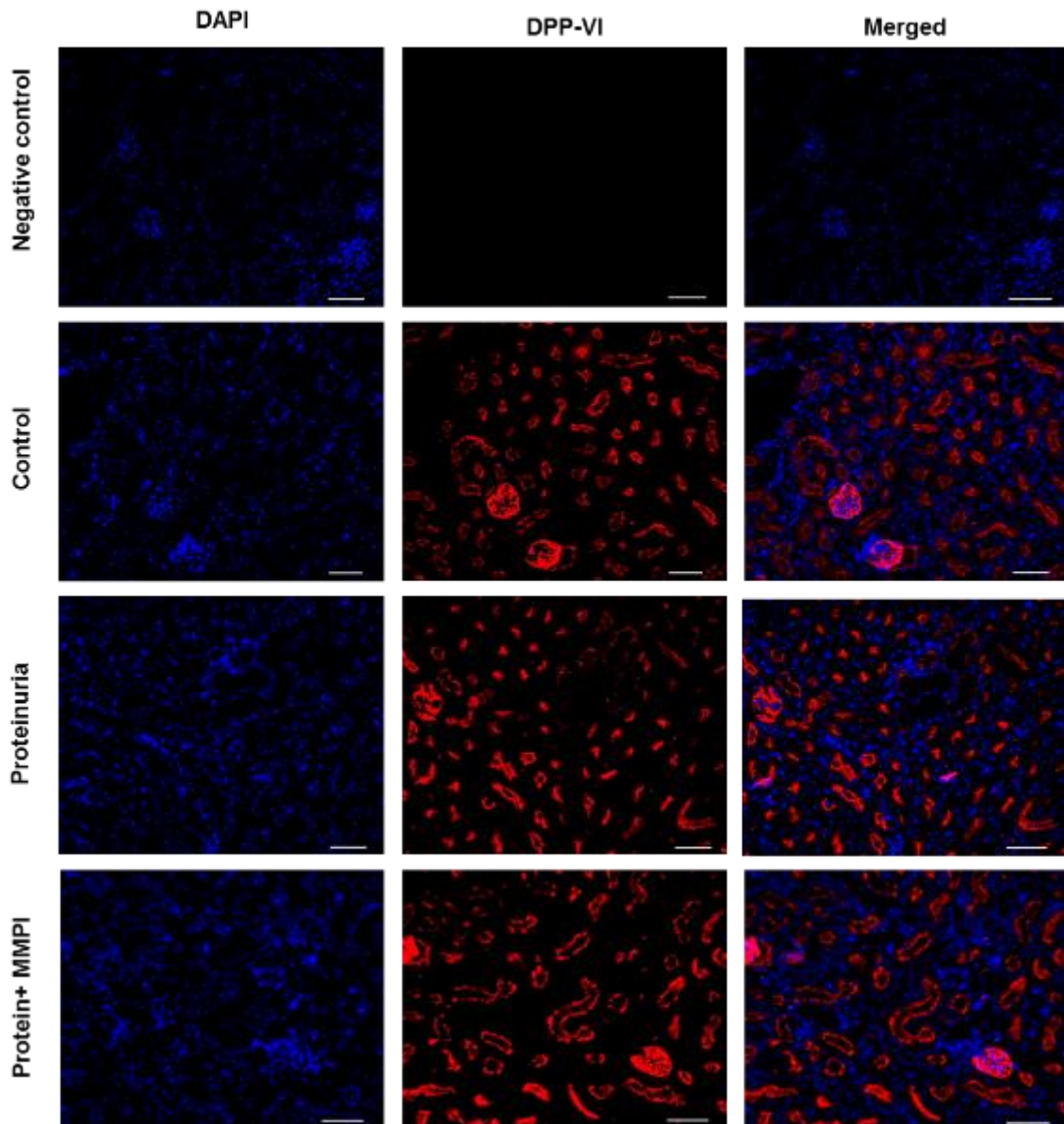


Figure.5.31. IF analysis of mouse kidney tissue for DPP-IV.

Representative photomicrographs showing negative control, control mice, proteinuric mice and protein injected mice treated with the MMPI. Nuclei were stained blue with DAPI (left panels). Middle panels represent DPP-IV (DPP-IV antibody) red-stained. Right-hand panels represent merged (DAPI and DPP-IV). Scale bars 100 μ M.

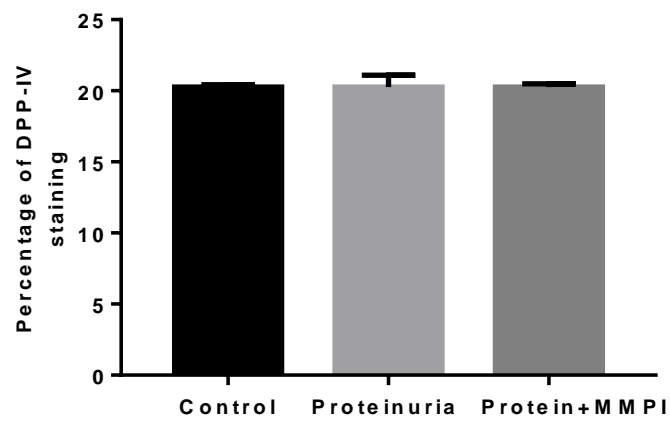


Figure.5.32. Semi-quantitative analysis of renal DPP-IV staining in control, proteinuric mice and protein injected mice treated with the MMPI.

Data are presented as mean \pm SEM of 4 mice per group. p =ns, one-way ANOVA.

5.3. Discussion

Cubam complex is responsible for reabsorption a wide range of glomerular ultrafiltered albumin (Pedersen et al., 2010, Amsellem et al., 2010). In the current study cubilin and amnionless receptors reduced on the cell surface of PTs and shed into the urine, which associated with loss of filtered proteins in the urine. This correlates with an increase of MMPs expression in proteinuria. These matrix enzymes could play an important role in the shedding of the extracellular domain of protein receptors by driving regulated intramembrane proteolysis (RIP) (Lichtenthaler et al., 2011, Lal and Caplan, 2011). The results of these experiments clearly showed that inhibition of MMPs reduced proteinuria and preserved the cell surface expression of cubilin and amnionless in the proximal tubules.

Previous investigators reported that albumin overload significantly revealed an increase in the expression and activity of MMPs. Albumin at diverse doses can increase the expression and activity of MMP-2 and MMP-9 in mouse podocytes (Zheng et al., 2009). Likewise, in vitro albumin overload led to upregulation and activation of MMP-9 in the glomerular parietal epithelial cell through activation of P44/42 MAPK pathway (Zhang et al., 2015). Another study found that albumin overload enhances the expression of MMP-9 by albumin endocytosis in renal tubule epithelial cells via the ERK signalling pathway (Chen et al., 2017). In a mouse model similar to the current study, Eddy et al (2000) revealed that the activity of MMP-9 increased but not significantly in TIMP-1 deficiency of albumin overload proteinuria (Eddy et al., 2000). However, our present study showed that MMP-2, MMP-3, MMP-7 and MMP-9 were significantly raised at both protein and mRNA expression in proteinuric animals. This activation of MMP in the kidney of

proteinuric mice may then contribute to the proximal tubular shedding of endocytic receptors.

The current findings detected that MMPI treatment reduced both the activity and expression of MMPs in proteinuric mice. MMPI (batimastat) is a broad-spectrum MMP inhibitor that mediates its action by the binding of a hydroxamate group to the zinc ion in the active site of MMPs (Botos et al., 1996). The previous investigator demonstrated that MMPI treatment reduced the activity of MMPs in various tissues. For instance, inhibition of MMPs activity by MMPI has been explored in acute kidney allograft rejection model. In this model, MMPI effectively inhibited MMP-2 and MMP-9 activity (Ermolli et al., 2003). Another study found that the enzymatic activity of MMPs considerably declined in skeletal muscle of mdx mice treated with MMPI (Kumar et al., 2010). Similarly, MMPI reduced the increased activity of MMP-2 and MMP-9 in a model of breast cancer (Low et al., 1996). Consistent with these studies, the findings of the present work displayed that MMPI treatment significantly reduced the increased MMP activity in proteinuric animals.

Although MMPI treatment inhibits the activity of MMPs the mechanism leading to a reduction of the MMPs expression by this treatment is not well described. The previous study demonstrated that reduced expression and activity of MMPs in animals and patients receiving MMP inhibitor (doxycycline). For instance, upregulation of expression and production of MMP-9 was reduced after doxycycline in the experimental aortic aneurysm (Petrinec et al., 1996). Likewise, both increased protein and mRNA expression of MMP-9 substantially declined in aneurysm tissues of patients treated with doxycycline (Curci et al., 2000). However, despite the fact that the models are different, MMPI treatment in the

present study showed a significant reduction in the expression of both protein and mRNA of MMP-2, MMP-3, MMP-7 and MMP-9 in proteinuric mice. Therefore, a decrease in the expression of MMPs by MMPI treatment could be related to the effect of this broad-spectrum inhibitor on the production and synthesis of this proteinase in the kidney. Consistent with these results Ermolli et al (2003) revealed that MMPI treatment (batimastat) caused a substantial reduction of MMP-2 mRNA production in acute kidney allograft rejection model (Ermolli et al., 2003). It seems that MMPI treatment is reducing the expression of MMPs, but the mechanism of downregulation is not well-defined.

An influence of MMPI treatment on reducing the risk of development of kidney diseases has been previously identified. For instance, MMPI treatment leads to a significant decline in cyst formation and kidney weight in a rat model of polycystic kidney disease (Obermuller et al., 2001b). Ermolli et al, (2003) illustrated that MMPI was effectively able to reduce proteinuria in transplanted animals (Ermolli et al., 2003). The significant point of the existing study showed that MMPI treatment is greatly reduced proteinuria and improved the renal function in proteinuric animals. This is proposing that MMPs activity may be contributing to alteration of the endocytic receptor expression of the proximal tubular or glomerular permselectivity in proteinuria. Another study supported that the antiproteinuric effect of MMPI: proteinuria was significantly decreased in hypertensive Dah1 salt-sensitive rats, and type 2 DN rats treated with MMPI (XL081 and XL784) (Williams et al., 2011). As a consequence, these MMPIs reduced glomerulosclerosis and renal injury in these animals, which might be by reduced proteinuria decreasing glomerular and renal injury (Williams et al., 2011). Furthermore, Lutz, et al (2005) revealed that early inhibition of MMPs after

transplantation is essential to reduce 24 hr protein and chronic allograft nephropathy (Lutz et al., 2005).

Synthetic broad-spectrum MMPi, such as minocycline and synthetic peptide MMPi showed that a significant decrease in the severity of the peritubular capillary injury, which led to a decline in AKI and improved renal function, decreasing serum creatinine after 24h in animals with ischemic AKI severity of PTC damage (Kunugi et al., 2011). Inhibition of MMP with GM6001 in hypertensive Dahl/SS rats found that reducing the intrarenal resistance, improved regional blood flow which consequently decreases serum creatinine and preserved renal function (Pushpakumar et al., 2013). Moreover, Ilomastat (GM6001) inhibited the activity and expression of MMPs resulting in an improvement in renal function and decreasing the blood urea nitrogen in cisplatin-induced injury (Ramesh and Reeves, 2004). The existing study depicted similar results to the previously mentioned studies that inhibition of MMPs by MMPi treatment decreases serum creatinine as a result of the improvement of renal function in proteinuric animals.

The current findings showed a significant reduction in cubilin complex receptors at both protein and gene levels in kidneys of proteinuric animals. Previous investigators in diabetic Goto–Kakizaki rats depicted that cubilin expression was significantly reduced in PTs associated with a rise in urinary albumin excretion, but after administration of gliquidone cubilin expression improved and urinary protein excretion decreased. This improvement in protein reabsorption was attributed to an amendment in endocytic receptors (Ke et al., 2014). Furthermore, another study found that cubilin reduction in proteinuria improved at the gene and protein level when treated with PPAR agonists. It appears that the mechanism of cubilin expression regulates at the gene level in the PTs by PPAR α and γ (Aseem

et al., 2013). Different mechanisms can regulate the expression of the cubam complex because the present study demonstrated that MMPI treatment improved cubilin and amnionless at cell surface expression and mRNA expression in proteinuric mice. However, the mechanism behind this effect is undetermined.

MMPs activity is obviously high in the tubular lumen of the diabetic kidney, associated with the shedding of endocytic receptors into the urine (Thraillkill et al., 2009b). Consistent with the above study, the findings of present work revealed that cubam complex endocytic receptors are elevated in the urine of proteinuric mice association with an increase of MMP activity. It is evident that MMPs are involved in the cleavage of the extracellular domain of membrane proteins by driving RIP (Nava et al., 2013, Lichtenthaler et al., 2011, Lal and Caplan, 2011). In vitro studies, for example, showed that megalin ectodomain was cleaved by RIP into the tubular lumen, whereas inhibition of MMP activity protected the cleavage of megalin (Zou et al., 2004). In our mouse model of protein overload proteinuria revealed that RIP could be an increase in urinary megalin excretion and its reduced expression in PTs of proteinuric mice (Fatah et al., 2017). Even though no evidence suggests that the RIP mechanism has a cleavage effect on cubam complex, this complex is close physically to megalin which may explain that cubam complex may be pulled free from the PTs as a consequence of megalin ectodomain shedding in proteinuria. Therefore, in the present experiment, MMPI treatment showed a significant decrease in cubilin and amnionless excretion in the urine of proteinuric mice. Furthermore, urinary excretion of albumin reduced in MMPI treated animals which indicate preservation of the cubam complex in the PTs. These observations suggest that maintaining the cubam complex expression is important in a reduction of proteinuria and the subsequent renal injury.

These data suggest that MMPI reduced the activity of MMP in the kidney. In addition, MMPI treatment reduced urinary excretion of plasma proteins which served to ameliorate cubam complex endocytic receptors expression in the PTs.

Chapter six

Matrix Metalloproteinase Inhibitor Ameliorates Renal Tubulointerstitial Fibrosis and Apoptosis in Proteinuric Mice

6.1. Introduction

Proteinuria contributes to progressive kidney damage by encouraging tubulointerstitial inflammation, fibrosis, tubular cell injury and death (Li et al., 2010). This sequence develops through various pathways, which leads to inflammatory cell infiltrate in the interstitium and sustained fibrogenesis (Abbate et al., 2006, Gorriz and Martinez-Castelao, 2012). MMPs have a key role in inflammatory cell recruitment and chemotaxis by regulating the inflammatory response and apoptosis (Tan and Liu, 2012). Apoptosis is a process that occurs in glomerular and tubulointerstitial areas of the kidney (Tejera et al., 2004), predominantly reliant on the activity of caspase-3 (Cryns and Yuan, 1998).

In chapter Four increased of MMP expression in proteinuria is described in association with reduced cubam expression. In these experiments, the effect of MMPI inhibition on the development of renal fibrosis, inflammation, renal proinflammatory mediators and apoptosis is examined.

6.2. Results

6.2.1. Renal histopathology in protein overload proteinuria and MMPI

The effect of MMPI on the renal histology of proteinuric mice and proteinuric mice with MMPI was investigated by histological assessment of H&E stained kidney sections. Mice with proteinuria showed a tubular injury with brush border loss, cellular swelling, and patchy tubular dilation and accumulation of tubular lumen casts (Figure 6.1B). By contrast, control mice showed no apparent histological changes in the kidney structure (Figure 6.1A). However, MMPI treatment resulted in an apparent reduction of the tubular injury in the kidneys of albumin injected mice (Figure 6.1C). The tubular injury scoring showed a significant increase in proteinuric mice compared to controls, whereas MMPI treated mice reduced (Figure.6.2). These results indicate that renal histological changes are reversible in the proteinuric animals when treated with MMPI.

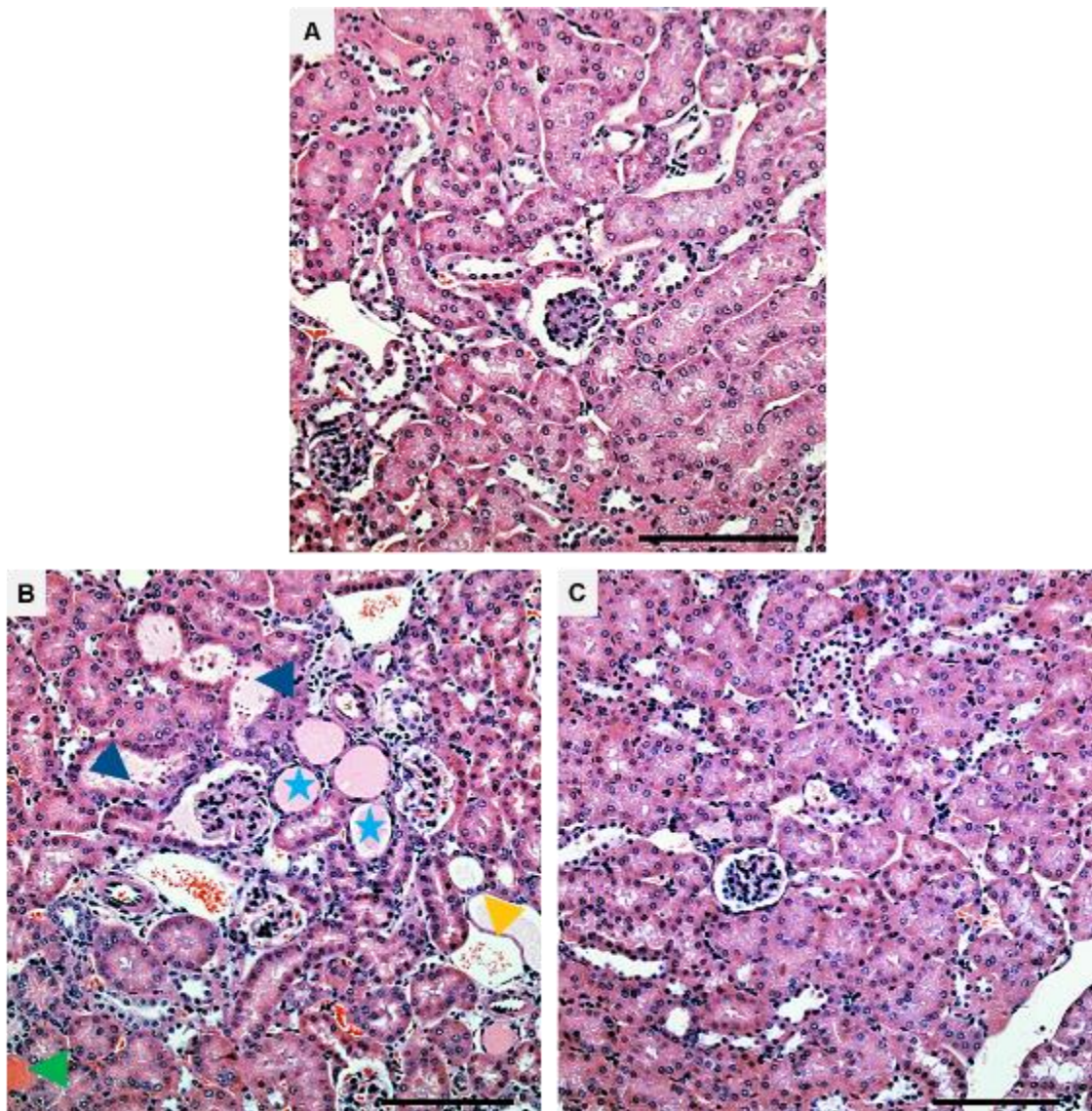


Figure.6.1. Kidney histology in control, proteinuric mice and protein injected mice treated with the MMPI.

Kidney injury was assessed in H&E stained kidney sections. (A) Control mice. (B) Proteinuric mice. (C) Protein injected mice treated with the MMPI. kidney sections of proteinuric mice illustrate the loss of brush border in renal tubules (yellow arrowheads), cast formation (blue asterisk), tubular dilatation (blue arrows), and intra-tubular blood cast (green arrowheads), Scale bars 100 μm .

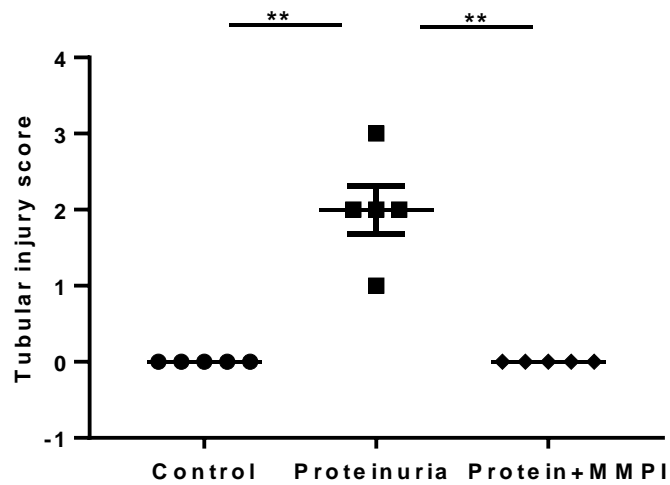


Figure.6.2. Renal tubular injury scoring in mouse kidney from control, proteinuric mice, and protein injected mice treated with the MMPI.

Data are expressed as mean \pm SEM of 4 mice per group. ** $p < 0.01$, one-way ANOVA.

6.2.2. Effect of MMPI treatment on collagen deposition in proteinuria

Sirius red staining was used to determine collagen deposition in the kidney of animals. Collagen deposition was barely detected in renal tissues from control mice (Figure 6.3A). Proteinuric mice displayed an increase in collagen deposition in the kidney (Figure 6.3B). Collagen in MMPI treated mice was significantly decreased (Figure 6.3C). The area of collagen staining displayed a significant rise in proteinuric mice ($11.8 \pm 0.7\%$ stained area) compared to control mice ($1.5 \pm 0.22\%$ stained area). However, MMPI treatment gave a significant decline of collagen to ($1.5 \pm 0.3\%$ stained area) in protein injected mice (Figure 6.4). This result indicates that the development of renal collagen in proteinuria is reversed by MMP inhibition.

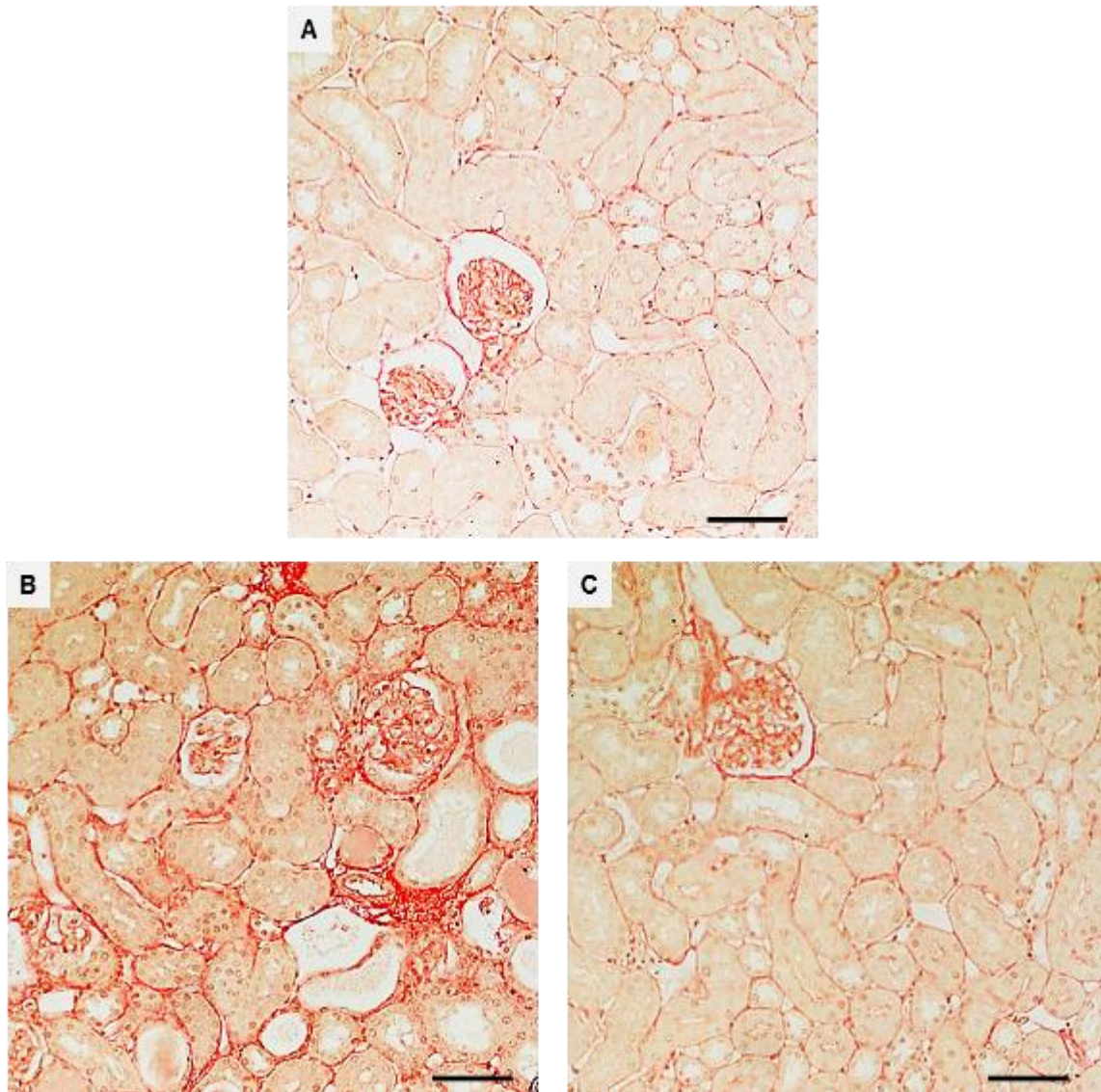


Figure.6.3. Sirius red staining of mouse kidney section for collagen deposition. Representative photomicrographs of showing (A) Control mice. (B) Proteinuric mice. (C) Protein injected mice treated with the MMPI. Scale bars 100 μ m

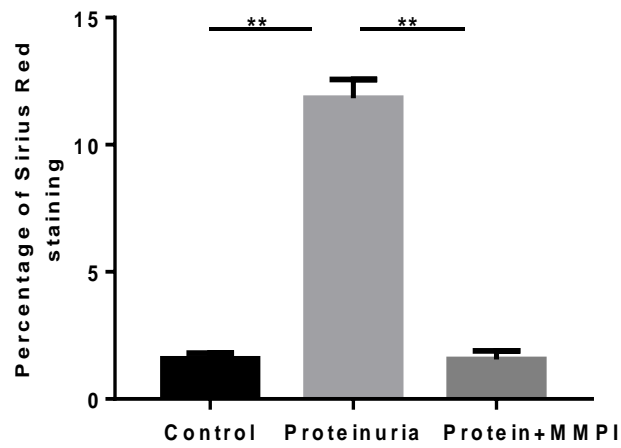


Figure.6.4. Semi-quantitative analysis of collagen deposition in mouse kidney from control, proteinuric mice and protein injected mice treated with the MMPI.

Results are expressed as mean \pm SEM of 4 mice per group. ** $p < 0.01$, one-way ANOVA.

6.2.3. Effect of MMPI treatment on renal macrophages in proteinuria

Macrophage F4/80 is a specific antigen marker on the surface of macrophages used to assess the degree of renal inflammation in protein overload proteinuria studies (Ma et al., 1998, Acosta et al., 2008, Donadelli et al., 2003). Immunoblotting was used to examine the macrophage expression in proteinuria. F4/80 bands at 160 kDa increased in proteinuric animals compared to controls and protein injected animals treated with the MMPI (Figure 6.5A). Results were quantified by densitometry and are shown in Figure 6.5B. A significant increase in F4/80 expression was seen in proteinuric mice (1.35 ± 0.034 relative intensity) in comparison with controls (0.43 ± 0.03 relative intensity), whereas protein injected mice treated with the MMPI was clearly reduced to (0.46 ± 0.09 relative intensity).

IHC results showed that greater F4/80 staining was detected in proteinuric mice compared with control groups, but this was not seen in protein injected mice treated with the MMPI (Figure 6.6). Semi-quantitative analysis of F4/80 staining revealed a significant increase in proteinuric mice to ($15.9 \pm 1.7\%$ stained area) compared to controls ($0.41 \pm 0.7\%$ stained area) but after MMPI treatment was significantly reduced to ($0.44 \pm 0.11\%$ stained area) (Figure.6.7).

qPCR studies (Figure.6.8) demonstrated that the expression of macrophage F4/80 mRNA was significantly increased to (7.9 ± 0.55 -fold) in proteinuric animals compared to controls (1 ± 0.2 -fold). When protein injected animals were treated with the MMPI this was substantially reduced to (0.99 ± 0.15 -fold). Together these results revealed that MMPI treatment decreased macrophages infiltration in kidneys proteinuria.

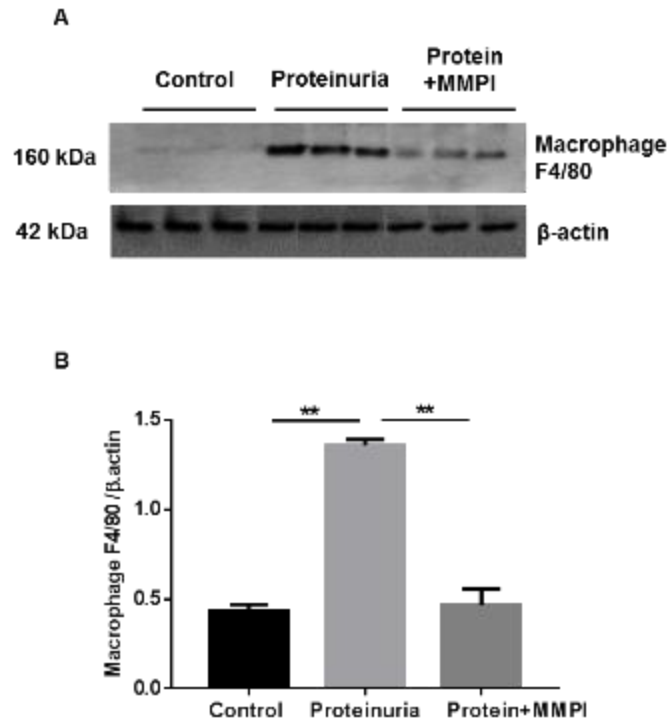


Figure.6.5. Analysis of macrophage F4/80 expression in mouse kidneys by immunoblotting.

(A) Kidney cortex from control, proteinuric mice and protein injected mice treated with the MMPI were evaluated for macrophage F4/80. Each lane represents a kidney sample from an individual animal from each group. The lower panel depicts a blot stripped and reprobbed for β -actin as a loading control. (B) Densitometric analysis of macrophage F4/80 expression as a ratio to β -actin. Results are expressed as mean \pm SEM of 3 mice per group. ** $p < 0.01$, one-way ANOVA.

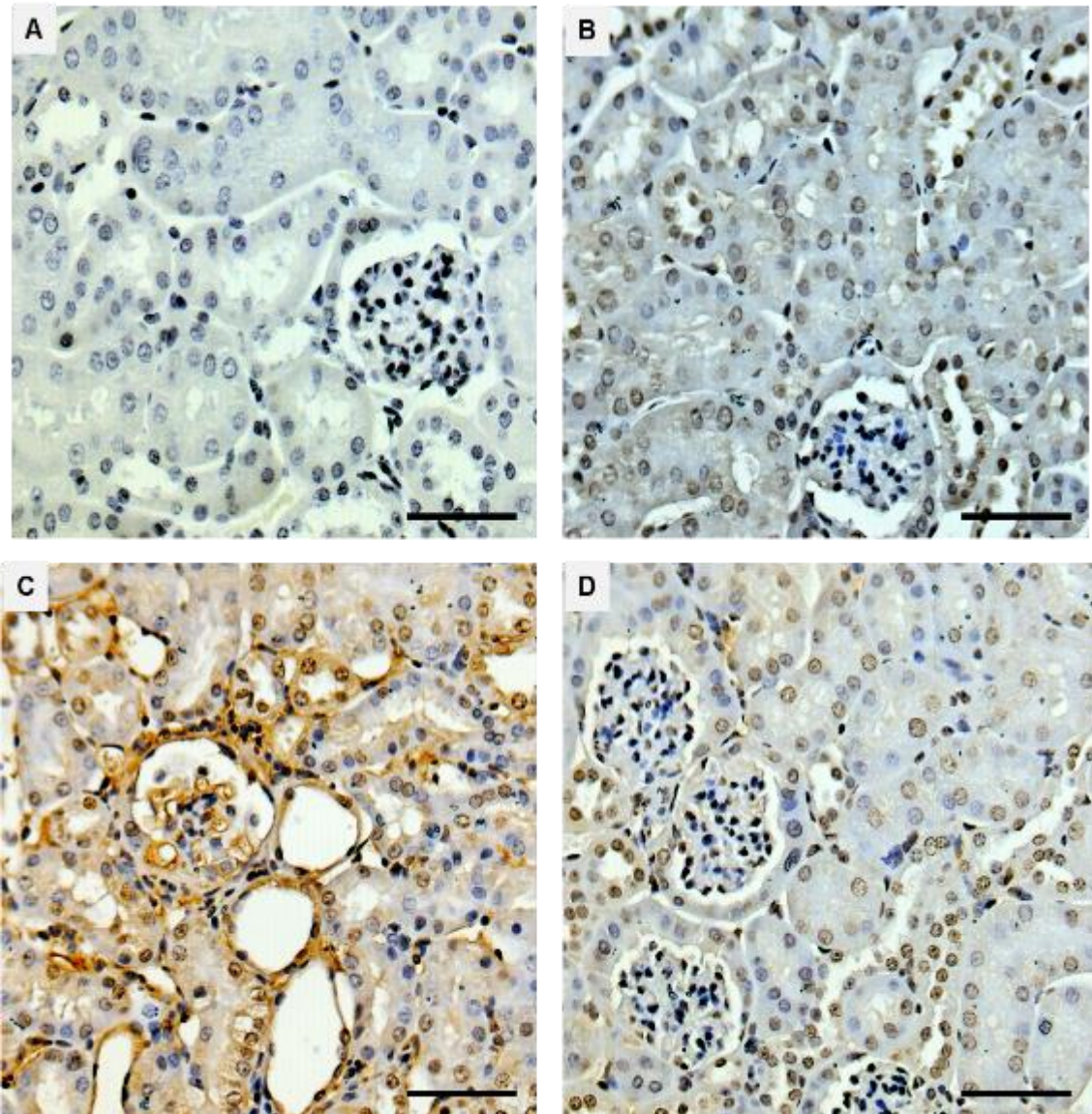


Figure.6.6. IHC analysis of mouse kidney tissue for macrophage F4/80 in control, proteinuric mice and protein injected mice treated with the MMPI.

Representative photomicrographs showing (A) Negative control sections from control animals prepared without primary antibody. (B) Control mice. (C) Proteinuric mice. (D) Protein injected mice treated with the MMPI. Scale bars 100 μ M.

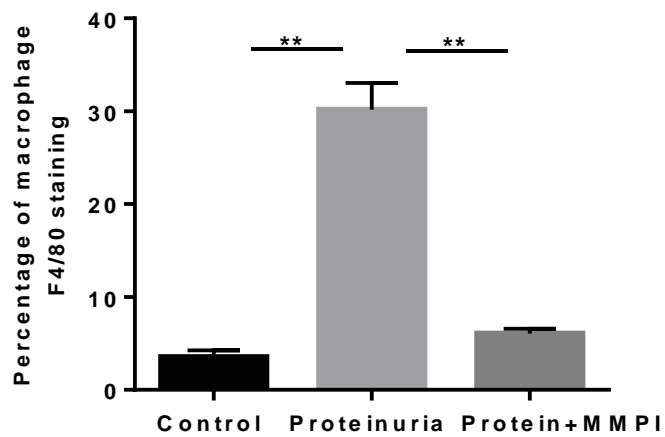


Figure.6.7. Semi-quantitative analysis of renal macrophage F4/80 staining in mouse kidney from control, proteinuric mice and protein injected mice treated with the MMPI.

Data are expressed as mean \pm SEM of 4 mice per group. ** $p < 0.01$, one-way ANOVA.

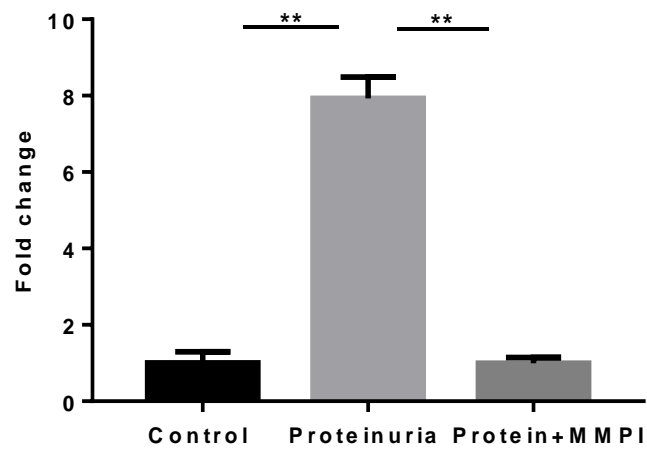


Figure.6.8. Fold change in macrophage F4/80 mRNA expression in mouse kidneys from control, proteinuric mice and protein injected mice treated with the MMPI.

mRNA was extracted from the kidney cortex and subjected to qPCR. Data are expressed as mean \pm SEM of 4 mice per group. **p < 0.01, one-way ANOVA.

6.2.4. Effect of MMPI treatment on renal interleukin-6 expression in proteinuria

To determine the effect of MMPI treatment on IL-6 in proteinuria, kidney tissues from each group were investigated by immunoblotting. IL-6 bands at 21 kDa were clearly detected in proteinuric animals. In contrast, IL-6 was virtually undetectable in both control and MMPI treated animals (Figure 6.9A). When quantified IL-6 protein was significantly higher in proteinuric groups (1.52 ± 0.1703 relative intensity) than in controls (0.14 ± 0.054 relative intensity). Conversely, IL-6 expression in protein injected groups treated with the MMPI was significantly lowered to (0.218 ± 0.085 relative intensity) (Figure.6.9B).

IHC displayed strong immunolabeling of IL-6 in the kidneys of proteinuric mice compared with controls (Figure 6.10C vs 6.10B), whereas protein injected mice treated with the MMPI exhibited no immunoreactive signals (Figure 6.10 D). Semi-quantitative analysis of the kidney sections revealed a significant rise in IL-6 expression in proteinuric mice (30.9 ± 0.9 % stained area) compared to control mice (2.5 ± 0.24 % stained area). However, MMPI treatment has significantly reduced to (5.1 ± 0.19 % stained area) in protein injected mice (Figure.6.11).

qPCR confirmed that IL-6 mRNA expression was markedly increased in proteinuric mice to (3.7 ± 0.52 -fold) compared with control mice (1 ± 0.26 -fold). While MMPI treatment of protein injected mice showed a significant decline in IL-6 mRNA expression to (1.06 ± 0.28 -fold) (Figure.6.12). These results suggest that MMPI treatment can decrease IL-6 expression and regulate its gene expression in proteinuria.

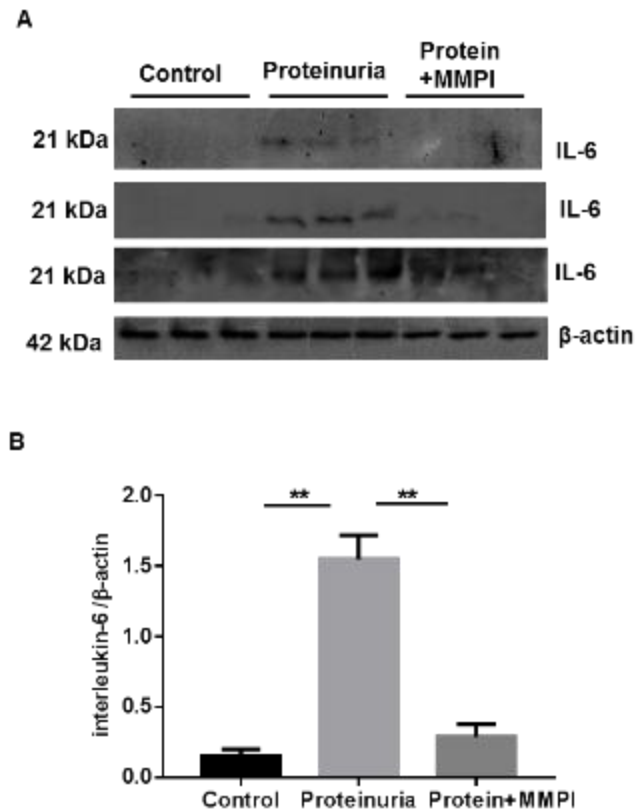


Figure.6.9. Analysis of IL-6 expression in mouse kidneys by immunoblotting.

(A) Kidney cortex from control, proteinuric mice and protein injected mice treated with the MMPI were evaluated for IL-6. Each lane represents a kidney sample from an individual animal from each group. The lower panel depicts a blot stripped and reprobbed for β -actin as a loading control. (B) Densitometric analysis of IL-6 expression as a ratio to β -actin. Results are expressed as mean \pm SEM of 3 mice per group. ** $p < 0.01$, one-way ANOVA.

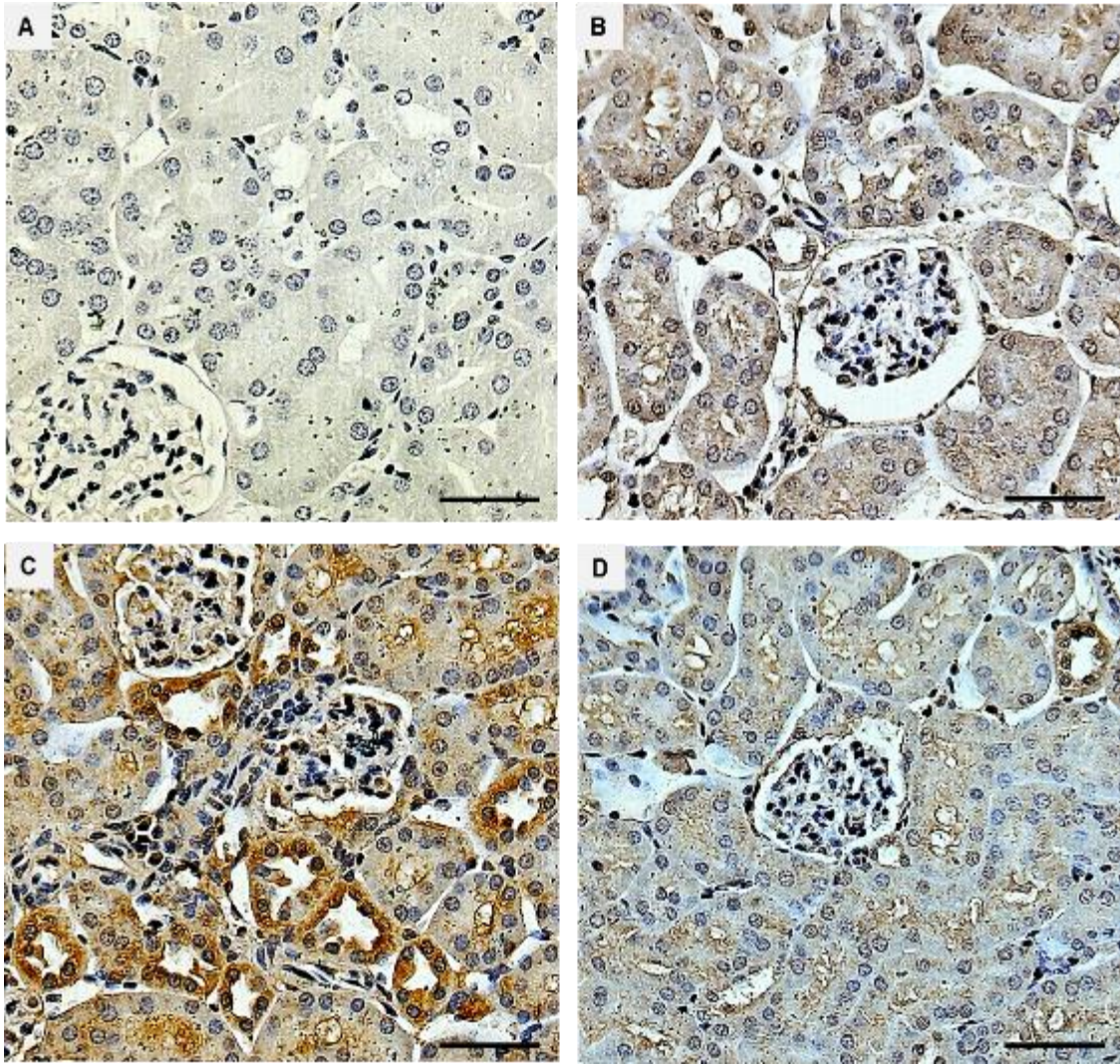


Figure.6.10. IHC analysis of mouse kidney tissue for IL-6 in control, proteinuric mice and protein injected mice treated with the MMPI.

Representative photomicrographs showing (A) Negative control sections from control animals prepared without primary antibody. (B) Control mice. (C) Proteinuric mice. (D) Protein injected mice treated with the MMPI. Scale bars 100 μ M.

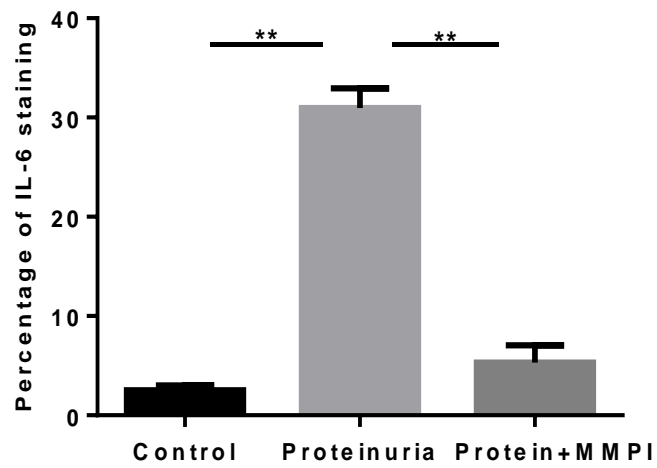


Figure.6.11. Semi-quantitative analysis of renal IL-6 staining in mouse kidney from control, proteinuric mice and protein injected mice treated with the MMPI.

Data are expressed as mean \pm SEM of 4 mice per group. ** $p < 0.01$, one-way ANOVA.

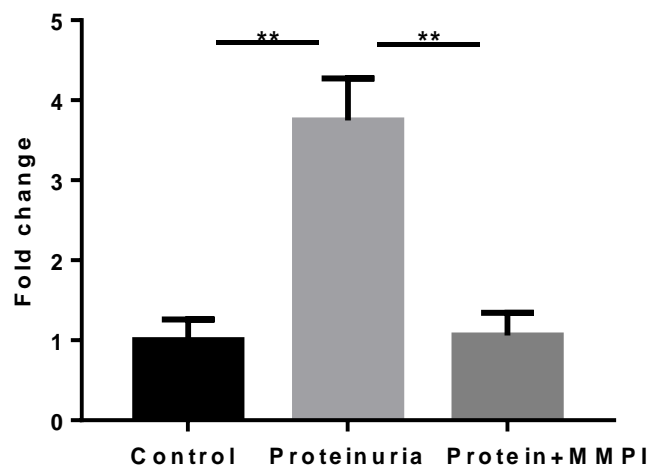


Figure.6.12. Fold change in IL-6 mRNA expression in mice kidneys from control, proteinuric mice and protein injected mice treated with the MMPI.

mRNA was extracted from the kidney cortex and subjected to qPCR. Data are expressed as mean \pm SEM of 4 mice per group. **p < 0.01, one-way ANOVA.

6.2.5. Effect of MMPI treatment on renal tumour necrosis factor-alpha (TNF- α) expression in proteinuria

To investigate the effect of MMPI treatment on TNF- α expression in proteinuria, kidney tissues from each group were assessed by immunoblotting. More prominent TNF- α bands at 17 kDa were revealed in proteinuric mice compared to controls. However, TNF- α bands were faintly detected in protein injected mice treated with the MMPI (Figure 6.13A). Quantified TNF- α expression showed a significant increase in proteinuric mice (1.3 ± 0.06 relative intensity) compared with controls (0.2 ± 0.06 relative intensity), while the MMPI treatment of protein injected mice substantially reduced this to (0.39 ± 0.04 relative intensity) (Figure 6.13B).

IHC results revealed TNF- α immunostaining was prominently detected in the kidneys of proteinuric animals (Figure. 6.14C). Conversely, in MMPI treated mice and in controls, this was not observed (Figure 6.14D and 6.14B). The semi-quantitative analysis showed a significant increase in proteinuric animals (25.0 ± 2.1 % stained area) compared with controls (3.7 ± 0.18 % stained area), whereas MMPI treatment remarkably reduced (5.1 ± 0.19 % stained area) (Figure.6.15).

By qPCR, proteinuric groups had a significant increase in mRNA levels of TNF- α (3.5 ± 0.58 -fold) compared with controls (1 ± 0.199 -fold) but MMPI treatment considerably reduced the mRNA level to (1.001 ± 0.07 -fold) (Figure.6.16). These data revealed that MMPI treatment suppresses TNF- α in the kidneys of protein injected animals.

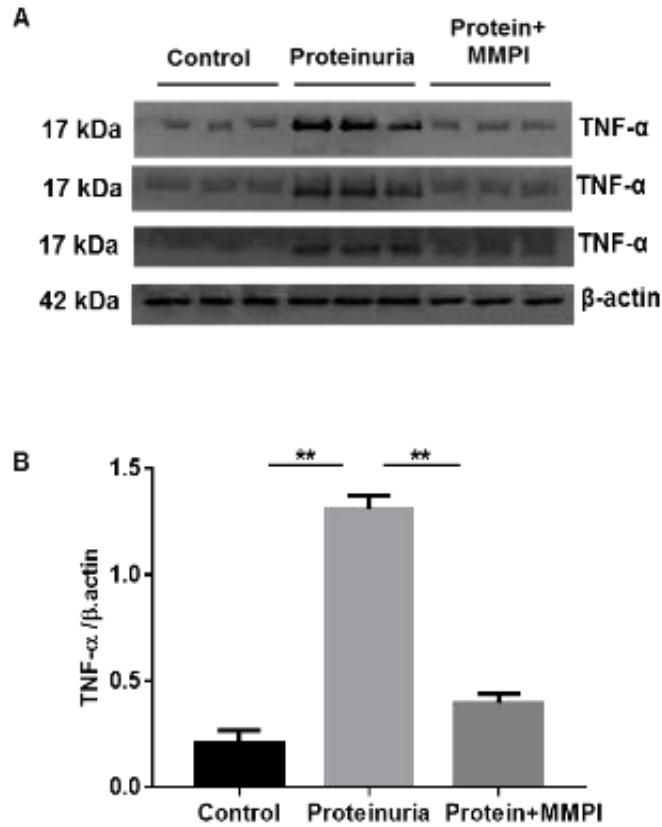


Figure.6.13. Analysis of TNF- α expression in mouse kidneys by immunoblotting. (A) Kidney cortex from control, proteinuric mice and protein injected mice treated with the MMPI were evaluated for TNF- α . Each lane represents a kidney sample from an individual animal from each group. The lower panel depicts a blot stripped and reprobbed for β -actin as a loading control. (B) Densitometric analysis of TNF- α expression as a ratio to β -actin. Results are expressed as mean \pm SEM of 3 mice per group. ** $p < 0.01$, one-way ANOVA.

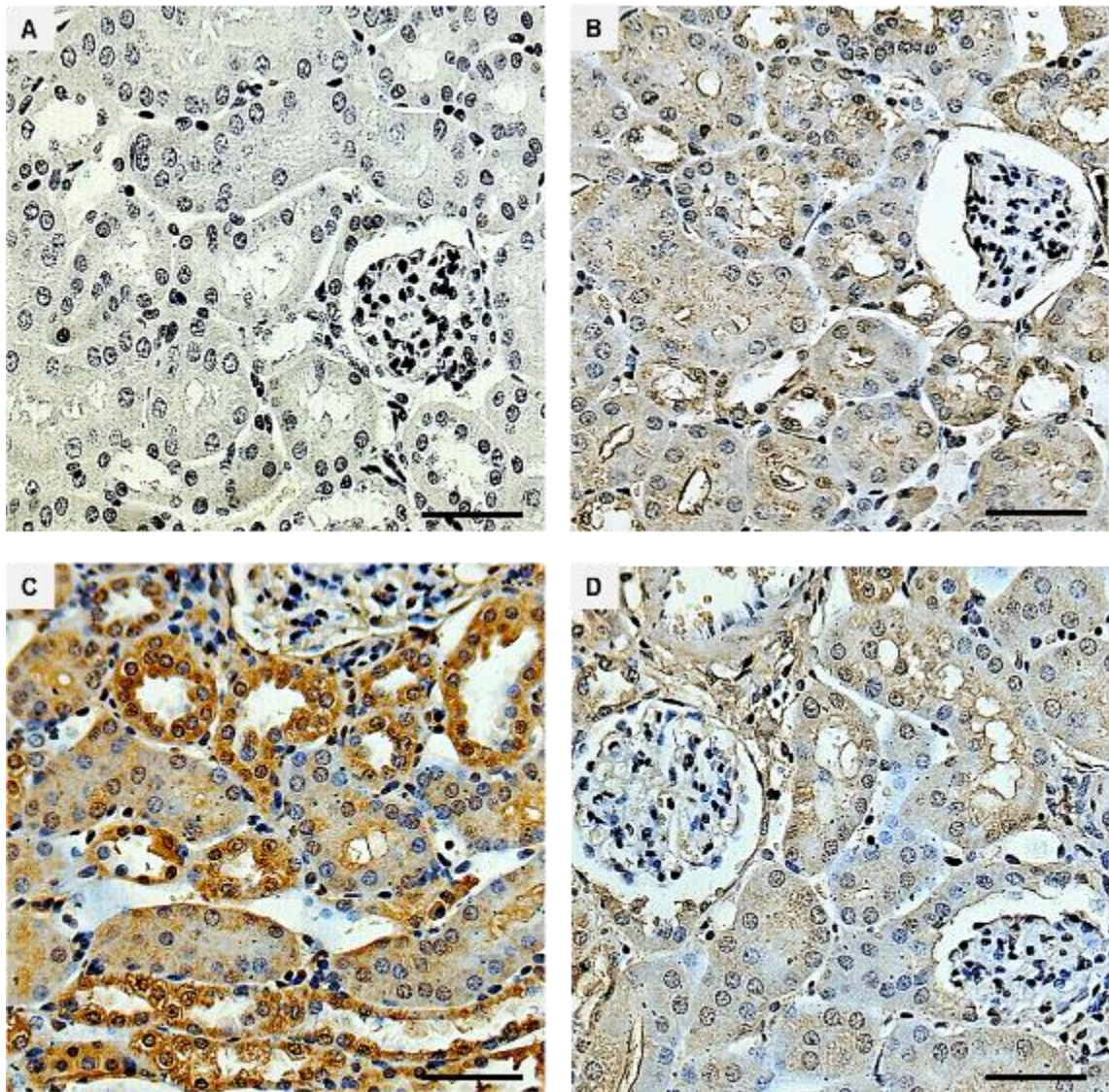


Figure.6.14. IHC analysis of mouse kidney tissue for TNF-alpha in control, proteinuric and protein injected mice treated with the MMPI.

Representative photomicrographs showing (A) Negative control sections from control animals prepared without primary antibody. (B) Control mice. (C) Proteinuric mice. (D) Protein injected mice treated with the MMPI. Scale bars 100 μ M.

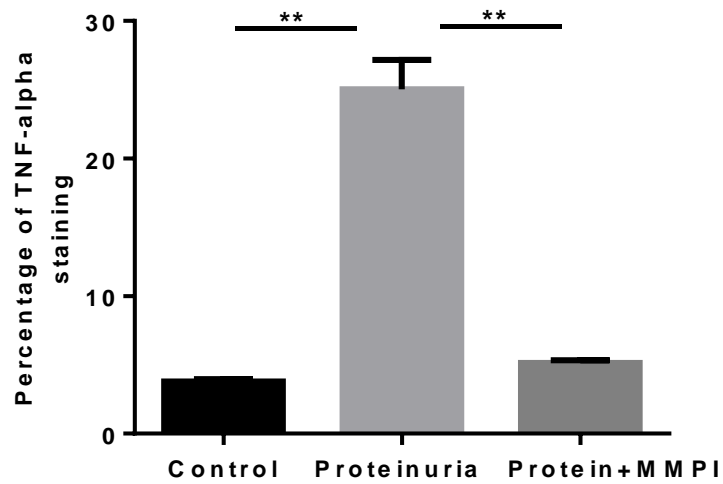


Figure.6.15. Semi-quantitative analysis of renal TNF-alpha staining in mouse kidney from control, proteinuric mice and protein injected mice treated with the MMPI.

Data are expressed as mean \pm SEM of 4 mice per group. ** $p < 0.01$, one-way ANOVA.

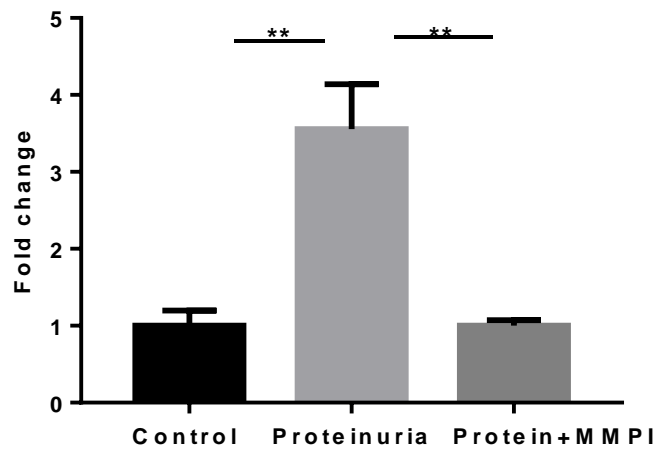


Figure.6.16. Fold change in TNF- α mRNA expression in mice kidneys from control, proteinuric mice and protein injected mice treated with the MMPI.

mRNA was extracted from the kidney cortex and subjected to qPCR. Data are expressed as mean \pm SEM of 4 mice per group. ** $p < 0.01$, one-way ANOVA.

6.2.6. Effect of MMPI treatment on renal transforming growth factor-beta (TGF- β) expression in proteinuria

TGF- β expression was studied either in proteinuria or proteinuria with MMPI. Kidney tissues from each group were studied by immunoblotting. More prominent TGF- β bands were detected at 25 kDa in proteinuric mice compared with controls. Similarly, their bands were faintly displayed in mice treated with MMPI (Figure 6.17A). By densitometric analysis, TGF- β expression was significantly increased in the kidney of proteinuric animals (1.17 ± 0.026 relative intensity) in comparison with controls (0.57 ± 0.02 relative intensity). However, MMPI treatment has dramatically decreased to (0.59 ± 0.022 relative intensity) in protein injected animals (Figure 6.17B).

To confirm the immunoblotting results, IHC found appreciable TGF- β staining in the kidneys of proteinuric mice (Figure. 6.18 C). In contrast, no staining was detected in mice with MMPI and controls (Figure.6.18D and 6.18B). Semiquantitative analysis of TGF- β expression revealed a substantial rise in animals with proteinuria (17.5 ± 0.9 % stained area) while in controls (2.47 ± 0.19 % stained area). In MMPI treatment of proteinuric animals, this was significantly decreased (3.81 ± 0.38 % stained area) (Figure.6.19).

In addition, the expression of TGF- β mRNA in proteinuric mice was greatly increased to (3.26 ± 0.36 -fold) compared with controls (1 ± 0.19 -fold). Whereas MMPI treatment has substantially reduced it to (1.1 ± 0.167 -fold) (Figure.6.20). These data demonstrated that MMPI treatment decreases the expression levels of TGF- β at protein and gene levels in the kidneys of proteinuric mice.

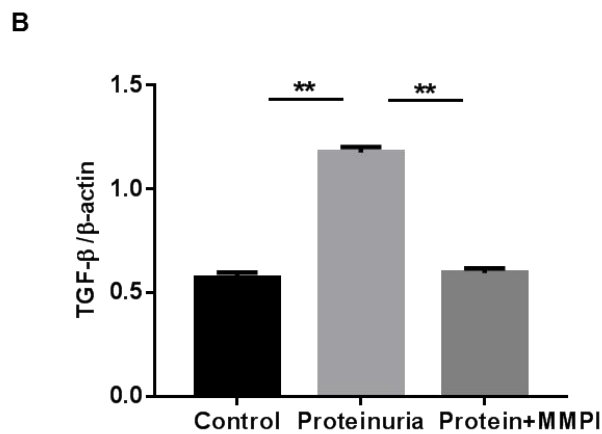
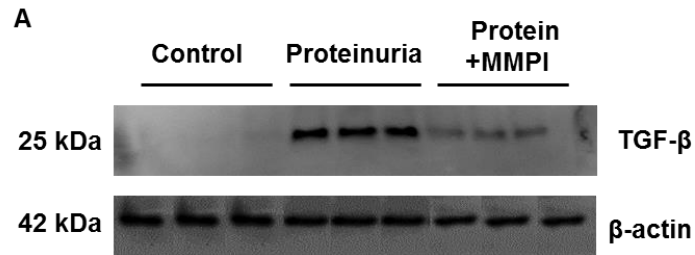


Figure.6.17. Analysis of TGF-β expression in mouse kidneys by immunoblotting. (A) Kidney cortex from control, proteinuric mice and protein injected mice treated with the MMPI were evaluated for TGF-β. Each lane represents a kidney sample from an individual animal from each group. The lower panel depicts a blot stripped and reprobbed for β-actin as a loading control. (B) Densitometry analysis of TGF-β immunoblots expressed as a ratio to β-actin. Results are expressed as mean ± SEM of 3 mice per group. **p < 0.01, one-way ANOVA.

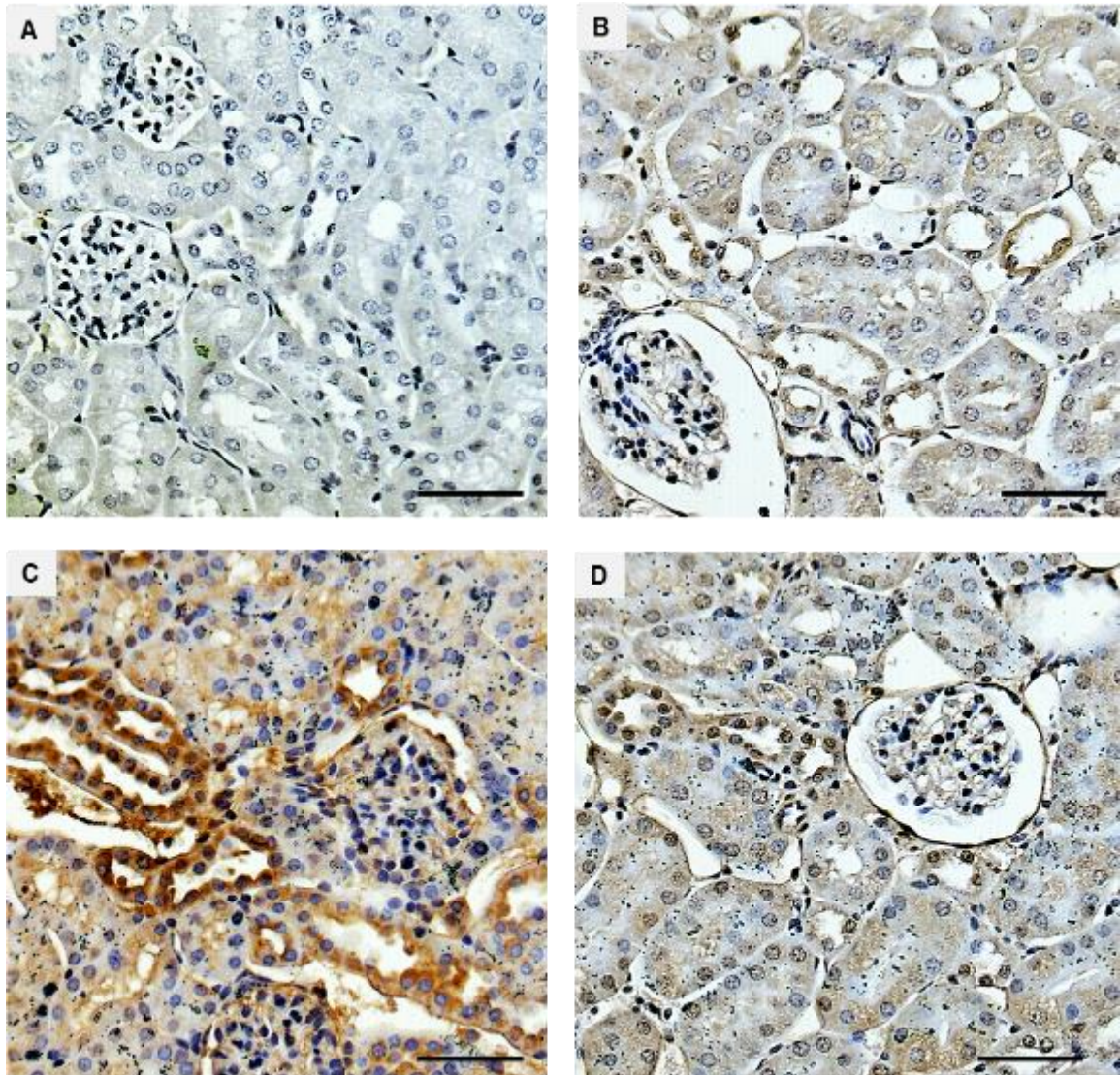


Figure.6.18. IHC analysis of mouse kidney tissue for TGF- β in control, proteinuric and protein injected mice treated with the MMPI.

Representative photomicrographs showing (A) Negative control sections from control animals prepared without primary antibody. (B) Control mice. (C) Proteinuric mice. (D) Proteinuric mice treated with MMPI, Scale bars 100 μ M.

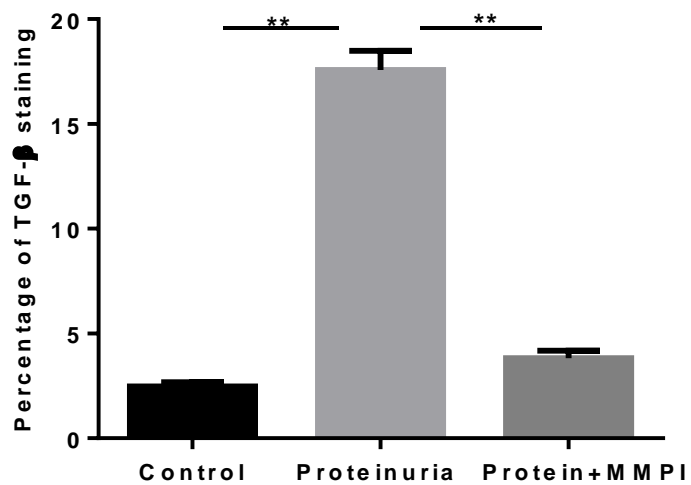


Figure.6.19. Semi-quantitative analysis of renal TGF- β staining in control, proteinuric mice and protein injected mice treated with the MMPI.

Data are expressed as mean \pm SEM of 4 mice per group. ** $p < 0.01$, one-way ANOVA.

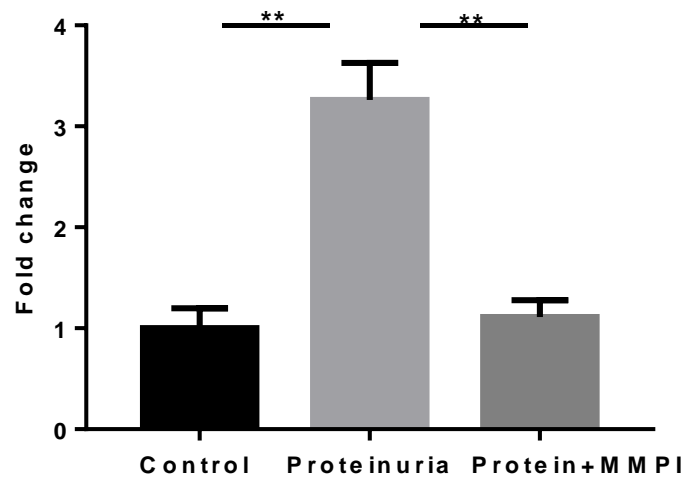


Figure.6.20. Fold change in TGF- β mRNA expression in mice kidneys from control, proteinuric mice and proteinuric mice treated with the MMPI.

mRNA was extracted from the kidney cortex and subjected to qPCR. Data are expressed as mean \pm SEM of 4 mice per group. ** $p < 0.01$, one-way ANOVA.

6.2.7. Effect of MMPI treatment on apoptosis in proteinuria

The influence of MMPI on apoptosis in proteinuria was studied by TUNEL assay. In proteinuric animals, TUNEL staining was increased compared with controls (Figure 6.21C vs 6.21B). In contrast, TUNEL staining was not detected in MMPI treated mice (Figure 6.21D). Similarly, apoptotic cells revealed a significant increase in proteinuric mice (32.4 ± 0.5) with respect to controls (1.1 ± 0.03). While MMPI treatment of protein injected mice showed a low number of apoptotic cells (1.2 ± 0.04) (Figure.6.22). These results indicate that MMPI treatment reduces the number of apoptotic cells in the kidneys of protein overload proteinuria mice.

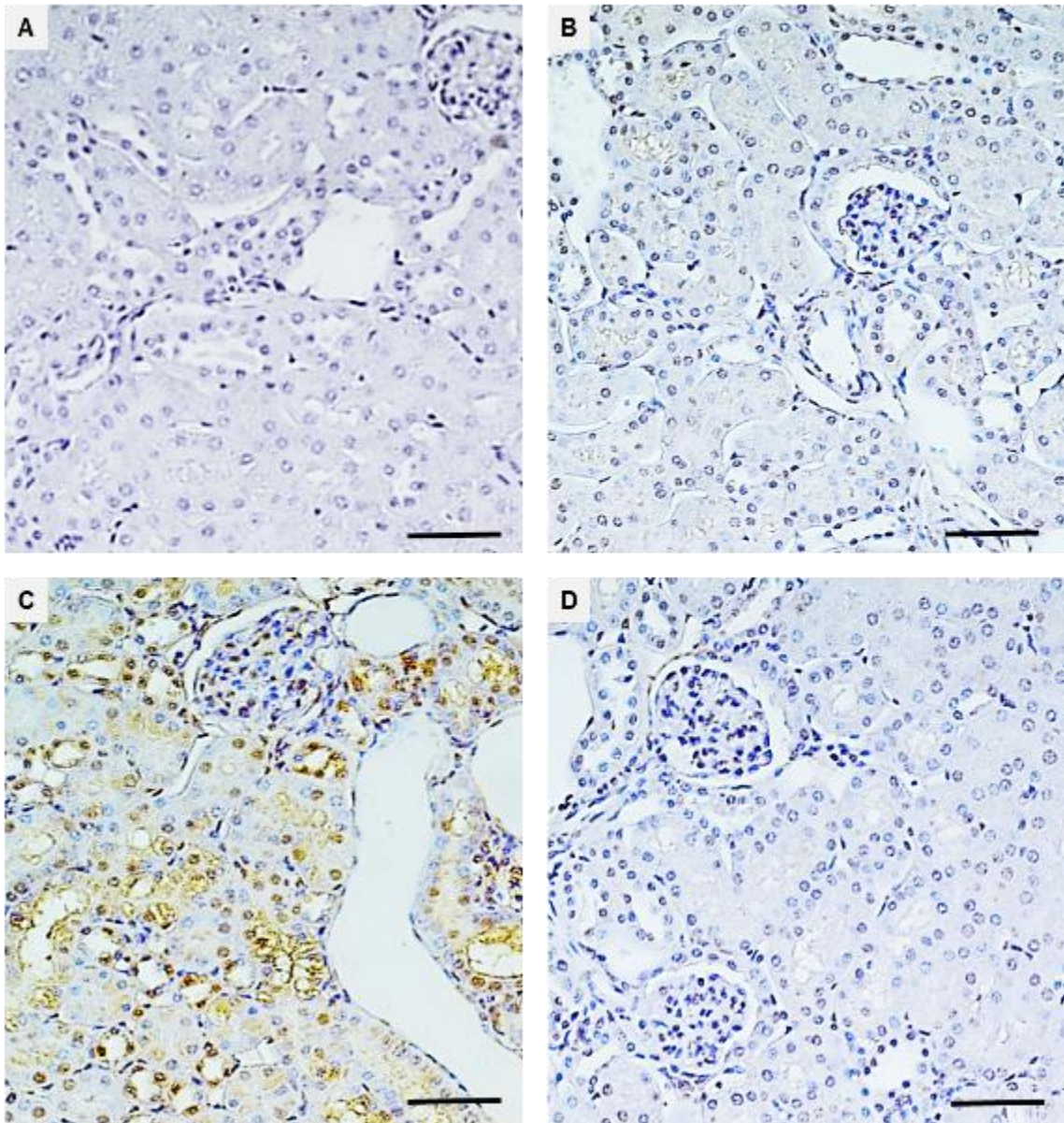


Figure.6.21. TUNEL stained mouse kidney sections for detection apoptosis.

Representative photomicrographs showing (A) Negative control sections from control animals prepared without TdT. (B) Control mice. (C) Proteinuric mice. (D) Protein injected mice treated with the MMPI. Scale bars 100 μ M.

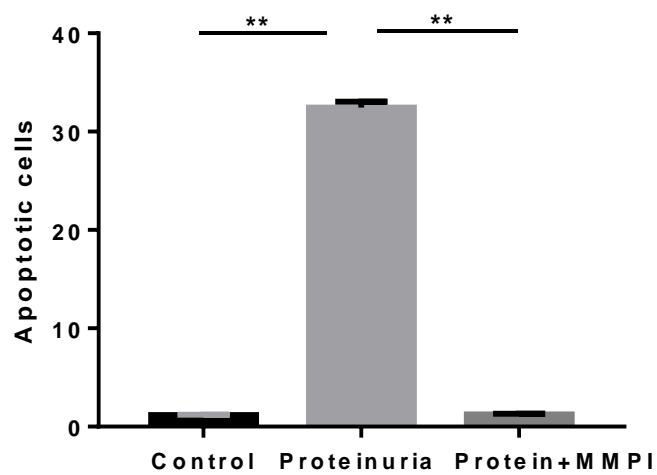


Figure.6.22. Numbers of apoptotic cells counted by Image J in control, proteinuric mice and protein injected mice treated with the MMPI.

Results are expressed as a percentage mean \pm SEM of 4 mice per group, $^{**}p < 0.01$, one-way ANOVA.

6.2.8. Effect of MMPI treatment on renal caspase-3 expression in proteinuria

MMPI effects on caspase-3 expression in proteinuria were studied by immunoblotting, IHC and IF. As shown in figure 6.23 A and B, caspase-3 bands at 35 kDa displayed a significant increase in proteinuric mice (1.08 ± 0.07 relative intensity) compared with controls (0.1 ± 0.02 relative intensity) but MMPI treated mice was considerably reduced to (0.12 ± 0.04 relative intensity).

IHC and IF results also confirmed that caspase-3 expression was substantially increased in proteinuric mice (23.6 ± 0.3 % stained area) compared with controls (0.8 ± 0.11 % stained area). Caspase-3 expression was substantially reduced in MMPI treated mice to (0.76 ± 0.12 % stained area) (Figure.6.24 to 6.27).

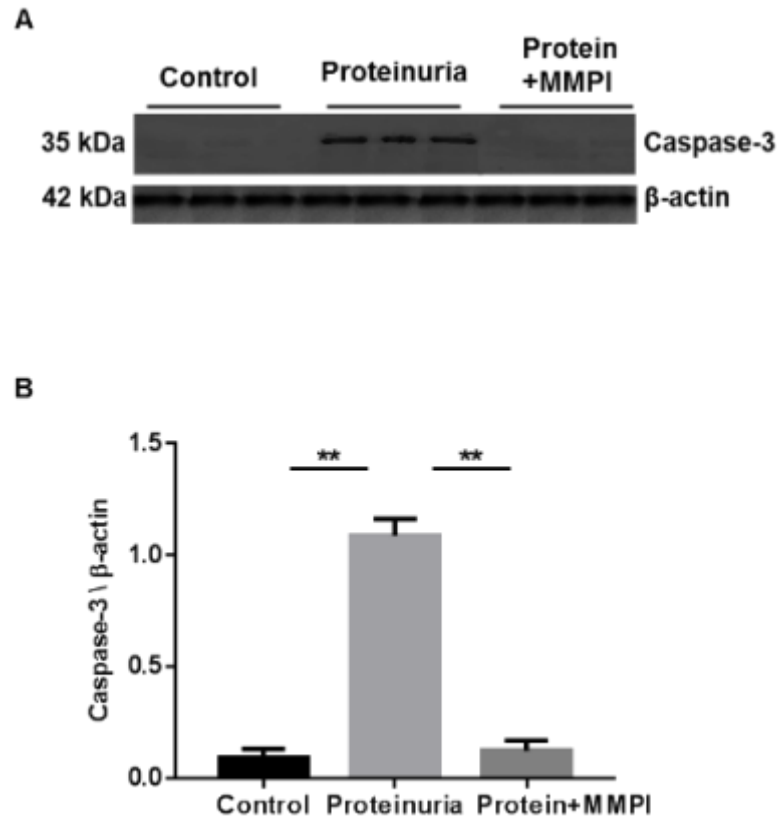


Figure.6.23. Analysis of caspase-3 expression in mouse kidneys by immunoblotting.

(A) Kidney cortex from control, proteinuric mice, and protein injected mice treated with the MMPI were evaluated by immunoblotting for caspase-3. Each lane represents a kidney sample from an individual animal from each group. The lower panel depicts a blot stripped and reprobed for β -actin as a loading control. (B) Densitometric analysis of caspase-3 expression, Results are expressed as a ratio to β -actin, mean \pm SEM of 3 mice per group. ** $p < 0.01$, one-way ANOVA.

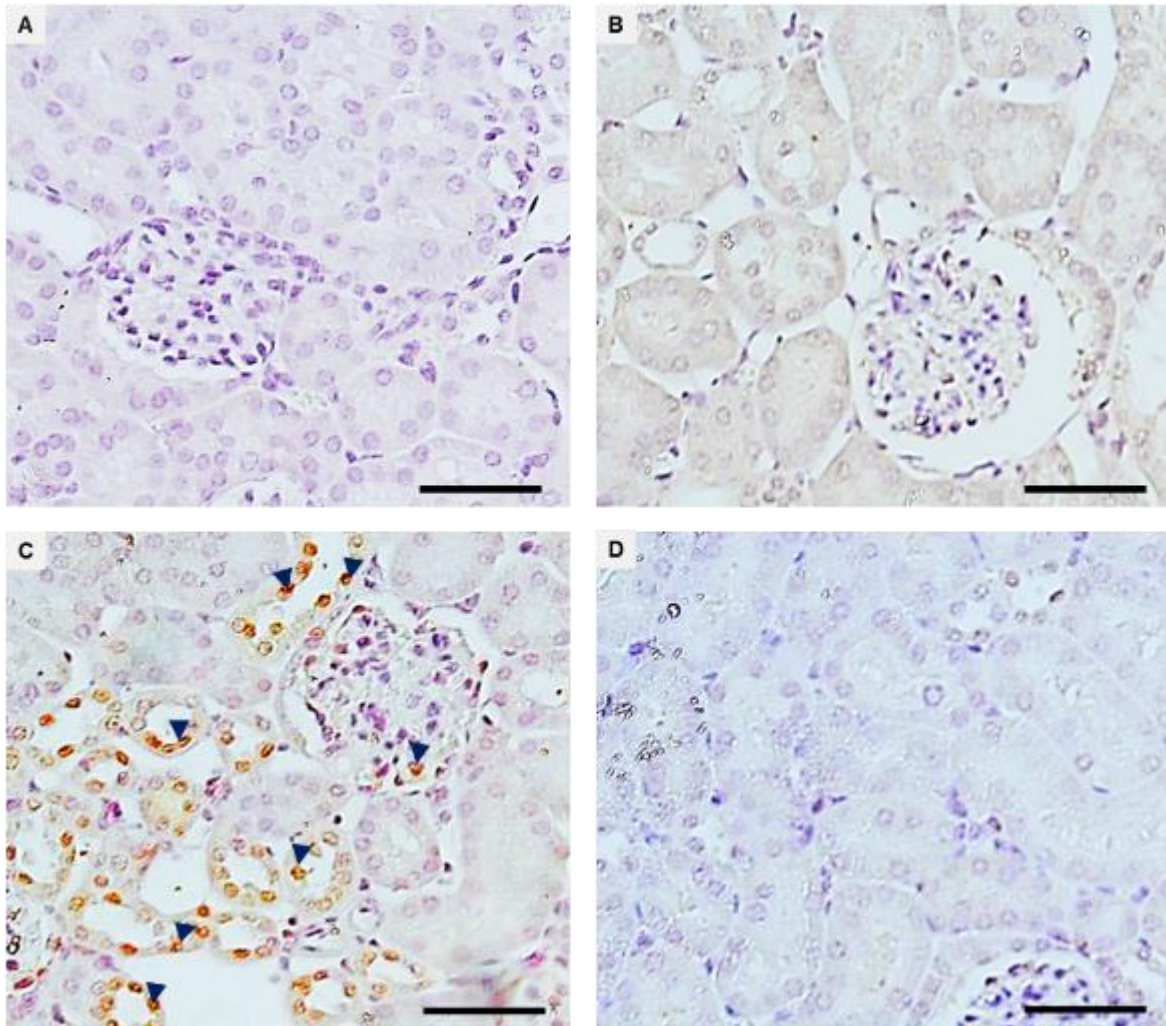


Figure.6.24. IHC analysis of mouse kidney tissue for caspase-3 in control, proteinuric mice and protein injected mice treated with the MMPI.

Representative photomicrographs showing (A) Negative control sections from control animals prepared without primary antibody. (B) Control mice. (C) Proteinuric mice. (D) Protein injected mice treated with the MMPI. Blue arrowheads represent the caspase-3 staining. Scale bars 100 μ M.

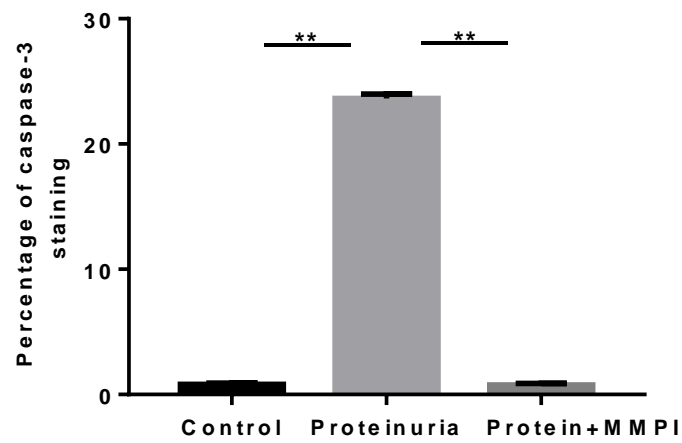


Figure.6.25. Semi-quantitative IHC analysis of renal caspase-3 staining in control, proteinuric mice and protein injected mice treated with the MMPI.

Data are expressed as mean \pm SEM of 4 mice per group. ** $p < 0.01$, one-way ANOVA.

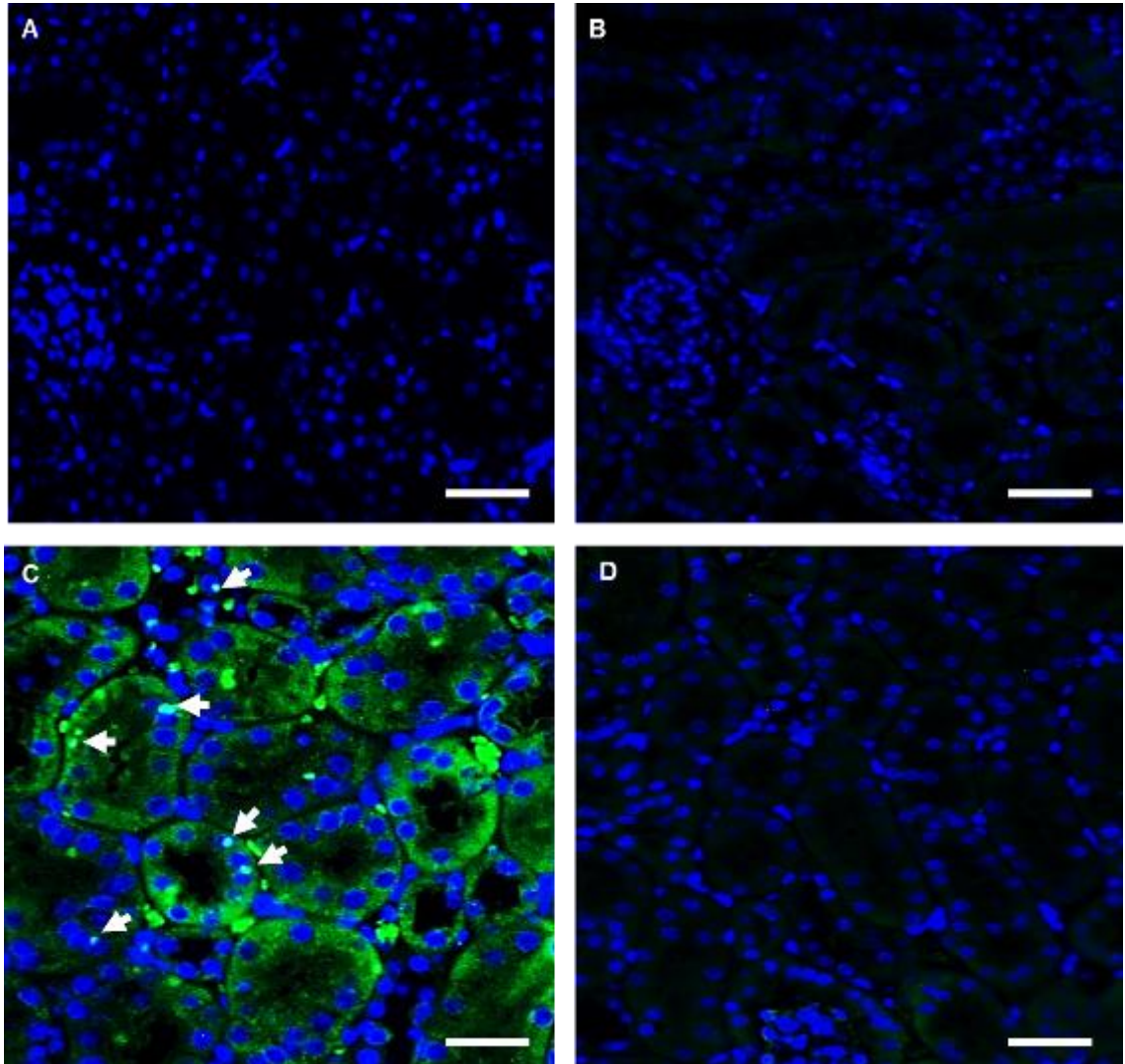


Figure.6.26. IF analysis of mouse kidney tissue for caspase-3.

Representative photomicrographs showing (A) Negative control sections from control animals prepared without primary antibody and DAPI nuclei stained. (B) Control mice (no staining of caspase-3 (green) expression) merged with DAPI nuclei stained. (C) Proteinuric mice (expression of caspase-3 (green) staining merged with DAPI nuclei stained). (D) Protein injected mice treated with the MMPI (no staining of caspase-3 (green) expression) merged with DAPI nuclei stained). White arrows indicate the caspase-3 staining. Scale bars 100 μ M.

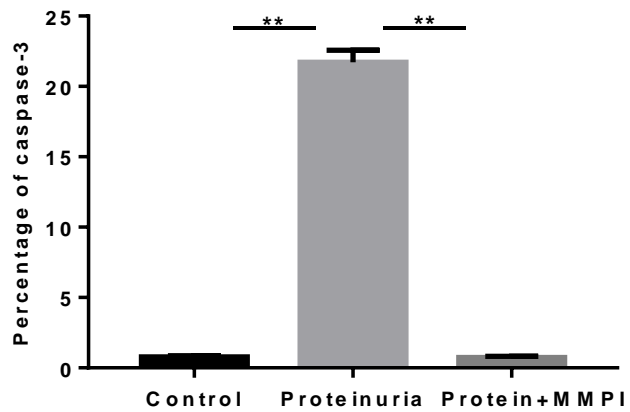


Figure.6.27. Semi-quantitative IF analysis of renal caspase-3 staining in control, proteinuric mice and protein injected mice treated with the MMPI. Data are expressed as mean \pm SEM of 4 mice per group. ** $p < 0.01$, one-way ANOVA.

6.3. Discussion

Abnormal protein trafficking is a causative factor of renal tubular cell injury and death (Li et al., 2010). This process stimulates a range of intracellular signalling pathways in renal cells and triggers tubular epithelial cells to enter a proinflammatory condition (Zoja et al., 2004, Tang et al., 2003). It then leads to a profibrotic microenvironment with an accumulation of extracellular matrix (Wu et al., 2014). MMPs were previously assumed to be an anti-fibrotic because of their ability to degrade and remodel of the ECM (Zhao et al., 2013). However, various studies found that MMPs regulate inflammatory response by recruitment of inflammatory cells and chemotaxis components (Tan and Liu, 2012). Although the biological functions of MMPs are much more complex and diverse, these enzymes have a role in the release and activation of extracellular matrix-bound growth factors and cytokines (Zhao et al., 2013). The current results reveal that the MMPI significantly reduced the levels of interstitial inflammation and fibrosis by decreasing the expression of proinflammatory cytokines and interstitial infiltration of macrophages. Similarly, the MMPI reduces apoptosis and caspase-3 in protein overload proteinuria.

Activation of MMP causes an accumulation of collagen-IV in the interstitial space of proteinuria kidney leading to the glomerular disease that progress to ESRD (Dimas et al., 2013). Previous studies also found that collagen deposition elevated in the kidney interstitium of BSA treated mice after 7 days of administration (Landgraf et al., 2014). Our present study showed that an increase in collagen deposition in the kidney of proteinuric animals occurred in association with a significant increase in TGF- β expression. This observation had found by Eddy et al (2000) who illustrated that TGF- β expression and collagen deposition

increased in albumin overload mice associated with interstitial fibrosis (Eddy et al., 2000). The current study revealed a significant increase in collagen deposition in animals with proteinuria; however, collagen deposition has decreased significantly when treated with MMPI. This might be explained by the inhibition of MMPs in this model. This finding was supported by a unilateral ureteral obstruction (UUO) which found that deposition of types III and I collagens were raised in the kidney associated with an increase in the expression levels of MMP-2 and MMP-9 in mice kidney (Du et al., 2012). Moreover, MMP-2^{+/+} mice treated with MMPI (minocycline) showed that the deposition of type III and type I collagen were diminished compared to MMP-2^{+/+} mice. This explains that MMPs play an important role in collagen deposition (Du et al., 2012). In salt-sensitive hypertension, it was demonstrated that MMP inhibition reduced type I collagen deposition and increased elastin in the intrarenal vessels with fibrosis reduction (Pushpakumar et al., 2013). According to our finding and previous studies, inhibition of MMP activity significantly reduced collagen deposition in proteinuric animals.

Macrophages are recognised in renal injury and fibrosis (Eddy, 2000). In the UUO model, it was confirmed that specific depletion of macrophages using CD11b-DTR was accompanied by a decrease in the severity of renal fibrosis (Henderson et al., 2008). The existing study demonstrated that macrophage was significantly increased in proteinuric mice. This result is in line with previous models of protein overload which revealed an increase of macrophage infiltration into the interstitium of proteinuric mice (Landgraf et al., 2014, Eddy et al., 2000). Interestingly, the current study detected an increase of macrophage into the interstitium associated with an elevation of MMP activity in proteinuric animals.

This data is consistent with a preceding study showing that MMP-2 expression increased with macrophage infiltration into the kidney of UUO mice (Nishida et al., 2007).

But MMP inhibition by MMPI in the present work showed a significant reduction in macrophages recruitment into the kidney of proteinuria. This data is consistent with Nishida et al. (2007) who discovered that inhibition of MMP-2 has significantly reduced macrophage infiltration and kidney fibrosis in UUO mice (Nishida et al., 2007). In addition, either MMP-2^{-/-} mice or MMP-2^{+/+} mice that treated with minocycline showed a considerable reduction in macrophage infiltration in the UUO model (Du et al., 2012). It is possible then that, a reduction in macrophages using batimastat may be correlated with MMP diminishing in proteinuric animals.

Clinical and experimental studies suggest that IL-6 contributes to the development of renal injury. For instance, IL-6 expression was elevated in kidneys and urine of patients with mesangial proliferative glomerulonephritis (Horii et al., 1989). Models of lupus nephritis revealed that IL-6 activities stimulated the progression of kidney damage while blocking of IL-6 using anti-IL-6 mAb showed prevention in the development of severe kidney disease (Liang et al., 2006). Furthermore, nephrotoxin-induced AKI study showed that IL-6 expression increased in the renal tubular epithelial cells associated with kidney damage. Nonetheless, mice with IL-6 deficiency have a reduced tendency towards neutrophil accumulation and are relatively resistant to the injury (Nechemia-Arbely et al., 2008). The finding in the present study revealed that IL-6 expression increased in the kidney with proteinuric animals, whereas batimastat treatment displayed a substantial decrease in the expression of IL-6 in the kidney of proteinuria. Consequently, IL-

6 as a proinflammatory factor its reduction could be associated with a decrease in macrophage and MMP expression.

TNF- α is another inflammatory cytokine increased in albuminuria of animal models of diabetic nephropathy when exposed to streptozotocin (Kalantarinia et al., 2003). This showed a similar result regarding the present study, TNF- α expression increased in proteinuric animals. An in vitro study presented evidence that effects of TNF- α increases MMP-9 in HK-2 (human proximal tubule cell line) through TNF-receptor I (Nee et al., 2004). Gearing et al (1995) found that inhibition of MMP-2/ MMP-9 activities might lead to inhibition of TNF- α activation (Gearing et al., 1995). This indicates that there is a correlation between an increase of TNF- α and MMPs activities (Gearing et al., 1994). This concept was supported in the current study when the expression of TNF- α was significantly reduced using MMPI treatment and ultimately ameliorated the renal injury in the animal model of protein overload proteinuria.

TGF- β is a profibrotic cytokine that stimulates renal cells to produce ECM proteins leading to glomerulosclerosis and tubulointerstitial fibrosis (Loeffler and Wolf, 2014). In vitro and in vivo studies showed that albumin activates the tubular synthesis of TGF- β (Abbate et al., 2002). Additionally, our study illustrated that an increase in TGF- β expression in the kidney of proteinuric animals occurred in association with a significant increase of MMP. This observation had found by Eddy et al (2000) who showed that TGF- β expression increased in albumin overload mice associated with interstitial fibrosis (Eddy et al., 2000). Moreover, TGF- β is associated with upregulation of MMP-2/MMP-7 expression in streptozotocin-induced diabetic nephropathy rats (Li et al., 2017). However, inhibition of MMP activity using MMPI treatment showed a significant decrease in

the expression of TGF- β levels accompanying a reduction in MMPs activities in proteinuria. An animal study also revealed that expressions of TGF- β , MMP-2 and MMP-7 are considerably reduced in diabetic nephropathy rats when treated with sodium hydrosulfide (Li et al., 2017).

Many experimental investigations and clinical observation proved that albumin overload is associated with tubular cell death (Tejera et al., 2004, Eddy, 1989, Sanz et al., 2008). In vitro studies described that renal tubular cell apoptosis plays a role in the pathogenesis of renal tubular injury (Morigi et al., 2002, Zoja et al., 1998). In albumin exposed PTCs, apoptosis has been detected due to an increase in TGF- β expression and fibrosis development (Gentle et al., 2013). Moreover, caspase-3 expression increased at both mRNA and protein levels during reperfusion in a rat model of acute renal ischemia associated with apoptosis (Kaushal et al., 1998).

These observations in the present experiment demonstrated that the apoptosis and caspase-3 expression were raised significantly in the kidney of proteinuric animals. Likewise, a previous study conducted on rats with protein-overload proteinuria revealed a substantial increase in the tubular cell apoptosis (Thomas et al., 1999); whereas pancaspase inhibitor diminished caspase-3 activity associated with a reduction in apoptosis and brush-border damage in ischemic mouse kidney (Jani et al., 2004). MMP expression in the current study has increased in the proteinuric mice concomitant with apoptosis and caspase-3. Although in the present findings the mechanism was not studied. Powell et al (1999) mentioned that MMP-7 encourage apoptosis via cleaving and generating active soluble Fas ligand (Powell et al., 1999). This may explain the inhibition

effect of MMPI treatment that showed a significant reduction in the apoptosis and caspase-3 expression in the existed model.

Taken together the results demonstrate increasing renal proinflammatory cytokines, inflammatory cell infiltration, collagen deposition and apoptosis in proteinuria reversed by MMP inhibition. The precise mechanisms of the MMPI effect remain to be identified.

Chapter Seven

Expression of Cubam complex in Human Nephrotic Syndrome

7.1. Introduction

Albumin is one of the filtered proteins reabsorbed in the proximal tubule mediated by the cubam endocytic complex (Zhang et al., 2013). Proteinuria is a sensitive marker and an adverse prognostic feature in renal diseases (Ruggenenti et al., 2001, Abbate et al., 2006). In a proteinuric disease such as minimal change nephrotic syndrome, a large amount of plasma proteins enters the tubules (Eddy, 2004). The mechanism behind these observations is unclear, but increasing the load of protein taken up and recycled by the proximal tubular cells potentially contributes to the development of inflammation and fibrosis (Gekle, 2005).

Nevertheless, expression of the cubam complex is not well studied in human proteinuric diseases. A recent report showed downregulation of endocytic protein receptors in mice protein overload nephropathy, but very little is known about the cubam complex expression in humans. Available data rely on the phenotypes of rare genetic disease resulting in dysfunction of cubilin and amnionless (Storm et al., 2013). Therefore, in this chapter, human patients' kidney biopsies from different nephrotic diseases were investigated to assess change in cubam expression.

7.2. Results

To determine whether cubam is altered in human nephrotic syndrome, renal biopsies from 29 patients with nephrotic syndrome due to minimal change disease (MCD), membranous nephropathy (MN) and focal segmental glomerulosclerosis (FSGS) were analysed for cubam complex by IHC.

Control biopsies harvested from the unaffected pole of nephrectomy specimens well clear of the tumour margin from age-matched renal cell carcinoma patients with normal eGFR were also studied by IHC (Table.7.1).

	Age	Gender	eGFR ml/min/1.73 m ²	Urine PCR mg/mmol	Glomeruli (n)
MCD	18	Female	> 90	500	18
	19	Male	> 90	364	13
	20	Male	> 90	800	18
	25	Male	> 90	> 1000	16
	28	Female	> 90	> 1000	7
	38	Male	> 90	601	30
	41	Female	73	400	18
	75	Male	60	618	14
	76	Male	72	> 1000	12
MN	24	Female	90	714	14
	33	Female	90	450	23
	41	Male	82	580	10
	41	Male	90	618	8
	47	Female	64	>1000	16
	48	Male	90	805	10
	70	Male	90	612	18
	71	Male	72	384	9
	73	Female	65	985	19
	73	Male	90	>1000	38
FSGS	32	Female	89	>1000	21
	50	Female	63	>1000	7
	51	Female	60	720	26
	53	Male	71	>1000	9
	63	Male	62	500	9
	63	Male	81	>1000	6
	64	Female	62	>1000	14
	72	Male	62	822	16
	82	Female	61	>1000	15

Table.7.1. Clinical parameters of nephrotic syndrome patients were provided that kidney biopsy samples, adapted from (Fatah et al., 2017).

7.2.1. Cubilin expression in human nephrotic syndrome

Cubilin expression in the kidney of proteinuric patients with the glomerular disease compared with normal controls was investigated. In normal control biopsies, cubilin expression was found on the apical membrane of proximal tubule as previously described (Christensen and Birn, 2002). Conversely, cubilin staining was noticeably reduced in the apical membrane of proximal tubules of MCD, MN and tissue biopsies from FSGS (Figure 7.1C to E). All sections of nephrotic patient's biopsies were compared with healthy controls (Figure 7.1B).

Semi-quantitative analysis of the sections using ImageJ revealed a significant reduction in cubilin expression in MND (9.0 ± 0.86 % stained area), MN (6.8 ± 0.69 % stained area) and FSGS patients (6.1 ± 0.65 % stained area) compared to healthy control biopsies (26.5 ± 0.9 % stained area) (Figure.7.2).

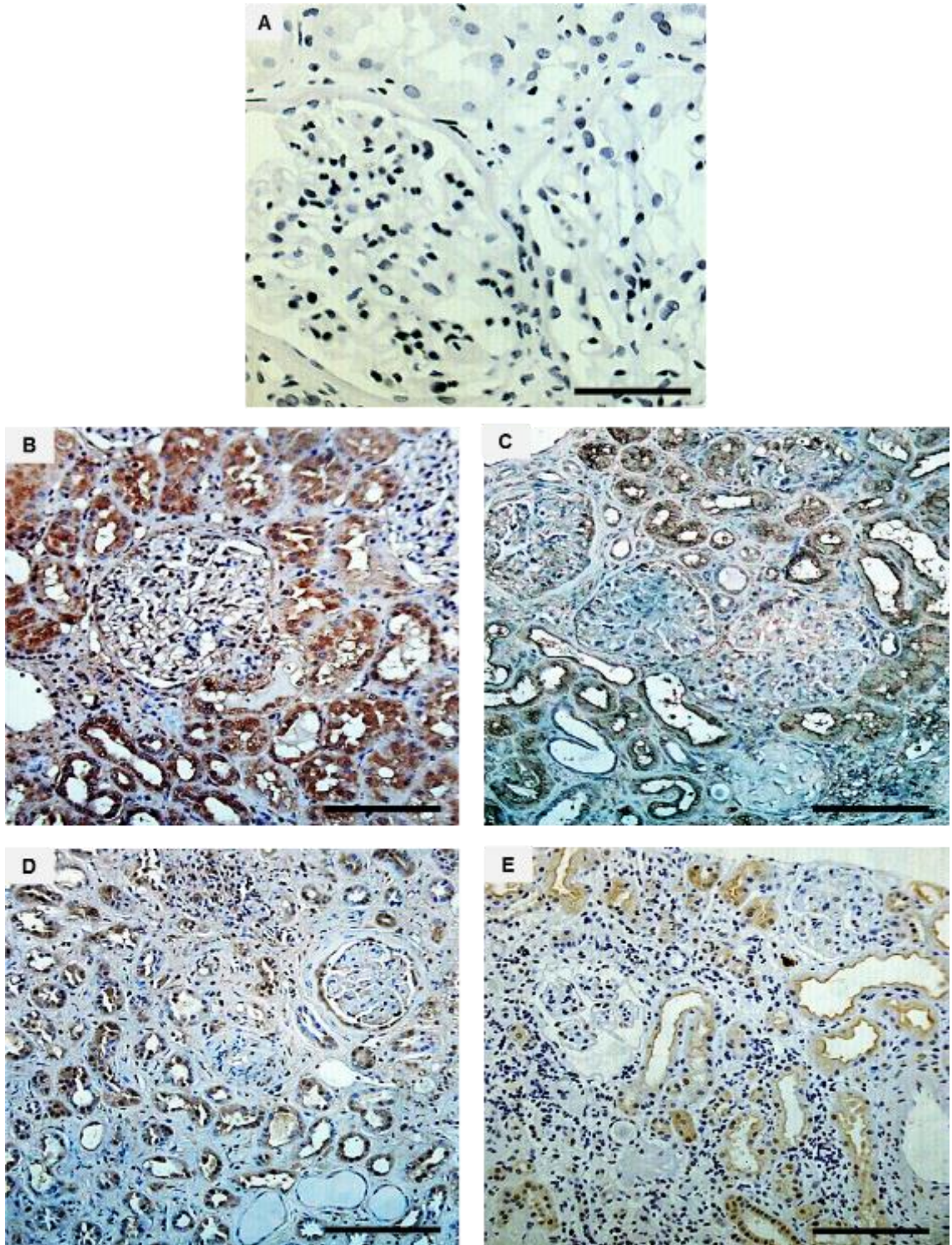


Figure.7.1. IHC analysis of human kidney biopsies for cubilin in patients with nephrotic syndrome.

Representative photomicrographs showing (A) Negative control from healthy control prepared without primary antibody, (B) Healthy human control, (C) MCD, (D) MN and (E) FSGS. All IHC was done in triplicate, Scale bars 100 μ M.

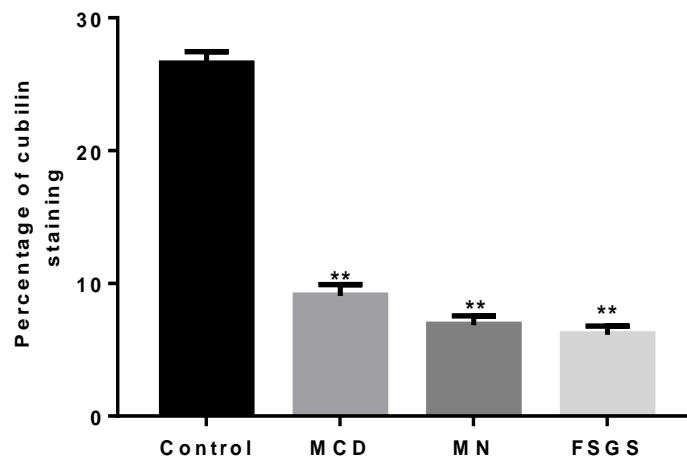


Figure.7.2. Semi-quantitative analysis of renal cubilin expression in human nephrotic syndrome.

Results are expressed as mean \pm SEM. ** $p < 0.01$ compared healthy controls (n=10 except for FSGS where n=9), one-way ANOVA.

7.2.2. Amnionless expression in human nephrotic syndrome

Amnionless expression was explored in the kidney of proteinuric patients with glomerular diseases. In normal control biopsies, amnionless expression was located at the apical surface of proximal tubules as previously defined (Coudroy et al., 2005). Amnionless staining was significantly decreased in the apical membrane of proximal tubules cells of patients with MCD, MN and tissue biopsies from FSGS (Figure 7.2 C to E) compared with healthy controls (Figure 7.3B).

Semiquantitative analysis of sections using ImageJ demonstrated a substantial decline in amnionless expression in patients with MND (11.3 ± 0.73 % stained area), MN (8.7 ± 0.73 % stained area) and FSGS (7.2 ± 0.62 % stained area) compared to control biopsies (25.4 ± 0.72 % stained area) (Figure 7.4).

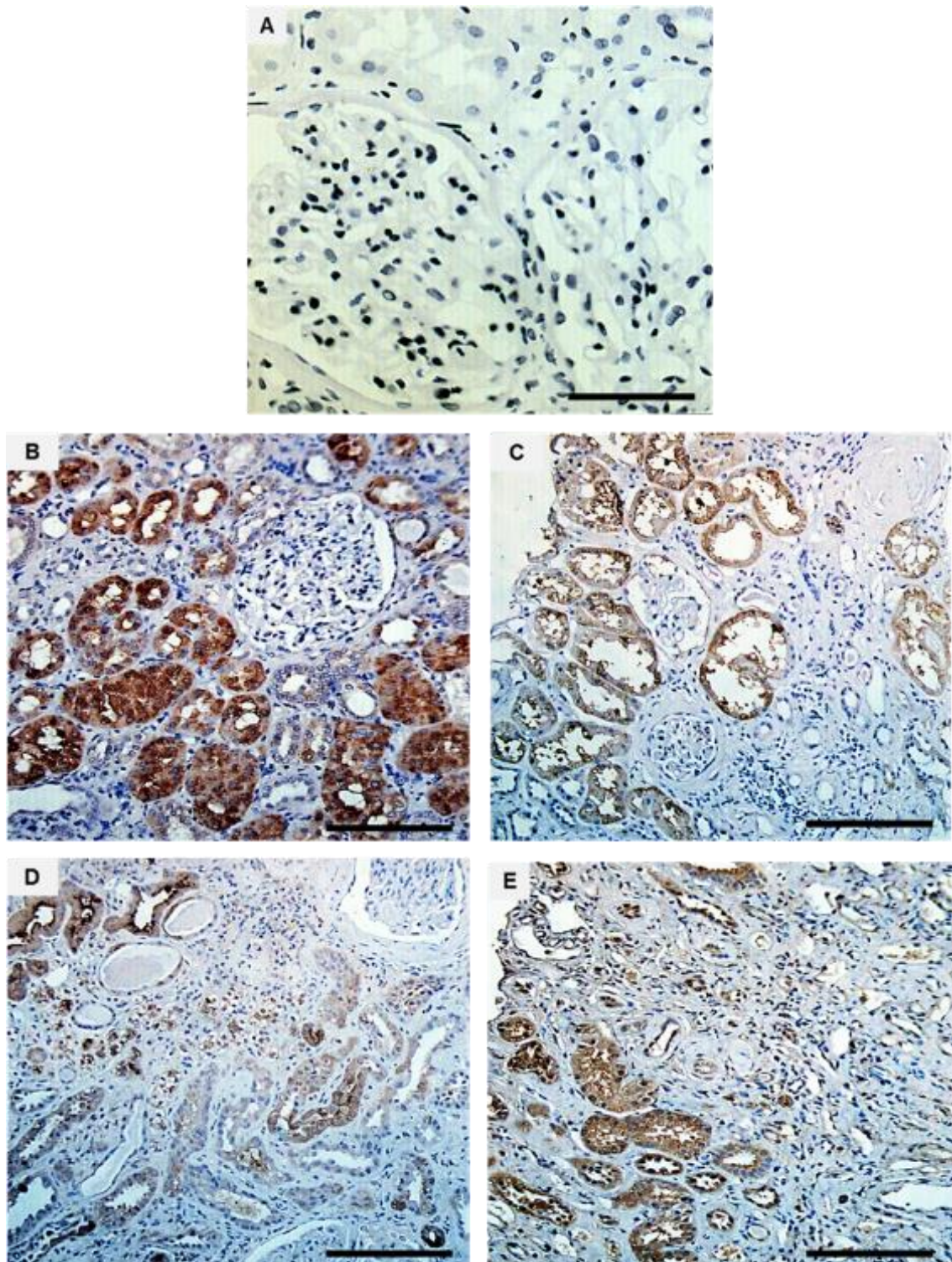


Figure.7.3. IHC analysis of human kidney biopsies for amnionless in patients with nephrotic syndrome.

Representative photomicrographs showing (A) Negative control from healthy control prepared without primary antibody, (B) Healthy human control, (C) MCD, (D) MN and (E) FSGS. All IHC was done in triplicate, Scale bars 100 μ M.

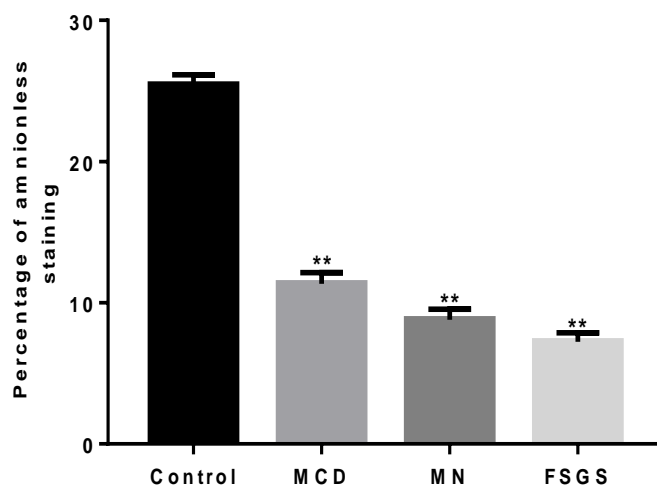


Figure.7.4. Semi-quantitative analysis of renal amnionless expression in human nephrotic syndrome.

Results are expressed as mean \pm SEM. **p < 0.01 compared healthy controls (n=10 except for FSGS where n=9), one-way ANOVA.

7.2.3. DPP- IV expression in human nephrotic syndrome

DPP-IV expression in proteinuric patients with the glomerular disease was studied by IHC. DPP-IV staining was initially expressed on the apical surface of proximal tubule as previous studies (Mentlein, 1999). Interestingly, DPP-IV immunostaining was clearly unchanged in the proximal tubules of proteinuric patients with MCD, MN and FSGS (Figure 7.5) In contrast with healthy controls (Figure 7.5B). Semiquantitative analysis of the sections confirmed no significant difference in DPP-IV expression between MND (23.6 ± 0.95 % stained area), MN (23.5 ± 0.92 % stained area) and FSGS (23.4 ± 0.98 % stained area) in comparison with healthy control biopsies ($23.6 \pm 1.7\%$ stained area)(Figure 7.6).

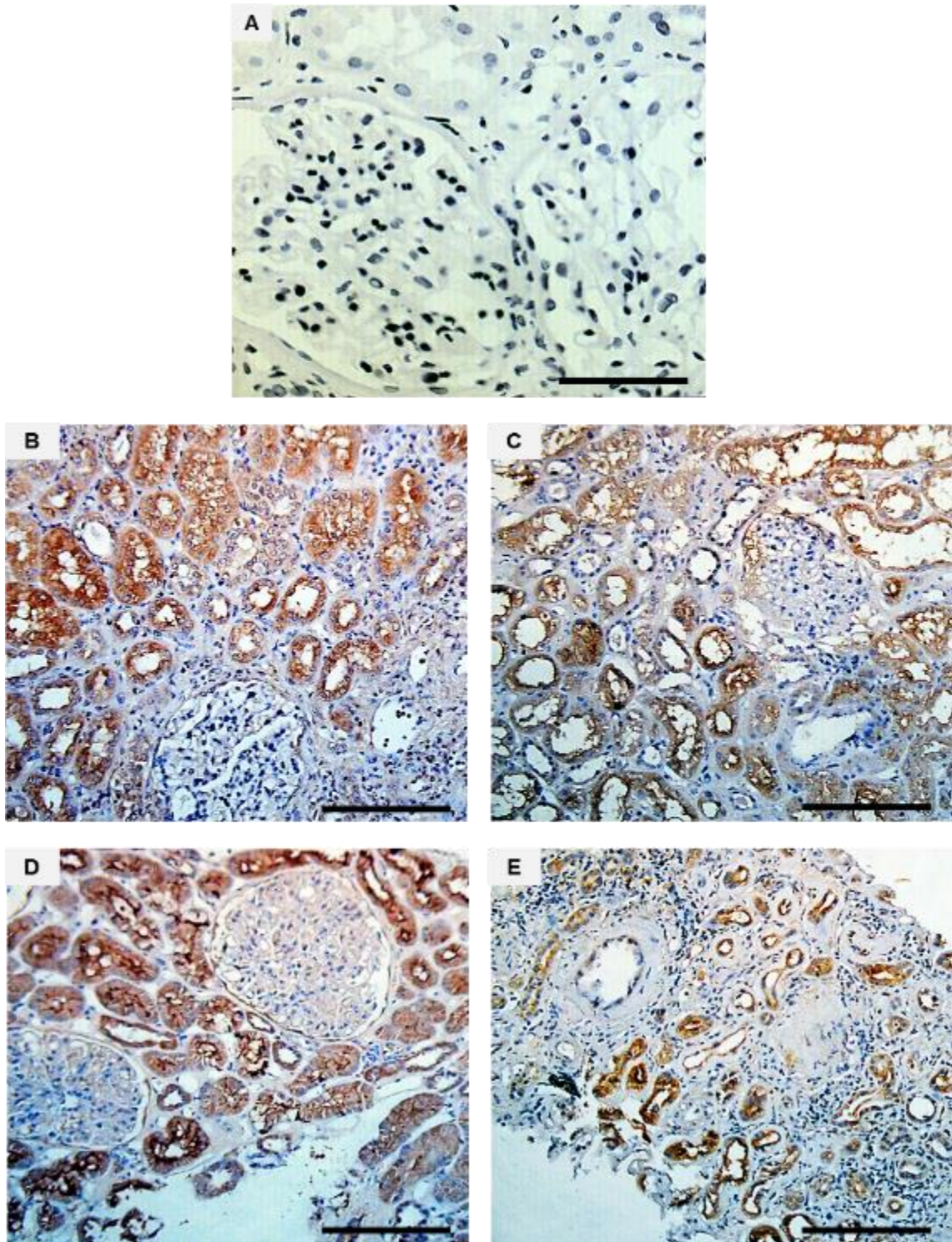


Figure.7.5. IHC analysis of human kidney biopsies for DPP-IV in patients with nephrotic syndrome.

Representative photomicrographs showing (A) Negative control from healthy control prepared without primary antibody, (B) Healthy human control. (C) MCD. (D) MN and (E) FSGS. All IHC was done in triplicate, Scale bars 100 μ M.

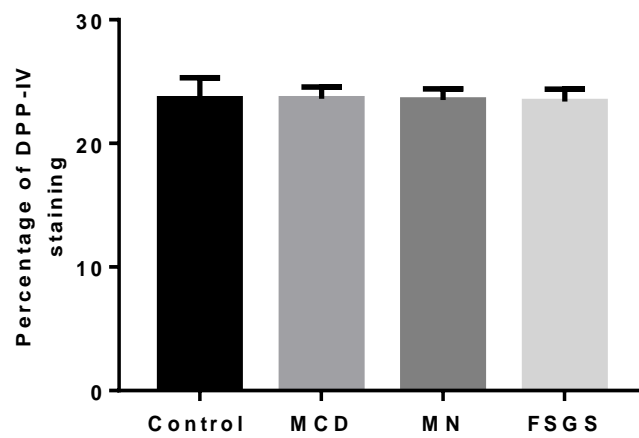


Figure.7.6. Semi-quantitative analysis of renal DPP-IV expression in human nephrotic syndrome.

Results are expressed as mean \pm SEM, p =ns, one-way ANOVA.

7.3. Discussion

Excessive reabsorption of proteins has been demonstrated to induce tubulointerstitial inflammation and fibrosis (Zoja et al., 2015). Proteinuria is thought to increase renal disease progression to ESRD (Abbate et al., 2006). The current study showed that cubam complex expression was significantly reduced in the proximal tubules from patients with MCD, MN and FSGS. In previous chapters on proteinuric mice, we found that the decrease of cubam complex correlated with an increase of MMPs expression and inflammatory markers. The mechanism behind these results had not been examined due to a limitation of human biopsies materials. However, reduction of the cubam complex in proteinuric human diseases is relatively consistent with findings in the mouse model. Therefore, endocytic receptors may be specifically downregulated in proteinuria to protect tubular cells from protein overload

The reduction in cubam complex expression in the PTs in proteinuria is to some degree selective as DPPIV unchanged. This is supported by a study on sub-chronic exposure to cadmium, a model which revealed a reduction of cubilin expression in the proximal tubule without alteration of DPP-IV expression in the rat kidney (Santoyo-Sanchez et al., 2013).

In summary, although the result of IHC showed a significant reduction of cubam complex, limitation of renal patient biopsies prevented mRNA or other more detailed analyses to examine mechanisms behind the cubam complex reduction.

Chapter Eight

Thesis discussion

8.1. Thesis summary

Proteinuria is prognostic of deteriorating renal function in patients with CKD (Gorriz and Martinez-Castelao, 2012). Albumin is the most abundant protein in the glomerular filtrate and is reabsorbed by the proximal tubule via endocytic receptors (Birn and Christensen, 2006). In proteinuria, proximal tubular cells are affected by abnormal filtered proteins which leads to renal inflammation and fibrosis (Eddy, 2004, Zoja et al., 2015). MMPs have a role in the regulation of the inflammatory response and apoptosis in proteinuric renal disease (Tan and Liu, 2012). This creates a pressing need for a better understanding of the molecular mechanisms of proteinuria. The primary aim of this thesis was to investigate the cubam complex endocytic receptor proteins that contribute to the interaction between the proximal tubular cells and proteins in the tubular lumen. However, little is known about the cubam complex expression in a renal disease characterized by heavy proteinuria.

In general protein excretion in the urine, particularly albumin is the result of both glomerular permselectivity and tubular reabsorption and this issue is still a debated question (Dickson et al., 2014, Peti-Peterdi, 2009, Comper et al., 2008b). Previous studies showed that tubular reabsorption of glomerular filtered proteins is contributing to proteinuria (Dickson et al., 2014, Comper et al., 2008b). This might show a relation between urinary protein excretion and impaired glomerular permselectivity (Peti-Peterdi, 2009). Immunogold staining of endogenous albumin by electron microscopy showed that endocytosed albumin appears to undergo transcytosis, to the basolateral membrane where the albumin is ejected back to

the peritubular blood supply (Russo et al., 2007). Moreover, the rate of uptake of albumin by the PT is reduced in nephrotic rats. This is consistent with the reduced expression of clathrin, megalin, and vacuolar H (+) ATPase A subunit, proteins that are important components of the PT endocytotic process (Russo et al., 2007). There is preliminary evidence that proposes more albumin leaks through the glomerular filtration barrier, and that much of this is returned to the circulation intact rather than being degraded (Comper et al., 2008a). These findings strongly support the concept that the glomerular filter normally leaks albumin at nephrotic levels. Albuminuria does not occur as this filtered albumin load is retrieved by proximal tubular cells, whereas dysfunction of this retrieval pathway leads to albuminuria (Comper et al., 2008a, Russo et al., 2007). The present study could not define between the increased glomerular leakages and /or decreased proximal tubular reabsorption of filtered protein via cubam complex endocytic receptors in proteinuria. These observations suggest that reducing tubular reabsorption of filtered proteins due to reduced expression of these endocytic receptors might likely contribute to a part of the increased urinary protein excretion.

This thesis has demonstrated that cubilin and amnionless are down-regulated in the PTs of proteinuric kidney compared with non-proteinuric proximal tubules, and this complex down-regulation was largely due to receptor shedding into the urine and reduction in gene expression. The decrease of this complex was associated with an increase in urinary excretion of albumin; increase the enzymatic activity of MMPs and increased cubilin and amnionless excretion into the urine of proteinuric animals. Although the present study could not differentiate between the increased glomerular leakage and/or decreased PT cells re-absorption of proteins via cubam

complex, reduced tubular reabsorption of filtered proteins as a result of reducing expression of these endocytic receptors could likely be a part of the increased protein specifically albumin in the urine of proteinuric mice.

Due to the role of cubilin and amnionless in vitamin B₁₂ absorption in the small intestine, cubilin expression was studied in the intestine in proteinuric animals. However, the receptor did not show any change at either the protein or gene expression level. This illustrated that in protein overload proteinuria had no systemic effect on cubam.

Investigating the mechanism of cubilin and amnionless reduction in proteinuric animals has provided an insight into how the cell surface expression of cubilin and amnionless are maintained in the PTs. The results demonstrate that increased cubilin and amnionless expression are important as in proteinuric animals when the expression and function of these endocytic receptors are downregulated, the urinary excretion of plasma proteins is increased. This could be a result of the increased enzymatic activity of metalloproteinases in the proteinuric animals. These results suggest that increased activity of MMPs has an association with the shedding of proteins endocytic receptors. Given the important associations between the increase of MMPs expression and urinary shedding of the cubam complex from proximal tubules surfaces (Thraillkill et al., 2009b), the current model of protein overload proteinuria showed that RIP may be explained as an increase in urinary megalin excretion and its reduced expression in PTs of proteinuric mice (Fatah et al., 2017). Because the cubam complex is close physically to megalin this could explain that complex may be pulled free from the PTs as a consequence of megalin ectodomain shedding in proteinuria.

Maintenance of cubilin and amnionless expression results in decreased urinary excretion of plasma proteins indicating the essential role of these receptors in normal reabsorption of glomerular filtered proteins in the kidney. Preservation of cubilin and amnionless cell surface expression was associated with the reduced activity of MMP that occurred by inhibiting by a broad-spectrum MMP inhibitor. Inhibition of MMPs activity reduced cubilin and amnionless shedding into the urine of proteinuric mice which in turn increased the expression of these receptors in the PTs and reduction of urinary albumin excretion in protein overload animals. Consequently, the reduced urinary excretion of plasma proteins is likely due to the effect of MMPI on the availability of cubam complex in the PT.

In chapter six, it is revealed that protein overload led to renal tubulointerstitial fibrosis, inflammation and apoptosis in experimental animals. In addition to the negative effect of increased filtered protein in the tubular lumen on the expression of endocytic receptors of the PTs, this resulted in a substantial increase in proinflammatory cytokines and chemokines (TNF- α , TGF- β , IL-6). It also increased the recruitment of inflammatory cells such as macrophage in the kidney of proteinuric mice. Furthermore, protein overload caused abnormal collagen deposition in the tubular interstitial space of proteinuric animals. Also, apoptotic cells were markedly high in mice with proteinuria. Interestingly, Inhibition of MMPs activity in the kidney of proteinuric animals with MMPI significantly ameliorated renal tubulointerstitial fibrosis and inflammation as the all proinflammatory markers expression decreased; reduced macrophage infiltration into the interstitial space was seen, apoptosis and collagen deposition also were decreased. These data illustrated that MMPI treatment was able to reduce the progression of tubulointerstitial fibrosis and inflammation in the kidney of protein injected animals.

Based on this, MMPI may be worthwhile therapeutic agents in proteinuric renal diseases.

Ultimately, chapter seven demonstrated that cubilin and amnionless endocytic receptors substantially declined in the PT in renal biopsies with minimal change disease, membranous nephropathy and focal segmental glomerulosclerosis. Interestingly, these findings were relatively consistent with the mouse model.

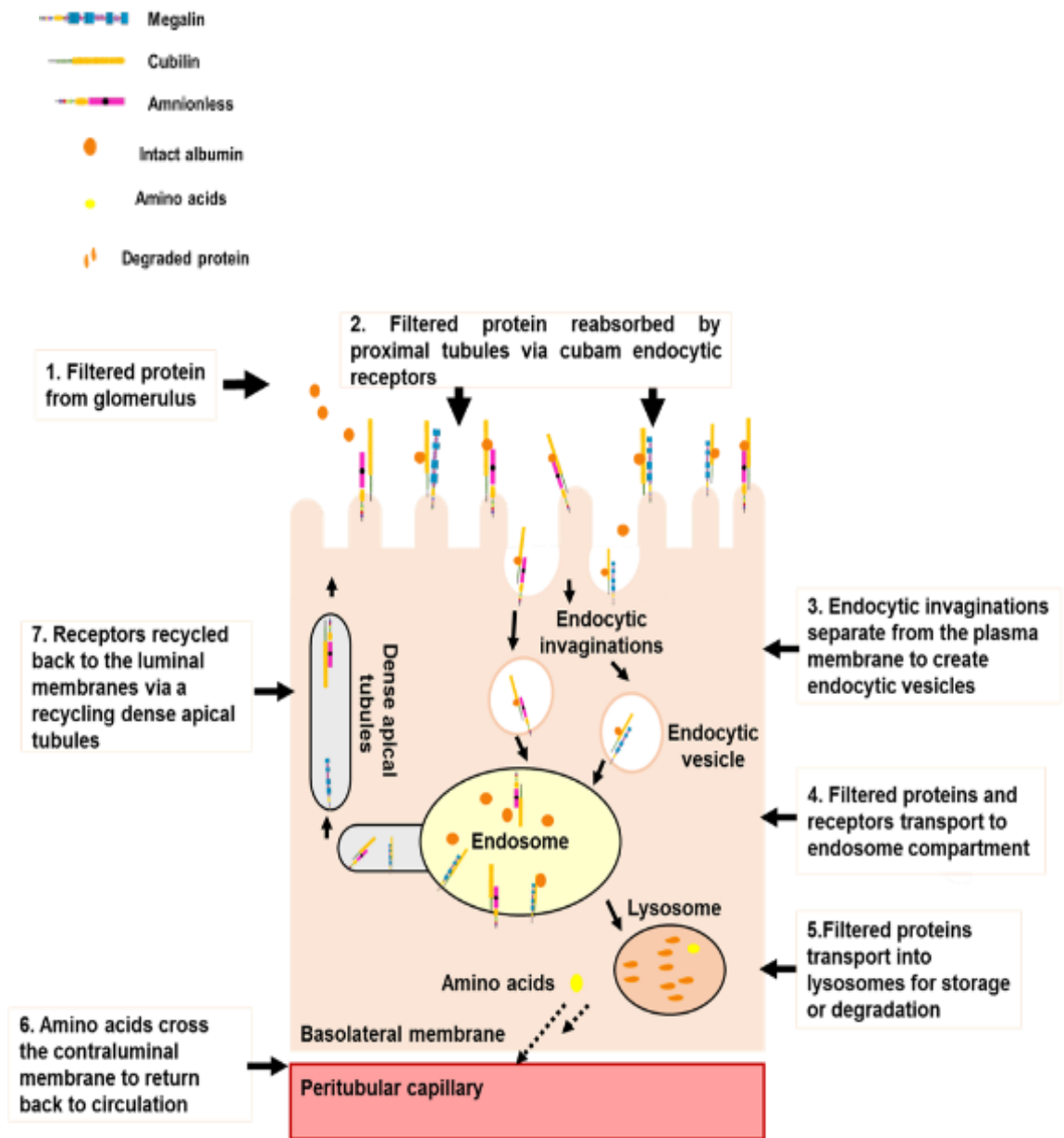


Figure 8.1. Schematic diagram illustrates the normal physiology process of proteins in the proximal tubules

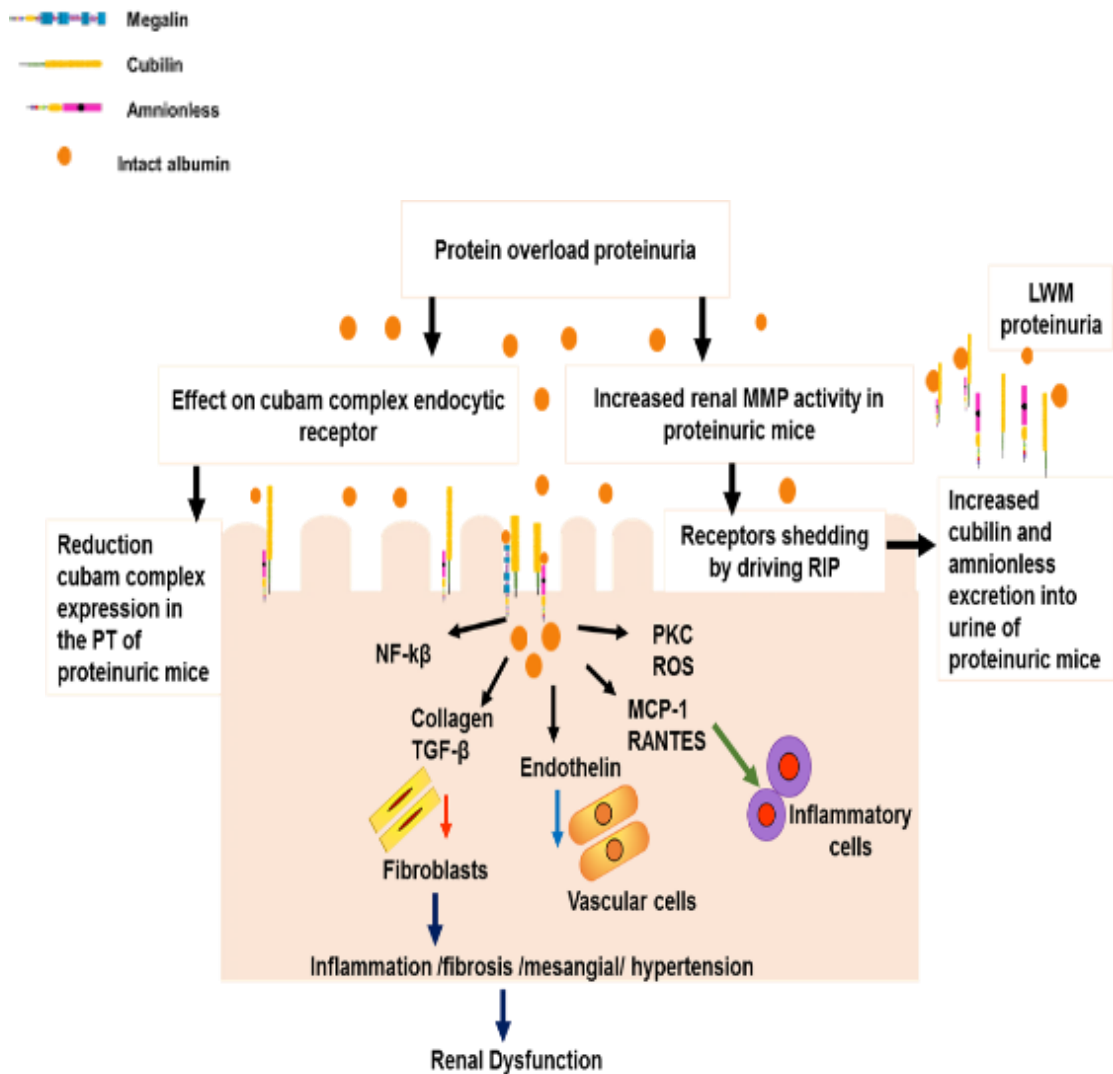


Figure 8.2. Schematic diagram illustrates the pathophysiological effect of protein overload proteinuria on the proximal tubules.

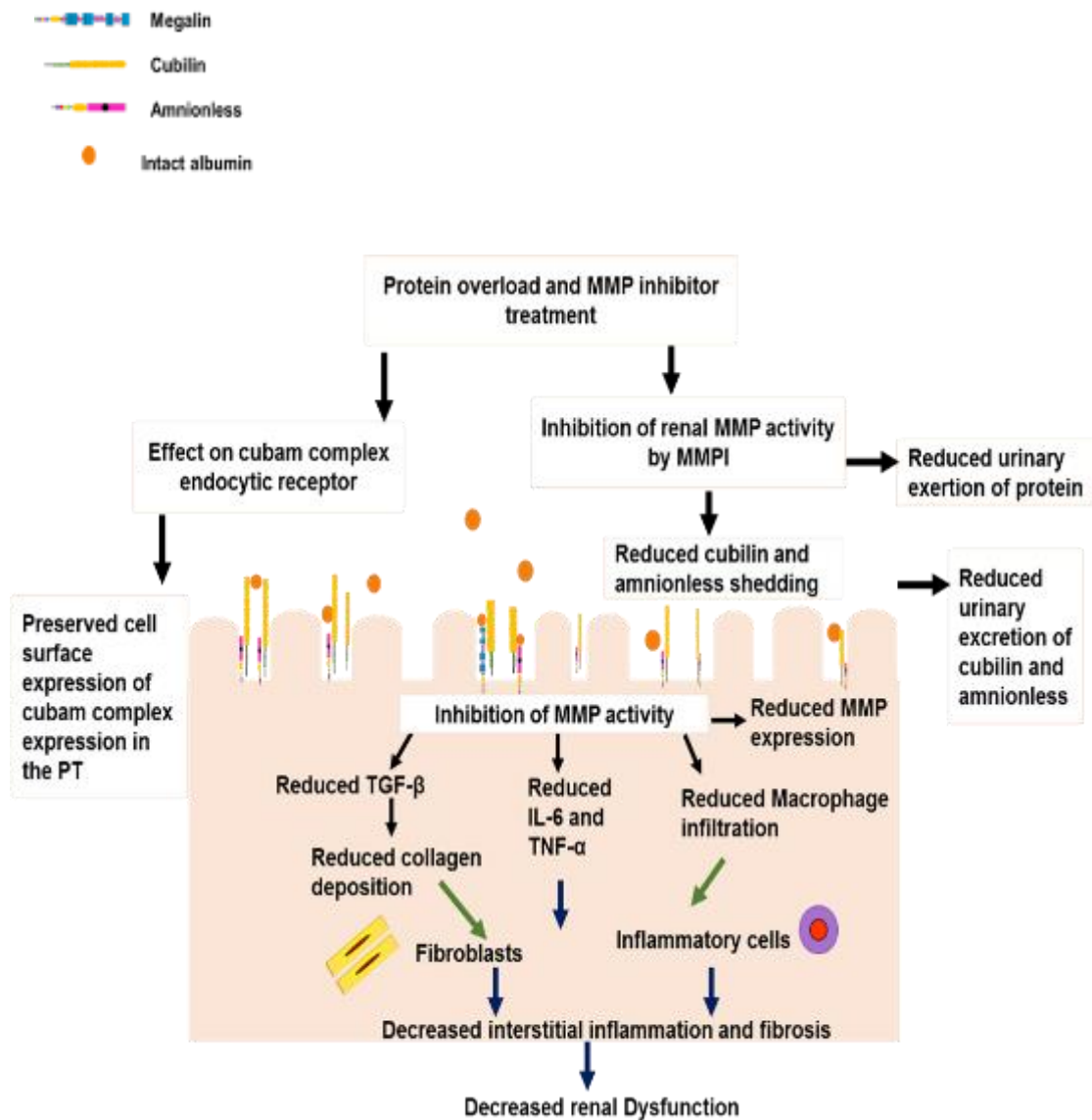


Figure 8.3. Schematic diagram illustrates the effect of MMP inhibition treatment on the proximal tubules in protein overload proteinuria.

8.2. Conclusion

Proteinuria is an important prognostic feature in CKD. Reducing proteinuria may be a therapeutic target to prevent the progression of renal impairments. This thesis has provided evidence of a decrease in renal cubam complex expression associated with albuminuria in the proteinuric animals and in human nephrotic syndrome.

Data indicated that downregulation of cubam complex was involved in the increased albumin excretion in the urine of proteinuric animals. Triggering MMP activity in proteinuric animals is associated with the loss of cubam complex receptors in the urine. However, inhibition of MMPs showed that preservation of the expression of cubam protein endocytic receptors in the proximal tubules, as well as reduced albuminuria in the proteinuric animals. Interestingly, MMPI treatment in the present study ameliorated renal inflammation and fibrosis in the proteinuric animals. This indicated a renoprotective action of MMP inhibitors in the proteinuric nephropathy.

Understanding the mechanism of the reduction of these endocytic receptors would be a great help for the future advance of this research field. It is clear that cubam complex could be physiological targets for the treatment of proteinuria and kidney diseases. This may have important clinical implications in the therapeutic approach to albuminuria.

8.3. Future work

Regarding cubam complex expression data, future study will examine the complex in a different proteinuric model with a long period of time as an alternative of two weeks of study to obtain more details about their expression. Further study will investigate the mechanism of how the MMPs lead to shedding of the cubilin and amnionless receptors from the apical membrane of the PTs in proteinuric animals. In addition, further investigation will explore the effect of MMPI treatment on renal impairment and cubam complex endocytic receptor following longer periods of protein overload proteinuria model and study which pathway is behind the effect of MMPI treatment. Further clinical studies are therefore needed to determine whether this MMPI treatment has a beneficial effect in lessening the development of proteinuria in human CKD. Recognizing the effectiveness of curative targeting of MMPI treatment may illuminate the interplay between MMPs and proteinuria.

Appendices

Appendix .1. Buffers, solutions and Materials used in this study

Appendix 1.1. Buffers and solutions

Block solution 2.5%

0.5 gram of milk powder in 20 ml TBST

Citrate buffer (PH 6.0)

2.94 gram of Sodium citrate in 1000 ml of distilled water

4x Laemmli sample buffer

900 μ l of 4x Laemmli buffer (#161-0747)

100 μ l of β -mercaptoethanol

Phosphate buffered saline (PBS) 1x (PH 7.4)

8 gram of Sodium chloride

0.2 gram of Potassium chloride

1.44 gram of Sodium phosphate, dibasic

0.24 gram of Potassium phosphate, monobasic in 1000 ml of distilled water

SDS Running Buffer x1(PH 8.3)

3.03 gram of 25 mM Tris-base

18.8 gram of 200 mM Glycine

1 gram of 0.1% (w/v) Sodium-dodecyl-sulphate (SDS) in 1000 ml Distilled water

Tis-buffered saline (TBS) PH 7.4

2.4 gram of 25 mM Tris-base

5.8 gram of Sodium Chloride in 1000 ml distilled water

Tis-buffered saline and Tween 20 (TBST) (PH 7.4)

2.4 gram of 25 mM Tris-base

5.8 gram of Sodium Chloride

500 μ L of Tween 20 (0.05%) in 1000 ml distilled water

Transfer Buffer for semi-dry Transfer

12 grams of 25 mM Tris –Base

35 grams of 200 mM Glycine

0.75 gram of Sodium-dodecyl-sulphate (SDS) in 1000 ml distilled water PH not adjusted.

Wash buffer 500 ml (1x) for ELISA

20ml concentrate wash buffer

480 ml distilled water

Biotin-antibody preparation (1x) for ELISA

10 µl of biotin antibody

990 µl of the antibody diluent

HRP-Avidin antibody preparation (1x) for ELISA

10 µl of HRP-Avidin antibody

990 µl of the antibody diluent

Appendix 1.2. Ready-made kits

The ready-made kits were purchased from Vector Laboratories (Peterborough, UK), BioAssay Systems, Universal Biologicals Ltd, (Cambridge, UK) and Bio-Rad Laboratories (Hemel Hempstead, UK).

Amnionless mouse ELISA kit EL001675MO)	Cusabio	Biotech	(CSB
ApopTag Peroxidase In situ detection kit	Millipore (S7100)		
Avidin/biotin blocking kit	Vector Laboratories (SP-2001)		
Coomassie Brilliant Blue R-250 staining kit	Bio-Rad Laboratories (161-0435)		
Cubilin mouse ELISA kit EL006213MO)	Cusabio	Biotech	(CSB
DC protein assay reagents kit	Bio-Rad Laboratories (500-0116)		
Mouse on Mouse (M.O.M™) Basic Kit	Vector Laboratories (BMK-2202)		
MMP Activity Assay Kit (Fluorometric)	Abcam (ab112146)		
Peroxidase substrate (DAB) kit	Vector Laboratories (SK-4100)		
Picro Sirius Red Stain Kit	Abcam (ab150681)		
ProteoSpin™ Urine protein concentration Micro Kit	Norgen Biotek corp (17400)		
QuantiChrom™ Creatinine Assay kit	Bioassay system (DICT-500)		
QuantiChrom™ Albumin Assay Kit	Bioassay Systems (DIAG-250)		
Reverse transcriptase system	Promega (A3500)		
RIPA Lysis Buffer system	Santa Cruz (Sc-24948A)		
RNeasy Mini plus Kit	Qiagen (74134)		
Vitamin B ₁₂ ELISA kit	Elabscience (E-EL010)		

Appendix 1.3. Pre-cast gels

A variety of pre-cast gels were obtained from Bio-Rad Laboratories and ThermoFisher Scientific (UK) as mentioned below: -

4-20% Tris-HCl gradient gel 10 well, 50 µl (cat no:161-1159),

7.5% Mini-PROTEAN® TGX™ Precast Protein Gels, 10-well, 30 µl (cat no: 456-1023),

7.5% Mini-PROTEAN® TGX™ Precast Protein Gels, 10-well, 50 µl (cat no: 456-1024),

4–20% Mini-PROTEAN® TGX™ Precast Protein Gels, 10-well, 50 µl (cat no: 456-1094),

10% Mini-PROTEAN® TGX™ Precast Protein Gels, 10-well, 50 µl (cat no: 456-1034).

Novex™ 10% Zymogram Plus (Gelatin) Protein Gels,1.0mm,10-well (cat no: ZY00100BOX).

Appendix 1.4. TaqMan® Gene Expression Assays

All TaqMan gene expression assays were used in a quantitative polymerase chain reaction that obtained from ThermoFisher Scientific, the UK with catalogue number 4331182.

Target	Assay ID
Mouse Amnionless	Mm00473870_m1
Mouse Cubilin	Mm01325077_m1
Mouse GAPDH	Mm99999915_g1
Mouse IL-6	Mm00446190_m1
Mouse MMP-2	Mm00439498_m1
Mouse MMP-3	Mm011168406_g1
Mouse MMP-7	Mm01168419_m1
Mouse MMP-9	Mm01240563_g1
Mouse Macrophage	Mm00802529_m1
Mouse TGF- β	Mm004417727_g1
Mouse TNF- α	Mm00443258_m1

Appendix 1.5. Primary and secondary antibodies dilution in immunoblotting analysis

Target	Primary Antibody	Dilution	Secondary Antibody
Amnionless	Amnionless (K-14) antibody (SC-46727)	1:1000	Rabbit anti-goat (HRP)
Cubilin	Cubilin (A-20) antibody (SC-20609)	1:1000	Rabbit anti-goat (HRP)
	Cubilin (T-16) antibody (SC-23644)	1:1000	Rabbit anti-goat (HRP)
MMP-7	MMP-7 Antibody (A-5) (SC-515703)	1:500	Rabbit anti-mouse (HRP)
MMP-3	MMP-3 Antibody (1B4) (SC-21732)	1:500	Rabbit anti-mouse (HRP)
MMP-9	MMP-9 goat polyclonal (AF902-SP)	1:500	Rabbit anti-goat (HRP)
MMP-2	MMP-2 goat polyclonal (AF909-SP)	1:500	Rabbit anti-goat (HRP)
Macrophage	F4/80 (C-7) monoclonal (SC-377009)	1:400	Rabbit anti-mouse (HRP)
TNF-alpha	TNF α antibody (52B83) monoclonal (SC-52746)	1:500	Rabbit anti-mouse (HRP)
Aquaporin-1	AQP1 antibody (B-11) (SC-25287)	1:1000	Rabbit anti-goat (HRP)
IL-6	IL-6 antibody (10E5) monoclonal (SC-57315)	1:500	Rabbit anti-mouse (HRP)
TGF-beta	TGF- β (3C11) monoclonal (SC-130348)	1:500	Rabbit anti-mouse (HRP)
DDP-IV	CD26/DPP IV goat polyclonal (AF954)	1:1000	Rabbit anti-goat (HRP)
Beta-actin	Beta-actin monoclonal (AC-15) (ab6276)	1:5000	Rabbit anti-mouse (HRP)

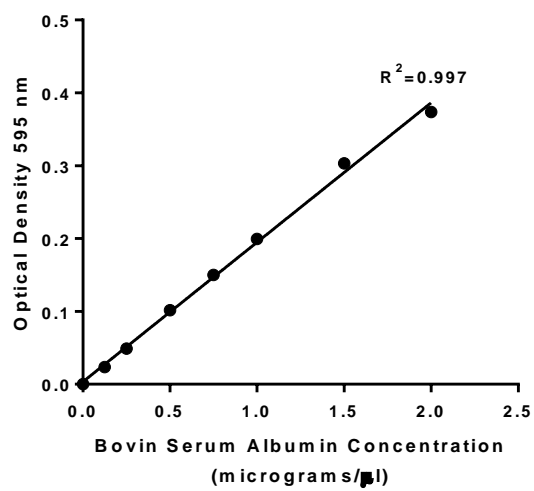
Appendix 1.6. Primary and secondary antibodies dilution in IHC analysis

Target	Primary antibody	Dilution	Secondary Antibody
Amnionless	Amnionless (K-14) goat polyclonal antibody (sc-46727)	1:100	Rabbit anti-goat(biotinylated)
Aquaporin-1	AQP1 mouse monoclonal Antibody (B-11) (sc-25287)	1:50	Goat anti-mouse(biotinylated)
Cubilin	Cubilin (A-20) goat polyclonal (sc-20609)	1:800	Rabbit anti-goat (biotinylated)
Cubilin	Human Cubilin sheep polyclonal (AF3700)	1:50	Rabbit antisheep (biotinylated)
DPP-IV	CD26/DPP IV goat polyclonal (AF954)	1:50	Rabbit anti-goat (biotinylated)
Caspase-3	Caspase-3 rabbit polyclonal (H-277) (sc-7148)	1:100	Swine anti-rabbit (biotinylated)
Interlukin-6	IL-6 (M-19) goat polyclonal (sc-1285)	1:100	Rabbit anti-goat(biotinylated)
Macrophage F4/80	Macrophage F4/80 (M-300) Rabbit polyclonal (sc-1348)	1:50	Rabbit anti-goat (biotinylated)
MMP-2	MMP-2 goat polyclonal (AF902-SP)	1:50	Rabbit anti-goat (biotinylated)
MMP-3	MMP-3 (1B4) mouse monoclonal (sc-21732)	1:50	Goat anti-mouse (biotinylated)
MMP-7	MMP-7 (A-5) mouse monoclonal (sc-515703)	1:200	Goat anti-mouse(biotinylated)
MMP-9	MMP-9 goat polyclonal (AF909-SP)	1:200	Rabbit anti-goat(biotinylated)
TNF- α	TNF- α (M-18) goat polyclonal (sc-1348)	1:100	Rabbit anti-goat(biotinylated)
TGF- β	TGF- β (H-112) Rabbit polyclonal (SC-7892)	1:100	Swine anti-rabbit (biotinylated)

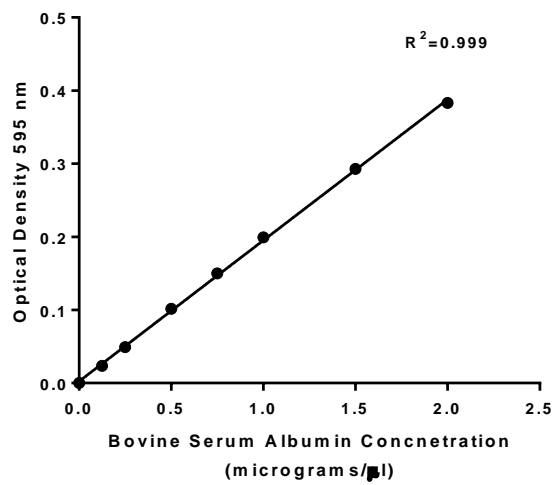
Appendix 1.7. Primary and secondary antibodies dilution in IF analysis

Target	Primary antibody	Dilution	Secondary Antibody
Amnionless	Amnionless (K-17) goat polyclonal (Santa Cruz, Germany),	1:100	Donkey anti-goat IgG, Alexa Fluor® 488 conjugate
Cubilin	Cubilin (A-20) goat polyclonal (Santa Cruz, Germany),	1:800	Donkey anti-goat IgG, Alexa Fluor® 568 conjugate
Caspase-3	Caspase-3 (H-277) rabbit polyclonal (Santa Cruz, Germany)	1:50	Goat anti-Rabbit IgG, Alexa Fluor 488
DPP- IV	DPP- IV goat polyclonal (1:50) (R&D Systems, US	1:100	Donkey anti-goat IgG, Alexa Fluor® 568 conjugate

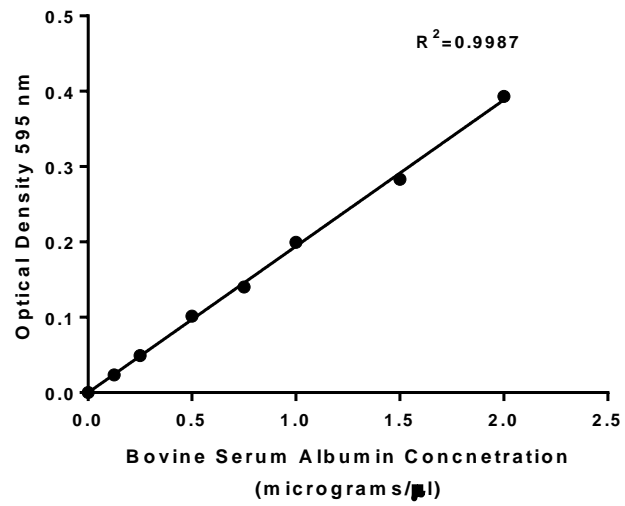
Appendix.2. Standard Curve



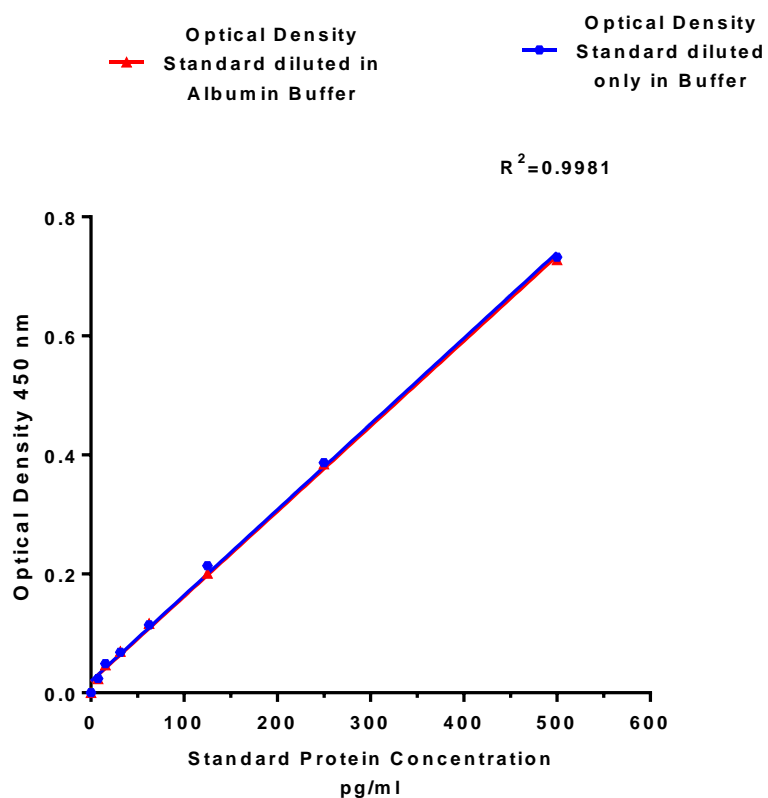
A standard curve for determining protein concentration in mouse kidney lysate. The concentrations were calculated by interpolating relative optical density 595 nm absorbance against a standard curve using Graph Pad Prism 7 analysis software.



A standard curve for determining protein concentration in mouse small intestine lysate. The concentrations were calculated by interpolating relative optical density 595 nm absorbance against a standard curve.

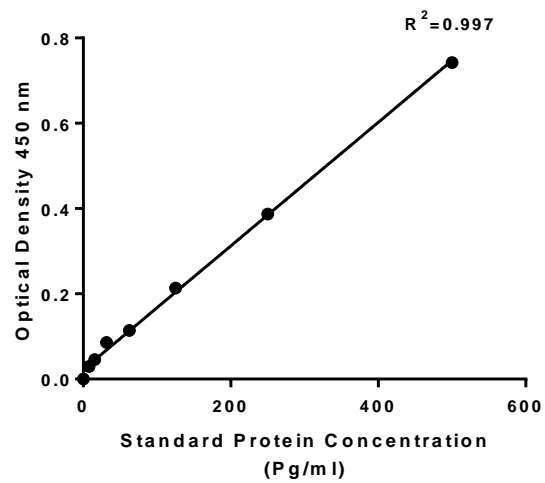


A standard curve for determining protein concentration in mouse urine. The concentrations were calculated by interpolating relative optical density (595 nm absorbance) against a standard curve.

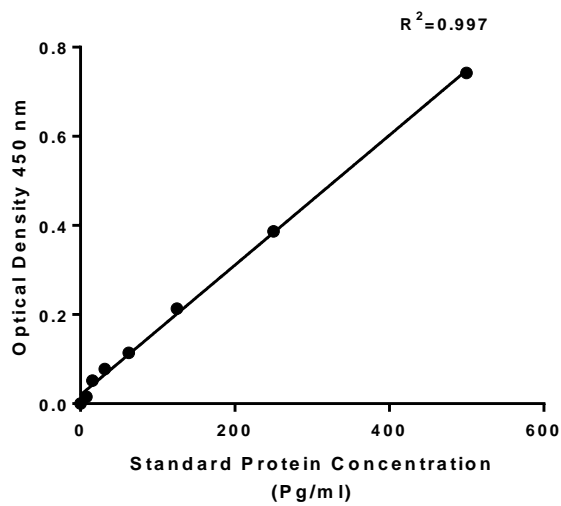


A standard curve for cubilin and amnionless ELISA assay.

The standard protein of ELISA is not affected by albumin. The relative optical density of standard protein at 450 nm increases with the increase of standard protein concentration. [BSA (0.003g) (Thermo Fisher Scientific) was dissolved in 1 ml of Sample Diluent Buffer. Two sets of standard protein were prepared as follows; standard protein (A) was diluted in Sample Diluent Buffer only. Another standard protein (B) was diluted in Sample Diluent Buffer with albumin].



A standard curve for determining the cubilin concentration in mouse urine. The concentrations were calculated by interpolating relative optical density (450 nm absorbance) against a standard curve.



A standard curve for determining the amnionless concentration in mouse urine. The concentrations were calculated by interpolating relative optical density (450 nm absorbance) against a standard curve.

Appendix.3. Computerised image analysis Macro code

These codes were recorded using the Java programming language of the ImageJ analysis processing software version 1.51h (Schneider et al., 2012). I hereby state that I have used these codes below for research purpose.

```
//The code starts:

run ("Image Sequence...", "open= [\"photo analysis image\\Image.tif] sort");
open (" image\\Image.tif");
run ("Colour Deconvolution", "vectors= [H DAB] show");
selectWindow ("Image.tif-(complemntaryColour_3)");
selectWindow ("Image.tif-(haemoxilyn Colour_1)");

selectWindow ("Image.tif-(DAB Colour_2)"); choose

run ("Subtract Background...", "rolling=50 light");

call ("ij.plugin. frame. Threshold Adjuster. Set Mode", "Red");

//run ("Threshold...");
//setThreshold (180, 255);
run ("Convert to Mask");
run ("Set Measurements...", "area min area_fraction limit display redirect=None decimal=2");
run ("Measure"); (Total area of non-staining IHC measurement);
run ("Save As");

Call ("ij.plugin. Frame. Threshold Adjuster. Set Mode", "Red");
//run ("Threshold..."); -
//set Threshold (0, 180);
run ("Convert to Mask");
run ("Set Measurements...", "area min area_fraction limit display redirect=None decimal=2");
run ("Measure"); (Area of interesting target staining IHC measurement);
run ("Save As");

run ("Result");
run ("Summarize");
run ("Save As");
run ("All Close");

// End of the code.
```

Analysis of IHC images through using Macro code ImageJ analysis software

```

//start of code:
run ("Image Sequence...", "open photo analysis image, sort");
open ("photo analysis image\\Compositennn.jpg");
run ("Split Channels");
selectWindow ("Compositennn.jpg (blue)");
selectWindow ("Compositennn.jpg (green)");
selectWindow ("Compositennn.jpg (red)");

selectWindow ("Compositennn.jpg (green)");
run ("8-bit");
run ("Subtract Background...", "rolling=50 create");

call ("ij.plugin.Frame.Threshold Adjuster.set Mode", "Red");

//run ("Threshold...");
setAutoThreshold ("Default dark");
//set Threshold (100, 225);
run ("Convert to Mask");
run ("Set Measurements...", "area min integrated area_fraction limit display redirect=None
decimal=2");
run("Measure"); Total Area of no fluorescence

setAutoThreshold ("Default dark");
//set Threshold (0, 180);
run ("Convert to Mask");
run ("Set Measurements...", "area min integrated area_fraction limit display redirect=None
decimal=2");
run("Measure"); Area of fluorescence
save As ("Results");
run("Summarize");
run ("Close");

selectWindow ("Compositennn.jpg (red)");
run ("8-bit");
setAutoThreshold ("Default dark");
//run ("Threshold...");
//set Threshold (100, 225);
run ("Convert to Mask");
run ("Set Measurements...", "area min integrated area_fraction limit display redirect=None
decimal=2");
run("Measure"); Total Area of no fluorescence

setAutoThreshold ("Default dark");
//set Threshold (0, 180);
run ("Convert to Mask");
run ("Set Measurements...", "area min integrated area_fraction limit display redirect=None
decimal=2");
run("Measure"); Area of fluorescence
save As ("Results");
run("Summarize");
run ("Close");

The End of code

```

Analysis of immunofluorescent image using Macro code ImageJ analysis software

References

- Abbate, M., Zoja, C. & Remuzzi, G. 2006. How does proteinuria cause progressive renal damage? *J Am Soc Nephrol*, 17, 2974-84.
- Abbate, M., Zoja, C., Rottoli, D., Corna, D., Tomasoni, S. & Remuzzi, G. 2002. Proximal tubular cells promote fibrogenesis by TGF-beta1-mediated induction of peritubular myofibroblasts. *Kidney Int*, 61, 2066-77.
- Acosta, E. G., Castilla, V. & Damonte, E. B. 2008. Functional entry of dengue virus into *Aedes albopictus* mosquito cells is dependent on clathrin-mediated endocytosis. *J Gen Virol*, 89, 474-84.
- Adamski, M. G., Gumann, P. & Baird, A. E. 2014. A method for quantitative analysis of standard and high-throughput qPCR expression data based on input sample quantity. *PLoS One*, 9, e103917.
- Ahuja, R., Yammani, R., Bauer, J. A., Kalra, S., Seetharam, S. & Seetharam, B. 2008. Interactions of cubilin with megalin and the product of the amnionless gene (AMN): effect on its stability. *Biochem J*, 410, 301-8.
- Aminoff, M., Carter, J. E., Chadwick, R. B., Johnson, C., Grasbeck, R., Abdelaal, M. A., Broch, H., Jenner, L. B., Verroust, P. J., Moestrup, S. K., De La Chapelle, A. & Krahe, R. 1999. Mutations in CUBN, encoding the intrinsic factor-vitamin B12 receptor, cubilin, cause hereditary megaloblastic anaemia 1. *Nat Genet*, 21, 309-13.
- Amsellem, S., Gburek, J., Hamard, G., Nielsen, R., Willnow, T. E., Devuyst, O., Nexø, E., Verroust, P. J., Christensen, E. I. & Kozyraki, R. 2010. Cubilin is essential for albumin reabsorption in the renal proximal tubule. *J Am Soc Nephrol*, 21, 1859-67.
- Anderson, S., Meyer, T. W., Rennke, H. G. & Brenner, B. M. 1985. Control of glomerular hypertension limits glomerular injury in rats with reduced renal mass. *J Clin Invest*, 76, 612-9.
- Appella, E., Weber, I. T. & Blasi, F. 1988. Structure and function of epidermal growth factor-like regions in proteins. *FEBS Lett*, 231, 1-4.
- Arif, E. & Nihalani, D. 2013. Glomerular Filtration Barrier Assembly: An insight. *Postdoc J*, 1, 33-45.
- Arnold, L. H., Butt, L. E., Prior, S. H., Read, C. M., Fields, G. B. & Pickford, A. R. 2011. The interface between catalytic and hemopexin domains in matrix

- metalloproteinase-1 conceals a collagen-binding exosite. *J Biol Chem*, 286, 45073-82.
- Asanuma, K., Yanagida-Asanuma, E., Takagi, M., Kodama, F. & Tomino, Y. 2007. The role of podocytes in proteinuria. *Nephrology (Carlton)*, 12 Suppl 3, S15-20.
- Aseem, O., Barth, J. L., Klatt, S. C., Smith, B. T. & Argraves, W. S. 2013. Cubilin expression is monoallelic and epigenetically augmented via PPARs. *BMC Genomics*, 14, 405.
- Baines, R. J. & Brunskill, N. J. 2011. Tubular toxicity of proteinuria. *Nat Rev Nephrol*, 7, 177-80.
- Barajas, L. 1997. Cell-specific protein and gene expression in the juxtaglomerular apparatus. *Clin Exp Pharmacol Physiol*, 24, 520-6.
- Barth, J. L. & Argraves, W. S. 2001. Cubilin and megalin: partners in lipoprotein and vitamin metabolism. *Trends Cardiovasc Med*, 11, 26-31.
- Benezra, M., Vlodaysky, I., Ishai-Michaeli, R., Neufeld, G. & Bar-Shavit, R. 1993. Thrombin-induced release of active basic fibroblast growth factor-heparan sulfate complexes from subendothelial extracellular matrix. *Blood*, 81, 3324-31.
- Bernstein, L. S., Grillo, A. A., Loranger, S. S. & Linder, M. E. 2000. RGS4 binds to membranes through an amphipathic alpha -helix. *J Biol Chem*, 275, 18520-6.
- Bertolatus, J. A. & Klinzman, D. 1991. Macromolecular sieving by glomerular basement membrane in vitro: effect of polycation or biochemical modifications. *Microvasc Res*, 41, 311-27.
- Bidani, A. K., Mitchell, K. D., Schwartz, M. M., Navar, L. G. & Lewis, E. J. 1990. Absence of glomerular injury or nephron loss in a normotensive rat remnant kidney model. *Kidney Int*, 38, 28-38.
- Biemesderfer, D. 2006. Regulated intramembrane proteolysis of megalin: linking urinary protein and gene regulation in proximal tubule? *Kidney Int*, 69, 1717-21.
- Birn, H. & Christensen, E. I. 2006. Renal albumin absorption in physiology and pathology. *Kidney Int*, 69, 440-9.
- Birn, H., Fyfe, J. C., Jacobsen, C., Mounier, F., Verroust, P. J., Orskov, H., Willnow, T. E., Moestrup, S. K. & Christensen, E. I. 2000. Cubilin is an

- albumin binding protein important for renal tubular albumin reabsorption. *J Clin Invest*, 105, 1353-61.
- Birn, H., Verroust, P. J., Nexø, E., Hager, H., Jacobsen, C., Christensen, E. I. & Moestrup, S. K. 1997. Characterization of an epithelial approximately 460-kDa protein that facilitates endocytosis of intrinsic factor-vitamin B12 and binds receptor-associated protein. *J Biol Chem*, 272, 26497-504.
- Blouch, K., Deen, W. M., Fauvel, J. P., Bialek, J., Derby, G. & Myers, B. D. 1997. Molecular configuration and glomerular size selectivity in healthy and nephrotic humans. *Am J Physiol*, 273, F430-7.
- Bode, W., Gomis-Ruth, F. X. & Stockler, W. 1993. Astacins, serralyins, snake venom and matrix metalloproteinases exhibit identical zinc-binding environments (HEXXHXXGXXH and Met-turn) and topologies and should be grouped into a common family, the 'metzincins'. *FEBS Lett*, 331, 134-40.
- Boger, C. A., Chen, M. H., Tin, A., Olden, M., Kottgen, A., De Boer, I. H., Fuchsberger, C., O'seaghdha, C. M., Pattaro, C., Teumer, A., Liu, C. T., Glazer, N. L., Li, M., O'connell, J. R., Tanaka, T., Peralta, C. A., Kutalik, Z., Luan, J., Zhao, J. H., Hwang, S. J., Akyzbekova, E., Kramer, H., Van Der Harst, P., Smith, A. V., Lohman, K., De Andrade, M., Hayward, C., Kollerits, B., Tonjes, A., Aspelund, T., Ingelsson, E., Eiriksdottir, G., Launer, L. J., Harris, T. B., Shuldiner, A. R., Mitchell, B. D., Arking, D. E., Franceschini, N., Boerwinkle, E., Egan, J., Hernandez, D., Reilly, M., Townsend, R. R., Lumley, T., Siscovick, D. S., Psaty, B. M., Kestenbaum, B., Haritunians, T., Bergmann, S., Vollenweider, P., Waeber, G., Mooser, V., Waterworth, D., Johnson, A. D., Florez, J. C., Meigs, J. B., Lu, X., Turner, S. T., Atkinson, E. J., Leak, T. S., Aasarod, K., Skorpen, F., Syvanen, A. C., Illig, T., Baumert, J., Koenig, W., Kramer, B. K., Devuyst, O., Mychaleckyj, J. C., Minelli, C., Bakker, S. J., Kedenko, L., Paulweber, B., Coassin, S., Endlich, K., Kroemer, H. K., Biffar, R., Stracke, S., Volzke, H., Stumvoll, M., Magi, R., Campbell, H., Vitart, V., Hastie, N. D., Gudnason, V., Kardia, S. L., Liu, Y., Polasek, O., Curhan, G., Kronenberg, F., Prokopenko, I., Rudan, I., Arnlov, J., Hallan, S., Navis, G., Consortium, C. K., Parsa, A., Ferrucci, L., Coresh, J., Shlipak, M. G., et al. 2011. CUBN is a gene locus for albuminuria. *J Am Soc Nephrol*, 22, 555-70.

- Boll, W., Rapoport, I., Brunner, C., Modis, Y., Prehn, S. & Kirchhausen, T. 2002. The mu2 subunit of the clathrin adaptor AP-2 binds to FDNPVY and YppO sorting signals at distinct sites. *Traffic*, 3, 590-600.
- Bolton, G. R., Deen, W. M. & Daniels, B. S. 1998. Assessment of the charge selectivity of glomerular basement membrane using Ficoll sulfate. *Am J Physiol*, 274, F889-96.
- Botos, I., Scapozza, L., Zhang, D., Liotta, L. A. & Meyer, E. F. 1996. Batimastat, a potent matrix metalloproteinase inhibitor, exhibits an unexpected mode of binding. *Proc Natl Acad Sci U S A*, 93, 2749-54.
- Bravo, D. A., Gleason, J. B., Sanchez, R. I., Roth, R. A. & Fuller, R. S. 1994. Accurate and efficient cleavage of the human insulin proreceptor by the human proprotein-processing protease furin. Characterization and kinetic parameters using the purified, secreted soluble protease expressed by a recombinant baculovirus. *J Biol Chem*, 269, 25830-7.
- Brenner, B. M., Hostetter, T. H. & Humes, H. D. 1978. Glomerular permselectivity: barrier function based on discrimination of molecular size and charge. *Am J Physiol*, 234, F455-60.
- Broch, H., Imerlund, O., Monn, E., Hovig, T. & Seip, M. 1984. Imerlund-Grasbeck anemia. A long-term follow-up study. *Acta Paediatr Scand*, 73, 248-53.
- Brunskill, N. J. 2004. Albumin signals the coming of age of proteinuric nephropathy. *J Am Soc Nephrol*, 15, 504-5.
- Brunskill, N. J., Cockcroft, N., Nahorski, S. & Walls, J. 1996. Albumin endocytosis is regulated by heterotrimeric GTP-binding protein G alpha i-3 in opossum kidney cells. *Am J Physiol*, 271, F356-64.
- Brunskill, N. J., Nahorski, S. & Walls, J. 1997. Characteristics of albumin binding to opossum kidney cells and identification of potential receptors. *Pflugers Arch*, 433, 497-504.
- Burmeister, R., Boe, I. M., Nykjaer, A., Jacobsen, C., Moestrup, S. K., Verroust, P., Christensen, E. I., Lund, J. & Willnow, T. E. 2001. A two-receptor pathway for catabolism of Clara cell secretory protein in the kidney. *J Biol Chem*, 276, 13295-301.

- Butler, G. S. & Overall, C. M. 2009. Updated biological roles for matrix metalloproteinases and new "intracellular" substrates revealed by degradomics. *Biochemistry*, 48, 10830-45.
- Cabezas, F., Lagos, J., Cespedes, C., Vio, C. P., Bronfman, M. & Marzolo, M. P. 2011. Megalin/LRP2 expression is induced by peroxisome proliferator-activated receptor-alpha and -gamma: implications for PPARs' roles in renal function. *PLoS One*, 6, e16794.
- Castrop, H. & Schiessl, I. M. 2017. Novel routes of albumin passage across the glomerular filtration barrier. *Acta Physiol (Oxf)*, 219, 544-553.
- Catania, J. M., Chen, G. & Parrish, A. R. 2007. Role of matrix metalloproteinases in renal pathophysiologies. *Am J Physiol Renal Physiol*, 292, F905-11.
- Cerda-Costa, N. & Gomis-Ruth, F. X. 2014. Architecture and function of metallopeptidase catalytic domains. *Protein Sci*, 23, 123-44.
- Chang, R. L., Ueki, I. F., Troy, J. L., Deen, W. M., Robertson, C. R. & Brenner, B. M. 1975. Permselectivity of the glomerular capillary wall to macromolecules. II. Experimental studies in rats using neutral dextran. *Biophys J*, 15, 887-906.
- Chatelet, F., Brianti, E., Ronco, P., Roland, J. & Verroust, P. 1986. Ultrastructural localization by monoclonal antibodies of brush border antigens expressed by glomeruli. I. Renal distribution. *Am J Pathol*, 122, 500-11.
- Chen, W. J., Goldstein, J. L. & Brown, M. S. 1990. NPXY, a sequence often found in cytoplasmic tails, is required for coated pit-mediated internalization of the low density lipoprotein receptor. *J Biol Chem*, 265, 3116-23.
- Chen, X., Cobbs, A., George, J., Chima, A., Tuyishime, F. & Zhao, X. 2017. Endocytosis of Albumin Induces Matrix Metalloproteinase-9 by Activating the ERK Signaling Pathway in Renal Tubule Epithelial Cells. *Int J Mol Sci*, 18.
- Cheng, S. & Lovett, D. H. 2003. Gelatinase A (MMP-2) is necessary and sufficient for renal tubular cell epithelial-mesenchymal transformation. *Am J Pathol*, 162, 1937-49.
- Christensen, E. I. 1982. Rapid membrane recycling in renal proximal tubule cells. *Eur J Cell Biol*, 29, 43-9.

- Christensen, E. I. & Birn, H. 2001. Megalin and cubilin: synergistic endocytic receptors in renal proximal tubule. *Am J Physiol Renal Physiol*, 280, F562-73.
- Christensen, E. I. & Birn, H. 2002. Megalin and cubilin: multifunctional endocytic receptors. *Nat Rev Mol Cell Biol*, 3, 256-66.
- Christensen, E. I. & Birn, H. 2013. Proteinuria: Tubular handling of albumin-degradation or salvation? *Nat Rev Nephrol*, 9, 700-2.
- Christensen, E. I., Birn, H., Storm, T., Weyer, K. & Nielsen, R. 2012a. Endocytic receptors in the renal proximal tubule. *Physiology (Bethesda)*, 27, 223-36.
- Christensen, E. I., Birn, H., Verroust, P. & Moestrup, S. K. 1998a. Megalin-mediated endocytosis in renal proximal tubule. *Ren Fail*, 20, 191-9.
- Christensen, E. I., Birn, H., Verroust, P. & Moestrup, S. K. 1998b. Membrane receptors for endocytosis in the renal proximal tubule. *Int Rev Cytol*, 180, 237-84.
- Christensen, E. I., Nielsen, R. & Birn, H. 2013. From bowel to kidneys: the role of cubilin in physiology and disease. *Nephrol Dial Transplant*, 28, 274-81.
- Christensen, E. I., Verroust, P. J. & Nielsen, R. 2009. Receptor-mediated endocytosis in renal proximal tubule. *Pflugers Arch*, 458, 1039-48.
- Christensen, E. I., Wagner, C. A. & Kaissling, B. 2012b. Uriniferous tubule: structural and functional organization. *Compr Physiol*, 2, 805-61.
- Chronic Kidney Disease Prognosis, C., Matsushita, K., Van Der Velde, M., Astor, B. C., Woodward, M., Levey, A. S., De Jong, P. E., Coresh, J. & Gansevoort, R. T. 2010. Association of estimated glomerular filtration rate and albuminuria with all-cause and cardiovascular mortality in general population cohorts: a collaborative meta-analysis. *Lancet*, 375, 2073-81.
- Chung, A. W., Yang, H. H., Kim, J. M., Sigrist, M. K., Chum, E., Gourlay, W. A. & Levin, A. 2009a. Upregulation of matrix metalloproteinase-2 in the arterial vasculature contributes to stiffening and vasomotor dysfunction in patients with chronic kidney disease. *Circulation*, 120, 792-801.
- Chung, A. W., Yang, H. H., Sigrist, M. K., Brin, G., Chum, E., Gourlay, W. A. & Levin, A. 2009b. Matrix metalloproteinase-2 and -9 exacerbate arterial stiffening and angiogenesis in diabetes and chronic kidney disease. *Cardiovasc Res*, 84, 494-504.

- Coffey, S., Costacou, T., Orchard, T. & Erkan, E. 2015. Akt Links Insulin Signaling to Albumin Endocytosis in Proximal Tubule Epithelial Cells. *PLoS One*, 10, e0140417.
- Cohen, A. H. 2006. Renal Anatomy and Basic Concepts and Methods in Renal Pathology. *In: AGNES B. FOGO, ARTHUR H. COHEN, J. CHARLES JENNETTE, JAN A. BRUIJN & COLVIN, R. B. (eds.) Fundamentals of Renal Pathology*. Springer, New York, NY: Springer, New York, NY.
- Comper, W. D., Haraldsson, B. & Deen, W. M. 2008a. Resolved: normal glomeruli filter nephrotic levels of albumin. *J Am Soc Nephrol*, 19, 427-32.
- Comper, W. D., Hilliard, L. M., Nikolic-Paterson, D. J. & Russo, L. M. 2008b. Disease-dependent mechanisms of albuminuria. *Am J Physiol Renal Physiol*, 295, F1589-600.
- Comper, W. D., Osicka, T. M., Clark, M., Macisaac, R. J. & Jerums, G. 2004. Earlier detection of microalbuminuria in diabetic patients using a new urinary albumin assay. *Kidney Int*, 65, 1850-5.
- Corbel, M., Caulet-Maugendre, S., Germain, N., Molet, S., Lagente, V. & Boichot, E. 2001. Inhibition of bleomycin-induced pulmonary fibrosis in mice by the matrix metalloproteinase inhibitor batimastat. *J Pathol*, 193, 538-45.
- Coudroy, G., Gburek, J., Kozyraki, R., Madsen, M., Trugnan, G., Moestrup, S. K., Verroust, P. J. & Maurice, M. 2005. Contribution of cubilin and amnionless to processing and membrane targeting of cubilin-amnionless complex. *J Am Soc Nephrol*, 16, 2330-7.
- Cryns, V. & Yuan, J. 1998. Proteases to die for. *Genes Dev*, 12, 1551-70.
- Curci, J. A., Mao, D., Bohner, D. G., Allen, B. T., Rubin, B. G., Reilly, J. M., Sicard, G. A. & Thompson, R. W. 2000. Preoperative treatment with doxycycline reduces aortic wall expression and activation of matrix metalloproteinases in patients with abdominal aortic aneurysms. *J Vasc Surg*, 31, 325-42.
- D'amico, G. & Bazzi, C. 2003. Pathophysiology of proteinuria. *Kidney Int*, 63, 809-25.
- Davies, M. 1994. The mesangial cell: a tissue culture view. *Kidney Int*, 45, 320-7.
- Davis, C. G. 1990. The many faces of epidermal growth factor repeats. *New Biol*, 2, 410-9.

- De, S., Kuwahara, S. & Saito, A. 2014. The endocytic receptor megalin and its associated proteins in proximal tubule epithelial cells. *Membranes (Basel)*, 4, 333-55.
- De Zeeuw, D., Remuzzi, G., Parving, H. H., Keane, W. F., Zhang, Z., Shahinfar, S., Snapinn, S., Cooper, M. E., Mitch, W. E. & Brenner, B. M. 2004. Proteinuria, a target for renoprotection in patients with type 2 diabetic nephropathy: lessons from RENAAL. *Kidney Int*, 65, 2309-20.
- Deen, W. M. 2004. What determines glomerular capillary permeability? *J Clin Invest*, 114, 1412-4.
- Deen, W. M., Lazzara, M. J. & Myers, B. D. 2001. Structural determinants of glomerular permeability. *Am J Physiol Renal Physiol*, 281, F579-96.
- Densupsoontorn, N., Sanpakit, K., Vijarnsorn, C., Pattaragarn, A., Kangwanpornsiri, C., Jatutipsompol, C., Tirapongporn, H., Jirapinyo, P., Shah, N. P., Sturm, A. C. & Tanner, S. M. 2012. Imerlund-Grasbeck syndrome: new mutation in amnionless. *Pediatr Int*, 54, e19-21.
- Dickson, L. E., Wagner, M. C., Sandoval, R. M. & Molitoris, B. A. 2014. The proximal tubule and albuminuria: really! *J Am Soc Nephrol*, 25, 443-53.
- Dimas, G., Iliadis, F. & Grekas, D. 2013. Matrix metalloproteinases, atherosclerosis, proteinuria and kidney disease: Linkage-based approaches. *Hippokratia*, 17, 292-7.
- Ding, W. Y. & Saleem, M. A. 2012. Current concepts of the podocyte in nephrotic syndrome. *Kidney Res Clin Pract*, 31, 87-93.
- Diwakar, R., Pearson, A. L., Colville-Nash, P., Brunskill, N. J. & Dockrell, M. E. 2007. The role played by endocytosis in albumin-induced secretion of TGF-beta1 by proximal tubular epithelial cells. *Am J Physiol Renal Physiol*, 292, F1464-70.
- Dixon, R. & Brunskill, N. J. 2000. Albumin stimulates p44/p42 extracellular-signal-regulated mitogen-activated protein kinase in opossum kidney proximal tubular cells. *Clin Sci (Lond)*, 98, 295-301.
- Donadelli, R., Abbate, M., Zanchi, C., Corna, D., Tomasoni, S., Benigni, A., Remuzzi, G. & Zoja, C. 2000. Protein traffic activates NF-kB gene signaling and promotes MCP-1-dependent interstitial inflammation. *Am J Kidney Dis*, 36, 1226-41.

- Donadelli, R., Zanchi, C., Morigi, M., Buelli, S., Batani, C., Tomasoni, S., Corna, D., Rottoli, D., Benigni, A., Abbate, M., Remuzzi, G. & Zoja, C. 2003. Protein overload induces fractalkine upregulation in proximal tubular cells through nuclear factor kappaB- and p38 mitogen-activated protein kinase-dependent pathways. *J Am Soc Nephrol*, 14, 2436-46.
- Drake, C. J., Fleming, P. A., Larue, A. C., Barth, J. L., Chintalapudi, M. R. & Argraves, W. S. 2004. Differential distribution of cubilin and megalin expression in the mouse embryo. *Anat Rec A Discov Mol Cell Evol Biol*, 277, 163-70.
- Drumond, M. C., Kristal, B., Myers, B. D. & Deen, W. M. 1994. Structural basis for reduced glomerular filtration capacity in nephrotic humans. *J Clin Invest*, 94, 1187-95.
- Du, X., Shimizu, A., Masuda, Y., Kuwahara, N., Arai, T., Kataoka, M., Uchiyama, M., Kaneko, T., Akimoto, T., Iino, Y. & Fukuda, Y. 2012. Involvement of matrix metalloproteinase-2 in the development of renal interstitial fibrosis in mouse obstructive nephropathy. *Lab Invest*, 92, 1149-60.
- Eddy, A. 2001. Role of cellular infiltrates in response to proteinuria. *Am J Kidney Dis*, 37, S25-9.
- Eddy, A. A. 1989. Interstitial nephritis induced by protein-overload proteinuria. *Am J Pathol*, 135, 719-33.
- Eddy, A. A. 2000. Molecular basis of renal fibrosis. *Pediatr Nephrol*, 15, 290-301.
- Eddy, A. A. 2004. Proteinuria and interstitial injury. *Nephrol Dial Transplant*, 19, 277-81.
- Eddy, A. A. & Giachelli, C. M. 1995. Renal expression of genes that promote interstitial inflammation and fibrosis in rats with protein-overload proteinuria. *Kidney Int*, 47, 1546-57.
- Eddy, A. A., Kim, H., Lopez-Guisa, J., Oda, T. & Soloway, P. D. 2000. Interstitial fibrosis in mice with overload proteinuria: deficiency of TIMP-1 is not protective. *Kidney Int*, 58, 618-28.
- Eddy, A. A., McCulloch, L., Liu, E. & Adams, J. 1991. A relationship between proteinuria and acute tubulointerstitial disease in rats with experimental nephrotic syndrome. *Am J Pathol*, 138, 1111-23.
- Eddy, A. A. & Michael, A. F. 1988. Acute tubulointerstitial nephritis associated with aminonucleoside nephrosis. *Kidney Int*, 33, 14-23.

- El-Nahas, A. M., Paraskevakou, H., Zoob, S., Rees, A. J. & Evans, D. J. 1983. Effect of dietary protein restriction on the development of renal failure after subtotal nephrectomy in rats. *Clin Sci (Lond)*, 65, 399-406.
- El Nahas, A. M. 1989a. Glomerulosclerosis: are we any wiser? *Klin Wochenschr*, 67, 876-81.
- El Nahas, A. M. 1989b. Glomerulosclerosis: insights into pathogenesis and treatment. *Nephrol Dial Transplant*, 4, 843-53.
- El Nahas, M. 2005. The global challenge of chronic kidney disease. *Kidney Int*, 68, 2918-29.
- Elger, M., Sakai, T. & Kriz, W. 1998. The vascular pole of the renal glomerulus of rat. *Adv Anat Embryol Cell Biol*, 139, 1-98.
- Ermolli, M., Schumacher, M., Lods, N., Hammoud, M. & Marti, H. P. 2003. Differential expression of MMP-2/MMP-9 and potential benefit of an MMP inhibitor in experimental acute kidney allograft rejection. *Transpl Immunol*, 11, 137-45.
- Evanko, D. S., Thiyagarajan, M. M. & Wedegaertner, P. B. 2000. Interaction with Gbetagamma is required for membrane targeting and palmitoylation of Galpha(s) and Galpha(q). *J Biol Chem*, 275, 1327-36.
- Falcone, D. J., Mccaffrey, T. A., Haimovitz-Friedman, A., Vergilio, J. A. & Nicholson, A. C. 1993. Macrophage and foam cell release of matrix-bound growth factors. Role of plasminogen activation. *J Biol Chem*, 268, 11951-8.
- Fang, Z., He, F., Chen, S., Sun, X., Zhu, Z. & Zhang, C. 2009. Albumin modulates the production of matrix metalloproteinases-2 and -9 in podocytes. *J Huazhong Univ Sci Technolog Med Sci*, 29, 710-4.
- Fatah, H., Benfaed, N., Chana, R. S., Chunara, M. H., Barratt, J., Baines, R. J. & Brunskill, N. J. 2017. Reduced proximal tubular expression of protein endocytic receptors in proteinuria is associated with urinary receptor shedding. *Nephrol Dial Transplant*.
- Fingleton, B. 2007. Matrix metalloproteinases as valid clinical targets. *Curr Pharm Des*, 13, 333-46.
- Fingleton, B. 2008. MMPs as therapeutic targets--still a viable option? *Semin Cell Dev Biol*, 19, 61-8.

- Fyfe, J. C., Giger, U., Hall, C. A., Jezyk, P. F., Klumpp, S. A., Levine, J. S. & Patterson, D. F. 1991a. Inherited selective intestinal cobalamin malabsorption and cobalamin deficiency in dogs. *Pediatr Res*, 29, 24-31.
- Fyfe, J. C., Madsen, M., Hojrup, P., Christensen, E. I., Tanner, S. M., De La Chapelle, A., He, Q. & Moestrup, S. K. 2004. The functional cobalamin (vitamin B12)-intrinsic factor receptor is a novel complex of cubilin and amnionless. *Blood*, 103, 1573-9.
- Fyfe, J. C., Ramanujam, K. S., Ramaswamy, K., Patterson, D. F. & Seetharam, B. 1991b. Defective brush-border expression of intrinsic factor-cobalamin receptor in canine inherited intestinal cobalamin malabsorption. *J Biol Chem*, 266, 4489-94.
- Gansevoort, R. T., Correa-Rotter, R., Hemmelgarn, B. R., Jafar, T. H., Heerspink, H. J., Mann, J. F., Matsushita, K. & Wen, C. P. 2013. Chronic kidney disease and cardiovascular risk: epidemiology, mechanisms, and prevention. *Lancet*, 382, 339-52.
- Gburek, J., Verroust, P. J., Willnow, T. E., Fyfe, J. C., Nowacki, W., Jacobsen, C., Moestrup, S. K. & Christensen, E. I. 2002. Megalin and cubilin are endocytic receptors involved in renal clearance of hemoglobin. *J Am Soc Nephrol*, 13, 423-30.
- Gearing, A. J., Beckett, P., Christodoulou, M., Churchill, M., Clements, J., Davidson, A. H., Drummond, A. H., Galloway, W. A., Gilbert, R., Gordon, J. L. & Et Al. 1994. Processing of tumour necrosis factor-alpha precursor by metalloproteinases. *Nature*, 370, 555-7.
- Gearing, A. J., Beckett, P., Christodoulou, M., Churchill, M., Clements, J. M., Crimmin, M., Davidson, A. H., Drummond, A. H., Galloway, W. A., Gilbert, R. & Et Al. 1995. Matrix metalloproteinases and processing of pro-TNF-alpha. *J Leukoc Biol*, 57, 774-7.
- Gekle, M. 1998. Renal Proximal Tubular Albumin Reabsorption: Daily Prevention of Albuminuria. *News Physiol Sci*, 13, 5-11.
- Gekle, M. 2005. Renal tubule albumin transport. *Annu Rev Physiol*, 67, 573-94.
- Gekle, M., Mildenerger, S., Freudinger, R. & Silbernagl, S. 1996. Functional characterization of albumin binding to the apical membrane of OK cells. *Am J Physiol*, 271, F286-91.

- Gentle, M. E., Shi, S., Daehn, I., Zhang, T., Qi, H., Yu, L., D'agati, V. D., Schlondorff, D. O. & Bottinger, E. P. 2013. Epithelial cell TGFbeta signaling induces acute tubular injury and interstitial inflammation. *J Am Soc Nephrol*, 24, 787-99.
- Gharagozlian, S., Svennevig, K., Bangstad, H. J., Winberg, J. O. & Kolset, S. O. 2009. Matrix metalloproteinases in subjects with type 1 diabetes. *BMC Clin Pathol*, 9, 7.
- Gialeli, C., Theocharis, A. D. & Karamanos, N. K. 2011. Roles of matrix metalloproteinases in cancer progression and their pharmacological targeting. *FEBS J*, 278, 16-27.
- Gibb, D. M., Tomlinson, P. A., Dalton, N. R., Turner, C., Shah, V. & Barratt, T. M. 1989. Renal tubular proteinuria and microalbuminuria in diabetic patients. *Arch Dis Child*, 64, 129-34.
- Gibbons, G. H., Pratt, R. E. & Dzau, V. J. 1992. Vascular smooth muscle cell hypertrophy vs. hyperplasia. Autocrine transforming growth factor-beta 1 expression determines growth response to angiotensin II. *J Clin Invest*, 90, 456-61.
- Goldstein, J. L., Anderson, R. G. & Brown, M. S. 1979. Coated pits, coated vesicles, and receptor-mediated endocytosis. *Nature*, 279, 679-85.
- Gomis-Ruth, F. X. 2009. Catalytic domain architecture of metzincin metalloproteases. *J Biol Chem*, 284, 15353-7.
- Gorriz, J. L. & Martinez-Castelao, A. 2012. Proteinuria: detection and role in native renal disease progression. *Transplant Rev (Orlando)*, 26, 3-13.
- Grande, M. T., Perez-Barriocanal, F. & Lopez-Novoa, J. M. 2010. Role of inflammation in tubulo-interstitial damage associated to obstructive nephropathy. *J Inflamm (Lond)*, 7, 19.
- Grasbeck, R. 2006. Imerslund-Grasbeck syndrome (selective vitamin B(12) malabsorption with proteinuria). *Orphanet J Rare Dis*, 1, 17.
- Greka, A. & Mundel, P. 2012. Cell biology and pathology of podocytes. *Annu Rev Physiol*, 74, 299-323.
- Guan, S., Ma, J., Zhang, Y., Gao, Y., Zhang, Y., Zhang, X., Wang, N., Xie, Y., Wang, J., Zhang, J. & Chu, L. 2013. Danshen (*Salvia miltiorrhiza*) injection suppresses kidney injury induced by iron overload in mice. *PLoS One*, 8, e74318.

- Gudehithlu, K. P., Pegoraro, A. A., Dunea, G., Arruda, J. A. & Singh, A. K. 2004. Degradation of albumin by the renal proximal tubule cells and the subsequent fate of its fragments. *Kidney Int*, 65, 2113-22.
- Gut, A., Kappeler, F., Hyka, N., Balda, M. S., Hauri, H. P. & Matter, K. 1998. Carbohydrate-mediated Golgi to cell surface transport and apical targeting of membrane proteins. *EMBO J*, 17, 1919-29.
- Hammad, S. M., Barth, J. L., Knaak, C. & Argraves, W. S. 2000. Megalin acts in concert with cubilin to mediate endocytosis of high density lipoproteins. *J Biol Chem*, 275, 12003-8.
- Haraldsson, B., Nystrom, J. & Deen, W. M. 2008. Properties of the glomerular barrier and mechanisms of proteinuria. *Physiol Rev*, 88, 451-87.
- Haub, P. & Meckel, T. 2015. A Model based Survey of Colour Deconvolution in Diagnostic Brightfield Microscopy: Error Estimation and Spectral Consideration. *Sci Rep*, 5, 12096.
- Hauck, F. H., Tanner, S. M., Henker, J. & Laass, M. W. 2008. Imlerslund-Grasbeck syndrome in a 15-year-old German girl caused by compound heterozygous mutations in CUBN. *Eur J Pediatr*, 167, 671-5.
- He, G., Gupta, S., Yi, M., Michaely, P., Hobbs, H. H. & Cohen, J. C. 2002. ARH is a modular adaptor protein that interacts with the LDL receptor, clathrin, and AP-2. *J Biol Chem*, 277, 44044-9.
- He, Q., Madsen, M., Kilkenney, A., Gregory, B., Christensen, E. I., Vorum, H., Hojrup, P., Schaffer, A. A., Kirkness, E. F., Tanner, S. M., De La Chapelle, A., Giger, U., Moestrup, S. K. & Fyfe, J. C. 2005. Amnionless function is required for cubilin brush-border expression and intrinsic factor-cobalamin (vitamin B12) absorption in vivo. *Blood*, 106, 1447-53.
- Hebert, L. A., Bain, R. P., Verme, D., Cattran, D., Whittier, F. C., Tolchin, N., Rohde, R. D. & Lewis, E. J. 1994. Remission of nephrotic range proteinuria in type I diabetes. Collaborative Study Group. *Kidney Int*, 46, 1688-93.
- Henderson, N. C., Mackinnon, A. C., Farnworth, S. L., Kipari, T., Haslett, C., Iredale, J. P., Liu, F. T., Hughes, J. & Sethi, T. 2008. Galectin-3 expression and secretion links macrophages to the promotion of renal fibrosis. *Am J Pathol*, 172, 288-98.
- Hooper, N. M., Karran, E. H. & Turner, A. J. 1997. Membrane protein secretases. *Biochem J*, 321 (Pt 2), 265-79.

- Hopsu-Havu, V. K. & Ekfors, T. O. 1969. Distribution of a dipeptide naphthylamidase in rat tissues and its localisation by using diazo coupling and labeled antibody techniques. *Histochemie*, 17, 30-8.
- Horii, Y., Muraguchi, A., Iwano, M., Matsuda, T., Hirayama, T., Yamada, H., Fujii, Y., Dohi, K., Ishikawa, H., Ohmoto, Y. & Et Al. 1989. Involvement of IL-6 in mesangial proliferative glomerulonephritis. *J Immunol*, 143, 3949-55.
- Hosaka, M., Nagahama, M., Kim, W. S., Watanabe, T., Hatsuzawa, K., Ikemizu, J., Murakami, K. & Nakayama, K. 1991. Arg-X-Lys/Arg-Arg motif as a signal for precursor cleavage catalyzed by furin within the constitutive secretory pathway. *J Biol Chem*, 266, 12127-30.
- Hostetter, T. H., Olson, J. L., Rennke, H. G., Venkatachalam, M. A. & Brenner, B. M. 1981. Hyperfiltration in remnant nephrons: a potentially adverse response to renal ablation. *Am J Physiol*, 241, F85-93.
- Hou, F. F., Xie, D., Zhang, X., Chen, P. Y., Zhang, W. R., Liang, M., Guo, Z. J. & Jiang, J. P. 2007. Renoprotection of Optimal Antiproteinuric Doses (ROAD) Study: a randomized controlled study of benazepril and losartan in chronic renal insufficiency. *J Am Soc Nephrol*, 18, 1889-98.
- Hudson, B. G., Tryggvason, K., Sundaramoorthy, M. & Neilson, E. G. 2003. Alport's syndrome, Goodpasture's syndrome, and type IV collagen. *N Engl J Med*, 348, 2543-56.
- Hurst, R. J. & Else, K. J. 2012. Retinoic acid signalling in gastrointestinal parasite infections: lessons from mouse models. *Parasite Immunol*, 34, 351-9.
- Ishola, D. A., Jr., Van Der Giezen, D. M., Hahnel, B., Goldschmeding, R., Kriz, W., Koomans, H. A. & Joles, J. A. 2006. In mice, proteinuria and renal inflammatory responses to albumin overload are strain-dependent. *Nephrol Dial Transplant*, 21, 591-7.
- Jani, A., Ljubanovic, D., Faubel, S., Kim, J., Mischak, R. & Edelstein, C. L. 2004. Caspase inhibition prevents the increase in caspase-3, -2, -8 and -9 activity and apoptosis in the cold ischemic mouse kidney. *Am J Transplant*, 4, 1246-54.
- Jeansson, M., Bjorck, K., Tenstad, O. & Haraldsson, B. 2009. Adriamycin alters glomerular endothelium to induce proteinuria. *J Am Soc Nephrol*, 20, 114-22.

- Jefferson, J. A., Shankland, S. J. & Pichler, R. H. 2008. Proteinuria in diabetic kidney disease: a mechanistic viewpoint. *Kidney Int*, 74, 22-36.
- Johnson, R. J., Alpers, C. E., Yoshimura, A., Lombardi, D., Pritzl, P., Floege, J. & Schwartz, S. M. 1992. Renal injury from angiotensin II-mediated hypertension. *Hypertension*, 19, 464-74.
- Jones, C. L., Buch, S., Post, M., Mcculloch, L., Liu, E. & Eddy, A. A. 1992. Renal extracellular matrix accumulation in acute puromycin aminonucleoside nephrosis in rats. *Am J Pathol*, 141, 1381-96.
- Jouret, F., Bernard, A., Hermans, C., Dom, G., Terryn, S., Leal, T., Lebecque, P., Cassiman, J. J., Scholte, B. J., De Jonge, H. R., Courtoy, P. J. & Devuyst, O. 2007. Cystic fibrosis is associated with a defect in apical receptor-mediated endocytosis in mouse and human kidney. *J Am Soc Nephrol*, 18, 707-18.
- Junqueira, L. C., Bignolas, G. & Brentani, R. R. 1979. Picrosirius staining plus polarization microscopy, a specific method for collagen detection in tissue sections. *Histochem J*, 11, 447-55.
- Kalantarinia, K., Awad, A. S. & Siragy, H. M. 2003. Urinary and renal interstitial concentrations of TNF-alpha increase prior to the rise in albuminuria in diabetic rats. *Kidney Int*, 64, 1208-13.
- Kalantry, S., Manning, S., Haub, O., Tomihara-Newberger, C., Lee, H. G., Fangman, J., Distech, C. M., Manova, K. & Lacy, E. 2001. The amnionless gene, essential for mouse gastrulation, encodes a visceral-endoderm-specific protein with an extracellular cysteine-rich domain. *Nat Genet*, 27, 412-6.
- Kamijo, A., Kimura, K., Sugaya, T., Yamanouchi, M., Hase, H., Kaneko, T., Hirata, Y., Goto, A., Fujita, T. & Omata, M. 2002. Urinary free fatty acids bound to albumin aggravate tubulointerstitial damage. *Kidney Int*, 62, 1628-37.
- Kanwar Nasir M. Khan, G. C. H., Carl L. Alden 2013. Kidney. In: WANDA M. HASCHEK, C. G. R., MATTHEW A. WALLIG (ed.) *Haschek and Rousseaux's Handbook of Toxicologic Pathology* Third Edition ed.: Academic Press is an Imprint of Elsevier.
- Kaushal, G. P., Singh, A. B. & Shah, S. V. 1998. Identification of gene family of caspases in rat kidney and altered expression in ischemia-reperfusion injury. *Am J Physiol*, 274, F587-95.

- Kayama, F., Yoshida, T., Kodama, Y., Matsui, T., Matheson, J. M. & Luster, M. I. 1997. Pro-inflammatory cytokines and interleukin 6 in the renal response to bacterial endotoxin. *Cytokine*, 9, 688-95.
- Kazancioglu, R. 2013. Risk factors for chronic kidney disease: an update. *Kidney Int Suppl* (2011), 3, 368-371.
- Ke, J. T., Li, M., Xu, S. Q., Zhang, W. J., Jiang, Y. W., Cheng, L. Y., Chen, L., Lou, J. N. & Wu, W. 2014. Gliquidone decreases urinary protein by promoting tubular reabsorption in diabetic Goto-Kakizaki rats. *J Endocrinol*, 220, 129-41.
- Kim, H. J., Moradi, H., Yuan, J., Norris, K. & Vaziri, N. D. 2009. Renal mass reduction results in accumulation of lipids and dysregulation of lipid regulatory proteins in the remnant kidney. *Am J Physiol Renal Physiol*, 296, F1297-306.
- Klahr, S., Levey, A. S., Beck, G. J., Caggiula, A. W., Hunsicker, L., Kusek, J. W. & Striker, G. 1994. The effects of dietary protein restriction and blood-pressure control on the progression of chronic renal disease. Modification of Diet in Renal Disease Study Group. *N Engl J Med*, 330, 877-84.
- Kozyraki, R., Fyfe, J., Kristiansen, M., Gerdes, C., Jacobsen, C., Cui, S., Christensen, E. I., Aminoff, M., De La Chapelle, A., Krahe, R., Verroust, P. J. & Moestrup, S. K. 1999. The intrinsic factor-vitamin B12 receptor, cubilin, is a high-affinity apolipoprotein A-I receptor facilitating endocytosis of high-density lipoprotein. *Nat Med*, 5, 656-61.
- Kozyraki, R., Fyfe, J., Verroust, P. J., Jacobsen, C., Dautry-Varsat, A., Gburek, J., Willnow, T. E., Christensen, E. I. & Moestrup, S. K. 2001. Megalin-dependent cubilin-mediated endocytosis is a major pathway for the apical uptake of transferrin in polarized epithelia. *Proc Natl Acad Sci U S A*, 98, 12491-6.
- Kozyraki, R., Kristiansen, M., Silaharoglu, A., Hansen, C., Jacobsen, C., Tommerup, N., Verroust, P. J. & Moestrup, S. K. 1998. The human intrinsic factor-vitamin B12 receptor, cubilin: molecular characterization and chromosomal mapping of the gene to 10p within the autosomal recessive megaloblastic anemia (MGA1) region. *Blood*, 91, 3593-600.
- Kristiansen, M., Kozyraki, R., Jacobsen, C., Nexø, E., Verroust, P. J. & Moestrup, S. K. 1999. Molecular dissection of the intrinsic factor-vitamin B12 receptor,

- cubilin, discloses regions important for membrane association and ligand binding. *J Biol Chem*, 274, 20540-4.
- Kriz, W. & Bankir, L. 1988. A standard nomenclature for structures of the kidney. The Renal Commission of the International Union of Physiological Sciences (IUPS). *Kidney Int*, 33, 1-7.
- Kriz, W. & Elger, M. 2010. Renal Anatomy. In: JÜRGEN FLOEGE, R. J. J., JOHN FEEHALLY (ed.) *Comprehensive Clinical Nephrology*. 4th ed. United States of America: Elsevier.
- Kriz, W., Hackenthal, E., Nobiling, R., Sakai, T., Elger, M. & Hahnel, B. 1994. A role for podocytes to counteract capillary wall distension. *Kidney Int*, 45, 369-76.
- Kruegel, J., Rubel, D. & Gross, O. 2013. Alport syndrome--insights from basic and clinical research. *Nat Rev Nephrol*, 9, 170-8.
- Kumar, A., Bhatnagar, S. & Kumar, A. 2010. Matrix metalloproteinase inhibitor batimastat alleviates pathology and improves skeletal muscle function in dystrophin-deficient mdx mice. *Am J Pathol*, 177, 248-60.
- Kunugi, S., Shimizu, A., Kuwahara, N., Du, X., Takahashi, M., Terasaki, Y., Fujita, E., Mii, A., Nagasaka, S., Akimoto, T., Masuda, Y. & Fukuda, Y. 2011. Inhibition of matrix metalloproteinases reduces ischemia-reperfusion acute kidney injury. *Lab Invest*, 91, 170-80.
- Lal, M. & Caplan, M. 2011. Regulated intramembrane proteolysis: signaling pathways and biological functions. *Physiology (Bethesda)*, 26, 34-44.
- Lan, H. Y. 2011. Diverse roles of TGF-beta/Smads in renal fibrosis and inflammation. *Int J Biol Sci*, 7, 1056-67.
- Lan, H. Y., Nikolic-Paterson, D. J., Zarama, M., Vannice, J. L. & Atkins, R. C. 1993. Suppression of experimental crescentic glomerulonephritis by the interleukin-1 receptor antagonist. *Kidney Int*, 43, 479-85.
- Landgraf, S. S., Silva, L. S., Peruchetti, D. B., Sirtoli, G. M., Moraes-Santos, F., Portella, V. G., Silva-Filho, J. L., Pinheiro, C. S., Abreu, T. P., Takiya, C. M., Benjamin, C. F., Pinheiro, A. A., Canetti, C. & Caruso-Neves, C. 2014. 5-Lipoxygenase products are involved in renal tubulointerstitial injury induced by albumin overload in proximal tubules in mice. *PLoS One*, 9, e107549.

- Lauhio, A., Sorsa, T., Srinivas, R., Stenman, M., Tervahartiala, T., Stenman, U. H., Gronhagen-Riska, C. & Honkanen, E. 2008. Urinary matrix metalloproteinase -8, -9, -14 and their regulators (TRY-1, TRY-2, TATI) in patients with diabetic nephropathy. *Ann Med*, 40, 312-20.
- Lee, S. Y., Horbelt, M., Mang, H. E., Knipe, N. L., Bacallao, R. L., Sado, Y. & Sutton, T. A. 2011. MMP-9 gene deletion mitigates microvascular loss in a model of ischemic acute kidney injury. *Am J Physiol Renal Physiol*, 301, F101-9.
- Lee, Y. K., Kwon, T., Kim, D. J., Huh, W., Kim, Y. G., Oh, H. Y. & Kawachi, H. 2004. Ultrastructural study on nephrin expression in experimental puromycin aminonucleoside nephrosis. *Nephrol Dial Transplant*, 19, 2981-6.
- Leheste, J. R., Rolinski, B., Vorum, H., Hilpert, J., Nykjaer, A., Jacobsen, C., Aucouturier, P., Moskaug, J. O., Otto, A., Christensen, E. I. & Willnow, T. E. 1999. Megalin knockout mice as an animal model of low molecular weight proteinuria. *Am J Pathol*, 155, 1361-70.
- Lenz, O., Elliot, S. J. & Stetler-Stevenson, W. G. 2000. Matrix metalloproteinases in renal development and disease. *J Am Soc Nephrol*, 11, 574-81.
- Leonard, M., Ryan, M. P., Watson, A. J., Schramek, H. & Healy, E. 1999. Role of MAP kinase pathways in mediating IL-6 production in human primary mesangial and proximal tubular cells. *Kidney Int*, 56, 1366-77.
- Levey, A. S., Atkins, R., Coresh, J., Cohen, E. P., Collins, A. J., Eckardt, K. U., Nahas, M. E., Jaber, B. L., Jadoul, M., Levin, A., Powe, N. R., Rossert, J., Wheeler, D. C., Lameire, N. & Eknoyan, G. 2007. Chronic kidney disease as a global public health problem: approaches and initiatives - a position statement from Kidney Disease Improving Global Outcomes. *Kidney Int*, 72, 247-59.
- Levey, A. S., De Jong, P. E., Coresh, J., El Nahas, M., Astor, B. C., Matsushita, K., Gansevoort, R. T., Kasiske, B. L. & Eckardt, K. U. 2011. The definition, classification, and prognosis of chronic kidney disease: a KDIGO Controversies Conference report. *Kidney Int*, 80, 17-28.
- Lewis, J. B., Berl, T., Bain, R. P., Rohde, R. D. & Lewis, E. J. 1999. Effect of intensive blood pressure control on the course of type 1 diabetic nephropathy. Collaborative Study Group. *Am J Kidney Dis*, 34, 809-17.

- Li, X., Pabla, N., Wei, Q., Dong, G., Messing, R. O., Wang, C. Y. & Dong, Z. 2010. PKC-delta promotes renal tubular cell apoptosis associated with proteinuria. *J Am Soc Nephrol*, 21, 1115-24.
- Li, Y., Li, L., Zeng, O., Liu, J. M. & Yang, J. 2017. H₂S improves renal fibrosis in STZ-induced diabetic rats by ameliorating TGF-beta1 expression. *Ren Fail*, 39, 265-272.
- Liang, B., Gardner, D. B., Griswold, D. E., Bugelski, P. J. & Song, X. Y. 2006. Anti-interleukin-6 monoclonal antibody inhibits autoimmune responses in a murine model of systemic lupus erythematosus. *Immunology*, 119, 296-305.
- Lichtenthaler, S. F., Haass, C. & Steiner, H. 2011. Regulated intramembrane proteolysis--lessons from amyloid precursor protein processing. *J Neurochem*, 117, 779-96.
- Liu, G., Thomas, L., Warren, R. A., Enns, C. A., Cunningham, C. C., Hartwig, J. H. & Thomas, G. 1997. Cytoskeletal protein ABP-280 directs the intracellular trafficking of furin and modulates proprotein processing in the endocytic pathway. *J Cell Biol*, 139, 1719-33.
- Liu, J., Li, K., He, Y., Zhang, J., Wang, H., Yang, J., Zhan, J. & Liang, H. 2011. Anticubilin antisense RNA ameliorates adriamycin-induced tubulointerstitial injury in experimental rats. *Am J Med Sci*, 342, 494-502.
- Liu, S., Li, Y., Zhao, H., Chen, D., Huang, Q., Wang, S., Zou, W., Zhang, Y., Li, X. & Huang, H. 2006. Increase in extracellular cross-linking by tissue transglutaminase and reduction in expression of MMP-9 contribute differentially to focal segmental glomerulosclerosis in rats. *Mol Cell Biochem*, 284, 9-17.
- Loeffler, I. & Wolf, G. 2014. Transforming growth factor-beta and the progression of renal disease. *Nephrol Dial Transplant*, 29 Suppl 1, i37-i45.
- Loffek, S., Schilling, O. & Franzke, C. W. 2011. Series "matrix metalloproteinases in lung health and disease": Biological role of matrix metalloproteinases: a critical balance. *Eur Respir J*, 38, 191-208.
- Lote, C. J. 2012. Essential Anatomy of the Kidney. *Principles of Renal Physiology*. 5th ed. New York, NY: Springer.
- Lovejoy, B., Cleasby, A., Hassell, A. M., Longley, K., Luther, M. A., Weigl, D., Mcgeehan, G., Mcelroy, A. B., Drewry, D., Lambert, M. H. & Et Al. 1994.

- Structure of the catalytic domain of fibroblast collagenase complexed with an inhibitor. *Science*, 263, 375-7.
- Low, J. A., Johnson, M. D., Bone, E. A. & Dickson, R. B. 1996. The matrix metalloproteinase inhibitor batimastat (BB-94) retards human breast cancer solid tumor growth but not ascites formation in nude mice. *Clin Cancer Res*, 2, 1207-14.
- Lund, U., Rippe, A., Venturoli, D., Tenstad, O., Grubb, A. & Rippe, B. 2003. Glomerular filtration rate dependence of sieving of albumin and some neutral proteins in rat kidneys. *Am J Physiol Renal Physiol*, 284, F1226-34.
- Lutz, J., Yao, Y., Song, E., Antus, B., Hamar, P., Liu, S. & Heemann, U. 2005. Inhibition of matrix metalloproteinases during chronic allograft nephropathy in rats. *Transplantation*, 79, 655-61.
- Ma, J., Nishimura, H., Fogo, A., Kon, V., Inagami, T. & Ichikawa, I. 1998. Accelerated fibrosis and collagen deposition develop in the renal interstitium of angiotensin type 2 receptor null mutant mice during ureteral obstruction. *Kidney Int*, 53, 937-44.
- Maack, T. 1975. Renal handling of low molecular weight proteins. *Am J Med*, 58, 57-64.
- Maack, T., Johnson, V., Kau, S. T., Figueiredo, J. & Sigulem, D. 1979. Renal filtration, transport, and metabolism of low-molecular-weight proteins: a review. *Kidney Int*, 16, 251-70.
- Marinides, G. N., Groggel, G. C., Cohen, A. H. & Border, W. A. 1990. Enalapril and low protein reverse chronic puromycin aminonucleoside nephropathy. *Kidney Int*, 37, 749-57.
- Marshansky, V., Bourgoin, S., Londono, I., Bendayan, M., Maranda, B. & Vinay, P. 1997. Receptor-mediated endocytosis in kidney proximal tubules: recent advances and hypothesis. *Electrophoresis*, 18, 2661-76.
- Matejas, V., Hinkes, B., Alkandari, F., Al-Gazali, L., Annexstad, E., Aytac, M. B., Barrow, M., Blahova, K., Bockenhauer, D., Cheong, H. I., Maruniak-Chudek, I., Cochat, P., Dotsch, J., Gajjar, P., Hennekam, R. C., Janssen, F., Kagan, M., Kariminejad, A., Kemper, M. J., Koenig, J., Kogan, J., Kroes, H. Y., Kuwertz-Broking, E., Lewanda, A. F., Medeira, A., Muscheites, J., Niaudet, P., Pierson, M., Saggari, A., Seaver, L., Suri, M., Tsygin, A., Wuhl, E., Zurowska, A., Uebe, S., Hildebrandt, F., Antignac, C. & Zenker, M.

2010. Mutations in the human laminin beta2 (LAMB2) gene and the associated phenotypic spectrum. *Hum Mutat*, 31, 992-1002.
- Maunsbach, A. B., Marples, D., Chin, E., Ning, G., Bondy, C., Agre, P. & Nielsen, S. 1997. Aquaporin-1 water channel expression in human kidney. *J Am Soc Nephrol*, 8, 1-14.
- Menon, M. C., Chuang, P. Y. & He, C. J. 2012. The glomerular filtration barrier: components and crosstalk. *Int J Nephrol*, 2012, 749010.
- Mentlein, R. 1999. Dipeptidyl-peptidase IV (CD26)--role in the inactivation of regulatory peptides. *Regul Pept*, 85, 9-24.
- Messina, A., Davies, D. J., Dillane, P. C. & Ryan, G. B. 1987. Glomerular epithelial abnormalities associated with the onset of proteinuria in aminonucleoside nephrosis. *Am J Pathol*, 126, 220-9.
- Miner, J. H. 2012. The glomerular basement membrane. *Exp Cell Res*, 318, 973-8.
- Miner, J. H. & Sanes, J. R. 1996. Molecular and functional defects in kidneys of mice lacking collagen alpha 3(IV): implications for Alport syndrome. *J Cell Biol*, 135, 1403-13.
- Mishra, V. K. & Palgunachari, M. N. 1996. Interaction of model class A1, class A2, and class Y amphipathic helical peptides with membranes. *Biochemistry*, 35, 11210-20.
- Mitani, O., Katoh, M. & Shigematsu, H. 2004. Participation of the matrix metalloproteinase inhibitor in Thy-1 nephritis. *Pathol Int*, 54, 241-50.
- Moestrup, S. K., Kozyraki, R., Kristiansen, M., Kaysen, J. H., Rasmussen, H. H., Brault, D., Pontillon, F., Goda, F. O., Christensen, E. I., Hammond, T. G. & Verroust, P. J. 1998. The intrinsic factor-vitamin B12 receptor and target of teratogenic antibodies is a megalin-binding peripheral membrane protein with homology to developmental proteins. *J Biol Chem*, 273, 5235-42.
- Mogensen, C. E. & Solling 1977. Studies on renal tubular protein reabsorption: partial and near complete inhibition by certain amino acids. *Scand J Clin Lab Invest*, 37, 477-86.
- Molloy, S. S., Bresnahan, P. A., Leppla, S. H., Klimpel, K. R. & Thomas, G. 1992. Human furin is a calcium-dependent serine endoprotease that recognizes the sequence Arg-X-X-Arg and efficiently cleaves anthrax toxin protective antigen. *J Biol Chem*, 267, 16396-402.

- Morelli, E., Loon, N., Meyer, T., Peters, W. & Myers, B. D. 1990. Effects of converting-enzyme inhibition on barrier function in diabetic glomerulopathy. *Diabetes*, 39, 76-82.
- Morigi, M., Macconi, D., Zoja, C., Donadelli, R., Buelli, S., Zanchi, C., Ghilardi, M. & Remuzzi, G. 2002. Protein overload-induced NF-kappaB activation in proximal tubular cells requires H₂O₂ through a PKC-dependent pathway. *J Am Soc Nephrol*, 13, 1179-89.
- Morris, S. M. & Cooper, J. A. 2001. Disabled-2 colocalizes with the LDLR in clathrin-coated pits and interacts with AP-2. *Traffic*, 2, 111-23.
- Morrison, C. J., Butler, G. S., Rodriguez, D. & Overall, C. M. 2009. Matrix metalloproteinase proteomics: substrates, targets, and therapy. *Curr Opin Cell Biol*, 21, 645-53.
- Morse, S. M., Shaw, G. & Larner, S. F. 2006. Concurrent mRNA and protein extraction from the same experimental sample using a commercially available column-based RNA preparation kit. *Biotechniques*, 40, 54, 56, 58.
- Mundel, P. & Reiser, J. 2010. Proteinuria: an enzymatic disease of the podocyte? *Kidney Int*, 77, 571-80.
- Murphy, G., Stanton, H., Cowell, S., Butler, G., Knauper, V., Atkinson, S. & Gavrilovic, J. 1999. Mechanisms for pro matrix metalloproteinase activation. *APMIS*, 107, 38-44.
- Nagase, H. 1997. Activation mechanisms of matrix metalloproteinases. *Biol Chem*, 378, 151-60.
- Nagase, H. & Woessner, J. F., Jr. 1999. Matrix metalloproteinases. *J Biol Chem*, 274, 21491-4.
- Nakajima, H., Takenaka, M., Kaimori, J. Y., Hamano, T., Iwatani, H., Sugaya, T., Ito, T., Hori, M. & Imai, E. 2004. Activation of the signal transducer and activator of transcription signaling pathway in renal proximal tubular cells by albumin. *J Am Soc Nephrol*, 15, 276-85.
- Namour, F., Dobrovolski, G., Chery, C., Audonnet, S., Feillet, F., Sperl, W. & Gueant, J. L. 2011. Luminal expression of cubilin is impaired in Imlerslund-Grasbeck syndrome with compound AMN mutations in intron 3 and exon 7. *Haematologica*, 96, 1715-9.

- Nava, P., Kamekura, R. & Nusrat, A. 2013. Cleavage of transmembrane junction proteins and their role in regulating epithelial homeostasis. *Tissue Barriers*, 1, e24783.
- Navarro-Gonzalez, J. F. & Mora-Fernandez, C. 2008. The role of inflammatory cytokines in diabetic nephropathy. *J Am Soc Nephrol*, 19, 433-42.
- Nechemia-Arbely, Y., Barkan, D., Pizov, G., Shriki, A., Rose-John, S., Galun, E. & Axelrod, J. H. 2008. IL-6/IL-6R axis plays a critical role in acute kidney injury. *J Am Soc Nephrol*, 19, 1106-15.
- Nee, L. E., Mcmorrow, T., Campbell, E., Slattery, C. & Ryan, M. P. 2004. TNF-alpha and IL-1beta-mediated regulation of MMP-9 and TIMP-1 in renal proximal tubular cells. *Kidney Int*, 66, 1376-86.
- Negri, A. L. 2006. Proximal tubule endocytic apparatus as the specific renal uptake mechanism for vitamin D-binding protein/25-(OH)D3 complex. *Nephrology (Carlton)*, 11, 510-5.
- Newbold, A., Martin, B. P., Cullinane, C. & Bots, M. 2014. Detection of apoptotic cells using immunohistochemistry. *Cold Spring Harb Protoc*, 2014, 1196-201.
- Nielsen, R., Birn, H., Moestrup, S. K., Nielsen, M., Verroust, P. & Christensen, E. I. 1998. Characterization of a kidney proximal tubule cell line, LLC-PK1, expressing endocytotic active megalin. *J Am Soc Nephrol*, 9, 1767-76.
- Nielsen, R. & Christensen, E. I. 2010. Proteinuria and events beyond the slit. *Pediatr Nephrol*, 25, 813-22.
- Nielsen, R., Christensen, E. I. & Birn, H. 2016. Megalin and cubilin in proximal tubule protein reabsorption: from experimental models to human disease. *Kidney Int*, 89, 58-67.
- Nieuwdorp, M., Mooij, H. L., Kroon, J., Atasever, B., Spaan, J. A., Ince, C., Holleman, F., Diamant, M., Heine, R. J., Hoekstra, J. B., Kastelein, J. J., Stroes, E. S. & Vink, H. 2006. Endothelial glycocalyx damage coincides with microalbuminuria in type 1 diabetes. *Diabetes*, 55, 1127-32.
- Ninomiya, T., Perkovic, V., De Galan, B. E., Zoungas, S., Pillai, A., Jardine, M., Patel, A., Cass, A., Neal, B., Poulter, N., Mogensen, C. E., Cooper, M., Marre, M., Williams, B., Hamet, P., Mancia, G., Woodward, M., Macmahon, S., Chalmers, J. & Group, A. C. 2009. Albuminuria and kidney function

- independently predict cardiovascular and renal outcomes in diabetes. *J Am Soc Nephrol*, 20, 1813-21.
- Nishida, M., Okumura, Y., Ozawa, S., Shiraishi, I., Itoi, T. & Hamaoka, K. 2007. MMP-2 inhibition reduces renal macrophage infiltration with increased fibrosis in UUO. *Biochem Biophys Res Commun*, 354, 133-9.
- Norden, A. G., Lapsley, M., Lee, P. J., Pusey, C. D., Scheinman, S. J., Tam, F. W., Thakker, R. V., Unwin, R. J. & Wrong, O. 2001. Glomerular protein sieving and implications for renal failure in Fanconi syndrome. *Kidney Int*, 60, 1885-92.
- Norden, A. G., Scheinman, S. J., Deschodt-Lanckman, M. M., Lapsley, M., Nortier, J. L., Thakker, R. V., Unwin, R. J. & Wrong, O. 2000. Tubular proteinuria defined by a study of Dent's (CLCN5 mutation) and other tubular diseases. *Kidney Int*, 57, 240-9.
- Novak, K. B., Le, H. D., Christison-Lagay, E. R., Nose, V., Doiron, R. J., Moses, M. A. & Puder, M. 2010. Effects of metalloproteinase inhibition in a murine model of renal ischemia-reperfusion injury. *Pediatr Res*, 67, 257-62.
- Novick, A. C., Gephardt, G., Guz, B., Steinmuller, D. & Tubbs, R. R. 1991. Long-term follow-up after partial removal of a solitary kidney. *N Engl J Med*, 325, 1058-62.
- Nykjaer, A., Fyfe, J. C., Kozyraki, R., Leheste, J. R., Jacobsen, C., Nielsen, M. S., Verroust, P. J., Aminoff, M., De La Chapelle, A., Moestrup, S. K., Ray, R., Gliemann, J., Willnow, T. E. & Christensen, E. I. 2001. Cubilin dysfunction causes abnormal metabolism of the steroid hormone 25(OH) vitamin D(3). *Proc Natl Acad Sci U S A*, 98, 13895-900.
- Obeidat, M., Obeidat, M. & Ballermann, B. J. 2012. Glomerular endothelium: a porous sieve and formidable barrier. *Exp Cell Res*, 318, 964-72.
- Obermuller, N., Kranzlin, B., Blum, W. F., Gretz, N. & Witzgall, R. 2001a. An endocytosis defect as a possible cause of proteinuria in polycystic kidney disease. *Am J Physiol Renal Physiol*, 280, F244-53.
- Obermuller, N., Morente, N., Kranzlin, B., Gretz, N. & Witzgall, R. 2001b. A possible role for metalloproteinases in renal cyst development. *Am J Physiol Renal Physiol*, 280, F540-50.

- Ohlson, M., Sorensson, J. & Haraldsson, B. 2000. Glomerular size and charge selectivity in the rat as revealed by FITC-ficoll and albumin. *Am J Physiol Renal Physiol*, 279, F84-91.
- Ohlson, M., Sorensson, J. & Haraldsson, B. 2001. A gel-membrane model of glomerular charge and size selectivity in series. *Am J Physiol Renal Physiol*, 280, F396-405.
- Oken, D. E. & Flamenbaum, W. 1971. Micropuncture studies of proximal tubule albumin concentrations in normal and nephrotic rats. *J Clin Invest*, 50, 1498-505.
- Osicka, T. M., Panagiotopoulos, S., Jerums, G. & Comper, W. D. 1997. Fractional clearance of albumin is influenced by its degradation during renal passage. *Clin Sci (Lond)*, 93, 557-64.
- Otaki, Y., Miyauchi, N., Higa, M., Takada, A., Kuroda, T., Gejyo, F., Shimizu, F. & Kawachi, H. 2008. Dissociation of NEPH1 from nephrin is involved in development of a rat model of focal segmental glomerulosclerosis. *Am J Physiol Renal Physiol*, 295, F1376-87.
- Park, C. H. & Maack, T. 1984. Albumin absorption and catabolism by isolated perfused proximal convoluted tubules of the rabbit. *J Clin Invest*, 73, 767-77.
- Parsons, S. L., Watson, S. A. & Steele, R. J. 1997. Phase I/II trial of batimastat, a matrix metalloproteinase inhibitor, in patients with malignant ascites. *Eur J Surg Oncol*, 23, 526-31.
- Pearson, A. L., Colville-Nash, P., Kwan, J. T. & Dockrell, M. E. 2008. Albumin induces interleukin-6 release from primary human proximal tubule epithelial cells. *J Nephrol*, 21, 887-93.
- Pedersen, G. A., Chakraborty, S., Steinhauser, A. L., Traub, L. M. & Madsen, M. 2010. AMN directs endocytosis of the intrinsic factor-vitamin B(12) receptor cubam by engaging ARH or Dab2. *Traffic*, 11, 706-20.
- Peng, W. J., Yan, J. W., Wan, Y. N., Wang, B. X., Tao, J. H., Yang, G. J., Pan, H. F. & Wang, J. 2012. Matrix metalloproteinases: a review of their structure and role in systemic sclerosis. *J Clin Immunol*, 32, 1409-14.
- Peterson, J. C., Adler, S., Burkart, J. M., Greene, T., Hebert, L. A., Hunsicker, L. G., King, A. J., Klahr, S., Massry, S. G. & Seifert, J. L. 1995. Blood pressure

- control, proteinuria, and the progression of renal disease. The Modification of Diet in Renal Disease Study. *Ann Intern Med*, 123, 754-62.
- Peti-Peterdi, J. 2009. Independent two-photon measurements of albumin GSC give low values. *Am J Physiol Renal Physiol*, 296, F1255-7.
- Petrinec, D., Liao, S., Holmes, D. R., Reilly, J. M., Parks, W. C. & Thompson, R. W. 1996. Doxycycline inhibition of aneurysmal degeneration in an elastase-induced rat model of abdominal aortic aneurysm: preservation of aortic elastin associated with suppressed production of 92 kD gelatinase. *J Vasc Surg*, 23, 336-46.
- Pittayapruek, P., Meehansan, J., Prapapan, O., Komine, M. & Ohtsuki, M. 2016. Role of Matrix Metalloproteinases in Photoaging and Photocarcinogenesis. *Int J Mol Sci*, 17.
- Pohl, M., Shan, Q., Petsch, T., Styp-Rekowska, B., Matthey, P., Bleich, M., Bachmann, S. & Theilig, F. 2015. Short-term functional adaptation of aquaporin-1 surface expression in the proximal tubule, a component of glomerulotubular balance. *J Am Soc Nephrol*, 26, 1269-78.
- Powell, W. C., Fingleton, B., Wilson, C. L., Boothby, M. & Matrisian, L. M. 1999. The metalloproteinase matrilysin proteolytically generates active soluble Fas ligand and potentiates epithelial cell apoptosis. *Curr Biol*, 9, 1441-7.
- Prontera, C., Mariani, B., Rossi, C., Poggi, A. & Rotilio, D. 1999. Inhibition of gelatinase A (MMP-2) by batimastat and captopril reduces tumor growth and lung metastases in mice bearing Lewis lung carcinoma. *Int J Cancer*, 81, 761-6.
- Pushpakumar, S. B., Kundu, S., Metreveli, N., Tyagi, S. C. & Sen, U. 2013. Matrix Metalloproteinase Inhibition Mitigates Renovascular Remodeling in Salt-Sensitive Hypertension. *Physiol Rep*, 1, e00063.
- Ramanujam, K. S., Seetharam, S., Dahms, N. M. & Seetharam, B. 1994. Effect of processing inhibitors on cobalamin (vitamin B12) transcytosis in polarized opossum kidney cells. *Arch Biochem Biophys*, 315, 8-15.
- Ramesh, G. & Reeves, W. B. 2004. Inflammatory cytokines in acute renal failure. *Kidney Int Suppl*, S56-61.
- Rao, Z., Handford, P., Mayhew, M., Knott, V., Brownlee, G. G. & Stuart, D. 1995. The structure of a Ca(2+)-binding epidermal growth factor-like domain: its role in protein-protein interactions. *Cell*, 82, 131-41.

- Rasmussen, H. S. & Mccann, P. P. 1997. Matrix metalloproteinase inhibition as a novel anticancer strategy: a review with special focus on batimastat and marimastat. *Pharmacol Ther*, 75, 69-75.
- Reich, H., Tritchler, D., Herzenberg, A. M., Kassiri, Z., Zhou, X., Gao, W. & Scholey, J. W. 2005. Albumin activates ERK via EGF receptor in human renal epithelial cells. *J Am Soc Nephrol*, 16, 1266-78.
- Reiser, J. & Altintas, M. M. 2016. Podocytes. *F1000Res*, 5.
- Remuzzi, A., Puntorieri, S., Battaglia, C., Bertani, T. & Remuzzi, G. 1990. Angiotensin converting enzyme inhibition ameliorates glomerular filtration of macromolecules and water and lessens glomerular injury in the rat. *J Clin Invest*, 85, 541-9.
- Rennke, H. G., Patel, Y. & Venkatachalam, M. A. 1978. Glomerular filtration of proteins: clearance of anionic, neutral, and cationic horseradish peroxidase in the rat. *Kidney Int*, 13, 278-88.
- Richard S. Snell 2000. *Clinical Anatomy for Medical Students*, United States of America.
- Robinson, M. S. 1994. The role of clathrin, adaptors and dynamin in endocytosis. *Curr Opin Cell Biol*, 6, 538-44.
- Rodewald, R. & Karnovsky, M. J. 1974. Porous substructure of the glomerular slit diaphragm in the rat and mouse. *J Cell Biol*, 60, 423-33.
- Rodriguez-Iturbe, B. & Garcia Garcia, G. 2010. The role of tubulointerstitial inflammation in the progression of chronic renal failure. *Nephron Clin Pract*, 116, c81-8.
- Ronco, P. & Chatziantoniou, C. 2008. Matrix metalloproteinases and matrix receptors in progression and reversal of kidney disease: therapeutic perspectives. *Kidney Int*, 74, 873-8.
- Ronco, P., Lelongt, B., Piedagnel, R. & Chatziantoniou, C. 2007. Matrix metalloproteinases in kidney disease progression and repair: a case of flipping the coin. *Semin Nephrol*, 27, 352-62.
- Roscioni, S. S., Lambers Heerspink, H. J. & De Zeeuw, D. 2014. Microalbuminuria: target for renoprotective therapy PRO. *Kidney Int*, 86, 40-9.
- Ross, J. 2014. using the colour deconvolution plugin in imageJ. *Biomedical Imaging Research Unit*. School of Medical Sciences.

- Rostgaard, J. & Qvortrup, K. 2002. Sieve plugs in fenestrae of glomerular capillaries--site of the filtration barrier? *Cells Tissues Organs*, 170, 132-8.
- Ruggenenti, P., Mosconi, L., Sangalli, F., Casiraghi, F., Gambarà, V., Remuzzi, G. & Remuzzi, A. 1999. Glomerular size-selective dysfunction in NIDDM is not ameliorated by ACE inhibition or by calcium channel blockade. *Kidney Int*, 55, 984-94.
- Ruggenenti, P., Perna, A., Gherardi, G., Gaspari, F., Benini, R. & Remuzzi, G. 1998. Renal function and requirement for dialysis in chronic nephropathy patients on long-term ramipril: REIN follow-up trial. Gruppo Italiano di Studi Epidemiologici in Nefrologia (GISEN). Ramipril Efficacy in Nephropathy. *Lancet*, 352, 1252-6.
- Ruggenenti, P., Schieppati, A. & Remuzzi, G. 2001. Progression, remission, regression of chronic renal diseases. *Lancet*, 357, 1601-8.
- Ruifrok, A. C. & Johnston, D. A. 2001. Quantification of histochemical staining by color deconvolution. *Anal Quant Cytol Histol*, 23, 291-9.
- Ruotsalainen, V., Ljungberg, P., Wartiovaara, J., Lenkkeri, U., Kestila, M., Jalanko, H., Holmberg, C. & Tryggvason, K. 1999. Nephritin is specifically located at the slit diaphragm of glomerular podocytes. *Proc Natl Acad Sci U S A*, 96, 7962-7.
- Russo, L. M., Bakris, G. L. & Comper, W. D. 2002. Renal handling of albumin: a critical review of basic concepts and perspective. *Am J Kidney Dis*, 39, 899-919.
- Russo, L. M., Sandoval, R. M., Mckee, M., Osicka, T. M., Collins, A. B., Brown, D., Molitoris, B. A. & Comper, W. D. 2007. The normal kidney filters nephrotic levels of albumin retrieved by proximal tubule cells: retrieval is disrupted in nephrotic states. *Kidney Int*, 71, 504-13.
- Sahali, D., Mulliez, N., Chatelet, F., Dupuis, R., Ronco, P. & Verroust, P. 1988. Characterization of a 280-kD protein restricted to the coated pits of the renal brush border and the epithelial cells of the yolk sac. Teratogenic effect of the specific monoclonal antibodies. *J Exp Med*, 167, 213-8.
- Sahali, D., Mulliez, N., Chatelet, F., Laurent-Winter, C., Citadelle, D., Sabourin, J. C., Roux, C., Ronco, P. & Verroust, P. 1993. Comparative immunochemistry and ontogeny of two closely related coated pit proteins.

- The 280-kd target of teratogenic antibodies and the 330-kd target of nephritogenic antibodies. *Am J Pathol*, 142, 1654-67.
- Santoyo-Sanchez, M. P., Pedraza-Chaverri, J., Molina-Jijon, E., Arreola-Mendoza, L., Rodriguez-Munoz, R. & Barbier, O. C. 2013. Impaired endocytosis in proximal tubule from subchronic exposure to cadmium involves angiotensin II type 1 and cubilin receptors. *BMC Nephrol*, 14, 211.
- Sanz, A. B., Santamaria, B., Ruiz-Ortega, M., Egido, J. & Ortiz, A. 2008. Mechanisms of renal apoptosis in health and disease. *J Am Soc Nephrol*, 19, 1634-42.
- Satchell, S. 2013. The role of the glomerular endothelium in albumin handling. *Nat Rev Nephrol*, 9, 717-25.
- Satchell, S. C. & Braet, F. 2009. Glomerular endothelial cell fenestrations: an integral component of the glomerular filtration barrier. *Am J Physiol Renal Physiol*, 296, F947-56.
- Scheiffele, P., Peranen, J. & Simons, K. 1995. N-glycans as apical sorting signals in epithelial cells. *Nature*, 378, 96-8.
- Schneider, C. A., Rasband, W. S. & Eliceiri, K. W. 2012. NIH Image to ImageJ: 25 years of image analysis. *Nat Methods*, 9, 671-5.
- Schreiber, A., Theilig, F., Schweda, F. & Hoherl, K. 2012. Acute endotoxemia in mice induces downregulation of megalin and cubilin in the kidney. *Kidney Int*, 82, 53-9.
- Schwegler, J. S., Heppelmann, B., Mildenerger, S. & Silbernagl, S. 1991. Receptor-mediated endocytosis of albumin in cultured opossum kidney cells: a model for proximal tubular protein reabsorption. *Pflugers Arch*, 418, 383-92.
- Scindia, Y. M., Deshmukh, U. S. & Bagavant, H. 2010. Mesangial pathology in glomerular disease: targets for therapeutic intervention. *Adv Drug Deliv Rev*, 62, 1337-43.
- Scott, R. P., Hawley, S. P., Ruston, J., Du, J., Brakebusch, C., Jones, N. & Pawson, T. 2012. Podocyte-specific loss of Cdc42 leads to congenital nephropathy. *J Am Soc Nephrol*, 23, 1149-54.
- Seetharam, B., Alpers, D. H. & Allen, R. H. 1981. Isolation and characterization of the ileal receptor for intrinsic factor-cobalamin. *J Biol Chem*, 256, 3785-90.

- Seetharam, B., Christensen, E. I., Moestrup, S. K., Hammond, T. G. & Verroust, P. J. 1997. Identification of rat yolk sac target protein of teratogenic antibodies, gp280, as intrinsic factor-cobalamin receptor. *J Clin Invest*, 99, 2317-22.
- Seetharam, B., Levine, J. S., Ramasamy, M. & Alpers, D. H. 1988. Purification, properties, and immunochemical localization of a receptor for intrinsic factor-cobalamin complex in the rat kidney. *J Biol Chem*, 263, 4443-9.
- Selander-Sunnerhagen, M., Ullner, M., Persson, E., Teleman, O., Stenflo, J. & Drakenberg, T. 1992. How an epidermal growth factor (EGF)-like domain binds calcium. High resolution NMR structure of the calcium form of the NH₂-terminal EGF-like domain in coagulation factor X. *J Biol Chem*, 267, 19642-9.
- Shimamura, T. & Morrison, A. B. 1975. A progressive glomerulosclerosis occurring in partial five-sixths nephrectomized rats. *Am J Pathol*, 79, 95-106.
- Singh, A., Satchell, S. C., Neal, C. R., McKenzie, E. A., Tooke, J. E. & Mathieson, P. W. 2007. Glomerular endothelial glycocalyx constitutes a barrier to protein permeability. *J Am Soc Nephrol*, 18, 2885-93.
- Sorbi, D., Fadly, M., Hicks, R., Alexander, S. & Arbeit, L. 1993. Captopril inhibits the 72 kDa and 92 kDa matrix metalloproteinases. *Kidney Int*, 44, 1266-72.
- Steinmann-Niggli, K., Ziswiler, R., Kung, M. & Marti, H. P. 1998. Inhibition of matrix metalloproteinases attenuates anti-Thy1.1 nephritis. *J Am Soc Nephrol*, 9, 397-407.
- Sternlicht, M. D. & Werb, Z. 2001. How matrix metalloproteinases regulate cell behavior. *Annu Rev Cell Dev Biol*, 17, 463-516.
- Sterzel, R. B., Lovett, D. H., Stein, H. D. & Kashgarian, M. 1982. The mesangium and glomerulonephritis. *Klin Wochenschr*, 60, 1077-94.
- Stockand, J. D. & Sansom, S. C. 1998. Glomerular mesangial cells: electrophysiology and regulation of contraction. *Physiol Rev*, 78, 723-44.
- Stolt, P. C. & Bock, H. H. 2006. Modulation of lipoprotein receptor functions by intracellular adaptor proteins. *Cell Signal*, 18, 1560-71.
- Storm, T., Emma, F., Verroust, P. J., Hertz, J. M., Nielsen, R. & Christensen, E. I. 2011. A patient with cubilin deficiency. *N Engl J Med*, 364, 89-91.

- Storm, T., Zeitz, C., Cases, O., Amsellem, S., Verroust, P. J., Madsen, M., Benoist, J. F., Passemard, S., Lebon, S., Jonsson, I. M., Emma, F., Koldso, H., Hertz, J. M., Nielsen, R., Christensen, E. I. & Kozyraki, R. 2013. Detailed investigations of proximal tubular function in Imlerslund-Grasbeck syndrome. *BMC Med Genet*, 14, 111.
- Strope, S., Rivi, R., Metzger, T., Manova, K. & Lacy, E. 2004. Mouse amnionless, which is required for primitive streak assembly, mediates cell-surface localization and endocytic function of cubilin on visceral endoderm and kidney proximal tubules. *Development*, 131, 4787-95.
- Sugimoto, H., Mundel, T. M., Sund, M., Xie, L., Cosgrove, D. & Kalluri, R. 2006. Bone-marrow-derived stem cells repair basement membrane collagen defects and reverse genetic kidney disease. *Proc Natl Acad Sci U S A*, 103, 7321-6.
- Suh, J. H. & Miner, J. H. 2013. The glomerular basement membrane as a barrier to albumin. *Nat Rev Nephrol*, 9, 470-7.
- Sumpio, B. E. & Hayslett, J. P. 1985. Renal handling of proteins in normal and disease states. *Q J Med*, 57, 611-35.
- Sumpio, B. E. & Maack, T. 1982. Kinetics, competition, and selectivity of tubular absorption of proteins. *Am J Physiol*, 243, F379-92.
- Sutton, T. A., Kelly, K. J., Mang, H. E., Plotkin, Z., Sandoval, R. M. & Dagher, P. C. 2005. Minocycline reduces renal microvascular leakage in a rat model of ischemic renal injury. *Am J Physiol Renal Physiol*, 288, F91-7.
- Szczzech, L. A. & Lazar, I. L. 2004. Projecting the United States ESRD population: issues regarding treatment of patients with ESRD. *Kidney Int Suppl*, S3-7.
- Takase, O., Hirahashi, J., Takayanagi, A., Chikaraishi, A., Marumo, T., Ozawa, Y., Hayashi, M., Shimizu, N. & Saruta, T. 2003. Gene transfer of truncated I κ B α prevents tubulointerstitial injury. *Kidney Int*, 63, 501-13.
- Takaya, K., Koya, D., Isono, M., Sugimoto, T., Sugaya, T., Kashiwagi, A. & Haneda, M. 2003. Involvement of ERK pathway in albumin-induced MCP-1 expression in mouse proximal tubular cells. *Am J Physiol Renal Physiol*, 284, F1037-45.
- Tan, R. J. & Liu, Y. 2012. Matrix metalloproteinases in kidney homeostasis and diseases. *Am J Physiol Renal Physiol*, 302, F1351-61.

- Tan, T. K., Zheng, G., Hsu, T. T., Lee, S. R., Zhang, J., Zhao, Y., Tian, X., Wang, Y., Wang, Y. M., Cao, Q., Wang, Y., Lee, V. W., Wang, C., Zheng, D., Alexander, S. I., Thompson, E. & Harris, D. C. 2013. Matrix metalloproteinase-9 of tubular and macrophage origin contributes to the pathogenesis of renal fibrosis via macrophage recruitment through osteopontin cleavage. *Lab Invest*, 93, 434-49.
- Tan, T. K., Zheng, G., Hsu, T. T., Wang, Y., Lee, V. W., Tian, X., Wang, Y., Cao, Q., Wang, Y. & Harris, D. C. 2010. Macrophage matrix metalloproteinase-9 mediates epithelial-mesenchymal transition in vitro in murine renal tubular cells. *Am J Pathol*, 176, 1256-70.
- Tang, S., Lai, K. N., Chan, T. M., Lan, H. Y., Ho, S. K. & Sacks, S. H. 2001. Transferrin but not albumin mediates stimulation of complement C3 biosynthesis in human proximal tubular epithelial cells. *Am J Kidney Dis*, 37, 94-103.
- Tang, S., Leung, J. C., Abe, K., Chan, K. W., Chan, L. Y., Chan, T. M. & Lai, K. N. 2003. Albumin stimulates interleukin-8 expression in proximal tubular epithelial cells in vitro and in vivo. *J Clin Invest*, 111, 515-27.
- Tang, W. W., Qi, M., Warren, J. S. & Van, G. Y. 1997. Chemokine expression in experimental tubulointerstitial nephritis. *J Immunol*, 159, 870-6.
- Tanner, S. M., Aminoff, M., Wright, F. A., Liyanarachchi, S., Kuronen, M., Saarinen, A., Massika, O., Mandel, H., Broch, H. & De La Chapelle, A. 2003. Amnionless, essential for mouse gastrulation, is mutated in recessive hereditary megaloblastic anemia. *Nat Genet*, 33, 426-9.
- Tanner, S. M., Li, Z., Bisson, R., Acar, C., Oner, C., Oner, R., Cetin, M., Abdelaal, M. A., Ismail, E. A., Lissens, W., Krahe, R., Broch, H., Grasbeck, R. & De La Chapelle, A. 2004. Genetically heterogeneous selective intestinal malabsorption of vitamin B12: founder effects, consanguinity, and high clinical awareness explain aggregations in Scandinavia and the Middle East. *Hum Mutat*, 23, 327-33.
- Tashiro, K., Koyanagi, I., Ohara, I., Ito, T., Saitoh, A., Horikoshi, S. & Tomino, Y. 2004. Levels of urinary matrix metalloproteinase-9 (MMP-9) and renal injuries in patients with type 2 diabetic nephropathy. *J Clin Lab Anal*, 18, 206-10.

- Tejera, N., Gomez-Garre, D., Lazaro, A., Gallego-Delgado, J., Alonso, C., Blanco, J., Ortiz, A. & Egido, J. 2004. Persistent proteinuria up-regulates angiotensin II type 2 receptor and induces apoptosis in proximal tubular cells. *Am J Pathol*, 164, 1817-26.
- Tencer, J., Frick, I. M., Oquist, B. W., Alm, P. & Rippe, B. 1998. Size-selectivity of the glomerular barrier to high molecular weight proteins: upper size limitations of shunt pathways. *Kidney Int*, 53, 709-15.
- Tenten, V., Menzel, S., Kunter, U., Sicking, E. M., Van Roeyen, C. R., Sanden, S. K., Kaldenbach, M., Boor, P., Fuss, A., Uhlig, S., Lanzmich, R., Willemsen, B., Dijkman, H., Grepl, M., Wild, K., Kriz, W., Smeets, B., Floege, J. & Moeller, M. J. 2013. Albumin is recycled from the primary urine by tubular transcytosis. *J Am Soc Nephrol*, 24, 1966-80.
- Terryn, S., Tanaka, K., Lengele, J. P., Olinger, E., Dubois-Laforgue, D., Garbay, S., Kozyraki, R., Van Der Smissen, P., Christensen, E. I., Courtoy, P. J., Bellanne-Chantelot, C., Timsit, J., Pontoglio, M. & Devuyst, O. 2016. Tubular proteinuria in patients with HNF1alpha mutations: HNF1alpha drives endocytosis in the proximal tubule. *Kidney Int*, 89, 1075-1089.
- Thelle, K., Christensen, E. I., Vorum, H., Orskov, H. & Birn, H. 2006. Characterization of proteinuria and tubular protein uptake in a new model of oral L-lysine administration in rats. *Kidney Int*, 69, 1333-40.
- Thomas, M. E., Brunskill, N. J., Harris, K. P., Bailey, E., Pringle, J. H., Furness, P. N. & Walls, J. 1999. Proteinuria induces tubular cell turnover: A potential mechanism for tubular atrophy. *Kidney Int*, 55, 890-8.
- Thraillkill, K. M., Bunn, R. C., Moreau, C. S., Cockrell, G. E., Simpson, P. M., Coleman, H. N., Frindik, J. P., Kemp, S. F. & Fowlkes, J. L. 2007. Matrix metalloproteinase-2 dysregulation in type 1 diabetes. *Diabetes Care*, 30, 2321-6.
- Thraillkill, K. M., Clay Bunn, R. & Fowlkes, J. L. 2009a. Matrix metalloproteinases: their potential role in the pathogenesis of diabetic nephropathy. *Endocrine*, 35, 1-10.
- Thraillkill, K. M., Nimmo, T., Bunn, R. C., Cockrell, G. E., Moreau, C. S., Mackintosh, S., Edmondson, R. D. & Fowlkes, J. L. 2009b. Microalbuminuria in type 1 diabetes is associated with enhanced excretion

- of the endocytic multiligand receptors megalin and cubilin. *Diabetes Care*, 32, 1266-8.
- Tojo, A. & Endou, H. 1992. Intrarenal handling of proteins in rats using fractional micropuncture technique. *Am J Physiol*, 263, F601-6.
- Tojo, A. & Kinugasa, S. 2012. Mechanisms of glomerular albumin filtration and tubular reabsorption. *Int J Nephrol*, 2012, 481520.
- Tokito, A. & Jougasaki, M. 2016. Matrix Metalloproteinases in Non-Neoplastic Disorders. *Int J Mol Sci*, 17.
- Tomihara-Newberger, C., Haub, O., Lee, H. G., Soares, V., Manova, K. & Lacy, E. 1998. The amn gene product is required in extraembryonic tissues for the generation of middle primitive streak derivatives. *Dev Biol*, 204, 34-54.
- Tryggvason, K. 1999. Unraveling the mechanisms of glomerular ultrafiltration: nephrin, a key component of the slit diaphragm. *J Am Soc Nephrol*, 10, 2440-5.
- Turck, J., Pollock, A. S., Lee, L. K., Marti, H. P. & Lovett, D. H. 1996. Matrix metalloproteinase 2 (gelatinase A) regulates glomerular mesangial cell proliferation and differentiation. *J Biol Chem*, 271, 15074-83.
- Tveita, A., Rekvig, O. P. & Zykova, S. N. 2008. Glomerular matrix metalloproteinases and their regulators in the pathogenesis of lupus nephritis. *Arthritis Res Ther*, 10, 229.
- Van Der Velde, M., Matsushita, K., Coresh, J., Astor, B. C., Woodward, M., Levey, A., De Jong, P., Gansevoort, R. T., Chronic Kidney Disease Prognosis, C., Van Der Velde, M., Matsushita, K., Coresh, J., Astor, B. C., Woodward, M., Levey, A. S., De Jong, P. E., Gansevoort, R. T., Levey, A., El-Nahas, M., Eckardt, K. U., Kasiske, B. L., Ninomiya, T., Chalmers, J., Macmahon, S., Tonelli, M., Hemmelgarn, B., Sacks, F., Curhan, G., Collins, A. J., Li, S., Chen, S. C., Hawaii Cohort, K. P., Lee, B. J., Ishani, A., Neaton, J., Svendsen, K., Mann, J. F., Yusuf, S., Teo, K. K., Gao, P., Nelson, R. G., Knowler, W. C., Bilo, H. J., Joosten, H., Kleefstra, N., Groenier, K. H., Auguste, P., Veldhuis, K., Wang, Y., Camarata, L., Thomas, B. & Manley, T. 2011. Lower estimated glomerular filtration rate and higher albuminuria are associated with all-cause and cardiovascular mortality. A collaborative meta-analysis of high-risk population cohorts. *Kidney Int*, 79, 1341-52.

- Van Der Zijl, N. J., Hanemaaijer, R., Tushuizen, M. E., Schindhelm, R. K., Boerop, J., Rustemeijer, C., Bilo, H. J., Verheijen, J. H. & Diamant, M. 2010. Urinary matrix metalloproteinase-8 and -9 activities in type 2 diabetic subjects: A marker of incipient diabetic nephropathy? *Clin Biochem*, 43, 635-9.
- Van Wart, H. E. & Birkedal-Hansen, H. 1990. The cysteine switch: a principle of regulation of metalloproteinase activity with potential applicability to the entire matrix metalloproteinase gene family. *Proc Natl Acad Sci U S A*, 87, 5578-82.
- Varghese, F., Bukhari, A. B., Malhotra, R. & De, A. 2014. IHC Profiler: an open source plugin for the quantitative evaluation and automated scoring of immunohistochemistry images of human tissue samples. *PLoS One*, 9, e96801.
- Verroust, P. J., Birn, H., Nielsen, R., Kozyraki, R. & Christensen, E. I. 2002. The tandem endocytic receptors megalin and cubilin are important proteins in renal pathology. *Kidney Int*, 62, 745-56.
- Verroust, P. J. & Christensen, E. I. 2002. Megalin and cubilin--the story of two multipurpose receptors unfolds. *Nephrol Dial Transplant*, 17, 1867-71.
- Vielhauer, V. & Mayadas, T. N. 2007. Functions of TNF and its receptors in renal disease: distinct roles in inflammatory tissue injury and immune regulation. *Semin Nephrol*, 27, 286-308.
- Vinge, L., Lees, G. E., Nielsen, R., Kashtan, C. E., Bahr, A. & Christensen, E. I. 2010. The effect of progressive glomerular disease on megalin-mediated endocytosis in the kidney. *Nephrol Dial Transplant*, 25, 2458-67.
- Visse, R. & Nagase, H. 2003. Matrix metalloproteinases and tissue inhibitors of metalloproteinases: structure, function, and biochemistry. *Circ Res*, 92, 827-39.
- Viswanathan, V. & Rani, A. A. 2016. Proteinuria in nondiabetic patients: Clinical significance. *Hypertension Journal*, 2, pp.118-123.
- Wahlstedt-Froberg, V., Pettersson, T., Aminoff, M., Dugue, B. & Grasbeck, R. 2003. Proteinuria in cubilin-deficient patients with selective vitamin B12 malabsorption. *Pediatr Nephrol*, 18, 417-21.
- Wallace, M. A. 1998. Anatomy and physiology of the kidney. *AORN J*, 68, 800, 803-16, 819-20; quiz 821-4.

- Wang, C. W., Fennell, D., Paul, I., Savage, K. & Hamilton, P. 2011. Robust automated tumour segmentation on histological and immunohistochemical tissue images. *PLoS One*, 6, e15818.
- Wang, X., Fu, X., Brown, P. D., Crimmin, M. J. & Hoffman, R. M. 1994. Matrix metalloproteinase inhibitor BB-94 (batimastat) inhibits human colon tumor growth and spread in a patient-like orthotopic model in nude mice. *Cancer Res*, 54, 4726-8.
- Wang, Y., Wang, Y. P., Tay, Y. C. & Harris, D. C. 2000. Progressive adriamycin nephropathy in mice: sequence of histologic and immunohistochemical events. *Kidney Int*, 58, 1797-804.
- Watson, S. A., Morris, T. M., Parsons, S. L., Steele, R. J. & Brown, P. D. 1996. Therapeutic effect of the matrix metalloproteinase inhibitor, batimastat, in a human colorectal cancer ascites model. *Br J Cancer*, 74, 1354-8.
- Wedegaertner, P. B., Chu, D. H., Wilson, P. T., Levis, M. J. & Bourne, H. R. 1993. Palmitoylation is required for signaling functions and membrane attachment of Gq alpha and Gs alpha. *J Biol Chem*, 268, 25001-8.
- Weinbaum, S., Tarbell, J. M. & Damiano, E. R. 2007. The structure and function of the endothelial glycocalyx layer. *Annu Rev Biomed Eng*, 9, 121-67.
- Werb, Z. & Yan, Y. 1998. A cellular striptease act. *Science*, 282, 1279-80.
- West, B. L., Picken, M. M. & Leehey, D. J. 2006. Albuminuria in acute tubular necrosis. *Nephrol Dial Transplant*, 21, 2953-6.
- Weyer, K., Storm, T., Shan, J., Vainio, S., Kozyraki, R., Verroust, P. J., Christensen, E. I. & Nielsen, R. 2011. Mouse model of proximal tubule endocytic dysfunction. *Nephrol Dial Transplant*, 26, 3446-51.
- Whaley-Connell, A. T., Morris, E. M., Rehmer, N., Yaghoubian, J. C., Wei, Y., Hayden, M. R., Habibi, J., Stump, C. S. & Sowers, J. R. 2007. Albumin activation of NAD(P)H oxidase activity is mediated via Rac1 in proximal tubule cells. *Am J Nephrol*, 27, 15-23.
- Wheeler, D. S., Giuliano, J. S., Jr., Lahni, P. M., Denenberg, A., Wong, H. R. & Zingarelli, B. 2011. The immunomodulatory effects of albumin in vitro and in vivo. *Adv Pharmacol Sci*, 2011, 691928.
- Whiteside, C. I., Cameron, R., Munk, S. & Levy, J. 1993. Podocytic cytoskeletal disaggregation and basement-membrane detachment in puromycin aminonucleoside nephrosis. *Am J Pathol*, 142, 1641-53.

- Whittaker, P., Kloner, R. A., Boughner, D. R. & Pickering, J. G. 1994. Quantitative assessment of myocardial collagen with picosirius red staining and circularly polarized light. *Basic Res Cardiol*, 89, 397-410.
- Williams, A. J., Baker, F. & Walls, J. 1987. Effect of varying quantity and quality of dietary protein intake in experimental renal disease in rats. *Nephron*, 46, 83-90.
- Williams, J. D. & Coles, G. A. 1994. Proteinuria--a direct cause of renal morbidity? *Kidney Int*, 45, 443-50.
- Williams, J. M., Zhang, J., North, P., Lacy, S., Yakes, M., Dahly-Vernon, A. & Roman, R. J. 2011. Evaluation of metalloprotease inhibitors on hypertension and diabetic nephropathy. *Am J Physiol Renal Physiol*, 300, F983-98.
- Willnow, T. E., Moehring, J. M., Inocencio, N. M., Moehring, T. J. & Herz, J. 1996. The low-density-lipoprotein receptor-related protein (LRP) is processed by furin in vivo and in vitro. *Biochem J*, 313 (Pt 1), 71-6.
- Woessner, J. F., Jr. 1991. Matrix metalloproteinases and their inhibitors in connective tissue remodeling. *FASEB J*, 5, 2145-54.
- Woessner, J. F., Jr. 1999. Matrix metalloproteinase inhibition. From the Jurassic to the third millennium. *Ann N Y Acad Sci*, 878, 388-403.
- Wojtowicz-Praga, S. M., Dickson, R. B. & Hawkins, M. J. 1997. Matrix metalloproteinase inhibitors. *Invest New Drugs*, 15, 61-75.
- Wu, H. J., Yiu, W. H., Li, R. X., Wong, D. W., Leung, J. C., Chan, L. Y., Zhang, Y., Lian, Q., Lin, M., Tse, H. F., Lai, K. N. & Tang, S. C. 2014. Mesenchymal stem cells modulate albumin-induced renal tubular inflammation and fibrosis. *PLoS One*, 9, e90883.
- Xu, D. & Fyfe, J. C. 2000. Cubilin expression and posttranslational modification in the canine gastrointestinal tract. *Am J Physiol Gastrointest Liver Physiol*, 279, G748-56.
- Xu, D., Kozyraki, R., Newman, T. C. & Fyfe, J. C. 1999. Genetic evidence of an accessory activity required specifically for cubilin brush-border expression and intrinsic factor-cobalamin absorption. *Blood*, 94, 3604-6.
- Xu, X., Jackson, P. L., Tanner, S., Hardison, M. T., Abdul Roda, M., Blalock, J. E. & Gaggar, A. 2011. A self-propagating matrix metalloprotease-9 (MMP-9)

- dependent cycle of chronic neutrophilic inflammation. *PLoS One*, 6, e15781.
- Yamamoto, M., Tsujishita, H., Hori, N., Ohishi, Y., Inoue, S., Ikeda, S. & Okada, Y. 1998. Inhibition of membrane-type 1 matrix metalloproteinase by hydroxamate inhibitors: an examination of the subsite pocket. *J Med Chem*, 41, 1209-17.
- Yang Jurong, H. Y., SHEN Haiying, DING Hanlu, LI Kailong WH. 2008. Expression of renal cubilin and its potential role in tubulointerstitial inflammation induced by albumin overload. *Front Med*, 2, 25–34.
- Yang, X., Kume, S., Tanaka, Y., Isshiki, K., Araki, S., Chin-Kanasaki, M., Sugimoto, T., Koya, D., Haneda, M., Sugaya, T., Li, D., Han, P., Nishio, Y., Kashiwagi, A., Maegawa, H. & Uzu, T. 2011. GW501516, a PPARdelta agonist, ameliorates tubulointerstitial inflammation in proteinuric kidney disease via inhibition of TAK1-NFkappaB pathway in mice. *PLoS One*, 6, e25271.
- Zatz, R., Dunn, B. R., Meyer, T. W., Anderson, S., Rennke, H. G. & Brenner, B. M. 1986. Prevention of diabetic glomerulopathy by pharmacological amelioration of glomerular capillary hypertension. *J Clin Invest*, 77, 1925-30.
- Zeisberg, M., Khurana, M., Rao, V. H., Cosgrove, D., Rougier, J. P., Werner, M. C., Shield, C. F., 3rd, Werb, Z. & Kalluri, R. 2006. Stage-specific action of matrix metalloproteinases influences progressive hereditary kidney disease. *PLoS Med*, 3, e100.
- Zempo, N., Koyama, N., Kenagy, R. D., Lea, H. J. & Clowes, A. W. 1996. Regulation of vascular smooth muscle cell migration and proliferation in vitro and in injured rat arteries by a synthetic matrix metalloproteinase inhibitor. *Arterioscler Thromb Vasc Biol*, 16, 28-33.
- Zhai, X. Y., Nielsen, R., Birn, H., Drumm, K., Mildenerger, S., Freudinger, R., Moestrup, S. K., Verroust, P. J., Christensen, E. I. & Gekle, M. 2000. Cubilin- and megalin-mediated uptake of albumin in cultured proximal tubule cells of opossum kidney. *Kidney Int*, 58, 1523-33.
- Zhang, F., Zhao, Y., Chao, Y., Muir, K. & Han, Z. 2013. Cubilin and amnionless mediate protein reabsorption in *Drosophila* nephrocytes. *J Am Soc Nephrol*, 24, 209-16.

- Zhang, Y., Dean, W. L. & Gray, R. D. 1997. Cooperative binding of Ca²⁺ to human interstitial collagenase assessed by circular dichroism, fluorescence, and catalytic activity. *J Biol Chem*, 272, 1444-7.
- Zhang, Y., George, J., Li, Y., Olufade, R. & Zhao, X. 2015. Matrix metalloproteinase-9 expression is enhanced in renal parietal epithelial cells of Zucker diabetic Fatty rats and is induced by albumin in in vitro primary parietal cell culture. *PLoS One*, 10, e0123276.
- Zhao, H., Dong, Y., Tian, X., Tan, T. K., Liu, Z., Zhao, Y., Zhang, Y., Harris, D. & Zheng, G. 2013. Matrix metalloproteinases contribute to kidney fibrosis in chronic kidney diseases. *World J Nephrol*, 2, 84-9.
- Zheng, F., Cornacchia, F., Schulman, I., Banerjee, A., Cheng, Q. L., Potier, M., Plati, A. R., Berho, M., Elliot, S. J., Li, J., Fornoni, A., Zang, Y. J., Zisman, A., Striker, L. J. & Striker, G. E. 2004. Development of albuminuria and glomerular lesions in normoglycemic B6 recipients of db/db mice bone marrow: the role of mesangial cell progenitors. *Diabetes*, 53, 2420-7.
- Zheng, G., Lyons, J. G., Tan, T. K., Wang, Y., Hsu, T. T., Min, D., Succar, L., Rangan, G. K., Hu, M., Henderson, B. R., Alexander, S. I. & Harris, D. C. 2009. Disruption of E-cadherin by matrix metalloproteinase directly mediates epithelial-mesenchymal transition downstream of transforming growth factor-beta1 in renal tubular epithelial cells. *Am J Pathol*, 175, 580-91.
- Zhou, L., Liu, F., Huang, X. R., Liu, F., Chen, H., Chung, A. C., Shi, J., Wei, L., Lan, H. Y. & Fu, P. 2011. Amelioration of albuminuria in ROCK1 knockout mice with streptozotocin-induced diabetic kidney disease. *Am J Nephrol*, 34, 468-75.
- Zhuo, J. L. & Li, X. C. 2013. Proximal nephron. *Compr Physiol*, 3, 1079-123.
- Zoja, C., Abbate, M. & Remuzzi, G. 2015. Progression of renal injury toward interstitial inflammation and glomerular sclerosis is dependent on abnormal protein filtration. *Nephrol Dial Transplant*, 30, 706-12.
- Zoja, C., Benigni, A. & Remuzzi, G. 2004. Cellular responses to protein overload: key event in renal disease progression. *Curr Opin Nephrol Hypertens*, 13, 31-7.
- Zoja, C., Donadelli, R., Colleoni, S., Figliuzzi, M., Bonazzola, S., Morigi, M. & Remuzzi, G. 1998. Protein overload stimulates RANTES production by

proximal tubular cells depending on NF-kappa B activation. *Kidney Int*, 53, 1608-15.

Zou, Z., Chung, B., Nguyen, T., Mentone, S., Thomson, B. & Biemesderfer, D. 2004. Linking receptor-mediated endocytosis and cell signaling: evidence for regulated intramembrane proteolysis of megalin in proximal tubule. *J Biol Chem*, 279, 34302-10.